University of Zurich[UZH]

Department of Informatics

MESTRAN, a Variable Stiffness Actuator for Energy Efficient Legged Robots

A dissertation submitted to the Faculty of Economics, Business Administration and Information Technology of the University of Zurich

for the degree of
Doctor of Science (Ph.D.)

by

Hung Quy Vu

from Vietnam

Accepted on the recommendation of

Prof. Dr. Rolf Pfeifer, University of Zurich, Switzerland
Prof. Dr. Koh Hosoda, Osaka University, Japan

November 2013

The Faculty of Economics, Business Administration and Information Technology of the University of Zurich herewith permits the publication of the aforementioned dissertation without expressing any opinion on the views contained therein.

Zurich, September 24, 2013

Head of the Ph.D. program in informatics: Prof. Dr. Abraham Bernstein

Acknowledgements

My PhD studies at the Artificial Intelligence Laboratory (AI Lab), University of Zurich, over the past five years has been an exciting and life defining period. I would like to thank Professor Rolf Pfeifer very much for his continuous support in science and finance to make my chance possible. I am grateful for the great opportunity to work under his supervision and at a scientifically stimulating environment as the AI lab.

I would especially like to thank Professor Koh Hosoda from the Osaka University, Japan, for a number of constructive and thoughtful suggestions as a reviewer of this thesis.

My PhD studies would not have been possible without the uncountable support of three persons: Lijin Aryananda, Helmut Hauser and Fumiya Iida. Lijin was a postdoctal researcher at the AI Lab and my first PhD supervisor. She was very enthusiastically guiding and teaching me in the very first steps of my PhD. Helmut Hauser was also at the AI Lab as a postdoc. He came later as my second PhD supervisor from the second year. He offered me intensive support and insightful guidance from time to time to help me complete the EU funded project, so-called Locormorph, and advised me on my research. Fumiya Iida is the Professor of the Bio-inspired Robotic Laboratory (BIRL) at ETHZ. He is my external collaborator. I came to meet him in the fourth year of my PhD. He provided me with invaluable mentorship and enormous encouragement in doing research and writing papers.

To my colleagues at the AI Lab, I would like to mention Farrukh Iqbal Sheikh, my teammate, who has worked together with me over the past five years. We were discussing, chatting, and sharing thoughts day by day about science and life. I would like to send my thanks to many other friends at the AI Lab, the BIRL and in Zurich, with whom I enjoyed at lunches, coffee, beer, and so on.

This research has been fully supported by the Locomorph project, which is funded by the FET Proactive 'Embodied Intelligence' Initiative within the Information and Communication Technologies (ICT) Work Programme, under the Seventh Framework Program (FP7) of the European Union. I am extremely thankful for this support.

Last but not least, I would like to give an ultimate acknowledgment to my parents, my wife, my sister, and my whole family. I am here to finish my PhD because they made my life possible until this moment. They are the love of my life.

Abstract

One of the key features that enables animals and humans to perform agile, robust, adaptive yet efficient locomotion is their body's complex muscle-tendon-ligament system. Such systems provide body and limbs with the functionality that is used to efficiently absorb external shocks and exchange of mechanical energy, e.g. kinetic and potential energy, to exploit natural dynamics during locomotion. In biology, it has been found that animals and humans adjust their limb stiffness to accommodate for different speeds, gaits, and terrains. On contrary, in the field of legged robots, little has been known about how to control leg stiffness to efficiently adapt to changes of speed, terrain, and gait or stride frequency at which the leg oscillates. Therefore, this thesis aims at contributing to the primary understanding of the topic.

Until today, mechanical springs with fixed spring constants are still widely used as energy saving mechanisms and shock absorbers for legged robots. However, the compliance of those springs is not adjustable and manual assembly is required to make a robot leg stiffer or more compliant. Motivated by this fact, we present a systematic development and evaluation of a new variable compliance/stiffness actuator, named MESTRAN (MEchanism to vary Stiffness via Transmission ANgle) in this thesis. This actuator serves as a key tool to investigate energy efficient locomotion at various stride frequencies and on surfaces with different stiffness. MESTRAN can dynamically alter joint stiffness in an unlimited range. It is also capable of maintaining the stiffness without requiring energy and offering different types of compliance, e.g. linear, quadratic, or exponential.

In this thesis, we first designed and constructed an adjustable stiffness leg based on the MESTRAN design. We then validated the design by conducting a series of experiments by using the first leg prototype. Second, in order to investigate hopping locomotion with variable stiffness capability, we designed a single-legged robot, named L-MESTRAN (Linear-MESTRAN), which is an advanced version of the MESTRAN leg. We systematically analysed and demonstrated the mechanical performance of the legged robot using the simulations and a number of real-world hopping experiments. As a result, we found that a proper adjustment of leg stiffness can improve the hopping energy efficiency of the robot at various stride frequencies. Third, this finding was also investigated on surfaces with different stiffness by using the L-MESTRAN robot. The simulation and experimental results indicated that, for a particular stride frequency (3 - 6 [Hz]), the adjustment of the knee stiffness can accommodate for changes in surface compliance, resulting in an improvement of the energy efficiency of hopping.

The main message to take from this thesis is that the variable stiffness actuator is useful for legged robot locomotion because it allows optimizing the energy efficiency of hopping locomotion

under changes of speed, stride frequency, and surface stiffness.

Zusammenfassung

Eines der Hauptmerkmale, welches es Tieren und Menschen erlaubt sich agil, robust, anpassungsfähig und dennoch effizient fortzubewegen, ist das komplexe Muskel-Sehne-Band System ihrer Körper. Dieses System bietet Körper und Gliedern die Möglichkeit, Stösse zu absorbieren und mechanische Energie (z.B. kinetische und potentielle Energie) effizient umzuwandeln, um die Eigendynamik während der Fortbewegung auszunutzen. Die Biologie konnte zeigen, dass Tiere und Menschen die Steifigkeit ihrer Glieder anpassen um verschiedenen Geschwindigkeiten, Gangarten oder Untergründen Rechnung zu tragen. Im Gegensatz dazu wurde im Bereich der Laufroboter bislang wenig untersucht, wie die Steifigkeit der Glieder geregelt werden kann, um sich effizient an veränderte Geschwindigkeit, Untergrund oder Schrittfrequenz, mit der das Bein schwingt, anzupassen. Das Hauptziel dieser Arbeit ist es deshalb dem Verständnis der Beinsteifigkeit beizutragen, um die Energieeffizienz bei der Fortbewegung zu erhöhen.

Bis heute sind mechanische Federn mit konstanter Federrate weit verbreitet im Einsatz zur Energieeinsparung und als Stossdämpfer bei Laufrobotern. Die Elastizität dieser Federn ist jedoch nicht automatisch einstellbar und ein manueller Umbau ist notwendig, um ein Roboterbein steifer oder nachgiebiger zu machen. Motiviert von dieser Tatsache präsentieren wir in dieser Arbeit die systematische Entwicklung und Evaluierung eines neuen Antriebs mit variabler Steifigkeit/ Nachgiebigkeit genannt MESTRAN (MEchanism to vary Stiffness via Transmission ANgle). Dieser Antrieb dient als Schlüsselwerkzeug um die energieeffiziente Fortbewegung bei verschiedenen Schrittfrequenzen und auf unterschiedlich harten Oberflächen zu untersuchen. MESTRAN kann im Prinzip die Gelenksteifigkeit dynamisch in einem unbegrenzten Bereich anpassen. Er kann ausserdem die Steifigkeit ohne Energieverbrauch beibehalten und bietet verschiedene Arten der Nachgiebigkeit, beispielsweise linear, quadratisch oder exponentiell.

In dieser Arbeit haben wir erstens ein Bein mit anpassbarer Steifigkeit basierend auf dem Designkonzept von MESTRAN entworfen und konstruiert. Anschliessend haben wir das Design in einer Serie von Experimenten validiert. Zweitens, um den Einfluss variabler Steifigkeit beim Hüpfen zu untersuchen, haben wir einen einbeinigen Roboter namens L-MESTRAN (Linear-MESTRAN) entwickelt, welcher eine Verbesserung des MESTRAN Beines ist. Die mechanische Leistungsfähigkeit des Beinroboters haben wir in Simulation und etlichen Hüpfexperimenten systematisch analysiert und demonstriert. Diese Untersuchung ergab, dass eine geeignete Einstellung der Beinsteifigkeit die Energieeffizienz des Roboters beim Hüpfen mit verschiedenen Schrittfrequenzen verbessern kann. Diese Ergebnisse haben wir drittens auch mit Oberflächen unterschiedlicher Härte mit Hilfe des L-MESTRAN-Roboters untersucht. Die Resultate zeigen, dass bei einer Erhöhung der Härte

des Untergrunds die Steifigkeit des Beines reduziert werden muss, um die Energieeffizienz beim Hüpfen zu verbessern.

Die Kernaussage dieser Doktorarbeit ist, dass ein Antrieb mit variable Steifigkeit für Laufroboter von Vorteil ist, weil er es erlaubt die, Energieeffizienz bei Veränderungen von Geschwindigkeit, Schrittfrequenz und Oberflächenhärte zu optimieren.

Contents

List of Figures

List of Tables

Chapter 1

Introduction

1.1 Motivation

Human society encounters critical challenges of how we can improve the quality of life at work, at home or during leisure activities. Developing better robots is one way to tackle such challenges and potentially makes our daily lives easier and better. For example, thanks to advanced technologies of automatic machines, many menial tasks in factories are now performed by machinery. Those tasks that humans prefer to avoid are usually dangerous, heavy, tedious, or require highly precise and reliable operations (Khatib (1999); Khatib et al. (1999)). Robots are special types of machines that are capable of performing a variety of complex and repetitive tasks. In fact, there are many different types of robots, e.g. automatic systems that are used in car assembly automotive lines to pick and place parts and to weld the parts together; in manufacturing processes, machines that cut materials with high precision and reliability; robotic assistants that can support doctors in surgical operations; robotic English teachers that are used in interactive education, and so on.

Despite the diversity of existing robots, their capability to adapt to changes in their environments remains very limited. Operation of robots generally relies heavily on their prior knowledge about the world and themselves. They have the model of their work environment, the objects with which they interact, and a set of behavioral rules that precisely determine their states during task execution, and guide what actions to perform next. Robots will most likely fail when an unexpected event occurs.

Although robotic technology has been rapidly developing in the last few decades, it is still challenging for robots to work outside their full-modeled environments. Thus, their ability to support humans in daily life activities remains limited. In the future, robots should be able to offer more assistance to humans, more flexibility in task execution and more adaptability to new environments (Pfeifer et al. (2012)). In order to achieve these goals, scientists and engineers have invested a lot of effort in designing and manufacturing robots that offer locomotion capability, safe manipulation, and energy efficiency (Khatib et al. (1999), Albu-Schaffer et al. (2005), Khatib (1999)). Progressing along this direction, this thesis places a particular emphasis on locomotion capability and energy efficiency of legged robot research,

Locomotion capabilities (i.e. stability, versatility, robustness) and energy efficiency are indeed two important concerns in the field of legged robotic research. The reasons for this are as follows. Firstly, robots should be able to move stably. Secondly, in order to complete certain tasks in complex environments, robots need to be versatile and robust enough to deal with unexpected disturbances. Thirdly, for "field robots", i.e. robots that operate outdoors, energy efficiency is an inevitable factor for long operation as the next charging station may be far away. Thus, the ability to increase energy efficiency and locomotion capability are highly desirable in the future development of legged

robots.

Until now, locomotion performance of the state-of-the-art legged robots is still far inferior to that of biological systems, e.g. humans or animals. In nature, biological legged systems can efficiently traverse many different terrains at various speeds and with amazing agility. One of the challenges in developing robot systems that are comparable with animals or humans in terms of locomotion capability is to design novel actuators that are capable of achieving similar performance as biological actuation systems. Conventional actuators have major limitations in shock absorbance, energy storage, bandwidth, and efficiency when compared with biological muscles (Madden et al. (2004); Zupan et al. (2002)). Thus, in the field of robotic research, there has been an increasing interest to develop novel actuators that can overcome those limitations of existing actuators. The actuators that integrate variable stiffness actuators (VSAs) are commonly recognized as potential candidates that improve energy efficiency and locomotion capability of legged robots (Hurst (2008); Li et al. (2012); Vanderborght et al. (2012, 2011)).

In 2009, when we started the thesis project, we reviewed the state of the art of VSA development (Ham et al. (2009a)). Most of the proposed VSAs at that time required energy to maintain stiffness and such requirements resulted in large and heavy legs (Ham et al. (2009a); Hurst et al. (2004b); Migliore (2008); Schiavi et al. (2008)). The VSAs that could maintain the stiffness without requiring energy (Wolf and Hirzinger (2008) and Galloway (2013); Hollander et al. (2005)) offered only a narrow range of deflection and stiffness adjustment, which was not suited to locomotion tasks. These designs were typically targeted towards prosthetic and manipulation applications. Thus, we decided to develop a new VSA that was specially designed to address the limitations of existing VSAs and was therefore more suited for locomotion tasks.

1.2 Research approach

Legged locomotion in nature exhibits elegant and efficient capability when an individual jumps, walks, and runs over many different terrains. As such, biological systems offer a great source of inspiration and useful insights that can contribute to locomotion research. This has led to a new field of robotic research that is often referred to as "bio-inspired robotics" or "bio-mimetics" (Floreano and Mattiussi (2008); Pfeifer et al. (2007)). On the one hand, studying biological systems allows abstracting underlying principles that can help engineers to design better systems, or even to solve long-standing problems. On the other hand, the results from engineering approaches can contribute to a deeper understanding of biological systems. Progressing along the line between robotics and biology, many biological hypotheses and even concrete evidence about the influence of leg stiffness on locomotion have been taken into account as useful resources to study in this thesis.

So far, the research on leg stiffness has gained a lot of interest from roboticists, biologists, physicists, etc., and many studies based on human and animal running experiments and mathematical analyses have been reported. However, the question of whether there exists optimal mechanical stiffness required for running and walking is still under debate. There are several approaches to address this topic, for example, the theory-based and robotics-based approaches. The theoretical approach abstracts the leg into a very simplified configuration, usually as a concentrated mass and a massless spring like SLIP (Spring Loaded Inverted Pendulum). Despite its simplicity, the SLIP

has been widely accepted as a powerful model to capture running dynamics of humans and animals, e.g. trajectory of the center of mass, ground reaction forces (Blickhan (1989); Blickhan and Full (1993)). However, it is not yet clear how such a simple model can be employed to the design of a robot, which is obviously far more complicated than just a mass connecting to a spring. A complement to the SLIP approach is the synthetic approach, namely "Understanding by building"Iida (2006); Pfeifer and Bongard (2007); Pfeifer and Scheier (1999)) that we adopt in this thesis. There are three steps associated with this approach. The first step is to model aspects of biological systems, the second step is to abstract and explore general principles, and the third step is to apply those principles to design robots.

The goal of this thesis is to explore potential contributions of leg stiffness to the energy efficiency of legged locomotion. Guided by the "Understanding by building" approach, we first develop hopping models in which the leg stiffness could be varied during locomotion. This step provides a basic understanding of the system behaviours and guidelines for real-world experiments. To narrow down the modeling gap between the locomotion behaviours of the simulated and physical leg, we implement numerical simulations in which the model closely represents the physical leg. Based on the results of the simulations, we then design real robotic legs that are capable of varying stiffness variability. We conduct a number of real-world experiments and analyse experimental results in comparison to the simulation results. Finally, the underlying control and design principles of leg stiffness adjustment that influence the energy efficiency of locomotion is drawn.

1.3 Thesis contributions

This thesis provides three main contributions to the field of legged robots.

It provides analytical approaches to systematically analyse the performance of the existing VSA designs and presents guidelines for the future development of optimal VSAs. In order to implement the analysis on VSAs, a new classification that captures the key features of VSA and categorizes them into classes is presented. Five determinants are analytically formulated on the basis of seven VSA classes. This will give additional insights into intrinsic pros and cons of different classes of stiffness adjustment mechanisms that enable a systematic future development of variable stiffness actuators and their applications.

To address the limitation of existing VSA designs, we propose a novel design of a VSA, named MESTRAN. Although other mechanisms were designed to vary stiffness dynamically, we argue that the MESTRAN is more beneficial for locomotion than the others, in particular those that require energy to maintain the stiffness and offer a limited range of adjustable stiffness. In particular, MESTRAN has a large range of stiffness variability as, theoretically, the stiffness can range from zero to infinity. This mechanism requires no energy to maintain stiffness. Another feature of MESTRAN is that the stiffness can be decoupled from the external load. As a result of the decoupling, the actuator can function as a linear torsional spring with stiffness variability.

Throughout a number of numerical analysis and experiments, we demonstrate the underlying mechanism to improve energy efficiency of a legged hopping robot, which is equipped with a specific class of VSA (**C6**), and explain how behavioural diversity can be enhanced with modest impact on energy efficiency. Our result suggests that the energy efficiency of hopping locomotion is directly related to Eigen frequency of the system, which can be used as an effective indicator

of the adjustment of knee stiffness. We also show how the actuator, which results in variations of stride frequencies and locomotion speed while increasing energy efficiency, can vary the natural dynamics of a hopping robot. Extending further the exploration for the optimal knee stiffness on hard ground, we show that the adaptation of the knee stiffness to the stride frequency can increase the energy efficiency of the hopping legged robot on surfaces with different stiffness.

Apart from the materials presented in the main body of this thesis, we have contributed four papers to the community as a dissemination of the thesis project. In addition, two journal papers are under revision.

1. Hung Q. Vu, Yu Xiaoxiang, Fumiya Iida, and Rolf Pfeifer. "*Improving energy efficiency of hopping locomotion by using a variable stiffness actuator*" under revision of The IEEE/ASME Transactions on Mechatronics, 2014 in Jan. 2014

2. Amir Jafari, Hung Q. Vu, Fumiya Iida, "*Determinants of Variable Stiffness Mechanisms*," submitted to The International Journal of Robotics Research in Oct. 2013

3. Hung Q. Vu, L. Aryananda, F. I. Sheikh, F. Casanova, and R. Pfeifer, "*A novel mechanism for varying stiffness via changing transmission angle*," Robotics and Automation (ICRA), 2011 IEEE International Conference on 9-13 May 2011, pp. 5076-5081.

4. Hung Q.Vu, Helmut Hauser, and R. Pfeifer, "*A variable stiffness mechanism for improving energy efficiency of a planar single-legged hopping robot*," Advanced Robotics (ICAR), 2013 16th International Conference on 25-29 Nov. 2013, pp. 1-7.

5. Hung Q. Vu . "*Knee stiffness adjustment for energy efficient locomotion of a legged robot on surfaces with different stiffnes*" Robotics and Biomimetics (ROBIO), 2013 IEEE International Conference on 12-14 Dec. 2013, pp. 1825-1831.

6. Hung Vu Quy, Gilles Ramstein, Flurin Casanova, Lijin Aryananda, Matej Hoffmann, Farrukh Iqbal Sheikh and Helmut Hauser "*Gait Versatility Through Morphological Changes in a New Quadruped Robot*," International Symposium on Adaptive Motion of Animals and Machines, pp. 59-60, 2011.

This thesis has six chapters. In Chapter 2, the background of this thesis work is presented. First, we discuss why the study of legged locomotion is necessary given the fact that wheeled vehicles have been widely used in many applications. Then, the state of the art of legged robot development focusing on the energy efficiency is presented. The biological background is addressed in the following section to introduce basic mechanisms that underlying energy efficient locomotion in nature. We start introducing variable stiffness actuators in the next section. Some classifications of legged robots are also discussed. In the end of Chapter 2, we introduce some advancements in material science dedicated to develop a new generation of VSAs that do not use mechanical springs. Finally, some legged robots equipped with VSAs and the summary of the chapter are presented.

A part of this chapter was presented in a paper named "Determinants of Variable Stiffness Mechanisms" available in Appendix A.

To develop a basic tool for our exploration, in Chapter 3, we present the development of a new VSA, namely, MESTRAN. Since the content of this chapter has been published in an IEEE paper, which is available in Appendix B, we only summarize the main results.

Chapter 4 presents an investigation of leg stiffness adjustment using MESTRAN to improve energy efficiency of hopping locomotion in a single-legged robot. We also refer to the published and submitted papers for more detail, which is available in Appendix C and D.

In Chapter 5, we extend the work from Chapter 4 by varying the surface compliance. The materials of this chapter were presented in an published paper available in Appendix E.

In Chapter 6, we summarize our whole thesis, and discuss the overall outcomes of the research. Some future perspectives are presented.

Additionally, we provide the stability analysis of the simulated leg on surfaces with different stiffness and the Matlab model implemented to simulate the leg in hopping locomotion in Appendices F and H, respectively, for more details.

Chapter 2

Background and Related Work

In this chapter, we present the background that supports the development of this thesis. We begin by addressing the reasons to study legged locomotion given the fact that wheeled vehicles are widely used in many fields of transportation nowadays. Following that we present four studies in the state of the art of legged robots to discuss the energy efficiency issue. We then introduce the studies in biology and biomechanics about how legged animals and humans employ variable stiffness mechanisms to improve their locomotion efficiency while traversing many different types of terrains and performing various tasks.

In the following section, an introduction of VSAs including potential applications, classifications, smart-material based VSAs, and legged robots that utilise VSAs is presented. Lastly, we conclude the chapter. One part of this chapter focusing on a systematic review of the state of the art of VSAs was presented in the paper "'*Determinants of Variable Stiffness Mechanism*" submitted to ***The International Journal of Robotics Research*** (see the Appendix A).

2.1 Legged locomotion

There is an interesting fact that most of artificial transportation machines on land use wheels, whereas biological systems use legged mechanisms for travelling. In the following section, we will present the advantages of legged locomotion in comparison to wheeled locomotion. To continue, a review on the state of the art of legged robots focusing on locomotion energy efficiency will be introduced in the last part of this section.

2.1.1 Legged versus wheeled locomotion

Wheeled vehicles were developed during the early history of mankind and have been used for thousands of years. Nowadays they make an indispensable contribution to transportation in human society. In fact, in our daily lives, many wheeled vehicles that substantially support our living to achieve transportation demands surround us. In general, wheeled vehicles exhibit advanced features such as high speed, stability, ease of control and energy efficiency in comparison to legged ones. Thus, the question arises "under which circumstances legged vehicles could be advantageous?".

In fact, although the wheel is one of the greatest inventions of human civilization, true wheels have not been found in biological systems (Dawkins (1996)). While some animals use rolling mechanisms as a means for moving, these are not exactly the same as wheels that operate through one part of the body rotating relative to the rest around a fixed axis (Kruszelnicki (2008)). The main reason for the non-existence of wheeled mechanisms in nature is potentially their low locomotion efficiency on uneven terrains. Due to this limitation, only a small part of the Earth's surface is accessible by wheels, whereas a much larger part can be reached by legged animals (Raibert (1986a)),

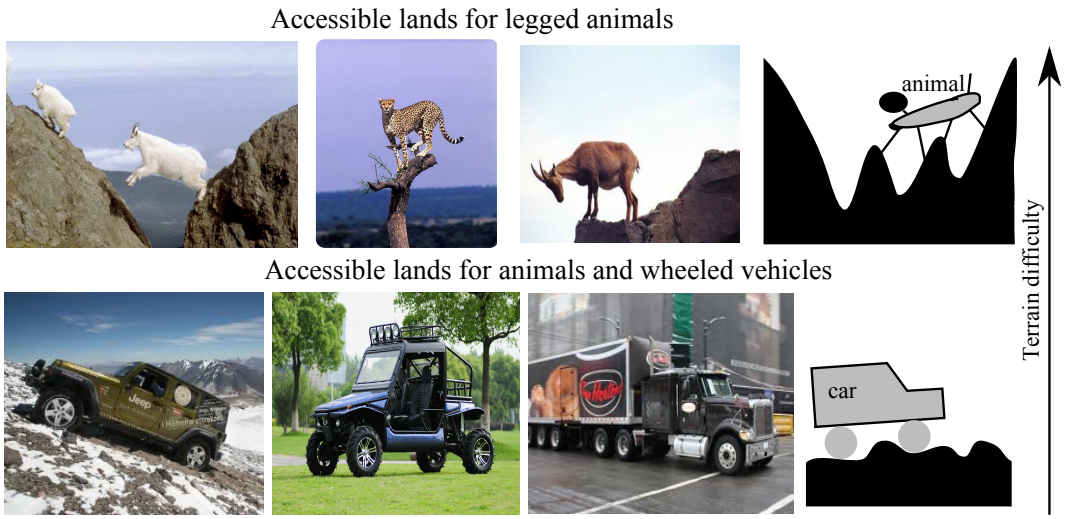

Figure 2.1: Accessibility for legged animals versus wheeled vehicles. Wheeled vehicles can only reach shallow slopes or flat terrains, whereas legged animals can traverse many different kinds of terrains.

as shown in Fig. 2.1. In general, legged mechanisms have three main advantages over wheeled mechanisms:

- **Foothold**

  In rough and unstructured terrains, legged animals have the capability to select foothold. This allows them to optimize their support posture and to increase traction force for stability and mobility. In contrast, the morphology of wheels requires a continuous contact between the wheels and the ground and this prevents them from travelling across different terrains. For example, wheels often get stuck in deep holes, slippery terrains, or are stopped by high obstacles as the wheel size is not sufficiently large.

- **Traction force**

  Traction forces refer to the maximum resistive forces between two contacting surfaces. Large traction force is desirable when vehicles/animals move on highly inclined or slippery terrains. In such situations, legged animals can achieve large traction force by putting their feet down into the ground, or actively anchoring their feet to terrain surfaces. This force can be much higher than the maximum friction force between two surfaces. For example, mountain goats can anchor their feet to rocks to increase traction, which enables them to traverse highly inclined terrains or cliffs. In contrast, wheeled vehicles cannot achieve a traction force that is higher than the friction force due to the circular shape of the wheel. Therefore, high-slope terrains are often not suitable for wheeled vehicles.

- **Load carrying capability**

  While travelling, wheels tend to be in continuous contact with the ground. Due to the constant radius of the wheels, the center of mass of the wheeled vehicles must follow the fluctua-

tion of the terrain's height, which results in vibrations of the carried load. In contrast, legged animals can "negotiate" with terrains to identify optimal footholds that allow them to maintain a more stable center of mass and posture, thus, the payload is carried more smoothly, regardless of the roughness of the ground. The abilities to retract and protract the leg of animals can also help them to maintain stable movements even when the optimal footholds cannot be chosen.

Due to the aforementioned advantages, subjects that move using legged mechanisms could have a wider range of terrain accessibility than those using wheels. However, there are in exchange fundamental challenges to overcome such as stability, robustness, energy efficiency, etc. In the past 50 years, a number of legged robots have been developed to study legged locomotion from many aspects. One of those aspects is how to improve the energy efficiency of locomotion. This is also one of the research goals of this thesis. In the next section, we briefly introduce the development of legged robots and their efficiency of locomotion.

2.1.2 Locomotion Energy Efficiency of the State of the Art Legged Robots

Before starting this section, we introduce a widely accepted measurement of energy efficiency, so-called Cost of Transport (CoT) originated from (Gabrielli and Von Karman (1950)). It is defined as

$$CoT = \frac{P}{M_s \times g \times v}, \tag{2.1}$$

where P denotes the power consumption of the subject to perform locomotion. M_s, g, and v denote the total mass of the subject, gravitational acceleration, and travelling speed. The low CoT implies high locomotion energy efficiency and vice versa. This indicator of energy efficiency will be used throughout the whole thesis

Since Marc Raibert developed the first series of dynamic legged robots in the 1980s (Raibert et al. (1984); Raibert and Brown (1984); Raibert et al. (1986); Raibert (1986b)), over 30 years, there have been a number of legged robots developed to study locomotion in many different aspects, e.g. stability, speed, versatility, energy efficiency, etc. One of the central concerns in the field of legged locomotion research is how to design a new class of mechanisms that can be equipped with robots and enable them to achieve high-energy efficiency without losing too much versatility, i.e. the ability to exhibit many locomotion behaviours. As the matter of fact, in the state of the art of legged robots, improving the energy efficiency of locomotion is still a long-standing problem in legged robots, especially for those required versatility to a large extent. Figure 2.2 shows a comprehensive comparison of energy efficiency across different robots, animals, humans, and other vehicles. Four state of the art legged robots which are marked by a circle in this figure will be analysed as followed.

- *The legged robots built by Boston Dynamics Inc (BDI).*: In the past ten years, BDI has introduced a number of impressive dynamic legged robots which have always pushed beyond the state of the art in the field of legged robots. In 2005, BDI presented the first version of the quadruped robot, called BigDog, as shown in Fig. 2.4A. The robot exhibited an astonishing performance

in a way that it could walk, trot on very rough terrains, inclined slopes, slippery ice, etc. However, in terms of locomotion energy efficiency, this robot achieving CoT of 6.3 is known to be much higher than those estimated from many other robots (Kuo (2007); Reis and Iida (2013)). There have been a number of iterations after the first Bigdog and the most recent legged robots made by BDI is LS3 as shown in Fig. 2.4C. LS3 is a dynamic robot that can manoeuvre in difficult terrains and carry up to 180kg of load with a need of refuel after 32km of travelling (BostonDynamics (2013)).

Although the series of legged robots developed by the Boston Dynamics (Fig. 2.4A-C) undoubtedly outperform the existing legged robots in terms of speed, robustness, load carrying capability, their locomotion energy efficiency is still questionable. As shown in Fig. 2.4, the CoT of BigDog is significantly higher than that of many other robots and biological systems.

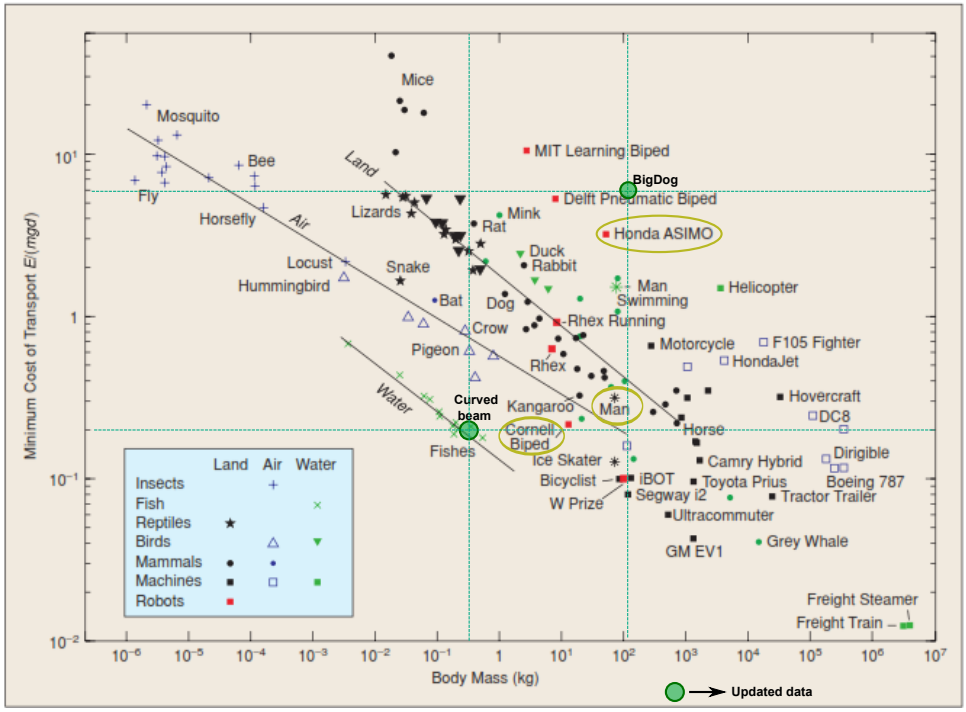

Figure 2.2: An estimation of CoT versus locomotion speed for different robots and animals adapted from (Kuo (2007)). Several robots are represented in this graph, including Honda ASIMO (Sakagami et al. (2002)), Curved Beam (Reis et al. (2013)) , Cornell Biped (Collins and Ruina (2005)), and BigDog (Raibert et al. (2008)).

- *The ASIMO robot built by Honda Inc.*: At the end of the second millennium, Honda Inc. presented the most human resembling robot called ASIMO. Its name stands for Advanced Step in Innovative Mobility. The robot kinematics consists of 26 degrees of freedom (two on the neck, six on each arm, and six on each leg). This robot is capable of a large variety of locomo-

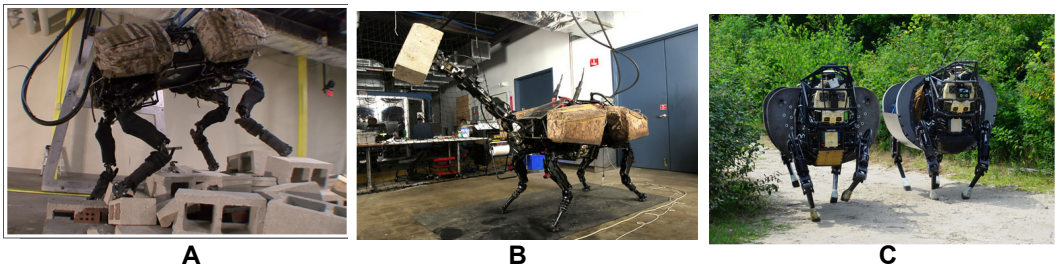

Figure 2.3: A series of quadruped robots developed by Boston Dynamics Inc., since 2005. A) First version of the BigDogs released in 2005, B) The most recently updated Bigdog, C) The LS3 robot.

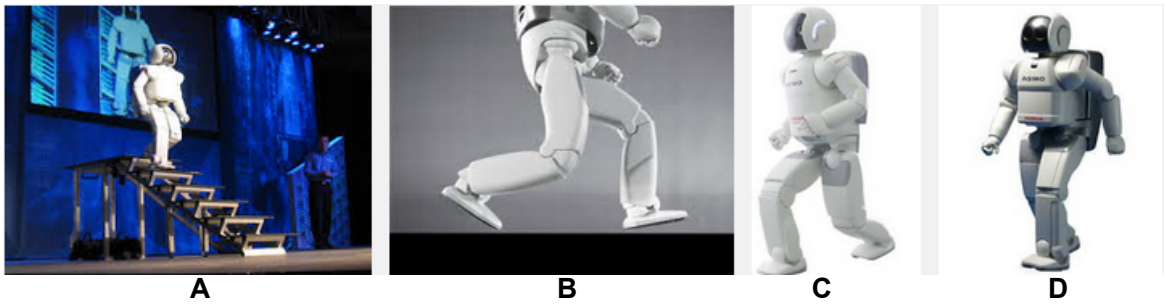

Figure 2.4: The ASIMO robots in several locomotion patterns (A-D)

tion behaviours including walking, running, and climbing up stairs, etc. as well as cognitive tasks such as recognizing faces and voices. However, as a walking robot, it is far from energy efficient. Based on the robot mass and its energy consumption per unit distance, the CoT of this robot is approximately 3.2, which is about 30 times higher than that of humans in walking (i.e. about 0.3) as shown in (Fig. 2.2). One of the fundamental differences between ASIMO and humans is the use of physical compliance in walking. Whereas the ASIMO structure does not employ any mechanical springs for energy storage and shock absorbance, the human musculo-skeleton efficiently makes use of biological springs, i.e. tendons and muscles. They exploit their passive dynamics in such a way that the energy for walking can be recycled from the potential energy storage in the elastic tendons. (Alexander (1990); Kuo (2007)). Thus, humans can walk with very low energy consumption compared to all existing robots. In contradiction, the walking behaviour of ASIMO is implemented by means of the Zero-moment point algorithm (Sakagami et al. (2002); Sardain and Bessonnet (2004)), which requires precise modelling of the robot and the environment it interacts with. As consequence, it demands expensive computational efforts, high-gain control over all joint angles during execution of locomotion tasks, and, therefore, largely eliminates the effect of passive dynamics. In addition, due to the absence of physical elasticity in actuation, no energy is potentially stored during stance phase of the foot.

- *The curved-beam robot built by BIRL at ETH Zurich*: Mainly targeting energy efficiency, this robot was designed to make use of free vibration of elastic curved beam during hopping

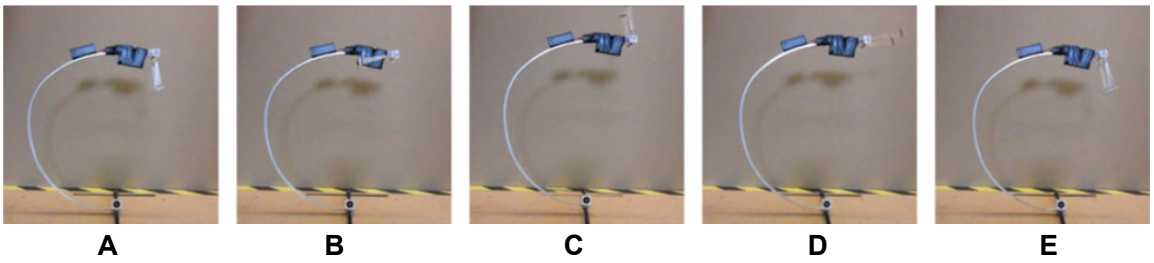

Figure 2.5: Time-lasped figures of the hopping motion during a hopping cycle from A to E.

locomotion (Reis and Iida (2013)). The robot leg is essentially an elastic curved beam with a specific shape. A small mass rotating/vibrating at the top of the robot body induces free vibration of the entire robot structure, as shown in Fig. 2.5. The weight of the vibrating mass is indeed negligible when compared to the robot body weight (0.015/0.5 [kg]). Unlike the conventional actuation principle employed by many other robots in which most of the energy driving locomotion is generated by the actuation sources, i.e. on-board batteries or external power supply, the actuation approach implemented in this curved beam hopper is only to trigger the natural vibration of the elastic beam in a way that the elastic strained energy of the beam can be recycled for locomotion. The electrical power source in this case mainly compensates for friction losses in the robot structure and energy losses by the impact between the foot and the ground. Moreover, the minimalistic control that is to keep the mass continuously rotated in one direction around the motor shaft requires very little energy for actuation. As a result, the CoT measurement on this robot in hopping is impressively low, about 0.2, which is comparable to that of human walking.

However, humans do not just walk at one speed or on one type of ground. They are very adaptive to changes of those. The performance of the curved-beam hopper is clearly limited in this aspect. The design of this type of robot is highly non-trivial and the mechanical structure has to be carefully optimized for specific locomotion behaviours and the environment with which it interacts.

- *Passive Dynamic Walkers (PDWs)*: There are basically two main approaches to control walking (Clark (2008)). First, as intuitively guided, the traditional approach is to control the joint-angles of all joints at the whole time. A typical example is the control of ASIMO as mentioned previously. This approach requires complicated walking controllers and is computationally expensive. Eventually, it results in low energy efficiency of walking gaits. Second, the alternative is so-called passive-dynamics, which was proposed by Tad McGeer (McGeer (1990)) in the 1990s, that mainly exploits the robot's mechanical dynamics for walking instead of drawing the energy from supply, e.g. batteries. In principle, the energy to power this type of robots is purely derived from gravity-induced forces, thus, the robot could walk down a shallow slope without any actuators. Plus a well designed mechanical body for a given specific slope, such robots could potentially achieve stable and energy-free walking performance. This method was successfully demonstrated by several teams, i.e. A. Ruina (Collins and Ru-

Figure 2.6: A series of Passive Dynamic Walkers developed by Mc Geer et. al (A), Ruina et al. (B), Wisse et al., (C), and Collins et al., (D).

ina (2005)), S.H. Collins (Collins et al. (2001)), M. Wisse (Wisse (2005)) as shown in Fig. 2.6. After the first generation of PDWs that did not employ any motors, the critical limitations (i.e. robots can only walk on downward slope) were eliminated by introducing small actuators that only supplied the necessary energy to compensate for gravity and the energy losses from ground impacts such that the robot could walk on flat terrains or normal office floors. For the moment, the Cornell Ranger developed by the team of Andy Ruina is the world record holder for distance walking about 65 kilometres with only one battery charge. This types of robot typically represents for ones that are mainly optimized for energy efficiency of locomotion.

Similar to the curved-beam hopper, the passive-dynamic walkers also encounter limitations of what they can do beyond passive walking. The walking behaviours of such robots are highly sensitive to any changes of the walking environments and they can only walk with a naturally defined gait. As such, their robustness and versatility are very poor.

So far, we have presented some state-of-the art legged robots, i.e. the BDI robots, the ASIMO robot, the curved-beam based robots, the PDWs robots, which are representatives of two groups of robots employing two different approaches to solve locomotion problems. On the one hand, the first group (i.e. ASIMO and BigDog) strongly relies on the joint-angle control approach, which requires large amount of energy supply and complicated control. On the other hand, the second group (e.g. PDWs, curved-beam) implements the passivity based control approach to exploit the mechanical dynamics of robots during locomotion. As the result, while the first group of robots could offer a much larger set of locomotion behaviours, the versatility is very poor for the robots in the second group. Solving the trade-off between energy efficiency and locomotion versatility is therefore challenging (Kuo (2007)) in legged robot research.

In contradiction, biological systems for example humans and animals can balance this trade-off very well. Animals and humans exhibit an amazing capability to move across various rough terrains while keeping energy consumption impressively low compared to that of legged robots

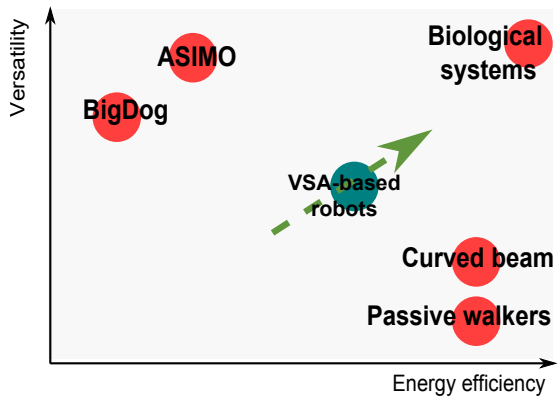

Figure 2.7: The energy efficiency versus locomotion versatility of the robots and biological systems.

(Alexander (2003); Collins and Ruina (2005)). The relationship between energy efficiency and versatility of locomotion can be graphically represented as shown in Fig. 2.7, where biological systems appear as "top performers" surpassing all robots in both aspects. One of the reasons could potentially be taken into consideration is that humans and animals are able to adjust their inherent mechanical dynamics via changing body/limb' stiffness to adapt to changes of locomotion dynamics and environment's conditions, e.g. the ground property changes from soft to hard. VSAs belong to a new class of actuation systems that could be equipped with the legged robots and vary their mechanical stiffness during locomotion to actively exploit potential energy returning from elastic elements on robots. We expect our robot built on the basis of a new VSA presented later in this thesis can achieve energetically efficient locomotion while still being robust and versatile.

In the next section, we will present the biological background focusing on underlying mechanisms of biological systems to improve their energy efficiency and locomotion versatility.

2.2 Energy Efficient Legged Locomotion in Nature

Since most animals have to move to find food, mates, avoid predators, hunt prey, etc., locomotion is one of the most important ecological functions of animals (Irschick and Garland (2001)). Locomotion cannot occur without energy supply. Thus, given a certain amount of energy, the more economically it is used, the longer the period of time over which an animal can perform locomotion (Meek et al. (2009); Schmidt et al. (2007)).

In biological studies, energy economy has been discovered as a central principle that drives locomotion behaviours, e.g. speed, gaits (Alexander (2003); Hoyt and Taylor (1981); Minetti et al. (1995); Umberger (2008)). Note that in some cases when animals need to avoid predators, catch prey, or jump over deep holes/high obstacles, the priority is not energy economy but high acceleration and manoeuvrability. In the scope of this thesis, we are only concerned with the energy economy in steady-state locomotion. We will focus on the mechanisms that have been found beneficial for improving locomotion energy efficiency as follows.

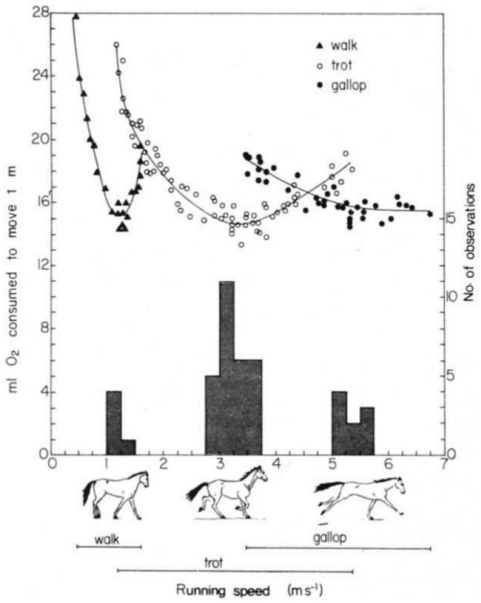

Figure 2.8: Oxygen consumption measurements taken during experiments in which horses ran on a treadmill. Horses were trained to move with intended gaits while the speed of the treadmill was varied. (Hoyt and Taylor (1981))

2.2.1 Gait transition

Gait is the pattern of the movement of the limbs of animals during locomotion. Depending on the state of locomotion or the kind of animals, different gait patterns may be selected. It has been found that given a specific locomotion speed, animals prefer a specific gait in order to minimize metabolic cost. Hoyt and Taylor investigated the oxygen consumption of horses during three different locomotion gait patterns as walking, trotting, and galloping (Hoyt and Taylor (1981)). The horses were trained to run on a treadmill at a certain speed. The experimental results showed that there was a distinct range of speed suited to a particular locomotion pattern in terms of oxygen consumption. For example, the minimum oxygen consumption for walking, trotting, and galloping achieved at 1.2 m/s, 3.2 m/s, and 6 m/s, respectively. Furthermore, the speeds at which the horses changed from walking to trotting, and trotting to galloping are about 1.8 m/s, and 4.5 m/s, respectively. Fig. 2.8 demonstrates strong relationships between speeds and preferred gait patterns. Similar relationships were also found in human locomotion. The preferable speed for humans to walk was found to be 1.5 m/s, whereas the speed at which the humans voluntarily change from walking to running was about 2 m/s (McNeill (2002)). It is commonly agreed that the gait transition can improve energetic efficiency Cavagna et al. (1977); Heglund and Taylor (1988), however, the other way is unlikely true. The level of energy consumption is not necessarily a trigger to the gait transition (Raynor et al. (2002)).

2.2.2 Body weight

By collecting mass and mass-specific energy per unit distance across a large set of animals ranging from small ones like insects to mammals, Taylor and his colleagues discovered an approximated linear relationship between the body weight and the metabolic cost of transport. Larger animals with large body weigh exhibit higher energy efficiency in locomotion compared to the small ones. For example, in general, lions and dogs achieve three times higher energy efficiency during locomotion than penguins or turkeys (Heglund et al. (1982); Heglund and Taylor (1988)). One of the explanations for this increase is that the energy cost on an unit body weight per one stride at different speeds is about the same for all animals, which is independent of body size. Due to the fact that smaller animals need to take more number of strides than larger animals to cover the same distance, the metabolic CoT will be higher for small animals. Furthermore, large animals are supposed to be more advantegous in exploiting the energy storage in their spring-like muscle-tendon systems during locomotion in comparison to the small animals (Taylor et al. (1982)).

2.2.3 Leg stiffness

The muscle-tendon in animals legged systems have been identified as energy saving mechanisms since they are capable of storing kinetic energy as potential energy and release it when necessary (Alexander (1990)). This mechanism allows the locomotion energy to be partially recycled from one cycle to the next, which potentially results in increased energy efficiency. Such capacity of storing energy characterizes by the leg elasticity/stiffness, which is defined as the resistance of the leg to external loads.

Many findings have revealed the spring-like bouncing motion of the leg systems with muscle-tendons systems in running animals. For example, as the finding of Roberts et al. (1997) indicated, in stance, the length of the gastrocnemius muscle fascicle (contractile muscle) on turkey's legs does not significantly change when compared to its change during flight. As measurement data indicated compliant tendons can store, return elastic energy, and vary their elastic responsive behavior, allowing the contractile components to act nearly isometrically, regardless of substantial length changes in the muscle–tendon unit. In another example, Biewener (1998) have found that when the horses changed gait from a walk to a slow trot, a maximum 40% recovery of mechanical work was provided by energy saving of the elastic tendons. This recovery percentage then decreased with the increased speed in trotting, but increased again to 36% when the horses switched to galloping. This significant amount revealed the contribution of the energy saving mechanism by the tendon elasticity. Many other studies that examined the influences of leg stiffness on energy efficiency can be found in these works (Alexander (2003); Ishikawa et al. (2005); Kuitunen et al. (2002)). It is therefore widely accepted that tendon elasticity at legs in biological systems plays a very important role to achieve high locomotion energy efficiency.

2.2.4 Coupling between the stride frequency and the leg stiffness

Despite the body's complex system of muscle and tendon systems, the mechanics of human walking and running has been captured successfully by a simple linear spring model, i.e. SLIP (Spring Loaded Inverted Pendulum) (Blickhan (1989)). When applying this model to analyze human run-

ning data, biologists have found that, when the leg stride frequency increases, both the leg stiffness, which is defined along the leg axis, and vertical stiffness, which is defined by the ratio of the center of mass displacement and the leg force in the vertical direction, increased (Farley and Gonzalez (1996)). Moreover, the relationship between the leg stiffness and the stride frequency in human running was rather linear. Such leg stiffness adjustments of humans during forward running are similar to those found in in-place hopping (Farley et al. (1991)). Zurrugh et al., found that when walking at a given speed, humans tend to choose a certain stepping frequency, which results in a minimum metabolic cost (McNeill (2002); Zarrugh and Radcliffe (1978)).

Animals are able to regulate their locomotion behaviours in different hierarchical levels from the high-level control as gait transition, speed variation to the lower level as reflexes-based control characterized by leg elasticity. Aiming at developing a controllable stiffness leg for an efficiently energetic and versatile robotic leg, in this thesis, we focus on VSA designs, implementation, and control in locomotion, inspired by stiffness variability of biological systems. Thus, in the next section, we introduce the background of VSA development.

2.3 Variable stiffness actuators

Industrial robots with stiff actuators that weld and assemble cars, categorize products, support automatic manufacturing, etc., have largely occupied factory automation environments for decades. These precise and stiff robots, although useful and impressive, are severely limited and even dangerous, when taken outside their fully modelled and controlled environments. Daily usage in human environments is extremely difficult for such robots due to the lacks of safety, adaptability and energy efficiency (Khatib (1999)).

Nowadays, an increasing effort has been giving to the development of robots that are capable of working in human environments and assisting humans to perform their daily activities. In the attempts to achieve these goals, roboticists face fundamental challenges. One of those is that robots have to work safely yet efficiently as companions of humans (Pfeifer et al. (2012)). These two requirements seem to contradict each other since the safety criterion usually limits the maximum speed and thus results in the inefficiency of operations. Another challenge is that autonomous robots, especially legged robots, should be able to adapt to changes in their outdoor environments, which are complex, unstructured, and most likely unknown without reducing energy efficiency (Hurst et al. (2005)).

Recently, VSAs have been considered as potential solutions to these issues. The actuators that have the ability to regulate stiffness of a system can be used to exploit the natural dynamics of that system, provide safe interaction between humans and robots, increase robustness to external disturbances, and allow for mechanical energy exchanges during locomotion. Many potential applications of VSAs are presented in the following section.

2.3.1 Variable stiffness actuator applications

Rehabilitation robotics devices are connected continuously to the human body in order to assist humans during rehabilitation therapy as shown in Fig. 2.9A for example. In design principle, such devices should provide a friendly mechanical interface to humans in use and, thus, support their disability in completing motion tasks. This is a basic requirement to design rehabilitation

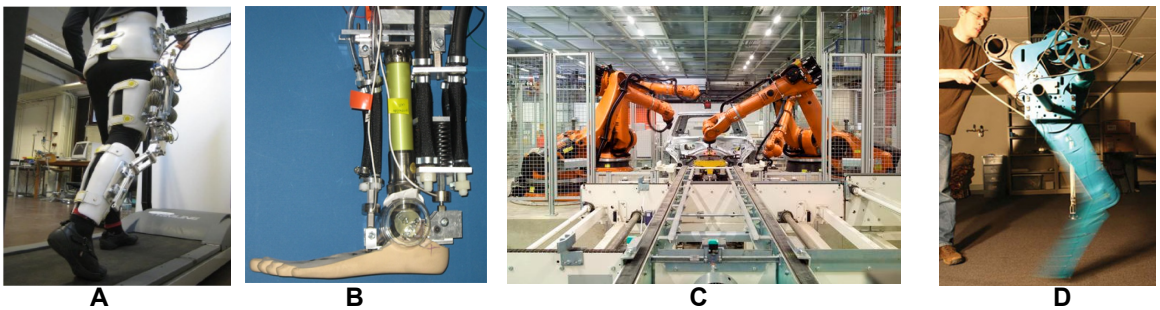

Figure 2.9: Potential application domains of variable stiffness actuators. (1): Rehabilitation robotics; (2): Prosthetic devices; (3) Industrial robot arms; (4) Legged locomotion

mechanisms that aims at safe human-machine interaction, agility in task execution, also energy efficiency, other mechanical behaviours indicated in (Beyl et al. (2011), Everarts et al. (2012)), similar to those of the muscular-tendon skeletal systems in the human body. Thus, VSAs could potentially be appropriate choices to design the devices.

Robotic prosthetic devices are used to help amputee people to restore some of their functionality in cases of limb loss as shown in Fig. 2.9B. Many tasks that humans perform on a daily basis require the variation of the limb's compliance, for energy efficiency, shock absorption, gait transition, variable speed locomotion (Hollander et al. (2005)). Therefore, the replacement of limbs by prosthetic devices should be able to replicate and produce the compliance variability of human limbs. As such, VSAs are potential solutions in designing prosthetic devices.

Industrial robots are developed for well-defined factory jobs, as shown in Fig. 2.9C. In general, they are precise, stiff, and powerful. Since most of them use off-board power supplies and work at isolated sites, energy efficiency and safety are often not critical consideration. However, the robots that work alongside humans in the factory have to be able to safely interact with workers while maintaining the speed needed for work efficiency. Thus, a control algorithm featuring the VSA has been proposed, which finds the minimum time to move between two defined configurations of the manipulator while guaranteeing a desired safety level of unexpected impacts at any given time (Bicchi and Tonietti (2004)). Other researchers have shown that the co-optimization of trajectory and stiffness can reduce energy consumption during throwing tasks (Kim and Song (2010b); Nakanishi and Vijayakumar (2012); Wolf and Hirzinger (2008)).

Legged locomotion robots, as shown in Fig. 2.9D, are usually aimed for energy efficient yet versatile and robust locomotion. As found in biology and biomechanics that legged animals and humans do change their stiffness for energy efficient locomotion (Alexander (2003); Biewener (1998); Roberts et al. (1997)), the field of studying VSAs for legged locomotion is growing rapidly in the recent years. For example, the variable stiffness leg employed in the Rhex robot was used to tune the leg's natural frequency to increase energy efficiency and speed (Galloway (2013)). In another example, it has been demonstrated that a proper adjustment of the knee stiffness using the MACCEPA actuator VSA during hopping can result in a higher hopping height compared to that achieved by using a stiff actuator (Vanderborght et al. (2011)). Hurst et al. investigated the influences of leg stiffness on the energy efficiency of the MABEL robot in in-place hopping experiments (Hurst (2011)).

He found that optimal stiffness maximizes the spring restitution of the robot, thus, it allowed for efficiently exploiting the energy storage in the springs.

Due to these potential applications of VSAs, there have been a number of VSAs developed in the past 20 years. We will provide a comprehensive review of VSAs in the next section.

2.3.2 Stiffness Adjustment Approaches

There is a large variety of VSAs in the literature. The mechanical designs of VSAs are very heterogeneous and can be implemented with different types of motors, speed-reducers and force/-torque transmission systems. Such components should be combined in a proper way to match encumbrances, weight, force, power and stiffness requirements. Therefore, their performances can be highly variable and hardly comparable. In order to systematically analyze their performance, a classification of different stiffness adjustment approaches is required. Some classifications have been already presented by (Ham et al. (2009b); Tagliamonte et al. (2012); Vanderborght et al. (2013)). However, since in this paper, the focus is on the stiffness adjustment mechanisms of VSAs, the classification presented here, is based on the arrangements of the essential elements within these mechanisms. A typical stiffness adjustment mechanism consists of two actuation units, e.g. motors, compliant elements, e.g. springs and the output link, which is in contact with the external environment. Such a classification is presented in Tab. 2.1. In general, there are two main approaches to regulate the stiffness, namely, antagonistic and series.

2.3.2.1 Antagonistic approach

Antagonistic approach is motivated by the arrangement of muscles such as biceps and triceps in the human arm (Hogan (1984)). When the biceps contracts and the triceps relaxes, the arm is flexed. When the triceps contracts and the biceps relaxes, the arm extends. However, when both biceps and triceps contract, the elbow becomes stiff and when they both relax, the elbow becomes very compliant and the arm hangs freely. In fact, the muscles in the human arm are controlled in a continuous way and, thus, the system can cover a range of positions and compliant behaviours. Inspired from the human musculoskeletal systems, in the antagonistic approach, two actuation units are antagonistically actuating an output link via elastic elements, e.g. springs. Springs which have nonlinear force-deflection profiles (nonlinear springs), are placed between the actuation units and the output link. Based on different arrangements of the actuation units and springs, this approach has been realized in three different classes: simple unidirectional (C1), cross-coupled (C2) and bidirectional mechanisms (C3).

- **C1**: Simple Antagonistic

  In the simplest class of antagonistic approaches, as it is shown in Tab. 2.1, each actuation unit is connected to the output link through a nonlinear unidirectional spring. Unidirectional springs can apply force in only one direction (either push or pull the output link). Therefore, only one actuation unit at each time can apply force to move the output link. Examples of this class are: Biologically inspired joint stiffness control (Migliore et al. (2005)), Actuator with Mechanically Adjustable Series Compliance (AMASC) (Hurst et al. (2010)), and Plated Pneumatic Artificial Muscles (PPAM) (Darden (1999)).

Table 2.1: Classification of different VSA classes. The VSAs in classes: C1, C2, C3, C4 change the stiffness by changing the pretension of nonlinear springs. Instead, the stiffness of VSAs in classes: C5, C6, and C7 is changed through (a) the load-spring transmission via altering the lever arm ratio in class C5, (b) the load-spring transmission via altering the transmission angle in class C6, and (c) changing the effective physical properties of compliant beams in class C7.

Approaches	Classes	Examples	Schemes
Antagonistic	**C1**: Simple antagonistic	Biologically inspired joint stiffness control (Migliore et al. (2005)) Actuator with Mechanically Adjustable Series Compliance (AMASC) (?) Plated Pneumatic Artificial Muscles (PPAM) (Darden (1999))	
	C2: Cross coupled	Variable Stiffness Actuator (VSA) (Tonietti et al. (2005))	
	C3: Bidirectional	Variable Stiffness Actuator-II (VSA-II) (Schiavi et al. (2008)) , VSA-CUBE (Catalano et al. (2011)), Bidirectional Antagonism with Variable Stiffness (BAVS) (Petit et al. (2010)) ,	
Series	**C4**: Pretension of nonlinear spring	Mechanically Adjustable and Controllable Compliance Equilibrium Position Actuator (MACCEPA) (Ham et al. (2006)) and (MACCEPA 2.0) (Vanderborght et al. (2011)), Variable Stiffness Joint (VS-joint) (Wolf and Hirzinger (2008)), Safe Joint Mechanism (SJM 1) (Park et al. (2009)) and (SJM II) (Park and Song (2010)), Floating Spring Joint (FSJ)(Wolf et al. (2011))	
	C5: Changing load-spring transmission ratio via lever arm ratio	Actuator with Adjustable Stiffness (AwAS-I) (Jafari et al. (2010)) and (AwAS-II) (Jafari et al. (2012)) Compact Variable Stiffness Actuator (ComPact-VSA) (Tsagarakis et al. (2011)) Energy Efficient Variable Stiffness Actuator (Visser et al. (2011)) Variable Stiffness Actuator University of Twente (Fumagalli et al. (2012); Groothuis et al. (2012)) Hybrid Dual Actuation Unit (HDAU) (Kim and Song (2010b),Kim and Song (2012))	
	C6: Changing load-spring transmission ratio via transmission angle	Mechanism for Varying Stiffness via Transmission Angle (Vu et al. (2011)), Floating Spring Joint (FSJ)(Wolf et al. (2011)), Human-friendly VSA (Hyun et al. (2010)),VSA-HD (Catalano et al. (2010)), DLR Q-A joint (Eiberger et al. (2010)).	
	C7: Changing effective physical properties	Structure Controlled Stiffness (SCS) (Hollander and Sugar (2004)), Jackspring (Hollander et al. (2005)), Changing beam length (Choi et al. (2011)); Morita and Sugano (1997)), Adjustable stiffness spring (Rodriguez et al. (2011))	

- **C2**: Cross coupled

  In this class, one additional nonlinear spring is placed between the two actuation units. The additional springs permits the full steering of the link by each actuator. Thanks to that, the maximum generated force per actuation unit can be set to the half of maximum force of the similar unidirectional mechanism to obtain an equivalent maximum force at the output link. The Variable Stiffness Actuator (VSA) (Tonietti et al. (2005)) is an example of this class.

- **C3**: Bidirectional

  In this class, each actuation unit is connected to the output link through a pair of nonlinear springs. Each pair consists of two nonlinear springs in opposite force direction. Therefore, each actuation unit is able to push and pull the output link due to the bidirectional arrangement of corresponding nonlinear springs. This solution again allows transmitting the maximum generated force of each actuation unit to the output link. Examples of this class are: Variable Stiffness Actuator-II (VSA-II) (Schiavi et al. 2008), VSA-CUBE (Castalano et al. 2011), Bidirectional Antagonism with Variable Stiffness (BAVS) (Petit et al. (2010)).

2.3.2.2 Series approach

In the other design approach, one actuation unit with springs in series is employed to control link position and other unit changes its stiffness, independently. Since in this approach, only the first actuation unit controls the desired position of the output link, thus, it is called series design approach. Typically, the second actuation unit is not employed to control the position, but the stiffness of the output link. As a contrast, the VSAs in antagonistic approaches employ the parallel actuation scheme in which the output position of the link is algebraically summed up by the displacement of two actuation units.

Based on the principles to change stiffness, VSAs that employs the series approach are categorized into four classes as follows. In the first series class, the spring's deflection is altered to tune the stiffness (C4). In addition to that, other series designs have also been implemented where the stiffness is regulated through changing either the lever arm ratio (C5), or the load-spring transmission ratio via transmission angle (C6) or the physical structural stiffness of elastic structure (C7).

- **C4**: Changing pretension of nonlinear spring

  In this class of series design approach, the first actuation unit is connected to the output link via springs to control the link position, whereas the second one regulates the pretension of such spring as shown in Tab. 1. Since the spring is nonlinear, the spring stiffness can be altered by changing the deflection. Some examples of this class are: Mechanically Adjustable and Controllable Compliance Equilibrium Position Actuator (MACCEPA) (Ham et al. (2006)), (MACCEPA 2.0) (Vanderborght et al. (2011)), Varaible Stiffness Joint (VS-joint) (Wolf and Hirzinger (2008)), Safe Joint Mechanism (SJM I) (Park et al. (2008)) and (SJM II) (Park and Song (2010)). It should be mentioned here that, these examples employ linear springs. However, the stiffness adjustment mechanisms in this class can provide nonlinear force-deflection profiles as the springs are deflected. Therefore, these springs are considered nonlinear springs.

- **C5**: Changing load-spring transmission ratio via lever arm ratio

  The VSAs in this class changes the transmission ratio between input force and the spring deflection through variation of a lever mechanism. In the mechanism design, a lever has three principal points: the pivot, i.e. the point around which the lever can rotate; the spring attachment point, i.e. the point at which springs are located; the force point, i.e. the point at which the force is applied to the lever. By changing the position of one of the three, the lever stiffness can be varied. As conceptually depicted in Tab. 2.1, the stiffness regulation in this class can be done without directly deflecting the springs. Some newly developed VSAs in this class are: Actuator with Adjustable Stiffness (AwAS-I) (Jafari et al. (2010)), (AwAS-II) (Jafari et al. (2012)), Compact Variable Stiffness Actuator (ComPact-VSA) (Tsagarakis et al. (2011)), Energy Efficient Variable Stiffness Actuator (Visser et al. (2011)) and Variable Stiffness Actuator University of Twente (Carloni et al. (2012)).

- **C6**: Changing load-spring transmission ratio via transmission angle

  Similar to class C5, the force transmission between the output link and the spring is also altered for different stiffnesses in this class. However, instead of regulating principal points of the lever arm, this class regulates the transmission angle between the direction of force applied to the spring and the spring neutral axis. Note that the spring is only deflected in specific direction under load, e.g. the direction that is parallel to spring neutral axis for linear springs. Thus, the force transmission ratio can be altered to any degree by varying the such angle. This design principle also allows for using linear springs. Some examples of VSAs belonging to this class are as follows. The Mechanism for Varying Stiffness via Changing Transmission Angle (MESTRAN) (Vu et al. (2011)), which regulates the stiffness by changing transmission angle between the output force and the deflection of the output link. The other example of this class is the FSJ actuator (Wolf et al. (2011)), which changes the stiffness of the output link by varying the pressure angle between the normal of the cam surface and the spring axis as a lower stiffness can be achieved when the pressure angle is reduced. Exploiting the transmission angle by different link configuration, VSA-HD (Catalano et al. (2010)) can also vary the stiffness in a relatively large range. Infinite stiffness can be achieved when two transmission links are straight-up. A simpler solution employing this approach can be obtained from (Hyun et al. (2010)), in which only two levels of stiffness are achieved by two separated fixed cam surfaces.

- **C7**: Changing effective physical properties

  Unlike the other VSA classes, in this class, the stiffness of the output link can be modulated by varying the effective physical structure of the structural elements. For example, the beam stiffness can be changed by varying the effective length, the sectional area, and elastic modulus of beam material. As it is presented in (Choi et al. (2011); Hollander et al. (2005); Morita and Sugano (1997); Rodriguez et al. (2011)), changing the length of the beam can provide a continuous range of stiffness modulation as long as the length can be changed in a continuous manner. The second approach is to vary the cross sectional areas W, that, basically, varies the anti-bending/twisting moment of the structure as shown by (Hollander and Sugar (2004)).

In this work, there however exist only two stiffness levels that are the low and high stiffness, corresponding to the two ways of orienting the elastic beam. In the practical implementation, it is impossible to change the stiffness while the link is under load. The third approach can potentially be implemented is to change the material modulus E. This approach is often implemented by employing some smart materials, e.g. Shape Memory Alloys and Dielectric Elastomer Polymers (Anderson et al. (2013); Carpi et al. (2008)). In the next section, we will review the potential materials that can be used for a new generation of VSAs. Currently, change of the stiffness in those materials is not sufficiently fast and requires impactical conditions, e.g. high voltage, critical heat treatment, to stimulate stiffness changes. As a result, no existing VSAs employ those materials to change stiffness yet.

Based on this classification, we have developed a systematic mathematical framework to evaluate performance of VSAs and provided some guidelines to design an optimal VSA as presented in the paper *Determinants of Variable Stiffness Mechanism* in the Appendix A.

Currently, most of VSAs use mechanical springs to realize compliance as reviewed this section. The compliances of those VSAs are changed by the actuation of DC motors. This conventional approach to obtain different levels of compliance requires a complex mechanical transmission system from the electrical motors to the stiffness mechanism and the output link, which eventually increases inertias, frictional effects, and reduces energy efficiency. Recently, in the field of material science, there is an increasing interest towards a new way of realizing controllable compliance based on smart materials. A number of "smart'-material based actuators have been studied, revealing new actuation principles (Madden et al. (2004)) as presented in Tab. 2.2. Among those materials, some of those materials are capable of changing their effective physical stiffness (class C7 as mentioned in section 2.3.2) by stimulations of, for example, high voltage or thermal activation (Kuder et al. (2013)) as presented in the following categories.

2.3.3 Stiffness Adjustment Approaches Using Smart Materials

- *Shape memory alloys (SMAs)*: Recently, there have been an increased interest in using SMAs in many different fields: robotics, aerospace, automative, etc. SMAs constitute a group of metallic materials capable of remembering their previous defined shapes when subjected to certain stimuli, e.g. thermal-mechanical or magnetic treatments. For specific types of alloys, e.g. NiTi, the micro-scaled structures inside the alloys are determined by the strutural phases (Bellouard (2008)). There exist two phases of alloy micro structure, i.e. Austenite and Martensite, resulting in different Young's moduli. By cooling the alloys at a high speed, Young's modulus increases due to the phase transition from Austenite to Martensite. Conversely, when the alloys are heated up, their micro structures return from Martensite to Austenite and Young's modulus decreases. Due to this temprature-dependent property, there have been many applications that utilize SMAs for stiffness variability. However, the large delay in transition from one phase to another limits the attainable actuation frequency. Moreover, the fatigue life cycle of the materials is really low with a typical maximum of about 10^4 (Patoor et al. (2006)). Thus, for applications in dynamic locomotion in which legged mechanisms are required to operate rapidly and repetitively, the use of SMA is still limited.

- *Shape Memory Polymers (SMPs):* Another way to vary the stiffness can be realized by using Shape Memory Polymers (SMPs). When the polymers are thermally stimulated at temperature T, they undergo a shape change process leading to the acquisition and the retainment of a different temporary configuration. The original shape can be resumed by a cooling-down process (Behl et al. (2010)). An important feature of SMPs is the transition temperature T_{tran} that marks the boundary between two polymer states, which is hard ($T < T_{trans}$) and soft ($T > T_{trans}$). This transition phenomenon varies the mechanical properties of SMP including Young's modulus as a key for stiffness variability. For example, increasing the temperature $T > T_{trans}$ induces rigidity changes up to 500 times, if compared to the changes of 3 times in the case of SMAs (Wei et al. (1998)). However, the main limitations of the SMP materials are the following: low actuation force compared to SMAs, danger of micro-scaled damage due to insufficient temperature, and durability in long term operations (Sun et al. (2012)).

- *Elastic Memory Composites (EMCs)*: In order to improve the performance of SMPs in terms of recovery of force and stiffness, there have been many attempts at engineering composite materials by appropriate reinforcement methods on SMPs (Abrahamson et al. (2003); Shan et al. (2009)). Although the reversible strain capacity of the SMPs is substantially reduced, the remaining range of adjustable stiffness is still sufficient in many applications. The stiffness of materials can be varied in a way that desired flexibility can be achieved under high temperature and rigidity under low temperature treatments. Due to a large change in structure of materials, the Young's modulus greatly varies. Compared to SMPs, EMCs can provide larger changes of Young's modulus. EMC materials are similar to traditional fiber-reinforced composites except for the use of a thermoset shape memory resin that enables much higher packaging strains than traditional composites without damage to the fibers or the resin (Lake and Campbell (2004)). EMCs also provide high strength, high modulus, but low density and that will result in light-weighted designs. The unique capacities of EMCs allows for the development of very efficient structural components in spacecraft systems (Tupper et al. (2001)).

- *Shape memory composite topology:* In general, the material structure of in this category makes use of two kinds: fixed stiffness and variable stiffness. The function of the fixed stiffness one is to carry the structural loads, whereas the variable stiffness materials, e.g. SMPs, are employed to regulate the behavior of the structural deformation via electrical, thermal, chemical, or magnetic stimuli. In other words, these stimuli control the connectivity between the fixed-stiffness materials (McKnight and Henry (2005)). When no stiffness variability is required, the variable stiffness materials are as rigid as the fixed stiffness ones. When needed, the stiffness of the sturcture could be controlled by changing the stiffness of variable stiffness materials. An advantage of SMPs is that the transition temperature is relatively large ranging from 2GPa to 50MPa for polyurethane based SMPs. Moreover, the transition temperature of SMPs can be adjusted to match a wide range of application requirements (McKnight and Henry (2008)).

Although there has been an increasing understanding of smart materials that are capable of changing stiffness, the applicability of these materials in the field of dynamic legged robots are still limited. As the main requirements of actuators for legged robots are high force output and high control bandwidth but light-weighted structure, using the current state-of-the art smart materials

Table 2.2: Variable stiffness actuators using smart materials (Adapted from Kuder et al. (2013)).

Variable stiffness actuators using smart materials			
Shape memory alloys	55-NiTiNOL	$E_{hot}/E_{cold} \approx 4^{\circ}$	$82-83^{\circ}$
Shape memory polymers	Polyurethane of polyester polyole series Polystyren-based CTD-DP-5.1 bulk thermoset resin	$E_{cold}/E_{hot} \approx 100$ $G_{cold}/G_{hot} \approx 326-517$ $G_{cold}/G_{hot} \approx 100$	Below and above $T_g = 95^{\circ}C$ at T_{room} and $T = 95^{\circ}$ $20-80^{\circ}$
Elastic memory composite	Reinforcement: cerbon fiber (T300) Resin: styren based Vertiflex S, VF62	$E_{hot}/E_{cold} \approx 79$	$23-90^{\circ}$
Shape memory composite	Constant-variable stiffness layer laminate Reinforcement: 1095 steel hexagonal elements Resin: Polyurethane-baed Diaplex	$E_{cold}/E_{hot} \approx 15-77$	Below and above $T_g = 35-75^{\circ}C$ at T_{room} and $T = 95^{\circ}$
Elastic memory composite	Tube: $\pm$ carbon fiber, silicone matrix Working fluid: water F^{2}MC sheet Four $\pm$ carbon fiber/silicone matrix tubes Sheet resin: silicone	$E_{closed}/E_{open} \approx 25.1$ $E_{hot}/E_{cold} \approx 21.6$	Discreted closed/open valve Discreted closed/open valve

are difficult to achieve such requirements. In legged locomotion, mechanical springs are still the most common choices to design VSAs and there are a number of potential uses to be exploited. After carefully reviewing the literature of materials in this field, we decided to use mechanical springs to develop a new VSA in this thesis.

2.3.4 Variable stiffness actuators in legged robots

One way to realize the functionality of variable stiffness at legs is to apply the force control technique to rigid actuators (DC motors) to simulate desired spring characteristics. This, however would be very challenging due to three reasons: large power output for the actuator, high bandwidth limitations due to delays of sensors, mechanism inertia, computational time of controller, and energy efficiency. Thus, VSAs with mechanical stiffness variability have been used to realize the variations of compliance in several legged robots as follows.

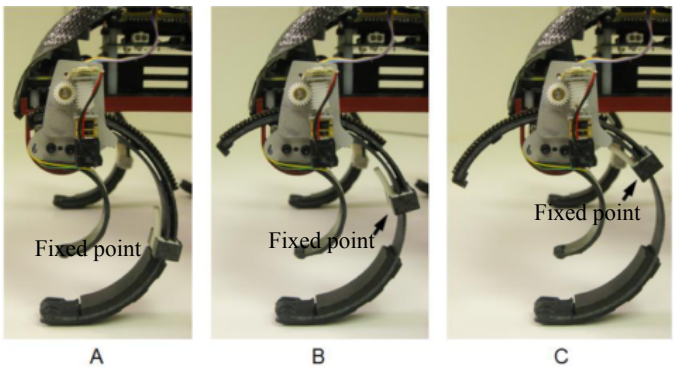

Figure 2.10: Side views of the RHex leg construction with three levels of stiffness adjustment. From (A) to (C), the leg stiffness decreases with the position of the fixed point.

Based on the principle of changing the effective structural compliance (class C7 (Section 2.3.2), the leg stiffness of the EDU-Rhex robot can be varied in a relatively large range. A number of design

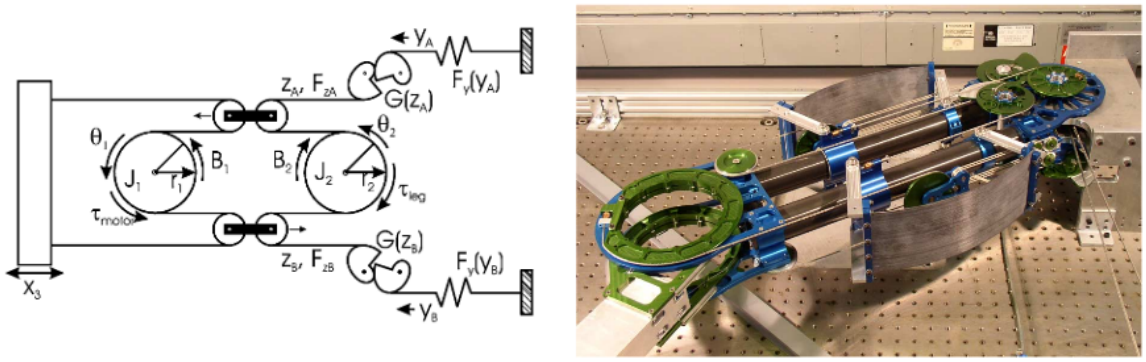

Figure 2.11: AMASC conceptual design and physical leg construction.

iterations such as delrin leg, hard four-link leg, and C-shaped leg have been implemented to improve the performance of the leg design. Figure 2.11 explains how the leg stiffness can be changed. Along the C-shape leg, a hard-circular frame attached with a circular rack gear is mounted to the leg. The position of this frame (represented by the fixed point) with respect to the tip of the foot can be regulated by a small motor connected to the worm-gear. The part of the leg remaining from the fixed point to the tip of the leg determines the effective leg stiffness. This design allows the leg to maintain the leg stiffness without requiring energy. In running experiments, the variable stiffness mechanism was used to tune the leg's natural frequency to increase energy efficiency and speed (Galloway (2013)). On terrains with different stiffness, the experimental results showed that higher leg stiffness enables faster and more efficient running performance in softer terrains. Although this variable stiffness mechanism has been successfully demonstrated in locomotion, there are some remaining design issues. First, the leg stiffness is actually coupled with the leg deflection such that the leg deflection increases with the leg compliance. This feature would not allow for linear stiffness. Second, based on the current design using a high ratio worm-gear unit it seems impossible to achieve a high speed of changing the leg stiffness. Because the small motor would have to rotate a number of revolutions to shift the fixed point along the C-shaped profile.

Another notable development of an adjustable stiffness leg is the AMASC robot (Hurst et al. (2004a, 2005)). Its conceptual design is based on the idea of the antagonistic muscle pair composed of bicep and tricep groups in human shoulder joint. The AMASC design requires two motors working against each other to maintain certain stiffness. Its stiffness is varied by regulating the co-contraction level of two opposed springs connected in series with two motors. Thus, the range of the adjustable stiffness is limitted by the maximum morminal torque of the motor. The important advanced feature of AMASC is that a large of elastic energy can be stored in fiberglass plates, which can subsequently benefit for energy efficient running. However, to maintain a fixed stiffness behavior of the leg, the robot requires energy. Especially, it is exhausted effort to maintain high stiffness at the robotic leg aiming highly dynamic locomotion. This feature clearly limits the real-world performance of AMASC in term of energy efficiency.

Instead of coil springs used in AMASC, two later developments based on the AMASC design, the MABEL and the Thumber robots use fiber-glass springs. Their leg stiffness is adjusted via motor

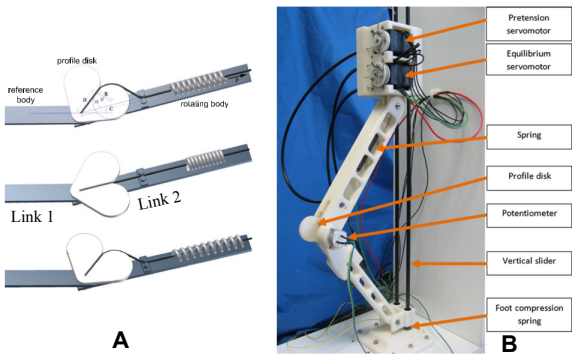

Figure 2.12: MACCEPA design and the hopping in-place robot, Chobino. A) The mechanical design of MACCEPA. B) Experimental setup of the Chobino hoppper.

control that varies the motor response to external loads to achieve the desired elastic behaviours (Grizzle et al. (2009)).

Adjustable leg stiffness was also implemented in a hopping robot, co-called Chobino whose design is based on MACCEPA (Vanderborght et al. (2011)) as shown in Fig. 2.12. The extensive description of the MACCEPA is provided in (Ham et al. (2006)). The design basically has one linear spring that connects across links. The joint stiffness can be tuned by one motor that varies the pretension of the spring, while the other motor controls the link position, independently. The joint stiffness profile can be adapted to desired shapes by mathematically designing the cam profile. As a result, a torsional stiffening-like spring, which is stiffer at larger joint deflection, was created at the knee joint of the Chobino leg, as shown in Fig. 2.12. Throughout a number of hopping experiments in which the knee stiffness was varied by changing the spring pretension, the results showed that by properly tuning the knee stiffness, a higher hopping height could be achieved in comparison to the hopping height when the knee was rigidly actuated without spring.

The limitation of the MACCEPA based design is that the mechanism requires two opposing motors pulling against each other to hold certain stiffness. Increasing stiffness leads to increased power consumption of two motors to pretension the linear spring. Moreover, increasing stiffness also decrease the spring capacity to release elastic energy since most of the spring length is already used for pretension. These limitations are the same as the ones the ASMASC design possesses.

2.3.5 Conclusion

In this chapter, we presented the background for this thesis. There are three important domains of knowledge that have been addressed. First, the background of legged robot locomotion is crucial to study, which defines the research field to which the thesis outcome is targeted to contribute. Second, studying biological locomotion systems is a strong focus of this thesis in order to understand and abstract principles that animals or humans employ in their daily locomotion. The further investigation in the following chapters strongly based on the biological background we presented in this chapter. Third, we introduced VSAs that could potentially that improve performance of legged robots to the extent comparable to animals.

Recently, the field of studying VSA has been growing rapidly and a number of novel actuators as described in Vanderborght et al. (2013) have been developed. Unfortunately, to the knowledge of the author, there are only three VSAs employed to investigate dynamic legged locomotion. Most of the other VSAs target manipulation applications or are at the state of proof of concept. Although the knowledge of how leg stiffness should be controlled in order to efficiently accommodate for changes of locomotion conditions, e.g. ground compliance, frequency to oscillate the leg, speed of locomotion, etc., is important, none of VSAs have been employed to investigate the role of variable compliance in forward dynamic running or hopping. Thus, in the next chapters, we will present study on this topic covering both aspects: the simulation and the real-world experiments.

Chapter 3

Design and Validation of a Novel Variable Stiffness Actuator, MESTRAN

In this chapter we present the development of a new VSA, named MESTRAN, which aims to address the limitations of existing VSAs. The main results of this chapter have been **published** in the paper: "Vu, H., Aryananda, L., Sheikh, F. I., Casanova, F., and Pfeifer, R., "**A novel mechanism for varying stiffness via changing transmission angle**," in *2011 IEEE International Conference on Robotics and Automation*, 2011, pp. 5076–5081.", available in Appendix B. Therefore, we summarize the results of the paper as follows.

3.1 Introduction

Compliant actuation contributes enormously to legged locomotion robotics since it is able to alleviate control efforts in improving the robot's adaptability and energy efficiency. In the past twenty years, there has been an increasing interest in developing VSAs that were targeted to improve the performance of existing actuators, which are limited in many aspects, e.g., energy efficiency, safety, power density, shock absorbance, robustness, and control bandwidth. For legged robots, these limitations become even more critical since legged robots are supposed to work outdoors in unknown environments with on-board power supply.

Many VSAs have been developed in the past (Vanderborght et al. (2013)), however, the focus on locomotion is still very limited as discussed in Section 2.3.4. In this paper, we present a novel design of a variable stiffness rotary actuator, called MESTRAN, which was especially targeted to address the limitations in terms of the amount of energy and time required to maintain and vary the stiffness of an actuated joint. This actuator belongs to class C6, i.e., Changing load-spring transmission ratio via transmission angle. The advanced features of VSAs in this class are that the stiffness can be changed in a very large range by a small angular displacement of the stiffness mechanism, that enables a high speed of changing the stiffness. In a combination with a worm-gear, the stifness can be held unchanged without requiring energy. Therefore, this mechanism would be beneficial for locomotion study as we will investigate in this chapter.

3.2 Conceptual design

The concept of MESTRAN design is derived from a basic mechanical setup, as illustrated in Fig. 3.3. Blocks A and B can slide on each other, while guided by a vertical and a horizontal wall. A spring is attached between block A and the black ceiling part. To simplify the concept, friction is neglected in this model.

Through the mechanical interaction of the components, a force F_x causes a displacement x and

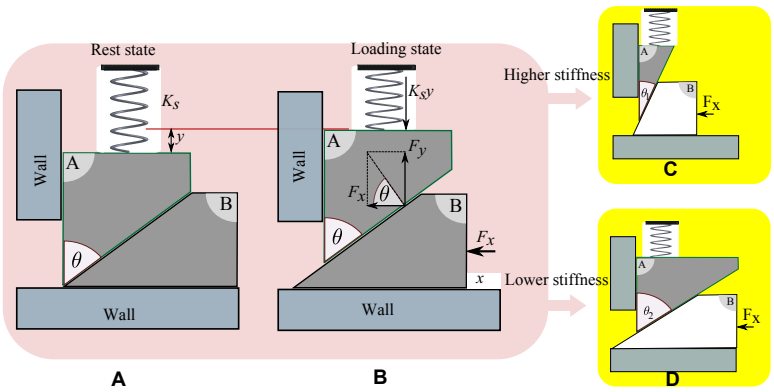

Figure 3.1: Operational principle of MESTRAN, force transmission via slopes; F_x: pressing force; θ: slope angle (transmission angle); y: spring deflection; x: displacement; K_s: stiffness of spring. (A) Initial state with no load. (B) Loading state. (C) Mechanism operation at high stiffness. (D) Mechanism operation at low stiffness.

a compression of spring y according to the following equation

$$F_x = \frac{K_s y}{(\tan\theta)} = \frac{K_s}{(\tan\theta)^2} x. \tag{3.1}$$

Thus, the system is compliant with a stiffness coefficient $K = \frac{K_s}{(\tan\theta)^2}$. Varying the stiffness level can be achieved by changing the transmission angle θ instead of replacing springs with different K_s. The mechanical design of MESTRAN is presented in Fig. 3.2.

3.3 Experimental results

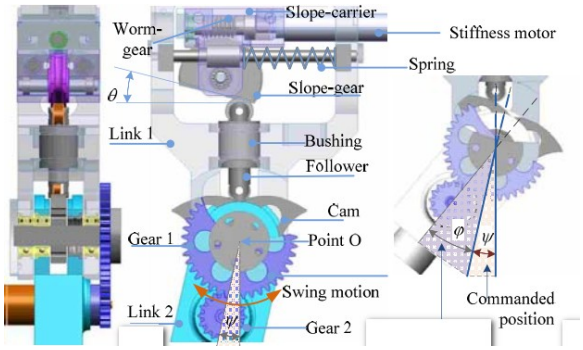

Figure 3.2: Implementation of the MESTRAN design on the rotary joint O formed by link 1 and 2. (a): the side view of the mechanical structure. (b): the configuration where link 2 is actuated by the knee motor by an angle ψ (the cam is not displaced). (c): the configuration where external load is presented and link 2 is displaced by an angle $\psi + \phi$ from both the knee motor and external load (the cam is displaced).

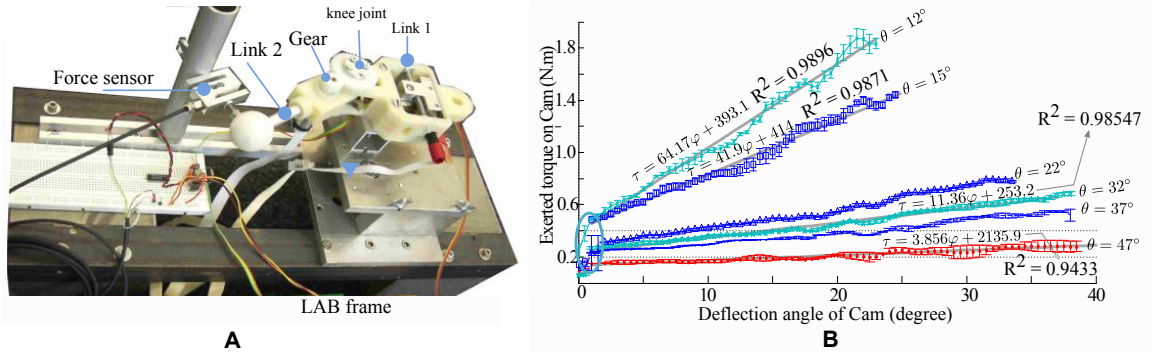

Figure 3.3: The exerted torque to a rotary joint is plotted respectively to the deflection angle of the cam for six transmission angles θ. The plotted results are the mean values of exerted torques in each transmission angle and the error bars show deviation of exerted torques. The linear relationship of the experiment data is validated by computing linear regression. The linear functions represent the approximated torque-angle relationship.

We have constructed a physical prototype to realize the concept and conducted a series of experiments to validate the performance of the MESTRAN actuator prototype as shown in Fig.3.3. The results from the theoretical analyses and experiments show that MESTRAN allows independent control of stiffness and position of an actuated rotary joint with a large operational range and high speed. The experiments were conducted within the slope angle θ ranging from $12° - 47°$. As a result of changing the slope angle, the stiffness ranges from 3Nm/$\circ$ to 64 Nm/$\circ$. The torque-displacement relationship is close to linear. Lastly, the MESTRAN actuator can maintain a certain stiffness without energy input.

3.4 Conclusion

The paper presented in this chapter shows a novel variable stiffness actuator design (MESTRAN), based on the concept of varying the transmission angle to change the force transmission which is a mechanical strategy to achieve varying stiffness. We have conducted modeling analysis, constructed a physical prototype, and carried out various experiments to validate the performance of the actuator. The preliminary results have shown that MESTRAN is capable of varying the joint stiffness with a large operational range and speed, and allows independent control of position and stiffness. We expect that the worm-gear mechanism would help legs equipped with MESTRAN, which is presented later in this thesis, to improve their energy efficiency of locomotion by saving the energy to maintain the stiffness. We will examine and verify this hypothesis in the next chapter. Preliminary experiment results are promising and we plan to integrate the MESTRAN actuator into a single-legged robot. We will carry out further experiments to investigate the energy efficiency and versatility of the legged robot in the context of dynamic locomotion in the next chapter.

Chapter 4

Stiffness Adjustment for Energy Efficient Locommotion on Hard Surfaces

In this chapter, we investigate how adjustment of leg stiffness can improve energy efficiency of hopping locomotion with different stride frequencies. A part of this chapter was presented in the the paper **"A variable stiffness mechanism for improving energy effciency of a planar single-legged hopping robot"** at *The 16th International Conference on Advanced Robotics, ICAR 2013, Nov. 2013*. In addition, the extension of this paper was presented in the submitted journal paper **"Improving energy efficiency of hopping locomotion by using a variable stiffness actuator"**. We will therefore only provide a summary of these papers in this chapter. For more details, we refer to Appendix C and D.

4.1 Introduction

The development of legged locomotion robots that can achieve both efficiency and versatility has been one of the most important challenges in robotics research. In general, fully-actuated systems that can achieve many variations of behaviors show comparatively low energy efficiency, while passivity-based systems that exhibit efficient behaviors suffer from a lack of behavioral diversity. Although many VSAs were proposed and developed in the past, it has not been clarified how such actuators can improve both energy efficiency and behavioral diversity. From this perspective, the goal of this chapter is to investigate the one-legged hopping robot that is equipped with the MESTRAN actuator to explain how behavioral diversity can be enhanced with modest impact on energy efficiency.

4.2 Modelling and simulation of a one-legged hoping robot

To study energy efficient locomotion of the hopping robot, first, we introduced a simulation model of a one-legged hopping robot with joint stiffness variability, as shown in Fig. 4.1. The stability of the model in locomotion was investigated to understand the hopping behaviors. We then examined the energy efficiency of the simulated locomotion with respect to different stride frequencies and knee stiffnesses. In order to explain the simulation results, we analytically derived a theoretical model of the leg to compute the Eigen frequencies with respect to different knee stiffness, as shown in Figure 4.2. This figure essentially indicates that the Eigen frequency increases with the knee stiffness. This figure also presents the simulation results on the energy efficiency of hopping when both knee stiffness and stride frequency vary. Usually, the variation of CoT shows a concave profile with respect to a stride frequency, thus we are able to identify the optimum CoT, which is depicted by the asterisks in Figure 4.2A.

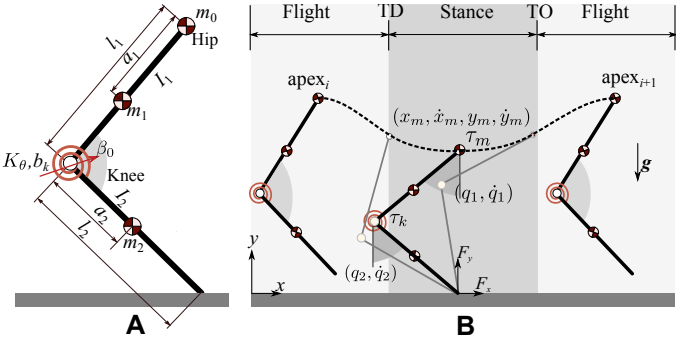

Figure 4.1: A model of legged hopping locomotion. (A) A two-segmented leg with a knee and hip joints. The knee joint is simulated with a torsion linear spring with stiffness variability. Three point masses m_0, m_1, m_2 are located at the hip joint, the center of mass of the link 1, and 2. (B) Hopping locomotion of the two-segmented leg in one hopping cycle. The hopping cycle is devided into three distinct phases: Flight, Stance, and Flight. The hopping locomotion cycle starts and ends at the apex point.

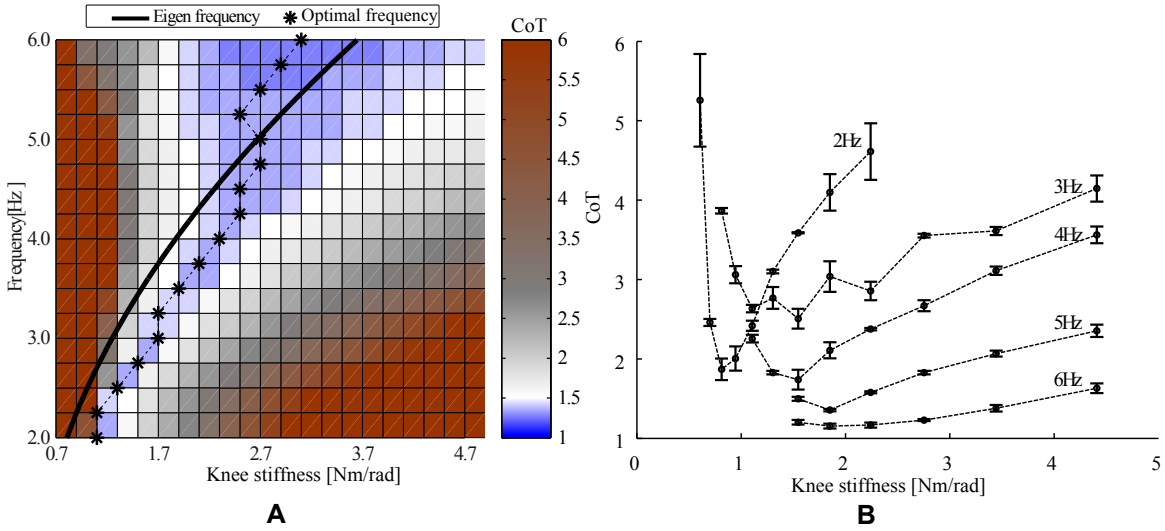

Figure 4.2: (A) CoT of simulated hopping locomotion with different knee stiffness K_θ ($0.7 - 4.7Nm/rad$ with every $0.2Nm/rad$) and stride frequency f ($2 - 6Hz$ with every $0.25Hz$). The bar on the right indicates the relationship between the values of CoT and color. The solid line shows the eigen frequency f_e with K_θ, while the dashed line connects the points at which the minimum CoT is achieved for each f. (B) Experimental CoT of the legged hopping with the leg stiffness K_θ for different stride frequencies f. The mean values (black dots) are avarages of three measured values shown with standard deviation bars.

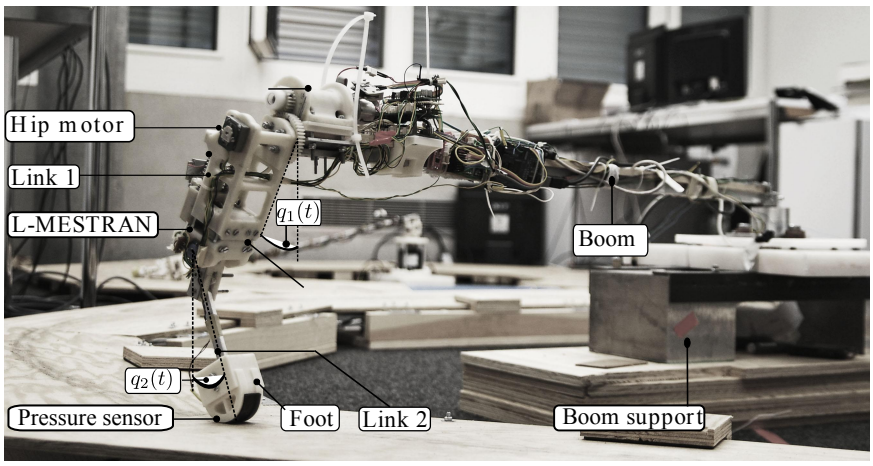

Figure 4.3: A legged hopping platform based on the hopping leg equipped with the variable stiffness mechanism L-MESTRAN.

We can learn two important implications from these simulation results. First, the variability of knee joint stiffness is very important in order to achieve high energy efficiency over different stride frequencies. Second, in order to achieve energy efficient hopping locomotion, the leg stiffness should be regulated such that the Eigen frequency of the leg structure is close to the imposed stride frequency. These results serve as guidelines to control the real-world hopping leg hopping, which is shown in Fig. 4.3, in the experiments.

4.3 A single-legged robot equipped with L-MESTRAN

As shown in Fig. 4.3, the design of the MESTRAN leg was adapted to a new leg, named L-MESTRAN. Compared to the previous one, the L-MESTRAN leg provides a linear joint stiffness, instead of an exponential one, and a more compact design. In addition, the symmetrical compliant joint in MESTRAN has been adapted to a uni-directional compliant joint. We utilized this mechanism to systematically investigate how to improve energy efficiency in forward hopping locomotion on a segmented leg robot. The design details of L-MESTRAN can be found in Appendix C.

4.4 Summary of experimental results

Through examining the results in Fig. 4.2B, the improvement of the CoT at different stride frequencies with the stiffness variability can be clarified as follows. At five stride frequencies: 2, 3,4,5,6 (Hz), the CoTs were improved 60, 40, 50, 40, and 25 (%), respectively. The minimum amount of 25 % was a significant improvement promoted by a proper setting of the knee stiffness according to the stride frequency. Moreover, the variations of the CoT over different stride frequencies further indicated that hopping at lower frequencies, e.g., 2 and 3 (Hz), requires higher precision of knee stiffness adjustment than hopping at higher frequencies, e.g., 5 and 6 (Hz). In particular, at the stride frequency of 6 Hz, the CoT only increased from 1.3 to 1.5 (13%) when the knee stiffness

varied from 1.5 Nm/rad to 4.7 Nm/rad (313%), whereas, at 2 Hz, a small change as 1Nm/rad of the knee stiffness could result in a rapid increase in CoT of 60%.

From the experimental results, we conclude that the variability of the leg stiffness is necessary for the improvement of the energy efficiency of one-leg robot hopping locomotion over the variations of stride frequencies.

4.5 Conclusion

The development of a legged robot that is capable of locomotion with high energy efficiency and diverse behaviours remains a significant challenge today. For a systematic investigation of this challenge, the paper presented in this chapter explored the relationship between energy efficiency, leg stiffness, and stride frequency. Through a series of simulation and real-world experiments of one-legged hopping locomotion, we showed that adjustment of knee joint stiffness is crucial in order to achieve efficient locomotion with variations of stride frequencies. In particular, we clarified that the energy efficiency of locomotion of the hopping robot can be significantly improved by at least approximately 25% over different stride frequencies with the joint stiffness variability. Furthermore, the model-based analysis suggested that the energy efficiency of hopping locomotion is significantly related to the Eigen frequency of the system, which can be used as an effective indicator of the adjustment of knee stiffness.

There are still a number of questions that need to be investigated in the future. In particular, this paper was limited to an investigation of only a partial set of control and design parameters, and the influences these had requires further clarification. In addition, it would be very interesting to investigate the design and control of different types of stiffness adjustment mechanisms in the same context. On top of these additional investigations, we will be able to develop a more comprehensive understanding about the efficiency and versatility of various types of legged locomotion such as bipedal or quadrupedal robot locomotion.

Progressing along this direction, in the next chapter, we present our study about leg stiffness adjustment on surfaces with different stiffness instead of on the hard surface.

Chapter 5

Stiffness Adjustment for Energy Efficient Locommotion on Compliant Surfaces

In Chapter 4, we investigated the stiffness adjustment of the hopping leg on only hard surface. In this chapter, we explore how the stiffness adjustment can improve the energy efficiency of hopping on surfaces with different stiffness. The main results of this work were presented in the **accepted** paper **"Knee stiffness adjustment for energy efficient locomotion of a legged robot on surfaces with different stiffness"** at *The Robotics and Biomimetics 2013 conference, 2013*. Thus, we refer to this paper in Appendix E for more details. In addition to the results presented in the submitted paper, we introduce a stability analysis of the leg hopping on surfaces with different stiffness, in Appendix F. The goal of this analysis is to provide insight into the relationship between the leg stiffness, the surface stiffness, and the stride frequency resulting in hopping stability.

5.1 Introduction

An important property that allows animals/humans to navigate on surfaces with different stiffness is the elasticity of their complex muscle-tendon-ligament systems (Spence et al. (2010)). Such a feature provides the body and legs with the functionality, e.g., compliance/stiffness, that they require to absorb external shocks and efficiently exchange of mechanical energy, i.e., kinetic and potential energy, to exploit natural dynamics during locomotion. For example, in the single jumping locomotion, it has been found that humans stiffen the legs to land on compliant surfaces, and soften the leg when landing on stiff surfaces (Sanders and Wilson (1992); Seyfarth et al. (1999)). Similarly, the leg stiffness adjustment for different surface stiffness has also been found in the in-place hopping studies (Ferris and Farley (1997)). When the ground stiffness was reduced from the most stiff value to the least, the leg stiffness of the subjects in the experiments was increased more than twice. The total stiffness, i.e., a series combination of the surface and the leg stiffness, remained unchanged regardless of the surface stiffness. In running, Farley et al. found that human runners adjust their leg stiffness to accommodate for changes in the surface stiffness (Ferris et al. (1998)). Such adjustment allows them to maintain their running mechanics over different surfaces with different stiffness. To address the underlying mechaanism of these adjustments, these studies, i.e., one that focused on hopping (Ferris and Farley (1997)) and another running at intermediate speeds (Kerdok et al. (2002)), predicted that the metabolic cost of the subjects, participating in the experiments, was reduced when they adjusted their leg stiffness according to changes of the surface stiffness.

In legged robot research, the studies of locomotion on compliant surfaces have just been at an early state. Little has been known about how to adjust leg stiffness to accommodate for changes of surface stiffness during locomotion. One of the difficulties associated with such studies could be that in order to cope with changes in the surface stiffness, one would need a VSA to dynamically

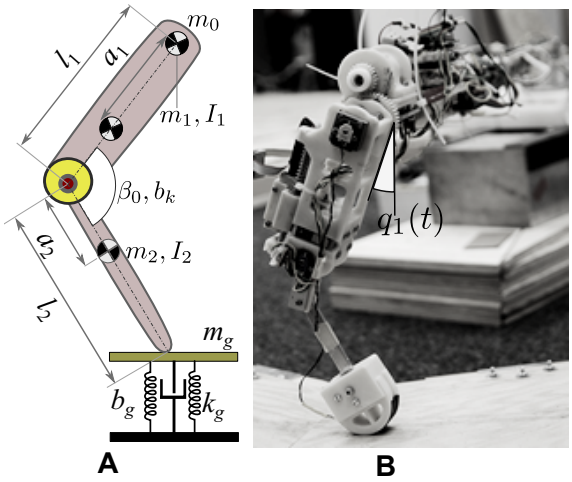

Figure 5.1: Mechanical design parameters of the real hopping leg and the leg model on the variable stiffness surface (A and B). The leg model consists of two links with two revolute joints which are referred to as the hip and the knee. The hip joint is considered as damping free whereas the knee joint is modeled with viscous-damping effect b_k. The rest angle formed by two links is β_0. The surface is modeled by a mass m_G supported by a linear spring with viscous damping b_G. The hip part of the leg is mounted on the boom arm, which allows the leg hopping around the boom base at the experimental arena

adjust leg stiffness. However, incorporating VSAs into a legged robot usually increases the size, weight, and, inertia, which degrade the agility and efficiency of legged robots for dynamic locomotion. Furthermore, the interaction of legs and surfaces during locomotion is highly complicated, which involves a number of locomotion parameters: leg stiffness, surface stiffness, leg damming, surface damming, and stride frequency. Thus, this topic remains challenging in the field of legged robots. To the author's knowledge, there has not been any empirical work along this direction. Thus, this chapter presents a study of how leg stiffness adjustment can accommodate for changes in surface stiffness, using the L-MESTRAN leg.

5.2 Investigation of stiffness adjustment for hopping on surfaces with different stiffness

We begin the study by modeling the legged robot hopping on a compliant surface instead of a rigid one. The model and the constructed leg are presented in Fig. 5.1. All design parameters of this model are presented in Fig. 5.1 and Tab.5.1, which closely abstracts the mechanical structure of the real robotic leg, shown in Fig. 4B, and the compliant surface. Note that since the hip part of the robotic leg was mounted on the boom, the hip pitching motion is omitted in the model by assuming no change of the hip orientation during hopping.

To investigate energy efficient locomotion at various stride frequencies, we simulated the hopping leg at the oscillation frequencies of 3, 4, 5, and 6 (Hz). To cover a large range of leg and surface

Table 5.1: Parameters used in the hopping simulation of the single leg.

Parameters	Value	Parameters	Value
l_1	0.115 m	l_2	0.155 m
m_1	0.32 kg	m_2	0.080 kg
I_1	4.1^{-4} kgm^2	I_2	8.1^{-6} kgm^2
a_1	0.06 m	a_2	0.1 m
β_θ	135°	m_0	0.6 kg
b_θ	0.1 Ns.m^{-1}	K_θ	0.7-4.7 Nm/rad
b_g	0.05 Ns.m^{-1}	K_g	3000→63000 (N/m)
m_g	0.5 kg		

parameters, we systematically varied three important parameters: knee stiffness K_θ, surface stiffness K_g, and, and stride frequency f from 1→15 (Nm/rad), 3000→63000 (N/m), and 3-6 (Hz) in a step size of 0.25, 6000, and 1, respectively. The detailed results are presented in Appendix E, section III.B.

In the real-world experiments, we let the hopping leg hop at four different frequencies of actuation: 3,4,5, and 6 (Hz) at two levels of the track compliance: stiff (Kg = 63000 N/m) and soft (Kg = 6300 N/m). Two locomotion measures, i.e., forward speed and CoT, were taken into account in analyzing the hopping performances. As we can observe in Fig. 5.2, the experimental results closely represent the simulation results.

As shown in the upper plots in Fig. 5.2A-B, the locomotion speed was strongly influenced by changes of the knee stiffness. For example, when the surface stiffness was set at a large value, i.e., 63000 N/m. It is clear that the variation profiles of the speed with respect to the knee stiffness show convex shapes. Thus, at a given stride frequency, high speed can be achieved when the knee stiffness are properly adjusted .

In the lower plots of Fig. 5.2A-B, when the surface stiffness reduced to a low level, e.g., 6300 N/m, the influence of the knee stiffness adjustment on the speed decreased. The data trends revealed that after the knee stiffness approached a minimum level, the increase of knee stiffness did not significantly affect the speed. The hopping leg achieved almost the same speed over a large range of the knee stiffness. Furthermore,the speed data also showed that increasing stride frequency requires to increase the knee stiffness in hopping on both levels of surface stiffness. Lastly, from the upper and lower figures, it was clear that on the lower stiffness surfaces, higher knee stiffness was required to achieve a similar level of speed which is comparable to the achievable speed on higher stiffness surfaces. We found that the influence of the knee stiffness on the CoT is similar to that on speed. Thus, the overall conclusion can be drawn that it is possible to optimize the speed and CoT of the hopping leg in different conditions of surface stiffness and stride frequency by a proper adjustment of the knee stiffness.

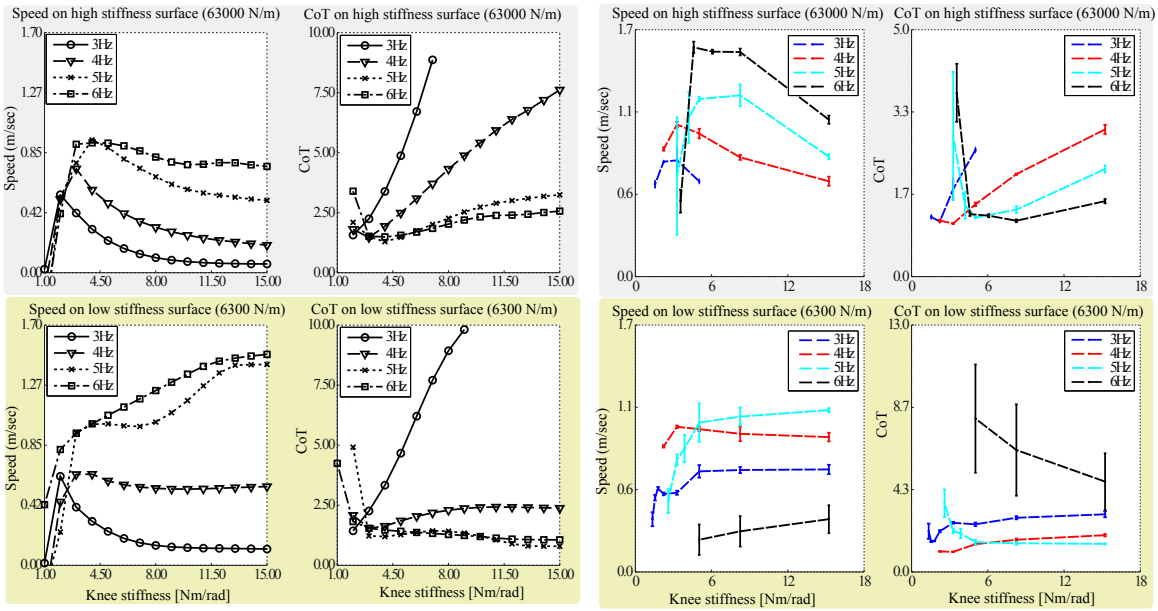

Figure 5.2: Knee stiffness versus CoT and speed at various hopping frequencies on surfaces with two different stiffness. The CoT is calculated by the average electrical power and average speed.

5.3 Conclusion

In this chapter, we presented a systematic exploration of how knee stiffness adjustment can accommodate the changes of surface stiffness to improve locomotion energy efficiency at various stride frequencies. First, we presented the mechanical design, the theoretical analysis, and the performance evaluation of the adjustable stiffness leg incorporating with L-MESTRAN. We, then, studied hopping locomotion on compliant surfaces by developing a hopping model which closely abstracted the physical properties of the robotic leg and the surface. Following that, based on the simulation results, we conducted a number of experiments to validate the results. The simulation results, shown in Fig. 5.2, are in the agreement with the experimental results.

Finally, the results obtained from this study demonstrated that for a given stride frequency and surface stiffness, a proper adjustment of knee stiffness can significantly improve the CoT of hopping locomotion. Despite the complex interaction of legs on surfaces, which involves a number of locomotion parameters: leg stiffness, leg oscillation amplitude, offset angle of leg oscillation, surface stiffness, stride frequency, etc., knee stiffness adjustment is found to be an effective approach to improve energy efficient locomotion at various stride frequencies on surfaces with different stiffness.

Chapter 6

Final Discussions and Conclusion

6.1 Discussions

In this section, we discuss how to improve the design of L-MESTRAN design and solutions to improve its mechanical performance. Following that, the potential applications to extend the usability of L-MESTRAN in a broader field will be provided. We conclude the discussion by presenting our future perspectives on the development of VSAs in general.

6.1.1 Development of VSAs for highly dynamic legged robots from 2009 to 2013

It has been five years since we started the thesis project in the beginning of 2009. Within this period, a number of new VSAs have been proposed and demonstrated as reviewed in section 2.3.2. However, so far, there are only two VSAs that are employed to study dynamic locomotion in a forward movement manner, i.e. C-shaped leg (Galloway (2013)) in the Rhex robots and L-MESTRAN (Vu (2013); Vu et al. (2011, 2013)). Other VSAs have been used to study variable stiffness locomotion in the context of in-place hopping within a very limited range of hopping frequency (Hurst et al. (2010); Vanderborght et al. (2011)). Most of other VSAs are typically targeted towards manipulation tasks.

Employed for dynamic legged locomotion, the C-shaped legged robots have demonstrated impressive dynamic performance on different terrains load carrying capability. However, due to the C shape it seems hard to implement such legs for for walking, hopping or running locomotion robots. To the author's knowledge, there are no other variable stiffness legged robots that can can achieve such performance.We have developed L-MESTRAN aiming at obtaining large benefit from stiffness variability and the mechanism can be used in segmented leg robots which are the common configurations for bio-inspired legs.

The common features of the C-shaped leg and the L-MESTRAN related to variable stiffness mechanisms are that both of them can keep stiffness constant without requiring supplied energy. They both showed that VSAs can be used to improve energy efficiency of locomotion

6.1.2 Design issues and solutions to improve performance of the LESTRAN legs

The first L-MESTRAN was constructed in 2009 to realize the concept. The mechanism was not robust enough for dynamic experiments. The legged platform built on the second version of the L-MESTRAN mechanism demonstrated a remarkable locomotion performance. A vast number of experiments have been carried out, using this leg as shown in Chapters 4 and 5. To further improve

the mechanical performance of L-MESTRAN, we analyse the current prototype to identify the remaining issues of the design and the prototype. Based on these, the solutions will be proposed.

1. Since the external force is not directly transferred to the spring but through several intermediate parts. This causes energy losses due to frictional forces between parts. Moreover, the frictional force can also result in mechanical damages between contacting surfaces.
2. Due to geometrical constraints, the springs are always preloaded, thus the accessibility to the full energy storage capacity of the springs is not possible.
3. Since the knee joint is compliant on the one side of the knee joint space, the collisions between Link 1 and Link 2 at the knee joint can cause energy losses when the leg is fully extended.
4. Several materials were used to construct the robotic leg, e.g., 3D-printer plastics, aluminium, etc., so that sturdiness and compactness requirements can be satisfied. However, the fragile and deformable parts, produced by 3D-printer, can influence the precision and repeatability of experimental measurements. They are not suitable for a long-term application.
5. Since this robotic leg was not manufactured by high precision machines, mechanical accuracy could be an issue and this may influence the precision of the leg operation.

Thus, we propose the following solutions to improve the current performance of the L-MESTRAN robotic leg:

1. Frictional effects are unavoidable in real mechanical systems, but we can reduce the frictional forces by using higher precision and strong ball bearings. Currently, the translational joints that are used to guide the rack gear are not equipped with ball bearings but sliding bushing instead. This can increase the damping of the legged robot under a large applied load.
2. To avoid the preload effects, the center of the slope gear that connects to the worm can be relocated to the canter of the bearing that interacts with the slope gear. Thus, the two centers are coincident and no preload on the spring is required while changing the slope.
3. Since the knee joint is asymmetrical, critical damping oscillations are unavoidable. To avoid damages to the leg structure, a rubber-like stopper at the neutral position of the knee joint should be introduced.
4. 3D printer is a great tool for fast prototyping the concept. However, for long-term and more reliable experiments, professional manufacturing is highly required.

6.1.3 Potential applications of MESTRAN-based variable stiffness mechanisms

In this thesis, we have presented the development of a new VSA from a conceptual design to the application levels. In particular, we have shown two case studies in which the MESTRAN-based VSA was employed to explore how to optimize the energy efficiency of hopping locomotion at various stride frequency by stiffness adjustment. Since the joints equipped with the MESTRAN mechanisms can theoretically obtain arbitrary stiffness, it is promising that MESTRAN-based mechanisms

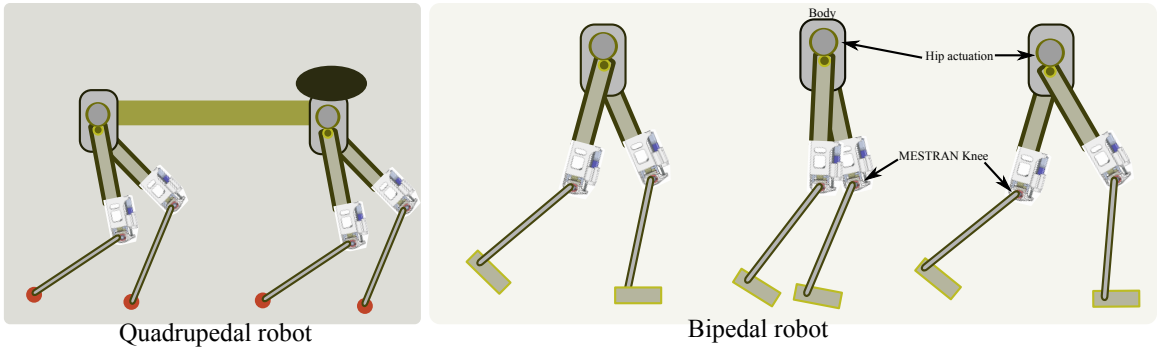

Figure 6.1: Potential applications of the MESTRAN mechanism on other types of legged robots

can be used in many locomotion machines that require a large range of stiffness adjustment and high energy efficiency.

Similar to what has been done for a single-legged hopping robot presented in this thesis, the mechanism can therefore be useful for studying stiffness variability in bipedal and quadrupedal robot locomotion. For example, Figure 6.1 shows how these robots quipped with L-MESTRAN can potentially designed. To make use of the results of this thesis, the leg design and controller can be analogously implemented as presented in Chapter 4 and 5 such that the mechanism is mounted to the knee joints and the actuation is sinusoidally provided from the hip joints. Along the leg, there is only a very small motor located at the knee joint, which is employed to control the knee stiffness. In our single-legged robot platform, we were able to achieve the speed of hopping up to 1m/sec, which is equivalent to 4 leg-length/sec with the minimal CoT of 1. Thus, this leg design demonstrated its relatively good performance, which shows the potential for further studies. In addition, physical joints could be realized in very compact forms due to the large range of stiffness adjustment offered by the design of MESTRAN. In many existing VSAs (Galloway (2013); Hurst et al. (2005, 2007); Kim and Song (2010a); Vanderborght et al. (2009)), the range of adjustable stiffness is limited by the physical constraint of the design, e.g., the spring size, the limited boundary dimension of the mechanisms, etc. Thus, the design of MESTRAN can feature the scalability of joint design, which is an important characteristic in order to achieve lightweight and compact robots.

Although this thesis only investigates two variations of the stiffness adjustment mechanism via transmission angle, the principle of changing stiffness via transmission angle expose promising characteristics, which can be adapted to other locomotion vehicles, e.g., cars, bicycles, etc. and not limited to legged robots. Such vehicles often require higher stiffness in sport modes and medium stiffness in normal modes for traveling (Anubi et al. (2013)). Variable stiffness mechanisms in suspension systems of wheeled vehicles are also an active research domain to which the conceptual design of MESTRAN could potentially contribute.

6.1.4 A future perspective in VSA development.

Biological actuators, e.g., muscles, are not better than artificial actuators at all aspects. For example, the power density of muscles is higher than that of the thermal expansion-based engines, but much lower than that of the combustible, hydraulic, and pneumatic engines (Zupan et al. (2002)).

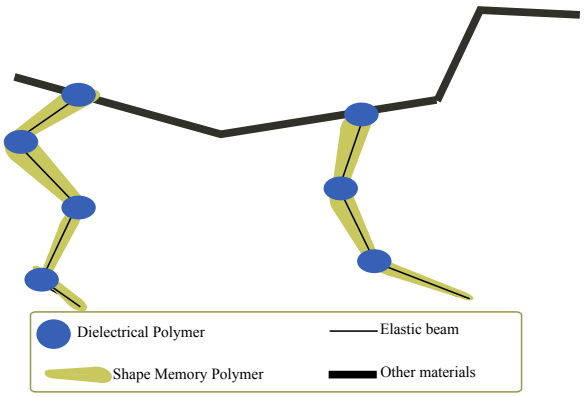

Figure 6.2: A legged robot design that employs smart materials for actuation and stiffness control.

In another aspect, the maximum strain of Elastic Memory Composite-based actuators are much larger than that of muscles (Kuder et al. (2013)). In terms of actuation stress, biological muscles are clearly not comparable to many other artificial actuators which are made of steel, aluminum, etc. Furthermore, artificial muscles such as piezoelectric and pneumatic actuators are capble of operating at high frequency which is orders of magnitude higher than the maximum plausible frequency of muscle contraction (Huber et al. (1997)). Surprisingly, despite all of these limitations, systems possessing biological muscles still outperform ones that are equipped with the artificial muscles.

One of the prominent features of biological muscles is stiffness variability via fiber recruitment processes. The muscle stiffness is graded by controlling the number of fibers which act in parallel. This process allows for optimizing the contraction efficiency of mucles over a large range of load. The inherent characteristics of muscle fibers made the whole process even more effective in a way that the inactive muscle fibers are relatively low in stiffness, and therefore do not require significant force to strain. Converntional materials in artificial muscles are commonly, for example, stainless steel, iron, aluminium, etc. that have a little ability to change the stiffness. Muscles connecting in series with tendons are also capable of storing kinetic energy into potential energy and release it later, as mechanical springs. Moreover, they connect and transfer motion across limbs. Another important feature, they can grow and self-repair. Such many functions enable animals to have the capability to travel across many irregular and unstructured terrains with high energy efficiency. In this regard, the state of the art legged robots are hardly comparable to animals.

VSAs are recognized as devices that can potentially mimic biological muscle characteristics force generation, varying stiffness, storing kinetic energy and releasing potential energy, etc.. However, current performance of VSAs is not applicable in a wide range of application. For example, one common limitation of VSAs are large size and weight added into robots. The leg equipped with VSAs is far more complicated and heavier than the ones without VSAs. The reason is that most of VSAs employ the double actuation method using two DC motors for stiffness and position control with complex transmission systems. Much power is lost at inertia and friction. Therefore, although the basic functionality of changing stiffness at such legs may be achievable, their dynamic capability drastically reduces due to insufficient power supply. This is a fundamental limitation, which is hard to eliminate.

As presented in section 2.3, there has been increasing understanding in the field of studying smart materials to realize variable stiffness. In the near future, the integration of these materials with traditional ones to design VSAs might lead to unexpected performance compared to that when only mechanical springs are used. These materials are Dielectric Polymers, Shape Memory Polymers, Elastic Memory Composites, etc. They can be used as force generators, stiffness regulators, sensors, and limb segments as shown in Fig. 6.2. In this figure, the structure of the robot is build up on many different materials depending on their requried finctionality in operation. Under either thermal or electrical stimulating processes on the desired parts of the structure, the local stiffness of the structure will be varied, inducing the change of the structural stiffness. Other advantages of the materials are large strain, high stress, high bandwidth, high power density, etc. Frictional and inertial effects could be minimized because only a minimal motion transmission system is needed. Currently, there are still technological barriers in using smart materials in legged robots such as high voltages (>1 kV), high temperature treatment, prestrained requirement, etc. As the technology develops smart materials will play a key role in advancing the stiffness adjustable technology in the near future.

However, mechanical springs will not be abandoned due to the development of such smart materials. The special advantages of those springs are simplicity and realiability. There is no controller needed to opearte them and they work right out-of-box. Thus studying VSAs using mechanical springs will go in parallel with those applying smart material technology. Depending on particular applications, appropriate solutions could be chosen.

6.2 Conclusion

This thesis presents the development of a new variable stiffness actuator, named MESTRAN, and two case studies using the actuator in legged robot locomotion. We began by introducing the background part containing of differnt types of locomotion, underlying mechanisms for energy efficient locomotion in nature, and variable stiffness actuators that serve as a basis for developing the thesis.

After covering the background, we proposed a new mechanism to change the stiffness. This mechanism possesses features that are suitable for legged locomotion such as the capability to keep stiffness constant without energy and large range of stiffness adjustment. A physical prototype was constructed and a series of experiments were carried out to validate the concept. We then used this concept for further investigations.

The first case study was to explore how the adjustment mechanism of leg stiffness employing MESTRAN could optimize the hopping energy efficiency at various stride frequencies. The simulation and experimental results have shown that a proper adjustment of leg stiffness results in improving energy efficiency of hopping locomotion at various stride frequencies.

In the second case study, we investigated the same variable stiffness mechanism employed in the first case study for hopping on surfaces with different stiffness. The results indicated that stiffness adjustment mechanism could be applied to improve energy efficiency of hopping locomotion under changes of speed, stride frequencies, and surface compliance.

The main message to take from this thesis is that variable stiffness actuator is useful for legged robot locomotion because it allows for optimizing energy efficiency under changes of speed, stride

frequency, and terrain compliance.

Bibliography

Abrahamson, E. R., Lake, M. S., Munshi, N. A., and Gall, K. (2003). Shape memory mechanics of an elastic memory composite resin. *Journal of Intelligent Material Systems and Structures*, 14(10):623–632.

Albu-Schaffer, A., Bicchi, A., Boccadamo, G., Chatila, R., De Luca, A., De Santis, A., Giralt, G., Hirzinger, G., Lippiello, V., Mattone, R., et al. (2005). Physical human robot interaction in anthropic domains: safety and dependability. In *Proceedings of the 4th IARP/IEEE-RAS/EURON Workshop on Technical Challenges for Dependable Robots in Human Environments, T17-06, Nagoya, June 16-18*.

Alexander, M. (1990). Three uses for springs in legged locomotion. *The International Journal of Robotics Research*, 9(2):53–61.

Alexander, R. (2003). *Principles of Animal Locomotion*. Princeton University Press, Princeton, NJ.

Anderson, W., Eshghinejad, a., Azadegan, R., Cooper, C., and Elahinia, M. (2013). A variable stiffness transverse mode shape memory alloy actuator as a minimally invasive organ positioner. *The European Physical Journal Special Topics*, 222(7):1503–1518.

Anubi, O. M., Patel, D. R., and Crane III, C. D. (2013). A new variable stiffness suspension system: passive case. *Mechanical Sciences*, 4(1):139–151.

Behl, M., Zotzmann, J., and Lendlein, A. (2010). Shape-memory polymers and shape-changing polymers. In *Shape-Memory Polymers*, pages 1–40. Springer.

Bellouard, Y. (2008). Shape memory alloys for microsystems: A review from a material research perspective. *Materials Science and Engineering: A*, 481:582–589.

Beyl, P., Knaepen, K., Duerinck, S., Van Damme, M., Vanderborght, B., Meeusen, R., and Lefeber, D. (2011). Safe and compliant guidance by a powered knee exoskeleton for robot-assisted rehabilitation of gait. *Advanced Robotics*, 25(5):513–535.

Bicchi, A. and Tonietti, G. (2004). Fast and soft arm tactics: Dealing with the safety-performance trade-off in robot arms design and control. *IEEE Robotics and Automation Magazine*, 11(2):22–33.

Biewener, A. A. (1998). Muscle-tendon stresses and elastic energy storage during locomotion in the horse. *Comparative Biochemistry and Physiology Part B: Biochemistry and Molecular Biology*, 120(1):73–87.

Blickhan, R. (1989). The spring-mass model for running and hopping. *Journal of Biomechanics*, 22(11-12):1217–1227.

Blickhan, R. and Full, R. (1993). Similarity in multilegged locomotion: bouncing like a monopode. *Journal of Comparative Physiology A*, 173(5):509–517.

BostonDynamics (2013). Ls3 - legged squad support systems,. Website: `http://www.bostondynamics.com/robot_ls3.html`.

Buchli, J., Righetti, L., and Ijspeert, A. J. (2006). Engineering entrainment and adaptation in limit cycle systems. *Biological Cybernetics*, 95(6):645–664.

Carloni, R., Visser, L., and Stramigioli, S. (2012). Variable stiffness actuators: A port-based power-flow analysis. *Robotics, IEEE Transactions on*, 28(1):1–11.

Carpi, F., DeRossi, D., Kornbluh, R., Pelrine, R., and Sommer-Larsen, P. (2008). *Dielectric elastomers as electromechanical transducers. Fundamentals, materials, devices, models and applications of an emerging electroactive polymer technology*. Elsevier Press.

Catalano, M., Grioli, G., Bonomo, F., Schiavi, R., and Bicchi, A. (2010). VSA-HD: From the enumeration analysis to the prototypical implementation. In *Intelligent Robots and Systems (IROS), 2010 IEEE/RSJ International Conference on*, pages 3676–3681.

Catalano, M., Grioli, G., Garabini, M., Bonomo, F., Mancinit, M., Tsagarakis, N., and Bicchi, A. (2011). Vsa-cubebot: A modular variable stiffness platform for multiple degrees of freedom robots. In *Robotics and Automation (ICRA), 2011 IEEE International Conference on*, pages 5090–5095.

Cavagna, G. A., Heglund, N. C., and Taylor, C. R. (1977). Mechanical work in terrestrial locomotion: two basic mechanisms for minimizing energy expenditure. *American Journal of Physiology-Regulatory, Integrative and Comparative Physiology*, 233(5):R243–R261.

Choi, J., Hong, S., Lee, W., Kang, S., and Kim, M. (2011). A robot joint with variable stiffness using leaf springs. *Robotics, IEEE Transactions on*, 27(2):229–238.

Clark, A. (2008). *Supersizing the Mind: Embodiment, Action, and Cognitive Extension*. Oxford University Press, New York.

Collins, S. and Ruina, A. (2005). A bipedal walking robot with efficient and human-like gait. In *Robotics and Automation, 2005. ICRA 2005. Proceedings of the 2005 IEEE International Conference on*, pages 1983–1988.

Collins, S. H., Wisse, M., and Ruina, A. (2001). A three-dimensional passive-dynamic walking robot with two legs and knees. *The International Journal of Robotics Research*, 20(7):607–615.

Darden, F. (1999). *Conception and Realization of Pleated Pneumatic Artificial Muscles and their Use as Compliant Actuation Elements*. PhD thesis, Vrije Universiteit Brussel.

Dawkins, R. (1996). Why dont animals have wheels? *The Sunday Times*, 24.

Eiberger, O., Haddadin, S., Weis, M., Albu-Schaeffer, A., and Hirzinger, G. (2010). On joint design with intrinsic variable compliance: derivation of the DLR QA-joint. In *Robotics and Automation (ICRA), 2010 IEEE International Conference on*, pages 1687–1694.

Everarts, C., Dehez, B., and Ronsse, R. (2012). Variable stiffness actuator applied to an active ankle prosthesis: Principle, energy-efficiency, and control. In *Intelligent Robots and Systems (IROS), 2012 IEEE/RSJ International Conference on*, pages 323–328.

Farley, C. T., Blickhan, R., Saito, J., and Taylor, C. R. (1991). Hopping frequency in humans: a test of how springs set stride frequency in bouncing gaits. *Journal of Applied Physiology*, 71(6):2127–2132.

Farley, C. T. and Gonzalez, O. (1996). Leg stiffness and stride frequency in human running. *Journal of Biomechanics*, 29(2):181–186.

Ferris, D. P. and Farley, C. T. (1997). Interaction of leg stiffness and surface stiffness during human hopping. *Journal of applied physiology*, 82(1):15–22.

Ferris, D. P., Louie, M., and Farley, C. T. (1998). Running in the real world: adjusting leg stiffness for different surfaces. *Proceedings of the Royal Society of London. Series B: Biological Sciences*, 265(1400):989–994.

Floreano, D. and Mattiussi, C. (2008). *Bio-inspired artificial intelligence: theories, methods, and technologies*. The MIT Press.

Fumagalli, M., Barrett, E., Stramigioli, S., and Carloni, R. (2012). The mvsa-ut: A miniaturized differential mechanism for a continuous rotational variable stiffness actuator. In *Biomedical Robotics and Biomechatronics (BioRob), 2012 4th IEEE RAS EMBS International Conference on*, pages 1943–1948.

Gabrielli, G. and Von Karman, T. (1950). What price speed? specific power required for propulsion of vehicles. *Mechanical Engineering*, 72:775–781.

Galloway, K. C. (2013). Variable Stiffness Legs for Robust, Efficient, and Stable Dynamic Running. *Journal of Mechanisms and Robotics*, 5(1):011009.

Gerritsen, K. G., van den Bogert, A. J., and Nigg, B. M. (1995). Direct dynamics simulation of the impact phase in heel-toe running. *Journal of Biomechanics*, 28(6):661–668.

Grizzle, J. W., Hurst, J., Morris, B., Park, H.-W., and Sreenath, K. (2009). Mabel, a new robotic bipedal walker and runner. In *Proceedings of the 2009 conference on American Control Conference*, ACC'09, pages 2030–2036, Piscataway, NJ, USA. IEEE Press.

Groothuis, S. S., Rusticelli, G., Zucchelli, A., Stramigioli, S., and Carloni, R. (2012). The vsaut-ii: A novel rotational variable stiffness actuator. In *Robotics and Automation (ICRA), 2012 IEEE International Conference on*, pages 3355–3360.

Ham, B. Y. R. V. A. N., Sugar, T. G., Vanderborght, B., Hollander, K. W., and Lefeber, D. (2009a). Review of Actuators with Passive Adjustable Compliance/Controllable Stiffness for Robotic Applications. (September):81–94.

Ham, R., Sugar, T., Vanderborght, B., Hollander, K., and Lefeber, D. (2009b). Compliant actuator designs. *Robotics Automation Magazine, IEEE*, 16(3):81–94.

Ham, R. V., Vanderborght, B., Verrelst, B., Damme, M. V., and Lefeber, D. (2006). MACCEPA : the Mechanically Adjustable Compliance and Controllable Equilibrium Position Actuator used in the ' Controlled Passive Walking ' biped Veronica.

Heglund, N. C., Fedak, M., Taylor, C., and Cavagna, G. (1982). Energetics and mechanics of terrestrial locomotion. iv. total mechanical energy changes as a function of speed and body size in birds and mammals. *Journal of Experimental Biology*, 97(1):57–66.

Heglund, N. C. and Taylor, C. R. (1988). Speed, stride frequency and energy cost per stride: how do they change with body size and gait? *Journal of Experimental Biology*, 138(1):301–318.

Hogan, N. (1984). Adaptive control of mechanical impedance by coactivation of antagonist muscles. *Automatic Control, IEEE Transactions on*, 29(8):681–690.

Hollander, K. and Sugar, T. (2004). Concepts for compliant actuation in wearable robotic systems. In *Proceeding of US-Korea Conference on Science, Technology and Entrepreneurship (UKC 04)*, volume 128, pages 644–650.

Hollander, K. W., Sugar, T. G., and Herring, D. E. (2005). Adjustable robotic tendon using a'jack spring'. In *Rehabilitation Robotics, 2005. ICORR 2005. 9th International Conference on*, pages 113–118. IEEE.

Hoyt, D. F. and Taylor, C. R. (1981). Gait and the energetics of locomotion in horses. *Nature*, 292(5820):239–240.

Huber, J., Fleck, N., and Ashby, M. (1997). The selection of mechanical actuators based on performance indices. *Proceedings of the Royal Society of London. Series A: Mathematical, Physical and Engineering Sciences*, 453(1965):2185–2205.

Hurst, J., Chestnutt, J., and a.a. Rizzi (2004a). An actuator with physically variable stiffness for highly dynamic legged locomotion. *IEEE International Conference on Robotics and Automation, 2004. Proceedings. ICRA '04. 2004*, pages 4662–4667 Vol.5.

Hurst, J. W. (2008). *The Role and Implementation of Compliance in Legged Locomotion*. PhD thesis, Robotics Institute, Carnegie Mellon University, Pittsburgh, PA.

Hurst, J. W. (2011). The electric cable differential leg: a novel design approach for walking and running. *I. J. Humanoid Robotics*, 8(2):301–321.

Hurst, J. W., Chestnutt, J. E., and Rizzi, A. A. (2004b). An actuator with physically variable stiffness for highly dynamic legged locomotion. In *IEEE International Conference on Robotics and Automation*, volume 5, pages 4662–4667.

Hurst, J. W., Chestnutt, J. E., and Rizzi, A. A. (2005). An Actuator with Mechanically Adjustable Series Compliance. *Robotics*, (April 2004).

Hurst, J. W., Chestnutt, J. E., and Rizzi, A. a. (2007). Design and Philosophy of the BiMASC, a Highly Dynamic Biped. *Proceedings 2007 IEEE International Conference on Robotics and Automation*, pages 1863–1868.

Hurst, J. W., Chestnutt, J. E., and Rizzi, A. A. (2010). The actuator with mechanically adjustable series compliance. *Robotics, IEEE Transactions on*, 26(4):597–606.

Hyun, D., Yang, H. S., Park, J., and Shim, Y. (2010). Variable stiffness mechanism for human-friendly robots. *Mechanism and Machine Theory*, 45(6):880 – 897.

Iida, F. (2006). *Cheap Design and Behavioral Diversity for Autonomous Adaptive Robots*. PhD thesis, University of Zurich.

Irschick, D. J. and Garland, T. (2001). Integrating function and ecology in studies of adaptation: Investigations of locomotor capacity as a model system. *Annual Review of Ecology and Systematics*, 32(1):367–396.

Ishikawa, M., Komi, P. V., Grey, M. J., Lepola, V., and Bruggemann, G.-P. (2005). Muscle-tendon interaction and elastic energy usage in human walking. *Journal of applied physiology*, 99(2):603–608.

Jafari, A., Tsagarakis, N., Vanderborght, B., and Caldwell, D. (2010). A novel actuator with adjustable stiffness (awas). In *Intelligent Robots and Systems (IROS), 2010 IEEE/RSJ International Conference on*, pages 4201–4206.

Jafari, A., Tsagarakis, N. G., Sardellitti, I., and Caldwell, D. G. (2012). A new actuator with adjustable stiffness based on a variable ratio lever mechanism. *Mechatronics, IEEE/ASME Transactions on*, PP(99):1–9.

Kerdok, A. E., Biewener, A. a., McMahon, T. a., Weyand, P. G., and Herr, H. M. (2002). Energetics and mechanics of human running on surfaces of different stiffnesses. *Journal of applied physiology (Bethesda, Md. : 1985)*, 92(2):469–78.

Khatib, O. (1999). Mobile manipulation: The robotic assistant. *Robotics and Autonomous Systems*, 26(2):175–183.

Khatib, O., Yokoi, K., Brock, O., Chang, K., and Casal, A. (1999). Robots in human environments. In *Robot Motion and Control, 1999. RoMoCo'99. Proceedings of the First Workshop on*, pages 213–221.

Kim, B.-s. and Song, J.-b. (2010a). Hybrid Dual Actuator Unit : A Design of a Variable Stiffness Actuator based. *Control*, pages 1655–1660.

Kim, B.-S. and Song, J.-B. (2010b). Hybrid dual actuator unit: A design of a variable stiffness actuator based on an adjustable moment arm mechanism. In *Robotics and Automation (ICRA), 2010 IEEE International Conference on*, pages 1655–1660.

Kim, B.-S. and Song, J.-B. (2012). Design and control of a variable stiffness actuator based on adjustable moment arm. *Robotics, IEEE Transactions on*, 28(5):1145–1151.

Kruszelnicki, K. (2008). Real wheel animals - part two. *Great Moments in Science. ABC Science*, pages 10–29.

Kuder, I. K., Arrieta, A. F., Raither, W. E., and Ermanni, P. (2013). Variable stiffness material and structural concepts for morphing applications. *Progress in Aerospace Sciences*.

Kuitunen, S., Komi, P. V., Kyrolainen, H., et al. (2002). Knee and ankle joint stiffness in sprint running. *Medicine and Science in Sports and Exercise*, 34(1):166–173.

Kuo, A. D. (2007). Choosing your steps carefully: Trade-offs between economy and versatility in dynamic walking bipedal robots. *IEEE Robotics & Automation Magazine*, 14(2):18–29.

Lake, M. S. and Campbell, D. (2004). The fundamentals of designing deployable structures with elastic memory composites. In *Aerospace Conference, 2004. Proceedings. 2004 IEEE*, volume 4, pages 2745–2756.

Li, Z., Vanderborght, B., Tsagarakis, N. G., Colasanto, L., and Caldwell, D. G. (2012). Stabilization for the compliant humanoid robot COMAN exploiting intrinsic and controlled compliance. *2012 IEEE International Conference on Robotics and Automation*, pages 2000–2006.

Madden, J. D., Vandesteeg, N. A., Anquetil, P. A., Madden, P. G., Takshi, A., Pytel, R. Z., Lafontaine, S. R., Wieringa, P. A., and Hunter, I. W. (2004). Artificial muscle technology: physical principles and naval prospects. *Oceanic Engineering, IEEE Journal of*, 29(3):706–728.

McGeer, T. (1990). Passive Dynamic Walking. *International Journal of Humanoid Robotics*, 09(02):62–82.

McKnight, G. and Henry, C. (2005). Variable stiffness materials for reconfigurable surface applications. In *Smart structures and materials*, pages 119–126.

McKnight, G. and Henry, C. (2008). Large strain variable stiffness composites for shear deformations with applications to morphing aircraft skins. In *The 15th International Symposium on: Smart Structures and Materials & Nondestructive Evaluation and Health Monitoring*, pages 692919–692919.

McNeill, A. R. (2002). Energetics and optimization of human walking and running: The 2000 raymond pearl memorial lecture. *American Journal of Human Biology*, 14(5):641–648.

Meek, T. H., Lonquich, B. P., Hannon, R. M., and Garland, T. (2009). Endurance capacity of mice selectively bred for high voluntary wheel running. *Journal of Experimental Biology*, 212(18):2908–2917.

Migliore, S., Brown, E., and DeWeerth, S. (2005). Biologically Inspired Joint Stiffness Control. *Proceedings of the 2005 IEEE International Conference on Robotics and Automation*, (April):4508–4513.

Migliore, S. A. (2008). *The Role of Passive Joint Stiffness and Active Knee Control in Robotic Leg Swinging: Applications to Dynamic Walking*. PhD thesis, Georgia Institute of Technology.

Minetti, A. E., Capelli, C., Zamparo, P., Di Prampero, P. E., Saibene, F., et al. (1995). Effects of stride frequency on mechanical power and energy expenditure of walking. *Medicine and science in sports and exercise*, 27:1194–1194.

Morita, T. and Sugano, S. (1997). Development and evaluation of seven dof mia arm. In *Robotics and Automation, 1997. Proceedings., 1997 IEEE International Conference on*, volume 1, pages 462–467.

Nakanishi, J. and Vijayakumar, S. (2012). Exploiting passive dynamics with variable stiffness actuation in robot brachiation. In *Robotics: Science and Systems*.

Park, J.-J., Kim, H.-S., and Song, J.-B. (2009). Safe robot arm with safe joint mechanism using nonlinear spring system for collision safety. In *Robotics and Automation, 2009. ICRA '09. IEEE International Conference on*, pages 3371–3376.

Park, J.-J., Lee, Y.-J., Song, J.-B., and Kim, H.-S. (2008). Safe joint mechanism based on nonlinear stiffness for safe human-robot collision. *2008 IEEE International Conference on Robotics and Automation*, pages 2177–2182.

Park, J.-J. and Song, J.-B. (2010). Safe joint mechanism using inclined link with springs for collision safety and positioning accuracy of a robot arm. In *Robotics and Automation (ICRA), 2010 IEEE International Conference on*, pages 813–818.

Parker, T. S. and Chua, L. O. (1987). Chaos: A tutorial for engineers. *Proceedings of the IEEE*, 75(8):982–1008.

Patoor, E., Lagoudas, D. C., Entchev, P. B., Brinson, L. C., and Gao, X. (2006). Shape memory alloys, part i: General properties and modeling of single crystals. *Mechanics of Materials*, 38(5):391–429.

Petit, F., Chalon, M., Friedl, W., Grebenstein, M., Albu-Schaeffer, A.ffer, A., and Hirzinger, G. (2010). Bidirectional antagonistic variable stiffness actuation: Analysis, design amp; implementation. In *Robotics and Automation (ICRA), 2010 IEEE International Conference on*, pages 4189–4196.

Pfeifer, R. and Bongard, J. (2007). *How the body shapes the way we think: a new view of intelligence*. MIT press.

Pfeifer, R., Lungarella, M., and Iida, F. (2007). Self-organization, embodiment, and biologically inspired robotics. *Science (New York, N.Y.)*, 318(5853):1088–93.

Pfeifer, R., Lungarella, M., and Iida, F. (2012). The challenges ahead for bio-inspired'soft'robotics. *Communications of the ACM*, 55(11):76–87.

Pfeifer, R. and Scheier, C. (1999). *Understanding intelligence*. MIT Press, Cambridge, MA, USA.

Raibert, M. (1986a). Legged robots that ballance. *MIT press, Cambridge*.

Raibert, M., Blankespoor, K., Nelson, G., Playter, R., et al. (2008). Bigdog, the rough-terrain quadruped robot. In *Proceedings of the 17th World Congress*, pages 10823–10825.

Raibert, M., Brown, B., and Chepponis, M. (1984). Experiments in balance with a 3d one-legged hopping machine. *The International Journal of Robotics Research*, 3(2):75–92.

Raibert, M. and Brown, H. B. (1984). Experiments in balance with a 2d one-legged hopping machine. *ASME Journal of Dynamic Systems, Measurement, and Control*, 106:75–81.

Raibert, M., Chepponis, M., and Brown Jr, H. (1986). Running on four legs as though they were one. *Robotics and Automation, IEEE Journal of*, 2(2):70–82.

Raibert, M. H. (1986b). Legged robots. *Communications of the ACM*, 29:499–514.

Raynor, A. J., Yi, C. J., Abernethy, B., and Jong, Q. J. (2002). Are transitions in human gait determined by mechanical, kinetic or energetic factors? *Human movement science*, 21(5):785–805.

Reis, M. and Iida, F. (2013). An energy-efficient hopping robot based on free vibration of a curved beam. *Mechatronics, IEEE/ASME Transactions on*, PP(99):1–12.

Reis, M., Yu, X., Maheshwari, N., and Iida, F. (2013). Morphological computation of multi-gaited robot locomotion based on free vibration. *Artificial life*, 19(1):97–114.

Roberts, T. J., Marsh, R. L., Weyand, P. G., and Taylor, C. R. (1997). Muscular force in running turkeys: The economy of minimizing work. *Science*, 275(5303):1113–1115.

Rodriguez, A. G., Chacon, J., Donoso, A., and Rodriguez, A. G. (2011). Design of an adjustable-stiffness spring: Mathematical modeling and simulation, fabrication and experimental validation. *Mechanism and Machine Theory*, 46(12):1970 – 1979.

Sakagami, Y., Watanabe, R., Aoyama, C., Matsunaga, S., Higaki, N., and Fujimura, K. (2002). The intelligent asimo: system overview and integration. In *IEEE/RSJ International Conference on Intelligent Robots and Systems*, volume 3, pages 2478–2483.

Sanders, R. H. and Wilson, B. D. (1992). Modification of movement patterns to accomodate to a change in surface compliance in a drop jumping task. *Human movement science*, 11(5):593–614.

Sardain, P. and Bessonnet, G. (2004). Forces acting on a biped robot. center of pressure-zero moment point. *Systems, Man and Cybernetics, Part A: Systems and Humans, IEEE Transactions on*, 34(5):630–637.

Schiavi, R., Grioli, G., Sen, S., and Bicchi, a. (2008). VSA-II: a novel prototype of variable stiffness actuator for safe and performing robots interacting with humans. *2008 IEEE International Conference on Robotics and Automation*, pages 2171–2176.

Schmidt, H., Werner, C., Bernhardt, R., Hesse, S., and Krüger, J. (2007). Gait rehabilitation machines based on programmable footplates. *Journal of neuroengineering and rehabilitation*, 4(1):2.

Seyfarth, A., Friedrichs, A., Wank, V., and Blickhan, R. (1999). Dynamics of the long jump. *Journal of Biomechanics*, 32(12):1259 – 1267.

Shan, Y., Philen, M., Lotfi, A., Li, S., Bakis, C. E., Rahn, C. D., and Wang, K.-W. (2009). Variable stiffness structures utilizing fluidic flexible matrix composites. *Journal of Intelligent Material Systems and Structures*, 20(4):443–456.

Spence, A. J., Revzen, S., Seipel, J., Mullens, C., and Full, R. J. (2010). Insects running on elastic surfaces. *The Journal of experimental biology*, 213(11):1907–20.

Sun, L., Huang, W., Ding, Z., Zhao, Y., Wang, C., Purnawali, H., and Tang, C. (2012). Stimulus-responsive shape memory materials: a review. *Materials & Design*, 33:577–640.

Tagliamonte, N. L., Sergi, F., Accoto, D., Carpino, G., and Guglielmelli, E. (2012). Double actuation architectures for rendering variable impedance in compliant robots: A review. *Mechatronics*, 22(8):1187–1203.

Taylor, C. R., Heglund, N. C., and Maloiy, G. (1982). Energetics and mechanics of terrestrial locomotion. i. metabolic energy consumption as a function of speed and body size in birds and mammals. *Journal of Experimental Biology*, 97(1):1–21.

Tonietti, G., Schiavi, R., and Bicchi, a. (2005). Design and Control of a Variable Stiffness Actuator for Safe and Fast Physical Human/Robot Interaction. *Proceedings of the 2005 IEEE International Conference on Robotics and Automation*, (April):526–531.

Tsagarakis, N., Sardellitti, I., and Caldwell, D. (2011). A new variable stiffness actuator (compact-vsa): Design and modelling. In *Intelligent Robots and Systems (IROS), 2011 IEEE/RSJ International Conference on*, pages 378–383.

Tupper, M., Munshi, N., Beavers, F., Gall, K., Mikuls Jr, M., and Meink, T. (2001). Developments in elastic memory composite materials for spacecraft deployable structures. In *Aerospace Conference, 2001, IEEE Proceedings.*, volume 5, pages 2541–2547. IEEE.

Umberger, B. R. (2008). Effects of suppressing arm swing on kinematics, kinetics, and energetics of human walking. *Journal of biomechanics*, 41(11):2575–2580.

Vanderborght, B., Albu-Schaeffer, A., Bicchi, A., Burdet, E., Caldwell, D., Carloni, R., Catalano, M., Eiberger, O., Friedl, W., Ganesh, G., et al. (2013). Variable impedance actuators: a review. *Robotics and Autonomous Systems*, 61(12):1601–1614.

Vanderborght, B., Albu-Schäffer, A., Bicchi, A., Burdet, E., Caldwell, D., Carloni, R., Catalano, M., Ganesh, G., Garabini, M., Grebenstein, M., et al. (2012). Variable impedance actuators: Moving the robots of tomorrow. In *Intelligent Robots and Systems (IROS), 2012 IEEE/RSJ International Conference on*, pages 5454–5455.

Vanderborght, B., Tsagarakis, N. G., Ham, R., Thorson, I., and Caldwell, D. G. (2011). MACCEPA 2.0: compliant actuator used for energy efficient hopping robot Chobino1D. *Autonomous Robots*, 31(1):55–65.

Vanderborght, B., Tsagarakis, N. G., Semini, C., Van Ham, R., and Caldwell, D. G. (2009). MACCEPA 2.0: Adjustable compliant actuator with stiffening characteristic for energy efficient hopping. *Proceedings of the IEEE International Conference on Robotics and Automation (2009)*, pages 544–549.

Visser, L. C., Carloni, R., and Stramigioli, S. (2011). Energy-efficient variable stiffness actuators. *IEEE Transactions on Robotics*, 27(5):865–875.

Vu, H. (2013). Knee stiffness adjustment for energy efficient locomotion of a legged robot on surfaces with different stiffnes. In *accepted to The IEEE Robotics and Biomimetics conference, ROBIO 2013*.

Vu, H., Aryananda, L., Sheikh, F. I., Flurin, C., and Rolf, P. (2011). A novel mechanism for varying stiffness via changing transmission angle. In *Proceedings of the RIEEE International Conference on Robotics and Automation*, pages 5076–5081.

Vu, H., Hauser, H., and Pfeifer, R. (2013). A variable stiffness mechanism for improving energy efficiency of a planar single-legged hopping robot. In *accepted to The 16th International Conference on Advanced Robotics, ICAR 2013*.

Wei, Z., Sandstroröm, R., and Miyazaki, S. (1998). Shape-memory materials and hybrid composites for smart systems: Part i shape-memory materials. *Journal of Materials Science*, 33(15):3743–3762.

Wisse, M. (2005). Three additions to passive dynamic walking: actuation, an upper body, and 3d stability. *International Journal of Humanoid Robotics*, 2(04):459–478.

Wolf, S., Eiberger, O., and Hirzinger, G. (2011). The DLR FSJ: Energy based design of a variable stiffness joint. In *Robotics and Automation (ICRA), 2011 IEEE International Conference on*, pages 5082 –5089.

Wolf, S. and Hirzinger, G. (2008). A new variable stiffness design: Matching requirements of the next robot generation. *2008 IEEE International Conference on Robotics and Automation*, pages 1741–1746.

Zarrugh, M. Y. and Radcliffe, C. W. (1978). Predicting metabolic cost of level walking. *European Journal of Applied Physiology and Occupational Physiology*, 38(3):215–223.

Zupan, M., Ashby, M. F., and Fleck, N. A. (2002). Actuator classification and selection - the development of a database. *Advanced engineering materials*, 4(12):933–940.

Chapter 7

Appendix

Appendix A

Determinants of Variable Stiffness Mechanisms

Reprinted from: Amir Jafari, Hung Q. Vu, Fumiya Iida, "Determinants of Variable Stiffness Mechanisms," submitted to The International Journal of Robotics Research, in Oct. 2013.

Determinants for Stiffness Adjustment Mechanisms

Amir Jafari[†], Hung Quy Vu[‡], and Fumiya Iida[†]

Abstract

Variable stiffness actuators (VSAs) are a new generation of robotic drives that are developed to enhance the robots efficiency and ability to safely interact with unknown and dynamic environments. To adjust the stiffness, different mechanisms have been implemented in VSAs, each to fulfill the requirements of certain applications. Each application determines some essential properties that have to be addressed by the stiffness adjustment mechanisms of VSAs. This paper explains these determinants and presents a comprehensive framework to systematically analyze performances of different stiffness adjustment mechanisms. First, a classification of different stiffness adjustment mechanisms is presented. Then, characteristics of each class regarding different determinants are evaluated and compared through numerical analyses. This will give additional insights into intrinsic pros and cons of different classes of stiffness adjustment mechanisms that enable a systematic future development of variable stiffness actuators and their applications.

Keywords- Variable Stiffness Actuators, Stiffness Adjustment Mechanisms, Determinants, Optimal Design, Mechanism Theory.

1 Introduction

There are many robotic applications where the ability to adjust the stiffness is a plus if not a must. The capability of stiffness regulation can enhance the robot's functions in several aspects. For instance, safety to humans and swiftness of motion are very important and can be guaranteed by tuning the stiffness while the robot is physically interacting or even possibly colliding with the humans and their environment [Bicchi and Tonietti (2004)]. Efficiency can also be improved by regulating the stiffness in e.g., natural gait generation [Vanderborght et al. (2008)], adaptation in legged locomotion applications [Stramigioli et al. (2008)] and prosthetics for lower limbs [Cherelle et al. (2012)]. In addition, adaptability and force accuracy of the interaction can also be increased through adjusting the stiffness. The continuous contact and accurate force exchange are vital in many applications such as in hands-on assistive devices, rehabilitation [Bureau et al. (2011)], exoskeletons [Beyl et al. (2009)] and haptics [Alaimo et al. (2011)]. Furthermore, ability to tune the stiffness improves robustness to external perturbations and unpredictable model errors. These uncertainties could be due to changes of the environment, of the robot kinematics and dynamics, or of the dynamics of a human interacting with it. The robustness to external perturbations is often required in tasks like hammering, holding cups, drumming [Catalano et al. (2011)]; typical tasks with tools such as screwdriving, cutting, polishing [Yang et al. (2011)], drawing [Grebenstein et al. (2010)] or stabilizing a humanoid [Li et al. (2012)].

Therefore, varying elasticity is widely acknowledged if its advantages are properly exploited. Consequently, different variable stiffness actuators (VSAs) have been developed so far, each to fulfill requirements of certain applications. The stiffness regulation in these VSAs is achieved by using different stiffness adjustment mechanisms.

Despite the remarkable potential advantages of VSAs, the practical use of such actuators is still very limited due to several reasons. First of all, usually a VSA occupies large space and has more weight/inertia compare to a traditional rigid or fixed compliant actuator. In addition, in many VSAs, regulating the stiffness requires considerable amount of energy consumption which prevents exploiting

*This research was funded by the Swiss National Science Foundation through the National Centre of Competence in Research Robotics.

‡Artificial Intelligence Laboratory, Department of Informatics, University of Zurich, Switzerland.

†Bio-Inspired Robotics Laboratory, Institute of Robotics and Intelligent Systems, Swiss Federal Institute of Technology Zurich, Switzerland.

stiffness variation in many tasks [Vanderborght et al. (2009)]. Furthermore changing the stiffness may affect the system's behavior which in turn requires employing sophisticated control approaches [Sardellitti et al. (2012)].

From this perspective, the main goal of this paper is to develop a comprehensive framework that systematically explains the performances and characteristics of VSAs. We believe that a deeper understanding about the inherent properties of the stiffness adjustment mechanisms, employed in different VSAs, is essential and would allow us to better exploit the advantages and avoid the disadvantages of such mechanisms in many applications. We particularly focus on five representative "determinants" that serve as the theoretical backbone of further developing VSAs for practical applications.

This paper is organized as follows; in section 2, a classification is made among different VSAs with respect to their stiffness adjustment mechanisms. Then in section 3, the representative determinants are introduced and evaluated for each class. Some numerical analysis is done to evaluate the performances of different classes. Section 4 compares the results and section 5 gives some insights about pros and cons of each mechanism and the conclusions.

2 Stiffness Adjustment Approaches

There is a large variety of VSAs in the literature. The mechanical designs of VSAs are very heterogeneous and can be implemented with different types of motors, speed-reducers and force/torque transmission systems. Such components should be combined in a proper way to match encumbrances, weight, force, power and stiffness requirements. Therefore their performances can be highly variable and hardly comparable. In order to systematically analyze their performance, a classification of different stiffness adjustment approaches is required. Some classifications have been already presented by [Ham et al. (2009); Tagliamonte et al. (2012); Vanderborght et al. (2013)]. However, since in this paper, the focus is on the stiffness adjustment mechanisms of VSAs, the classification presented here, is based on the arrangements of the essential elements within these mechanisms. A typical stiffness adjustment mechanism consists of two actuation units, e.g., motors, compliant elements, e.g., springs and the output link which is in contact with the external environment. Such a classification is presented in Tab. 1. In general, there are two main approaches to regulate the stiffness, namely, antagonistic and series.

2.1 Antagonistic approach

Antagonistic approach is motivated by the arrangement of muscles such as biceps and triceps in the human arm [Hogan (1984)]. When the biceps contract and the triceps relaxes, the arm is flexed. When the triceps contracts and the biceps relaxes, the arm extends. However, when both biceps and triceps contract, the elbow becomes stiff and when they both relax, the elbow becomes very compliant and the arm hangs freely. In fact, the muscles in the human arm are controlled in a continuous way and, thus, the system can cover a range of positions and compliant behaviors. Inspired from the human musculoskeletal system, in the antagonistic approach, two actuation units are antagonistically actuating an output link via elastic elements, e.g., springs. Springs which have nonlinear force-deflection profiles (nonlinear springs), are placed between the actuation units and the output link. Based on different arrangements of the actuation units and springs, this approach has been realized in three different classes: simple unidirectional (C1), cross coupled (C2) and bidirectional mechanisms (C3).

- **C1**: Simple Antagonistic

  In the simplest class of antagonistic approaches, as it is shown in Tab. 1, each actuation unit is connected to the output link through a nonlinear unidirectional spring. Unidirectional springs can apply force in only one direction (either push or pull the output link). Therefore, only one actuation unit at each time can apply force to move the output link. Examples of this class are: Biologically inspired joint stiffness control [Migliore et al. (2005)], Actuator with Mechanically Adjustable Series Compliance (AMASC) [Hurst et al. (2010)], and Plated Pneumatic Artificial Muscles (PPAM) [Darden (1999)].

- **C2**: Cross coupled

Table 1: Classification of different VSA classes. The VSAs in classes: C1, C2, C3, C4 change the stiffness by changing the pretension of nonlinear springs. Instead, the stiffnesses of VSAs in classes: C5, C6, and C7 are changed through (a) the load-spring transmission via altering the lever arm ratio in class C5, (b) the load-spring transmission via altering the transmission angle in class C6, and (c) changing the effective physical properties of compliant beams in class C7. The bold arrows (⟶)are presented as "regulators".

Approaches	Classes	Examples	Schemes
Antagonistic	**C1**: Simple antagonistic	Biologically inspired joint stiffness control [Migliore et al. (2005)] Actuator with Mechanically Adjustable Series Compliance (AMASC) [Hurst et al. (2010)] Plated Pneumatic Artificial Muscles (PPAM) [Darden (1999)]	
	C2: Cross coupled	Variable Stiffness Actuator (VSA) [Tonietti et al. (2005)]	
	C3: Bidirectional	Variable Stiffness Actuator-II (VSA-II) [Schiavi et al. (2008)] , VSA-CUBE [Catalano et al. (2011)], Bidirectional Antagonism with Variable Stiffness (BAVS) [Petit et al. (2010)] ,	
Series	**C4**: Pretension of nonlinear spring	Mechanically Adjustable and Controllable Compliance Equilibrium Position Actuator (MACCEPA) [Van Ham et al. (2006)] and (MACCEPA 2.0) [Vanderborght et al. (2011)] , Variable Stiffness Joint (VS-joint) [Wolf and Hirzinger (2008)], Safe Joint Mechanism (SJM I) [Park et al. (2009)] and (SJM II) [Park and Song (2010)], Floating Spring Joint (FSJ)[Wolf et al. (2011)]	
	C5: Changing load-spring transmission ratio via lever arm ratio	Actuator with Adjustable Stiffness (AwAS-I) [Jafari et al. (2010)] and (AwAS-II) [Jafari et al. (2012b)] Compact Variable Stiffness Actuator (ComPact-VSA) [Tsagarakis et al. (2011)] Energy Efficient Variable Stiffness Actuator [Visser et al. (2011)] Variable Stiffness Actuator University of Twente [Groothuis et al. (2012); Fumagalli et al. (2012)] Hybrid Dual Actuation Unit (HDAU) [Kim and Song (2010),Kim and Song (2012)]	
	C6: Changing load-spring transmission ratio via transmission angle	Mechanism for Varying Stiffness via Transmission Angle [Vu et al. (2011)], Floating Spring Joint (FSJ)[Wolf et al. (2011)], Human-friendly VSA [Hyun et al. (2010)],VSA-HD [Catalano et al. (2010)], DLR Q-A joint [Eiberger et al. (2010)].	
	C7: Changing effective physical properties	Structure Controlled Stiffness (SCS) [Hollander and Sugar (2004)], Jack-spring [Hollander et al. (2005)], Changing beam length [Morita and Sugano (1997); Choi et al. (2011)], Adjustable stiffness spring [Rodriguez et al. (2011)]	

In this class, one additional nonlinear spring is placed between the two actuation units. The additional springs permits the full steering of the link by each actuator. Thanks to that, the maximum generated force per actuation unit can be set to the half of maximum force of the similar unidirectional mechanism to obtain an equivalent maximum force at the output link. The Variable Stiffness Actuator (VSA) [Tonietti et al. (2005)] is an example of this class.

- **C3**: Bidirectional

  In this class, each actuation unit is connected to the output link through a pair of nonlinear springs. Each pair consists of two nonlinear springs in opposite force direction. Therefore, each actuation unit is able to push and pull the output link due to the bidirectional arrangement of corresponding nonlinear springs. This solution again allows to transmit the maximum generated force of each actuation unit to the output link. Examples of this class are: Variable Stiffness Actuator-II (VSA-II) [Schiavi et al. 2008], VSA-CUBE [Castalano et al. 2011], Bidirectional Antagonism with Variable Stiffness (BAVS) [Petit et al. (2010)].

2.2 Series approach

In the other design approach, one actuation unit with springs in series is employed to control link position and other unit changes its stiffness, independently. Since in this approach, the desired position of the output link is controlled only by the first actuation unit, thus, it is called series design approach. Typically, the second actuation unit is not employed to control the position, but the stiffness of the output link. As a contrast, the VSAs in antagonistic approaches employ the parallel actuation scheme in which the output position of the link is algebraically summed up by the displacement of two actuation units.

Based on the principles to change stiffness, VSAs that employs the series approach are categorized into four classes as follows. In the first series class, the spring's deflection is altered to tune the stiffness (C4). In addition to that, other series designs have also been implemented where the stiffness is regulated through changing either the lever arm ratio (C5), or the load-spring transmission ratio via transmission angle (C6) or the physical structural stiffness of elastic structure (C7).

- **C4**: Changing pretension of nonlinear spring

  In this class of series design approach, the first actuation unit is connected to the output link via springs to control the link position, whereas the second one regulates the pretension of such spring as shown in Tab. 1. Since the spring is nonlinear, the spring stiffness can be altered by changing the deflection. Some examples of this class are: Mechanically Adjustable and Controllable Compliance Equilibrium Position Actuator (MACCEPA) [Van Ham et al. (2006)], (MACCEPA 2.0) [Vanderborght et al. (2011)], Varaible Stiffness Joint (VS-joint) [Wolf and Hirzinger (2008)], Safe Joint Mechanism (SJM I) [Park et al. (2008)] and (SJM II) [Park and Song (2010)]. It should be mentioned here that, these examples employ linear springs. However, the stiffness adjustment mechanisms in this class can provide nonlinear force-deflection profiles as the springs are deflected. Therefore, these springs are considered nonlinear springs.

- **C5**: Changing load-spring transmission ratio via lever arm ratio

  The VSAs in this class changes the transmission ratio between input force and the spring deflection through variation of a lever mechanism. In the mechanism design, a lever has three principal points: the pivot, i.e., the point around which the lever can rotate; the spring attachment point, i.e., the point at which springs are located; the force point, i.e., the point at which the force is applied to the lever. By changing the position of one of the three, the lever stiffness can can be varied. As conceptually depicted in Tab. 1, the stiffness regulation in this class can be done without directly deflecting the springs. Some newly developed VSAs in this class are: Actuator with Adjustable Stiffness (AwAS-I) [Jafari et al. (2010)], (AwAS-II) [Jafari et al. (2012b)], Compact Variable Stiffness Actuator (ComPact-VSA) [Tsagarakis et al. (2011)], Energy Efficient Variable Stiffness Actuator [Visser et al. (2011)] and Variable Stiffness Actuator University of Twente [Carloni et al. (2012)].

- **C6**: Changing load-spring transmission ratio via transmission angle

Similar to class C5, the force transmission between the output link and the spring is also altered for different stiffness in this class. However, instead of regulating principal points of the lever arm, this class regulates the transmission angle between the direction of force applied to the spring and the spring neutral axis. Note that the spring is only delectable in specific direction under load, e.g., the direction that is parallel to spring neutral axis for linear springs. Thus, the force transmission ratio can be altered to any degree by varying the such angle. This design principle also allows for using linear springs. Some examples of VSAs belonging to this class are as follows. The Mechanism for Varying Stiffness via Changing Transmission Angle (MESTRAN) [Vu et al. (2011)], which regulates the stiffness by changing transmission angle between the output force and deflection of the output link. The other example of this class is the FSJ actuator [Wolf et al. (2011)], which changes the stiffness of the output link by varying the pressure angle between the normal of the cam surface and the spring axis as a lower stiffness can be achieved when the pressure angle is reduced. Exploiting the transmission angle by different link configuration, VSA-HD [Catalano et al. (2010)] can also vary the stiffness in a relatively large range. Infinite stiffness can be achieved when two transmission links are straight-up. A simpler solution employing this approach can be obtained from [Hyun et al. (2010)], in which only two levels of stiffness are achieved by two separated fixed cam surfaces.

- **C7**: Changing effective physical properties

  Unlike the other VSA classes, in this class, the stiffness of the output link can be modulated by varying the effective physical structure of the structural elements. For example, the beam stiffness can be changed by varying the effective length, the sectional area, and elastic modulus of beam material. As it is presented in [Morita and Sugano (1997); Hollander et al. (2005); Choi et al. (2011); Rodriguez et al. (2011)], changing the length of the beam can provide a continuous range of stiffness modulation as long as the length can be changed in a continuous manner. The second approach is to vary the cross sectional areas W, that, basically, varies the anti-bending/twisting moment of the structure as shown by [Hollander and Sugar (2004)]. In this work, there however exist only two stiffness levels that are the low and high stiffness, corresponding to the two ways of orienting the elastic beam. In the practical implementation, it is impossible to change the stiffness while the link is under load. The third approach can potentially be implemented is to change the material modulus E. This approach is often implemented by employing some smart materials as SMAs or EAPs [Anderson et al. (2013); Carpi et al. (2008)]. However, currently, the change of stiffness is not sufficiently fast and, in the state of the art VSAs, there are no known VSAs employing this principle yet.

Based on this classification, in the next section, we will introduce a mathematical framework by which the performance of seven representative class can be systematically analyzed. Although there are asymmetrical VSAs designs for antagonist and series classes, in this paper, we only consider symmetrical designs, in which the springs and the actuators are arranged symmetrically with respect to the output link. Furthermore, for a simplification of analysis, the whole performance analysis is based on translational models. Thus, we can neglect the effect of the radius of the pulley, which is usually attached to the output link. As a result, only three parameters, i.e., K_{max}, K_{min}, and x_{lmax} are sufficient to formulate all performance determinants of all classes. The proposed framework is presented in a generic manner so as to the same analyses can be implemented for a particular rotational VSA.

3 Performance Analysis

The seven classes of stiffness adjustment mechanisms mentioned in the previous section are comparable regardless of the actual mechanical implementation. This implies that all the different implementation can be built with components that shows equivalent performances. In this section, we systematically analyze the performances and characteristics of each class of stiffness adjustment mechanisms (C1 to C7) on the basis of seven representatives "determinants" (D1 to D5). These determinants are imperative measures in applications, where regulating the stiffness is essential.

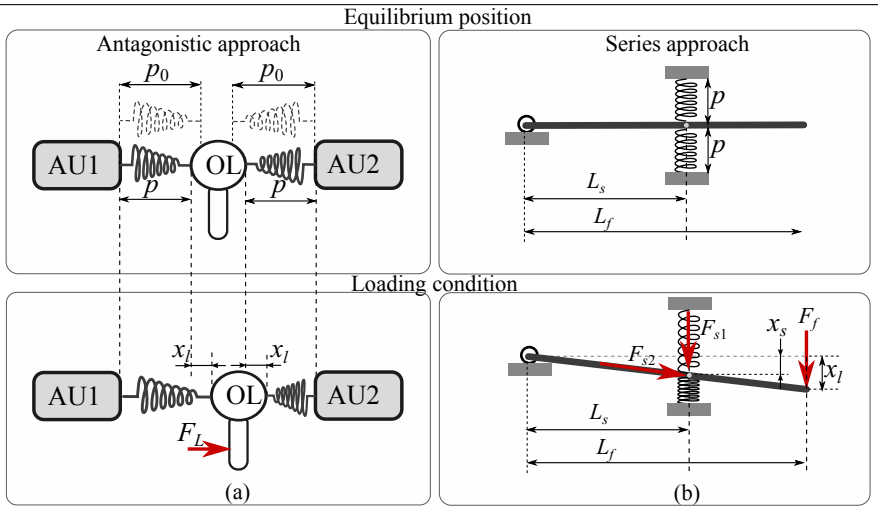

Figure 1: Two representative classes C1 and C5; AU and OL denote for actuation unit and output link. (a) from antagonistic approach- class C1: where the output link is deviated by x_l from its equilibrium due to the force F_L. p is the pre-deflection of the springs, (b) from series approach- class C5: Compliant lever mechanism: where the output link is deviated by x_l due to the applied force F_f. L_s is the distance between the spring's location and the pivot and L_f is the lever length. s is the spring's deflection and F_s1 and F_s2 are the spring force and the resistive force to increase the stiffness.

3.1 Mathematical formulation of stiffness

The evaluation of each determinant is based on the static case where friction forces and inertias of the moving objects can be neglected. To perform a fair comparison, the maximum output link deflection x_{lmax}, the minimum K_{min} and the maximum K_{max} stiffness of the output link (when the link is not deflected) are equally set for all the classes as 100 [N/m], 1000[N/m], and 0.01[m], respectively. For those classes which employ nonlinear springs, there are a number of possible choices on different types of nonlinearity, thus, a general mathematical framework to analyze those springs in a generic form is useful. For this reason, we mainly present a generic approach to derive the stiffness and determinant formulations through the whole paper. For numerical analysis via determinants, we specifically present the calculation of five determinants over two representative classes of VSA based on four types of springs: linear, quadratic, cubic, and exponential ones, which are commonly chosen for VSAs in the literature [Vanderborght et al. (2013)]. Eventhough we focus only on four types of spring, extending this approach to the other types of nonlinear spring can be implemented in a similar fashion.

The force due to the deflection for each type of linear and nonlinear springs can be given by:

$$F_x = f(x) = \begin{cases} K_s x & \rightarrow Linear \\ K_{sq} x^2 & \rightarrow Quadratic \\ K_{sc} x^3 & \rightarrow Cubic \\ K_{se}(e^x - 1) & \rightarrow Exponential, \end{cases} \tag{1}$$

where K_s, K_{sq}, K_{sc} and K_{se} denote the spring's constant in each type, and x is the spring deflection. For a linear spring, the spring's constant is also stiffness of the spring. However for nonlinear springs, stiffness is different from the spring's constant. The spring stiffness in each type is the derivative of the force with respect to the displacement:

$$K = g(x) = \frac{\partial f(x)}{\partial x}. \tag{2}$$

The energy stored in the spring due to the its deflection can be given by

$$h(x) = \int f(x)dx. \tag{3}$$

As we present later in this paper, there are five determinants to be investigated over seven classes of VSAs. Thus, to clarify the presentation of the paper, each determinant is analytically evaluated for one class (C1) of the antagonistic approach and one class (C5) of the series approach and then the results are presented. For other classes, the same method is applied, but only the results are presented. In addition, some of detailed implementation of the method can be founded in [Jafari et al. (2012a)].

3.1.1 Formulation of stiffness adjustment in C1

To formulate the stiffness in C1, let's consider Figure 1 where the output link deviates to the right side from its equilibrium position by x_l. In this configuration, the force applied to the output link can be given by:

$$F_L = f(p + x_l) - f(p - x_l), \tag{4}$$

where p is the pre-deflection of the springs when the output link is not loaded. Then the stiffness is the derivative of this force with respect to the position of the output link.

$$K = \frac{\partial[f(p + x_l) - f(p - x_l)]}{\partial x_l}. \tag{5}$$

When the output link is at its no-load equilibrium position ($x_l = 0$), based on Eq. 2, the stiffness can be re-written as:

$$K_{(x_l=0)} = \frac{\partial f(p + x_l)}{\partial(p + x_l)}\frac{\partial(p + x_l)}{\partial x_l} - \frac{\partial f(p - x_l)}{\partial(p - x_l)}\frac{\partial(p - x_l)}{\partial x_l} = 2g(p), \tag{6}$$

and the pre-deflection of the springs can then be calculated for both minimum and maximum levels of stiffness as:

$$p_{min} = g^{-1}(\frac{K_{min}}{2}); \quad p_{max} = g^{-1}(\frac{K_{max}}{2}), \tag{7}$$

where $g^{-1}(x)$ is inverse function of $g(x)$.

There is one important implementation concern; when the output link becomes fully deflected, the deflection in one spring increases while in the other one it reduces, both by the magnitude of x_{lmax}. The spring which reduces its deflection, however, cannot experience negative deflection due to its unidirectionality. In the worst case (where one spring has minimum pre-deflection and the output link is fully deflected toward the other spring), the deflection becomes zero. Therefore we constraint that:

$$p_{min} = x_{lmax}. \tag{8}$$

By substituting Eq. 7 and Eq. 8 into Eq. 6, we can obtain the link stiffness at no-load condition.

3.1.2 Formulation of stiffness adjustment in C5

Among the other classes which employ linear springs and alter the stiffness not by changing the deflection, i.e., C5 to C7, changing the load-spring transmission via the lever arm ratio (i.e., C5) is considered as a representative example. Let's consider Figure 1, where a lever with the length of L_f deflects (rotates around its pivot) by x_l due to the force applied at the output link. The position of the spring with respect to the pivot point is L_s. The deflection of the springs as the link is at displacement x_l can be found as:

$$s = x_l\frac{L_s}{L_f}, \tag{9}$$

and the spring force :

$$F_{s1} = K_s s. \tag{10}$$

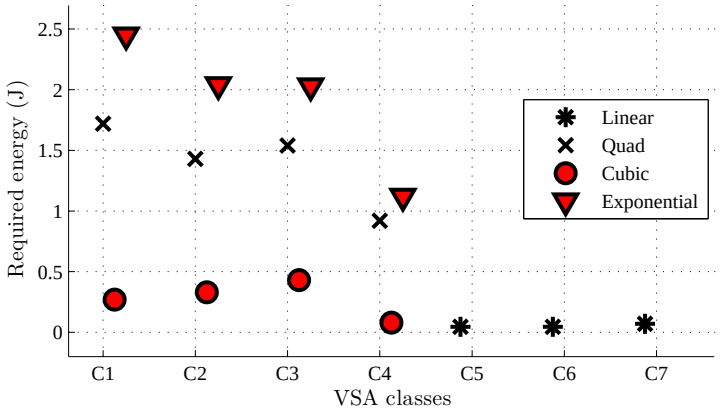

Figure 2: Energy required to change the stiffness (D1) from 100N/m to 1000N/m while the output link is deviated from its equilibrium position by 0.01m, using different types of springs from C1 to C7.

Therefore, the force applied to the link can be calculated as

$$F_L = F_{s1}\frac{L_s}{L_f}. \tag{11}$$

The vertical stiffness which is felt at the tip of the lever can be found as

$$K = \frac{F_L}{x_l} = K_s\left(\frac{L_s}{L_f}\right)^2. \tag{12}$$

3.2 Determinant evaluation

3.2.1 D1: Required energy to adjust the stiffness

Theoretically, changing the stiffness while the link is deflected regulates the potential energy stored at the link, thus, energy must be spent by actuation units to change the corresponding parameters: the spring deflection (C1-C4), lever arm ratio (C5), transmission angle (C6), or effective length of beams (C7). This required amount of energy varies with the amount of the link deflection and different principles of VSAs. For example, when the link is not loaded and the deflection of the output link is zero, some do not requires energy to maintain the stiffness [Jafari et al. (2012b); Visser et al. (2011), whereas others consume energy to keep the stiffness constant [Schiavi et al. (2008); Vanderborght et al. (2011)]. In order to calculate the energy required to change the stiffness, we need to integrate the resistive force produced by actuation units over the displacement of the stiffness mechanism, which is required to change the corresponding parameter.
In class C1, for a given type of spring we investigate, both actuation units have to apply force to increase the p from its minimum to the maximum, which results in increased stiffness. Therefore, the required energy to change the stiffness, while the link is fully deflected can be given by:

$$E = \int_{p_{min}}^{p_{max}} f(p + x_{lmax})dq + \int_{p_{min}}^{p_{max}} f(p - x_{lmax})dq, \tag{13}$$

where the first and the second terms in the right present the energy consumption of the first and the second actuation unit to increase the stiffness from K_{min} to K_{max} while the link is deflected to x_{lmax}.

From this perspective, we can call it, i.e., E in Eq. 13, the input energy E_{in}. Considering Eq. 2, Eq. 3, Eq. 13 and this energy can be re-formulated as:

$$E = E_{in} = \begin{aligned} & h\left[g^{-1}\left(\frac{K_{max}}{2}\right) + x_{lmax}\right] + h\left[g^{-1}\left(\frac{K_{max}}{2}\right) - x_{lmax}\right] \\ & -h\left[g^{-1}\left(\frac{K_{min}}{2}\right) + x_{lmax}\right] - h\left[g^{-1}\left(\frac{K_{min}}{2}\right) - x_{lmax}\right]. \end{aligned} \tag{14}$$

Until this step, the values of the three already set parameters ($K_{min}, K_{max}$and x_{lmax}) are not sufficient to numerically calculate this energy as the term K_s (spring constant) will appear in the formula. However, based on Eq. 7 and Eq. 8 the spring's constant K_s can be determined and then the required energy for changing the stiffness can be calculated as a function of $K_{min,}K_{max}$ and x_{lmax}. The same method can be used to calculate E_{in} for other classes which tune the stiffness by changing the spring's deflection i.e., classes C2 to C4.

In class C5, when the link is deflected, the force due to the spring's deflection will have a projection (resistive force F_{s2}) along the lever as:

$$F_{s2} = F_{s1}\sin\alpha = K_s\frac{L_s}{L_f}x_{lmax}\sin\alpha. \tag{15}$$

Assuming α is small, the resistive force can be simplified as

$$F_{s2} \approx K_s\frac{L_s}{L_f}x_{lmax}. \tag{16}$$

To increase the stiffness, this resistive force F_{s2} has to be overcome along the lever while the springs are moving. Therefore the required energy to change the stiffness is:

$$E_{in} = \int_{L_{smin}}^{L_{smax}} F_{s2}dL_s. \tag{17}$$

Let the maximum allowable ratio L_s/L_f be 1, we obtain $L_{smax} = L_f$. From Eq. 12, the following relations can be achieved:

$$K_{min} = K_s\left(\frac{L_{smin}}{L_f}\right)^2 \qquad \text{and} \qquad K_{max} = K_s\left(\frac{L_{smax}}{L_f}\right)^2 = K_s\left(\frac{L_f}{L_f}\right)^2. \tag{18}$$

From Eq. 18, we can write:

$$L_{smin} = L_f\left(\frac{K_{min}}{K_{max}}\right)^{0.5}. \tag{19}$$

Therefore, substituting Eq. 16 and Eq. 19 into Eq. 17, the required energy to change the stiffness while the output link is deflected to its maximum deflection can be formulated as:

$$E_{in} = \frac{1}{2}[K_{max} - K_{min}]x_{lmax}^2 \tag{20}$$

Figure 2 summarizes the required energy to change the stiffness for C1 to C7, considering linear, quadratic, exponential and cubic springs. To calculate the maximum required input energy, the output link is considered to be always deflected to its maximum deflection while the stiffness is regulated. As the figure suggests, classes of series approach, require less input energy than the classes of antagonistic approach. Furthermore, in antagonistic approach, using the cubic springs leads to require less input energy than using quadratic or exponential springs.

3.2.2 D2: Required force to maintain the stiffness

The force to keep the stiffness constant while the link is deflected is obviously not avoidable for all classes of VSA design and also proportionally changed with the load. However, the forces that the actuation units have to hold the corresponding parameters, e.g., spring deflection, in order to maintain the stiffness unchanged significantly varies, depending on specific designs. In many applications, e.g., legged robots running at a constant frequency or speed, the stiffness can be kept constant for most of

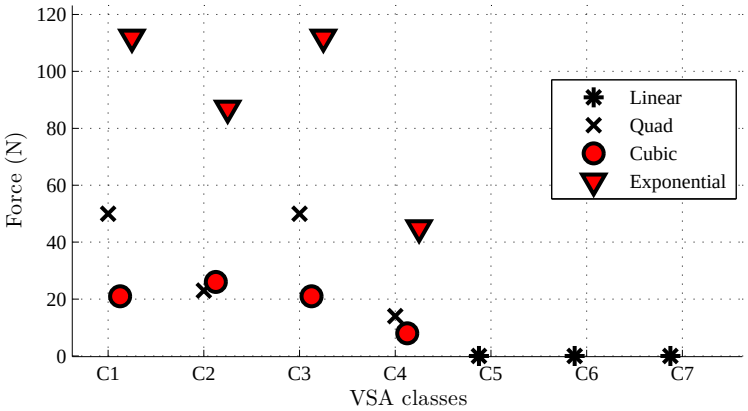

Figure 3: Force requirement to keep the maximum stiffness (D2) 1000N/m using different types of springs in C1 to C7 .

the operational time and is only required to change when necessary. For the systems employed VSAs in such applications, it is crucial to design VSAs that can maintain the stiffness with a minimal amount of energy or, optimally, no requiring energy. Thus, the determinant of force requirement to hold the stiffness while the link is at its equilibrium is essential to be investigated.

To calculate the force to hold the stiffness mechanism under no-load condition, the same for the previous determinant D1, here, the force required to maintain the stiffness is formulated for two classes of stiffness adjustment mechanisms, i.e., C1 and C5.

In C1, to maintain the stiffness at a certain level, each actuation unit has to insert force to keep the springs deflected. Therefore, the force required to maintain the stiffness at its maximum level K_{max} depends on the force which corresponds to the maximum deflection p_{max}. In simple antagonistic class C1, when the output link is not deflected, this force is given by:

$$\begin{aligned} F_{\binom{K=K_{max}}{\&x_l=0}} &= f(p_{max} + x_{lmax}) + f(p_{max} - x_{lmax}) \\ &= 2f\left(g^{-1}(\frac{K_{max}}{2})\right). \end{aligned} \tag{21}$$

In the class C5, however, when the lever is not deflected, spring's force would have no projection as it is perpendicular to the lever. Thus no force would be required to maintain the stiffness when the output link is not deflected. The same holds true for class C6 and C7.

Figure 3 shows the force requirement to maintain the maximum stiffness for the same classes and springs. It is obvious that the series approach requires less force to maintain the stiffness than the antagonistic approach. Using the cubic springs in the antagonistic approach, however, reduces the required force to maintain the stiffness. It can be observed that employing systems with the VSA in class C1, C2, and C3 in the applications where the stiffness is rarely required to change would reduce the energy efficiency of systems drastically.

Nevertheless, the choice of the series versus the antagonistic approach for a VSA design is not trivial. In principle, the force to keep the stiffness constant can be held without requiring energy via mechanical solutions as non-back drivable gear mechanisms. On the one hand, such gear mechanisms allow for the removal of the energy to hold stiffness, thus, it can significantly improve the energy efficiency of the stiffness actuation unit if changing stiffness are not required frequently. This advantage would then suggest VSA designers to choose the series design, instead of the antagonistic one. On the other hand, employing back-drivable gear mechanisms can reduce mechanical complexity, thus, leading to the reduction of power losses in friction and added inertias, in comparison to non-back drivable ones. For those VSAs with back-drivable mechanisms, Figure 3 presents the actual force that has to be generated by actuation units, which can serve as one of criteria for design selection between different mechanism

solutions.

3.2.3 D3: Energy efficiency of stiffness adjustment

In conventional rigid actuator, actuation unit is rigidly connected to the output link. However in a VSA, there is the stiffness adjustment mechanism between the output link and the actuation units. The stiffness adjustment mechanism receives energy from the actuation unit (E_i) and delivers energy to the output link (E_0). In the static case, where only the stiffness of the output link is changing through the actuation units and the position is fixed, the output energy is in fact the potential energy of the output link. Therefore it can be calculated as

$$E_0 = \int_0^{x_l} \int_0^{x_l} K dx. \tag{22}$$

The input energy is the energy which is supplied by the actuation units into the stiffness adjustment mechanism during stiffness regulation. The energy efficiency of the stiffness adjustment mechanism can be defined as the ratio between the output and the input energy:

$$\eta = \frac{E_0}{E_{in}} \tag{23}$$

To make the concept of energy efficiency of stiffness adjustment more clear, lets consider the output link of a VSA as a spring (with adjustable stiffness). If the output link is deflected by an external load to a certain deflection, then there is a potential energy stored in the link due to its compliance. Now assume that the stiffness of the VSA increases while the deflection in kept fixed. The potential energy of the link will increase in this case, since it is a function of joint stiffness and the deflection. However, on the other hand, to increase the stiffness, the VSA has to consume energy. In the optimal scenario, this consumed energy is equal to the added potential energy of the output link. This means all the energy spent to regulate the stiffness is stored in the output link which can be used later to move it. For the numerical analysis of this determinant, again classes C1 and C5 are considered. In the simple antagonistic design C1, when the link is fully deflected and its stiffness is minimum, the potential energy is:

$$E_{p_{min}} = \int_0^{x_{lmax}} \int_0^{x_{lmax}} K_{min} dx. \tag{24}$$

By increasing the stiffness to its maximum level, the link's potential energy becomes:

$$E_{p_{max}} = \int_0^{x_{lmax}} \int_0^{x_{lmax}} K_{max} dx. \tag{25}$$

Therefore, the potential energy added to the link can be given by:

$$E_0 = E_{p_{max}} - E_{p_{min}}. \tag{26}$$

Using Eq. 8 and Eq. 26 and based on Eq. 23, the energy efficiency of stiffness adjustment can be calculated for the simple antagonistic mechanism. Figure 4 presents the energy efficiency of the stiffness adjustment for the same mechanisms and springs mentioned in Table 2. In AwAS [Jafari et al. (2010)], as an example for the C5 class, the potential energy of the lever can be calculated as:

$$\begin{aligned} E_0 &= \int_0^{x_{lmax}} \int_0^{x_{lmax}} K_{max} dx - \int_0^{x_{lmax}} \int_0^{x_{lmax}} K_{min} dx \\ &= \frac{1}{2}[K_{max} - K_{min}] x_{lmax}^2. \end{aligned} \tag{27}$$

This energy is exactly equal to Eq. 20. Therefore the energy efficiency of stiffness adjustment for this mechanism is 100%. The energy efficiency of stiffness adjustment for C6 and C7 is also 100% as presented in Figure 4.

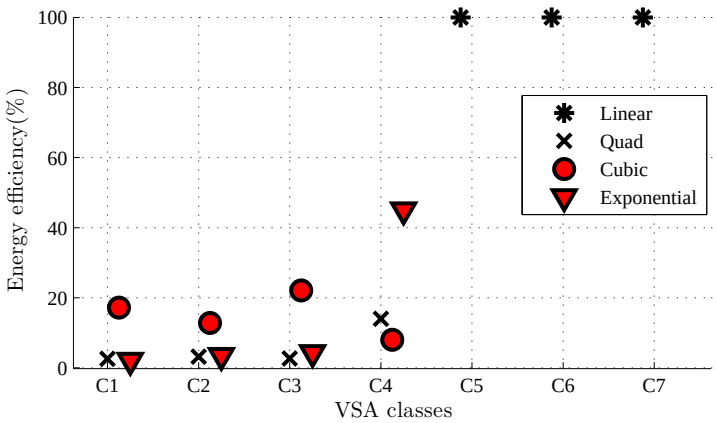

Figure 4: Energy efficiency of stiffness adjustment (D3) from 100N/m to 1000N/m using different types of springs in C1 to C7 .

3.2.4 D4: Accessibility to the maximum energy storage

This determinant is complementary to the previous one. As it was mentioned before, due to the compliant elements, e.g., springs, the stiffness adjustment mechanisms can store the energy. When all the springs are fully deflected, the maximum amount of energy is stored into this mechanism. This energy can be formulated as:

$$E_s = \sum_{i=1}^{n} \int_0^{s_{imax}} \int_0^{s_{imax}} K_{s_i} ds_i, \tag{28}$$

where s_i and K_{si} are deflection and stiffness of the ith spring, respectively. n is the number of springs and s_{imax} is the maximum allowable deflection of the ith spring. Accessibility to the maximum energy storage can be defined as a ratio between the maximum potential energy of the output link and the maximum energy storage of the stiffness adjustment mechanism.

$$\alpha = \frac{E_0}{E_s} \tag{29}$$

In an optimal case, this maximum energy should be accessible by the output link. This means that the full capacity of energy storage can be transmitted to the output link ($E_0 = E_s$) and so no fraction of this storage is wasted due to the other implementation constraints. Here again, this determinant is formulated for C1 from the antagonistic and C5 from the series approaches.

In the simple antagonistic design C1, two springs are used. The maximum energy which can be stored at the stiffness adjustment mechanism is

$$E_s = 2 \int_{p_{min}}^{p_{max}} f(p + x_{l_{max}}) dp. \tag{30}$$

Using Eq. 26 and Eq. 30 and based on Eq. 29, the accessibility to the maximum energy storage can be calculated for the simple antagonistic mechanism. Figure 5 presents the accessibility to the maximum energy storage for the same mechanisms and springs mentioned in Figure 4. In AwAS [Jafari et al. (2010)], as an example for the C5 class, there is an implementation concern. In principle, springs are either compression or extension. Therefore two springs are placed at each side of the lever to realize the compliant behavior in both directions (upward and downward). Now, suppose the lever is deflected downward (as it was shown in Tab. 1), thus the bottom springs becomes deflected. However, we need to guarantee the connection between the lever and the upper spring. This means that springs have t be inserted with a pre-deflection. In fact, this pre-deflection has to be half of the spring's maximum deflection ($p = 0.5 s_{max}$). The maximum energy which can be stored in the stiffness adjustment mechanism is

$$E_s = 2 \int_0^{s_{max}} K_s s ds \tag{31}$$

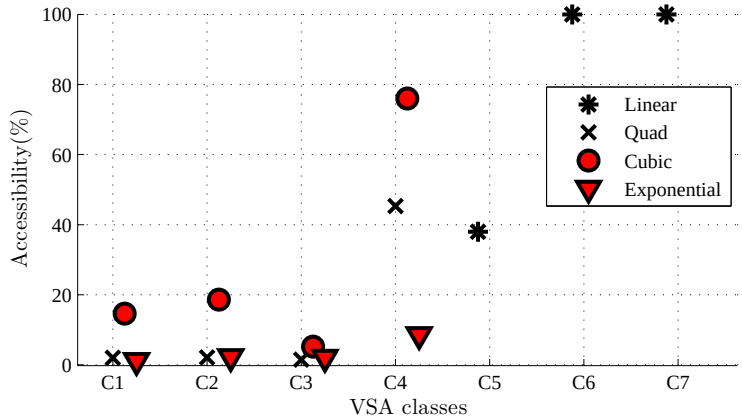

Figure 5: Accessibility to the maximum energy storage (D4) in C1 to C7 with different types of springs .

Using Eq. 27 and Eq. 31 and based on Eq. 29, the accessibility to the maximum energy storage for this mechanism is about 38%. Therefore, even in this class of stiffness adjustment mechanism, some part of energy storage capacity is not transmittable to the link side. In contrast, in the case of C6 and C7, it is possible that the full capacity of the elastic elements as beams or springs can be fully exploited, the accessibility to the maximum energy storage can reach 100%.

3.2.5 D5:Coupling between the deflection and the stiffness

In many applications of VSAs such as impedance control of haptic devices, it is usually desired to set the stiffness to a preset level of stiffness and maintain this level while the output link deflects. Stiffness should be changed only through the mechanism dedicated for the stiffness adjustment but not by any external load. This implies the necessity of a linear relationship between the external load and angular deflection, or in the other words, stiffness should not be a function of external loads. This property makes force control easy as a fixed term of stiffness will be appeared in the dynamics of the link and the deflection of the link can be linearly converted to the contact force. For instance the control approach proposed by [Sardellitti et al. (2012)], is only applicable to VSAs in which stiffness and the load are decoupled. In most of the antagonistic designs, load and stiffness are strongly coupled, as the deflection of the output link changes the spring deflection and so the stiffness varies by the spring deflection. However, nonlinearity of the springs in antagonistic designs can greatly affect this coupling. In order to evaluate the decoupling between the load and the stiffness, we investigate in this subsection the degrees of coupling in the classes C1 and C5 by analyzing the correlation between external load and stiffness.

In the class C1, from Eq. 1 and Eq. 4, we can obtain force acting on four types of spring as follows:

$$F_x = \begin{cases} K_s[(p+x_l)-(p-x_l)] & \rightarrow Linear \\ K_{sq}[(p+x_l)^2-(p-x_l)^2] & \rightarrow Quadratic \\ K_{sc}[(p+x_l)^3-(p-x_l)^3] & \rightarrow Cubic \\ K_{se}[e^{(p+x_l)}-e^{(p-x_l)}], & \rightarrow Exponential \end{cases} \tag{32}$$

and, thus, the stiffness of the output link can be found as :

$$K = \frac{\partial F_x}{\partial x_l} = \begin{cases} 2K_s \\ 4K_{sq}p \\ 6K_{sc}[x_l^2+p^2] \\ K_{se}[e^p(e^{xl}-e^{-xl})]. \end{cases} \tag{33}$$

As it is clear from the above equation, the stiffness with linear springs is not adjustable by pretension and, in case of quadratic springs, stiffness is completely independent (i.e., decoupled) from deflection

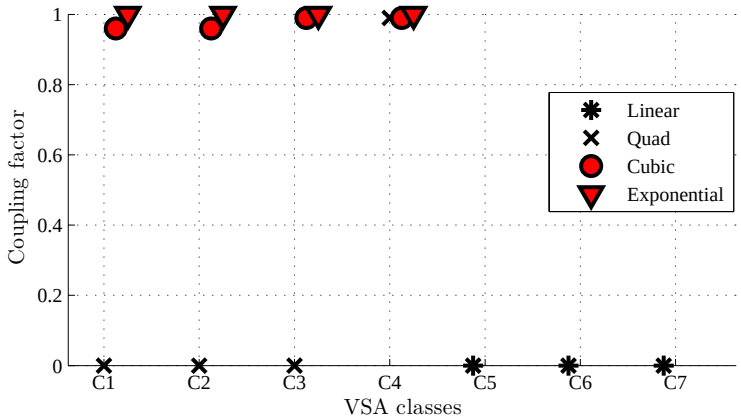

Figure 6: Evaluation of coupling between deflection and stiffness (D5) in C1 to C7 with different types of springs.

of the output link. However, for the other types of nonlinear springs, stiffness is a function of output link deflection x_l, thus the deflection and the stiffness are coupled. We analyze the degrees of the couplings by measuring a linear correlation (i.e., the Pearson product-moment correlation coefficient). More specifically the coefficient between between stiffness and deflection indicates zero when they are totally decoupled, whereas it increases as the stiffness changes with the deflection.

Here we only analyze the coupling coefficient of the cubic and exponential spring types when they are set to their maximum stiffness with $p \rightarrow p_{max}$ in order to emphasize the salient differences (We disregard the linear and quadratic spring types because we already know they are fully decoupled as explained above). For this calculation, we first rewrite the stiffness equation Eq.33 as follows:

$$K_x = \begin{cases} K_{sc}(6p_{sc.max}^2 + 6x_l^2) & \rightarrow Quadratic \\ K_{se}(e^{p_{se.max}+x_l} + e^{p_{se.max}-x_l}) & \rightarrow Exponential, \end{cases} \tag{34}$$

where

$$K_{sc} = K_{min}/(6x_{max}^2)$$
$$K_{se} = K_{min}/(2e^{x_{lmax}}),$$

and

$$p_{sc.max} = x_{lmax}\sqrt{K_{max}/K_{min}}$$
$$p_{se.max} = ln[K_{max}/K_{min}] + x_{lmax}.$$

From these equations, we are now able to calculate the coupling coefficients of these two spring types. Specifically, given K_s and p_{max}, we can numerically derive the degrees of correlation between deflection x_l and stiffness K_x. The same method can be also applied to the other antagonistic classes, and the results are shown in Figure 6. In case of the series classes, the stiffness is a function of spring deflection and spring constant. Moreover, in the first class of series design C4, stiffness is a function of spring's deflection and as the output load changes, it affects the stiffness. In the class of C5, however, the load has a minor effect on the stiffness as it is clear from Eq.12. In the class C6, MESTRAN [Vu et al. (2011)] achieves a linear relation between the force and link's deflection. In this mechanism, a cam profile is designed in such a way that rotating the output link linearly deflects the springs. In this way, stiffness and load are decoupled.

3.2.6 Other determinants

So far we introduced five determinants that can characterize performances of the different VSA classes. There are, however, many other determinants that can be critical for some robotic applications. In this subsection we introduce three other potentially important determinants that we analyzed additionally, although we keep the explanations minimum because these determinants are largely dependent on the design specifics of VSA mechanisms and difficult to generalize.

- Range of stiffness adjustment (D-RS)

  Range of stiffness adjustment is an important performance metric that can significantly influence application opportunities of VSAs. While the range should be ideally adjusted from zero stiffness (i.e., completely passive) to infinite (i.e., completely rigid), none of the existing VSAs can achieve such a performance because of the physical constraints originated in the mechanical designs.

  Among the VSAs introduced earlier in this paper, the largest range of stiffness adjustment can be achieved by AWAS-II [Jafari et al. (2012b)], VSA-compact[Tsagarakis et al. (2011)] from the class C5 or VSA-HD [Catalano et al. (2010)] and MESTRAN [Vu et al. (2011)] from the class C6, which are capable of varying stiffness from a very small value to almost infinity due to their specific mechanical designs. In contrast to these approaches, the ranges of the other VSAs are usually restricted by the maximum forces of nonlinear springs particularly in the classes C1, C2, and C3, thus it is challenging to make the mechanisms simple and compact.

  Another important factor of this determinant is continuity in the stiffness range. As an extreme case, a large range of adjustment can be achieved by a discrete coupling SCS Hollander and Sugar (2004) or [Leach et al. (2012)] although it is often necessary to have a continuous adjustment of stiffness over a large range.

- Added inertia to output link (D-IS)

  The output link is where the actuator is in contact with its surrounding environment. In human robot interaction applications, for example, it is vital to guarantee the safety where the robot physically contacts the human body. Therefore, the output link has to be as light and low inertia as possible such that the robots can be back drivable against the forces generated by humans. Compared to normal actuators, VSAs have some additional components due to their stiffness adjustment mechanisms which usually increase the inertia. The optimal design in this case is the one in which the inertia is added to the actuation units, rather than to the output link.

  In general, the antagonistic designs (C1 to C3) have a greater advantage since the output link does not carry the stiffness adjustment mechanism. In contrast, in all the series designs (C4 to C7), the stiffness adjustment mechanism as well as the second actuation unit is directly connected to the output link which considerably increases the inertia at the output link. The degrees of back drivability, however, are dependent on the mechanical design of the mechanisms.

- Speed to change stiffness (D-SS)

  Rapid adjustment of stiffness is always desired in the VSA applications, and often it is a must. Again the speed of stiffness adjustment is largely dependent on the specifics of mechanical and mechanism designs as well as the applications in which the actuators are used, and it is difficult to generalized. However we can extract a few principles based on the classifications of different VSA mechanisms. For example, in the classes C1, C2, C3 and C4, the mechanisms exploits adjustment of pretension in the nonlinear springs, and the actuation units have to work against the springs to adjust the stiffness even in the case of the output shaft at a rest position without load. This mechanism-oriented fact imposes the intrinsic slow speed of stiffness adjustment because the actuation units sacrifice speed for generating larger forces. In contrast, the classes C5, C6, and C7 have a better chance to increase the speed of stiffness adjustment, because the stiffness adjustment mechanisms are decoupled from the spring pretension, and a faster actuation unit (without large force output) can be used. It is also important to mention that mechanism of discrete stiffness adjustment can be superior for this determines if the applications require no continuous stiffness adjustment. Typically in this type of mechanisms, it is possible to optimize the mechanical designs for faster motion control with small force requirement [Leach et al. (2012)].

4 Discussion

Despite many case studies of mechanisms and applications of VSAs in the past, there are still a number of open problems and challenges in this area of research. The complex nature of this research field is, in our view, originated in two distinctive reasons: On the one hand, there are many tasks and applications where VSAs can be beneficial while different tasks require different specifications[Tagliamonte et al. (2012)]. On the other hand, every VSA has relatively complex mechanisms and requires many components to be optimized in many ways. This is why so many different types of VSAs were developed and reported in the past, and it is important to generalize the categories and the design principles among many of VSA mechanisms [Tagliamonte et al. (2012); Ham et al. (2009); Vanderborght et al. (2013)], which can be meaningful for both developers and researchers of VSAs in the future. From this perspective, based on the exploration of classes and determinants above, this section attempts to summarize the principles and case studies.

4.1 Design principles of VSAs

In general, there are two basic optimization criteria in the design and control strategies of VSAs. The first criterion is to focus on the optimization of energy and power requirements which are essentially exemplified by the determinants D1, D2, and D3. By designing efficient mechanisms and using smaller actuation units, the strategy toward these determinants usually leads to more compact and lighter VSAs as C5, C6, and C7, given a target performance of stiffness adjustment. In contrast, the second criterion considers more about the other performances of stiffness adjustment such as (D4) accessible energy capacity, (D5) stiffness-deflection coupling, and the other determinants. Compared to the first one, the VSAs based on the second criterion are typically larger and energetically inefficient, whereas they can generate better performances in terms of some of the determinants.

From the quantified analysis in some of the determinants above, these two optimization criteria can be explained as a trade-off. For example, VSAs in the series approach are usually more efficient and compact because they use smaller actuation units for stiffness adjustment. This mechanism, in turn, has to impose the other actuation unit to carry complex structures with significant mass, which degrades the back drivability of actuators due to the added inertial constraints. To achieve better back drivability, the antagonistic approach is the right choice although it sacrifices efficiency and compactness because two actuation units are always counteracting to each other (which eventually result in comparatively larger actuation units). It is however worth mentioning that VSAs in the antagonistic approach have usually simpler mechanical designs despite their requirements of comparatively large actuation units.

In addition to this basic trade-off, we have also learned many other potential design principles from the numerical analysis given earlier in this paper. For example, the best strategy to maximize accessibility of maximum energy capacity (D4) is the VSA class C4, although we found no solution to decouple the nonlinearity in the relation between stiffness and output link deflection (D5) when we have to employ the C4 mechanism. In contrast to the VSA class C1 to C4 in terms of the decoupling coefficient, the deflection of the output link in class C5, C6, and C7 is almost decoupled from the stiffness (D5). Another criterion that can potentially improve the performance of VSAs is the range of stiffness adjustment. For the classes C1-4, the range of stiffness adjustment depends on the stall torque of actuation units even when no load applies to the output link. However, the VSA class C5-7 can provide a unlimited range of stiffness adjustment,from zero to infinity, when the output at its equilibrium. Under the deflection of the output link, the range of stiffness adjustment for classes C5, C6, and C7 are also dependent on the provided stall torque of the actuation units. Nevertheless, the ability of C5,C6, and C7 to change the stiffness in a large range can significantly enhances the scalability of the mechanism, since it can be realized in a very small scale without affecting the stiffness range. Lastly, the criterion concerning the speed to change the stiffness is found also dependent on specific designs, e.g., the power of actuation units, and loading condition. The evaluation of the speed to change the stiffness has to be associated with the load applied to the output link.

The list of design principles here is by no means complete, and there should be many others depending on the types of VSAs to be included in the analysis. The intention of this analysis in this paper was to include as broad variations of VSAs as possible, while this approach makes it harder to obtain more generalized determinants. From this perspective, it is also important, in the future, to continue more detailed analysis of subset of VSA types by considering more specifics of mechanical designs, and so on.

4.2 Case studies of VSA applications

While there are many applications that can benefit from VSAs, they often require specific characteristics in VSAs to be implemented. Based on the exploration different types of VSAs in terms of performances and characteristics, we are now able to extend our analysis to discuss pros and cons for different applications. Again this analysis is not supposed to be a complete list of the analysis of VSA applications, but we attempt to demonstrate how the classes and determinants can be beneficial for the researchers and developers of the applications.

In the human-robot-interaction applications where a robot has to closely interact with humans, the robot needs to fulfill the safety requirement while performing fast and precise positioning tasks, for example [Khatib (1999); Albu-Schaffer et al. (2005); Albu-Schäffer et al. (2007); De Santis et al. (2008); Pfeifer et al. (2012)]. In such an application, back drivability of VSAs should be one of the most important features (D-IS) in addition to the capability of adjusting large range of stiffness (D-SS). For these reasons, this type of applications should make use of the VSA classes C1, C2 and C3, as demonstrated in the past by [Zinn et al. (2004); Bicchi and Tonietti (2004)].

When considering exoskeleton and prosthetic devices, VSAs to be implemented need to fulfill the energy efficiency and size/weight criteria to minimize the consumption of energy from onboard batteries and load exerted to human users [Hurst and Rizzi (2008)]. Even though this application require similar actuation characteristics to those in the human-robot-interaction applications, it is necessary to consider the determinants on energy efficiency and power requirements (i.e., D1, D2 and D3) , thus the VSA classes C4, C5, C6 and C7 become more preferable mechanisms for these applications [Hurst (2008); Vanderborght et al. (2011); Enoch et al. (2012); Galloway (2013)]. The legged robot locomotion has similar requirements as the prosthetic devices [Giorgio Carpino and Guglielmelli (2012)] but this application usually considers larger ranges of payload and controllability. From this perspective, we suggest the determinant D4 (accessibility to the maximum energy storage) in addition to D1, D2, and D3 for this application as explained above, as a result the VSA class C4 and C6 could be a superior choice among others. A similar argument holds also for the other dynamic tasks such as hammering and throwing which require a large amount of energy to be given to the output shaft thus C4 and C5 are recommended [Wolf and Hirzinger (2008); Park and Song (2010); Nakanishi and Vijayakumar (2012); Garabini et al. (2012); Haddadin et al. (2012)].

There are a series of applications that require accurate control of stiffness such as haptic devices and fine manipulation, in which the decoupling of stiffness and output shaft deflection (e.g., D5) is crucial. From our analysis above, these applications should consider the VSA class C5 and C6, in addition to C1 and C2 as long as they use the quadratic nonlinear springs. However, to enlarge the adjustable range of stiffness in these applications, the class C5 and C6 [Jafari et al. (2012b); Vu et al. (2011); Catalano et al. (2010); Groothuis et al. (2012)] seems to be a good option according to the discussion in D6 .

5 Conclusion

This paper presented a systematic analysis about design principles and performance of the current state of the art of variable stiffness actuators. To analyze the performances of different stiffness adjustment mechanisms for each determinant, a classification over existing VSAs was presented. Five determinants: D1 to D5 for stiffness adjustment mechanisms were analytically defined and analyzed.

Through the analysis in the paper, on the one hand, it is suggested that the classes of antagonist design approach are better choices toward safety while those of the series design approach are more energy efficient with a higher degree of functionality and controllability. On the other hand, the VSAs in series classes are more advantageous to improve energy efficiency of systems employed VSAs. Nevertheless, the important conclusion from the results of the whole paper is the fact that there is no class of stiffness adjustment mechanism which is suitable for all the applications. The reason is due to two conflicting drawbacks intrinsically associated with each design approach.

Finally, to develop an optimal stiffness adjustment mechanism which can satisfy all the determinants and can be used in any application, a new design approach, rather than antagonistic or series, is yet to be proposed.

References

Alaimo, S., Pollini, L., Bresciani, J.-P., and Bülthoff, H. (2011). Evaluation of direct and indirect haptic aiding in an obstacle avoidance task for tele-operated systems. pages 6472–6477, Red Hook, NY, USA. Max-Planck-Gesellschaft, Curran.

Albu-Schaffer, A., Bicchi, A., Boccadamo, G., Chatila, R., De Luca, A., De Santis, A., Giralt, G., Hirzinger, G., Lippiello, V., Mattone, R., et al. (2005). Physical human–robot interaction in anthropic domains: safety and dependability. In *Proceedings of the 4th IARP/IEEE-RAS/EURON Workshop on Technical Challenges for Dependable Robots in Human Environments, T17-06, Nagoya, June 16-18.*

Albu-Schäffer, A., Haddadin, S., Ott, C., Stemmer, A., Wimböck, T., and Hirzinger, G. (2007). The dlr lightweight robot: design and control concepts for robots in human environments. *Industrial Robot: An International Journal*, 34(5):376–385.

Anderson, W., Eshghinejad, a., Azadegan, R., Cooper, C., and Elahinia, M. (2013). A variable stiffness transverse mode shape memory alloy actuator as a minimally invasive organ positioner. *The European Physical Journal Special Topics*, 222(7):1503–1518.

Beyl, P., Cherelle, P., Knaepen, K., and Lefeber, D. (2009). A proof-of-concept exoskeleton for robot-assisted rehabilitation of gait. In Sloten, J., Verdonck, P., Nyssen, M., and Haueisen, J., editors, *4th European Conference of the International Federation for Medical and Biological Engineering*, volume 22 of *IFMBE Proceedings*, pages 1825–1829. Springer Berlin Heidelberg.

Bicchi, A. and Tonietti, G. (2004). Fast and soft arm tactics: Dealing with the safety-performance trade-off in robot arms design and control. *IEEE Robotics and Automation Magazine*, 11(2):22–33.

Bureau, M., Keller, T., Perry, J., Velik, R., and Veneman, J. (2011). Variable stiffness structure for limb attachment. In *Rehabilitation Robotics (ICORR), 2011 IEEE International Conference on*, pages 1–4.

Carloni, R., Visser, L., and Stramigioli, S. (2012). Variable stiffness actuators: A port-based power-flow analysis. *Robotics, IEEE Transactions on*, 28(1):1–11.

Carpi, F., DeRossi, D., Kornbluh, R., Pelrine, R., and Sommer-Larsen, P. (2008). *Dielectric elastomers as electromechanical transducers. Fundamentals, materials, devices, models and applications of an emerging electroactive polymer technology.* Elsevier Press.

Catalano, M., Grioli, G., Bonomo, F., Schiavi, R., and Bicchi, A. (2010). Vsa-hd: From the enumeration analysis to the prototypical implementation. In *Intelligent Robots and Systems (IROS), 2010 IEEE/RSJ International Conference on*, pages 3676–3681.

Catalano, M., Grioli, G., Garabini, M., Bonomo, F., Mancinit, M., Tsagarakis, N., and Bicchi, A. (2011). Vsa-cubebot: A modular variable stiffness platform for multiple degrees of freedom robots. In *Robotics and Automation (ICRA), 2011 IEEE International Conference on*, pages 5090–5095.

Cherelle, P., Matthys, A., Grosu, V. Brackx, B., Van Damme, M., Vanderborght, B., and Lefeber, D. (2012). Design of the amp-foot 2.0 : An active trans-tibial prosthesis that mimicks able-bodied ankle behavior. In *The 2nd Joint International Conference on Multibody System Dynamics.*

Choi, J., Hong, S., Lee, W., Kang, S., and Kim, M. (2011). A robot joint with variable stiffness using leaf springs. *Robotics, IEEE Transactions on*, 27(2):229–238.

Darden, F. (1999). *Conception and Realization of Pleated Pneumatic Artificial Muscles and their Use as Compliant Actuation Elements.* PhD thesis, Vrije Universiteit Brussel.

De Santis, A., Siciliano, B., De Luca, A., and Bicchi, A. (2008). An atlas of physical human?robot interaction. *Mechanism and Machine Theory*, 43(3):253–270.

Eiberger, O., Haddadin, S., Weis, M., Albu-Schaeffer, A., and Hirzinger, G. (2010). On joint design with intrinsic variable compliance: derivation of the DLR QA-joint. In *Robotics and Automation (ICRA), 2010 IEEE International Conference on*, pages 1687–1694.

Enoch, A., Sutas, A., Nakaoka, S., and Vijayakumar, S. (2012). BLUE : A Bipedal Robot with Variable Stiffness and Damping. *Proc. 12th IEEE-RAS International Conference on Humanoid Robots, Osaka, Japan (2012)*.

Fumagalli, M., Barrett, E., Stramigioli, S., and Carloni, R. (2012). The mvsa-ut: A miniaturized differential mechanism for a continuous rotational variable stiffness actuator. In *Biomedical Robotics and Biomechatronics (BioRob), 2012 4th IEEE RAS EMBS International Conference on*, pages 1943–1948.

Galloway, K. C. (2013). Variable Stiffness Legs for Robust, Efficient, and Stable Dynamic Running. *Journal of Mechanisms and Robotics*, 5(1):011009.

Garabini, M., Passaglia, A., Belo, F., Salaris, P., and Bicchi, A. (2012). Optimality principles in stiffness control: The vsa kick. In *Robotics and Automation (ICRA), 2012 IEEE International Conference on*, pages 3341–3346. IEEE.

Giorgio Carpino, Dino Accoto, F. S. N. L. T. and Guglielmelli, E. (2012). A novel compact torsional spring for series elastic actuators for assistive wearable robots. *Journal of Mechanical Design*, 134(12).

Grebenstein, M., Chalon, M., Hirzinger, G., and Siegwart, R. (2010). Antagonistically driven finger design for the anthropomorphic dlr hand arm system. In *Humanoid Robots (Humanoids), 2010 10th IEEE-RAS International Conference on*, pages 609–616. IEEE.

Groothuis, S. S., Rusticelli, G., Zucchelli, A., Stramigioli, S., and Carloni, R. (2012). The vsaut-ii: A novel rotational variable stiffness actuator. In *Robotics and Automation (ICRA), 2012 IEEE International Conference on*, pages 3355–3360.

Haddadin, S., Huber, F., and Albu-Schaffer, A. (2012). Optimal control for exploiting the natural dynamics of variable stiffness robots. In *Robotics and Automation (ICRA), 2012 IEEE International Conference on*, pages 3347–3354. IEEE.

Ham, R., Sugar, T., Vanderborght, B., Hollander, K., and Lefeber, D. (2009). Compliant actuator designs. *Robotics Automation Magazine, IEEE*, 16(3):81–94.

Hogan, N. (1984). Adaptive control of mechanical impedance by coactivation of antagonist muscles. *Automatic Control, IEEE Transactions on*, 29(8):681–690.

Hollander, K. and Sugar, T. (2004). Concepts for compliant actuation in wearable robotic systems. In *Proceeding of US-Korea Conference on Science, Technology and Entrepreneurship (UKC04)*, volume 128, pages 644–650.

Hollander, K., Sugar, T., and Herring, D. (2005). Adjustable robotic tendon using a 'jack spring' trade;. In *Rehabilitation Robotics, 2005. ICORR 2005. 9th International Conference on*, pages 113–118.

Hurst, J. and Rizzi, A. (2008). Series compliance for an efficient running gait. *Robotics & Automation Magazine, IEEE*, 15(3):42–51.

Hurst, J. W. (2008). *The Role and Implementation of Compliance in Legged Locomotion*. PhD thesis, Robotics Institute, Carnegie Mellon University, Pittsburgh, PA.

Hurst, J. W., Chestnutt, J. E., and Rizzi, A. A. (2010). The actuator with mechanically adjustable series compliance. *Robotics, IEEE Transactions on*, 26(4):597–606.

Hyun, D., Yang, H. S., Park, J., and Shim, Y. (2010). Variable stiffness mechanism for human-friendly robots. *Mechanism and Machine Theory*, 45(6):880 – 897.

Jafari, A., Tsagarakis, N., Sardellitti, I., and Caldwell, D. (2012a). How design can affect the energy required to regulate the stiffness in variable stiffness actuators. In *Robotics and Automation (ICRA), 2012 IEEE International Conference on*, pages 2792–2797.

Jafari, A., Tsagarakis, N., Vanderborght, B., and Caldwell, D. (2010). A novel actuator with adjustable stiffness (awas). In *Intelligent Robots and Systems (IROS), 2010 IEEE/RSJ International Conference on*, pages 4201–4206.

Jafari, A., Tsagarakis, N. G., Sardellitti, I., and Caldwell, D. G. (2012b). A new actuator with adjustable stiffness based on a variable ratio lever mechanism. *Mechatronics, IEEE/ASME Transactions on*, PP(99):1–9.

Khatib, O. (1999). Mobile manipulation: The robotic assistant. *Robotics and Autonomous Systems*, 26(2):175–183.

Kim, B.-S. and Song, J.-B. (2010). Hybrid dual actuator unit: A design of a variable stiffness actuator based on an adjustable moment arm mechanism. In *Robotics and Automation (ICRA), 2010 IEEE International Conference on*, pages 1655–1660.

Kim, B.-S. and Song, J.-B. (2012). Design and control of a variable stiffness actuator based on adjustable moment arm. *Robotics, IEEE Transactions on*, 28(5):1145–1151.

Leach, D., Gunther, F., Maheshwari, N., and Iida, F. (2012). Linear multi-modal actuation through discrete coupling. In *Intelligent Robots and Systems (IROS), 2012 IEEE/RSJ International Conference on*, pages 2437–2442.

Li, Z., Tsagarakis, N., and Caldwell, D. G. (2012). A passivity based admittance control for stabilizing the compliant humanoid COMAN. In *IEEE-RAS International Conference on Humanoid Robots*, pages 44–49, Osaka, Japan.

Migliore, S., Brown, E., and DeWeerth, S. (2005). Biologically inspired joint stiffness control. In *Robotics and Automation, 2005. ICRA 2005. Proceedings of the 2005 IEEE International Conference on*, pages 4508–4513.

Morita, T. and Sugano, S. (1997). Development and evaluation of seven dof mia arm. In *Robotics and Automation, 1997. Proceedings., 1997 IEEE International Conference on*, volume 1, pages 462–467 vol.1.

Nakanishi, J. and Vijayakumar, S. (2012). Exploiting Passive Dynamics with Variable Stiffness Actuation in Robot Brachiation.

Park, J.-J., Kim, H.-S., and Song, J.-B. (2009). Safe robot arm with safe joint mechanism using nonlinear spring system for collision safety. In *Robotics and Automation, 2009. ICRA '09. IEEE International Conference on*, pages 3371–3376.

Park, J.-J. and Song, J.-B. (2010). Safe joint mechanism using inclined link with springs for collision safety and positioning accuracy of a robot arm. In *Robotics and Automation (ICRA), 2010 IEEE International Conference on*, pages 813–818.

Park, J.-J., Song, J.-B., and Kim, H.-S. (2008). Safe joint mechanism based on passive compliance for collision safety. In Lee, S., Suh, I., and Kim, M., editors, *Recent Progress in Robotics: Viable Robotic Service to Human*, volume 370 of *Lecture Notes in Control and Information Sciences*, pages 49–61. Springer Berlin Heidelberg.

Petit, F., Chalon, M., Friedl, W., Grebenstein, M., Albu-Schaeffer, A.ffer, A., and Hirzinger, G. (2010). Bidirectional antagonistic variable stiffness actuation: Analysis, design amp; implementation. In *Robotics and Automation (ICRA), 2010 IEEE International Conference on*, pages 4189–4196.

Pfeifer, R., Lungarella, M., and Iida, F. (2012). The challenges ahead for bio-inspired 'soft' robotics. *Commun. ACM*, 55(11):76–87.

Rodriguez, A. G., Chacon, J., Donoso, A., and Rodriguez, A. G. (2011). Design of an adjustable-stiffness spring: Mathematical modeling and simulation, fabrication and experimental validation. *Mechanism and Machine Theory*, 46(12):1970 – 1979.

Sardellitti, I., Medrano-Cerda, G., Tsagarakis, N., Jafari, A., and Caldwell, D. (2012). A position and stiffness control strategy for variable stiffness actuators. In *Robotics and Automation (ICRA), 2012 IEEE International Conference on*, pages 2785–2791.

Schiavi, R., Grioli, G., Sen, S., and Bicchi, A. (2008). Vsa-ii: a novel prototype of variable stiffness actuator for safe and performing robots interacting with humans. In *Robotics and Automation, 2008. ICRA 2008. IEEE International Conference on*, pages 2171–2176.

Stramigioli, S., van Oort, G., and Dertien, E. (2008). A concept for a new energy efficient actuator. In *Advanced Intelligent Mechatronics, 2008. AIM 2008. IEEE/ASME International Conference on*, pages 671–675.

Tagliamonte, N. L., Sergi, F., Accoto, D., Carpino, G., and Guglielmelli, E. (2012). Double actuation architectures for rendering variable impedance in compliant robots: A review. *Mechatronics*, 22(8):1187–1203.

Tonietti, G., Schiavi, R., and Bicchi, A. (2005). Design and control of a variable stiffness actuator for safe and fast physical human/robot interaction. In *Robotics and Automation, 2005. ICRA 2005. Proceedings of the 2005 IEEE International Conference on*, pages 526–531.

Tsagarakis, N., Sardellitti, I., and Caldwell, D. (2011). A new variable stiffness actuator (compact-vsa): Design and modelling. In *Intelligent Robots and Systems (IROS), 2011 IEEE/RSJ International Conference on*, pages 378–383.

Van Ham, R., Vanderborght, B., Van Damme, M., Verrelst, B., and Lefeber, D. (2006). Mechanically adjustable and controllable compliance, equilibrium position actuator (maccepa). In *Proceeding of the IEEE International Conference on Robotics and Automation (ICRA)*, pages pp. 2195 – 2200.

Vanderborght, B., Albu-Schaeffer, A., Bicchi, A., Burdet, E., Caldwell, D., Carloni, R., Catalano, M., Eiberger, O., Friedl, W., Ganesh, G., Garabini, M., Grebenstein, M., Grioli, G., Haddadin, S., Hoppner, H., Jafari, A., Laffranchi, M., Lefeber, D., Petit, F., Stramigioli, S., Tsagarakis, N., Damme, M. V., Ham, R. V., Visser, L., and Wolf, S. (2013). Variable impedance actuators: A review. *Robotics and Autonomous Systems*, (0):–.

Vanderborght, B., Tsagarakis, N. G., Ham, R., Thorson, I., and Caldwell, D. G. (2011). MACCEPA 2.0: compliant actuator used for energy efficient hopping robot Chobino1D. *Autonomous Robots*, 31(1):55–65.

Vanderborght, B., Verrelst, B., Ham, R., Damme, M., Beyl, P., and Lefeber, D. (2008). Development of a compliance controller to reduce energy consumption for bipedal robots. *Autonomous Robots*, 24(4):419–434.

Vanderborght, B.and Van Ham, R., Lefeber, D., Sugar, T., and Hollander, K. (2009). Comparison of mechanical design and energy consumption of adaptable, passive-compliant actuators. *The International Journal of Robotics Research (IJRR)*, 28:90–113.

Visser, L., Carloni, R., and Stramigioli, S. (2011). Energy-efficient variable stiffness actuators. *Robotics, IEEE Transactions on*, 27(5):865–875.

Vu, H., Aryananda, L., Sheikh, F., Casanova, F., and Pfeifer, R. (2011). A novel mechanism for varying stiffness via changing transmission angle. In *Robotics and Automation (ICRA), 2011 IEEE International Conference on*, pages 5076 –5081.

Wolf, S., Eiberger, O., and Hirzinger, G. (2011). The DLR FSJ: Energy based design of a variable stiffness joint. In *Robotics and Automation (ICRA), 2011 IEEE International Conference on*, pages 5082–5089.

Wolf, S. and Hirzinger, G. (2008). A new variable stiffness design: Matching requirements of the next robot generation. In *Robotics and Automation, 2008. ICRA 2008. IEEE International Conference on*, pages 1741–1746.

Yang, C., Ganesh, G., Haddadin, S., Parusel, S., Albu-Schaeffer, A., and Burdet, E. (2011). Human-like adaptation of force and impedance in stable and unstable interactions. *Robotics, IEEE Transactions on*, 27(5):918–930.

Zinn, M., Khatib, O., Roth, B., and Salisbury, J. K. (2004). Playing it safe [human-friendly robots]. *Robotics & Automation Magazine, IEEE*, 11(2):12–21.

Appendix B

A novel mechanism for varying stiffness via changing transmission angle

Reprinted from: H. Vu Quy, L. Aryananda, F. I. Sheikh, F. Casanova, and R. Pfeifer, "A novel mechanism for varying stiffness via changing transmission angle," in 2011 IEEE International Conference on Robotics and Automation, 2011, pp. 5076–5081.

A Novel Mechanism for Varying Stiffness via Changing Transmission Angle

Hung Vu Quy, Lijin Aryananda, Farrukh Iqbal Sheikh, Flurin Casanova, Rolf Pfeifer

***Abstract*- Compliant actuation contributes enormously in legged locomotion robotics since it is able to alleviate control efforts in improving the robot's adaptability and energy efficiency. In this paper, we present a novel design of a variable stiffness rotary actuator, called MESTRAN, which was especially targeted to address the limitations in terms of the amount of energy and time required to vary the stiffness of an actuated joint. We have constructed a mechanical model in simulation and a physical prototype. We conducted a series of experiments to validate the performance of the MESTRAN actuator prototype. The results from the simulation and experiments show that MESTRAN allows independent control of stiffness and position of an actuated rotary joint with a large operational range and high speed. The torque-displacement relationship is close to linear. Lastly, the MESTRAN actuator is energy-efficient since a certain stiffness level is maintained without energy input.**

I. Introduction

In this paper, we present a novel design for a rotary actuator with variable stiffness/compliance. The use of compliance has been widely explored in robotics to address the limitations of existing robots which use stiff structures, actuators with high-gear ratio, and well-established control algorithms, such as industrial manipulators and ZMP-based bipedal robots [1]. These precise and stiff robots, although useful and impressive, are severely limited and even dangerous when taken outside their fully-modeled and controlled environments. Daily usage in human environments is particularly difficult for such robots because of their lack of adaptability and energy efficiency. Essentially, integration of compliance actuator into the robot's joints and structures can alleviate some of these limitations.

In designing the variable stiffness actuators for robots in order to achieve adaptability and energy efficiency, there are some crucial points that have to be considered: 1-light in weight and compact in structure, 2-large operational range of joint deflection, 3-rapid change of stiffness, 4-high power density. 5-independent control of position and stiffness

In the field of robotics, there has been vast effort in the development of variable stiffness actuators. A class of approaches was mainly inspired by the agonist and antagonist muscle groups in the animal muscle system. The principle of operation relies on an antagonistic arrangement of the motors which are connected in series to the output shaft via elastic elements. Two motors control the stiffness and the position of the output shaft by changing the tension level of the elastic elements. Some examples of these approaches were presented in an antagonistically actuated robotic joint [2], the Variable Stiffness Actuator (VSA) [3] and the Actuator with Mechanically Adjustable Series Compliance (ASMASC) [4]. One limitation of this principle is that energy is consumed since the pre-tensioning motor controlling the spring stiffness has to be powered all the time even when there is no need for varying stiffness.

Instead of using an antagonistic arrangement, the MACCEPA actuator [5] uses two motors to regulate the pre-tension level and the equilibrium point of one linear spring to vary the stiffness and position independently. One motor moves the spring back and forth to drive the output link, while the other is in charge of tensioning the spring to alter the stiffness. Thus, the MACCEPA design still has the drawback of energy inefficiency. By using the screw-nut mechanism which is not back-drivable, the continuous requirement for energy to maintain the stiffness was resolved in the VS-Joint [6]. The joint uses one motor to control the spring compression on the cam surface and the other is used to control the joint position. The energy efficiency issue is pushed one step further in some recent designs [7, 8]. The idea is to move the slider which determines the activation level of the spring perpendicularly to the exerted force. In principle, no energy is needed to vary the stiffness level from one to another and to maintain the stiffness level. In addition, there is no coupling between the output stiffness and position. Nevertheless, from a control perspective, the non-linearity of the torque-displacement curve of these actuators still causes difficulties in their use.

The variable stiffness actuator presented in this paper, called MESTRAN (MEchanism for Varying Stiffness via changing TRansmission ANgle) is designed to address the main limitations of existing mechanisms, i.e. energy efficiency and the speed required to change the stiffness. A mechanical model has been built. A prototype has been constructed and integrated into the knee joint of the segmented limb. In order to validate the performance of MESTRAN, we have conducted a series of experiments which show that MESTRAN is able to vary the limb's compliance independently from its position with a large operational range and high speed. The relationship between exerted torque and angular deflection of the limbs is fairly linear with the minimum R^2 coefficient of 0.94, which is a statistical measure of how well the regression line

Manuscript received September 15, 2010. This work was funded by the European Commission's Seventh Framework Programme, Theme ICT-2007.8.5 as part of the project LOCOMORPH under grant no 231688.

Hung Vu Quy, Lijin Aryananda, Farrukh Iqbal Sheikh, Flurin Casanova and Rolf Pfeifer are with the AI Laboratory, Department of Informatics, University of Zurich, Switzerland (e-mail: vqhung@ifi.uzh.ch, lijin@ifi.uzh.ch, farrukh.ssuet@gmail.com, casanova@ifi.uzh.ch).

approximates the experiment data points as described in section III.B.1.

We begin by presenting a design concept in section II.A, followed by section II.B, where we present the mechanical implementation of the concept. In section II.B.2 and 3, we provide an analytical model. In order to validate the practical performance, we present the experimental data and discussion in section III. Finally, conclusions and future work are presented in section IV.

II. Actuator Design

A. Conceptual Model

The concept of the MESTRAN design is derived from a basic mechanical problem, as illustrated in Fig.1. Blocks A and B can slide on each other, while guided by a vertical and a horizontal wall. A spring is attached between block B and the other vertical wall. For simplification, friction is neglected in this model, but will be addressed later in the next section.

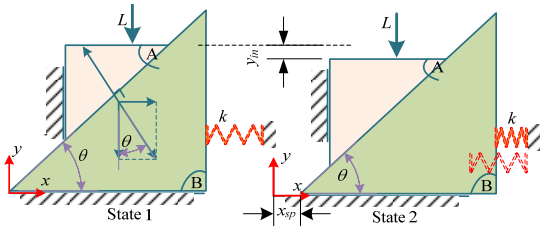

Fig.1 Concept of force transmission via slopes. L: pressing force; θ: slope angle (transmission angle); x_{sp}: spring deflection; y_{in}: displacement; k: stiffness of spring. Block A can slide on block B freely.

Through the mechanical interaction of the components, force L causes a displacement y_{in} and a compression of spring x_{sp}, according to the following equation.

$$L = \frac{kx_{sp}}{\tan\theta} = \frac{k}{(\tan\theta)^2} y_{in} \qquad (1)$$

In other words, the system is compliant with a stiffness coefficient of $\varepsilon = k/\tan\theta^2$. Varying the stiffness level can be achieved by changing the slope/transmission angle θ. The smaller the transmission angle θ is, the higher the system's stiffness ε is.

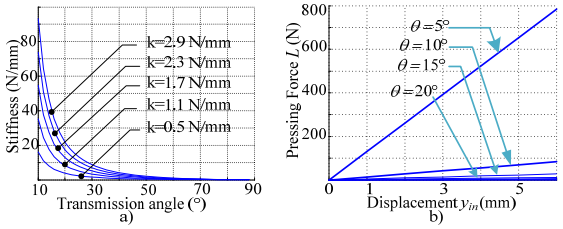

Fig.2 MESTRAN characteristics. a) System's stiffness values vary as a function of transmission angle θ with respect to spring stiffness values, k; b) Force values varies as a function of displacement y_{in} , respected to transmission angle values θ, according to Eq.1.

Fig.2a illustrates how the system's stiffness ε changes as a function of the transmission angle θ between 10° and 90° according to Eq.1, when the spring stiffness k is varied from 0.5 to 2.9 N/mm. The high spring stiffness k values correspond to the high rates of change of ε. Theoretically, regardless of the spring stiffness, the system's stiffness is either infinite or zero as the transmission angl e θ is 0° or 90°, respectively. Fig.2b shows the linear relationship between force L and displacement y_{in}, with varying values of transmission angle θ .

B. Mechanical Implementation

1) General Structure

Fig.3 illustrates our mechanical implementation of the variable stiffness mechanism on a rotary joint formed by two links (link 1 and 2) derived from the basic design concept described above.

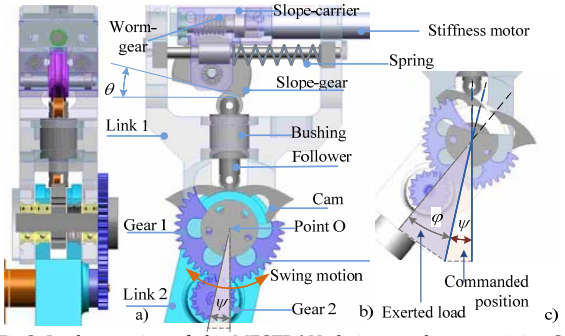

Fig.3 Implementation of the MESTRAN design on the rotary joint O formed by link 1 and 2. (a): the side view of the mechanical structure. (b): the configuration where link 2 is actuated by the knee motor by an angle ψ (the cam is not displaced). (c): the configuration where external load is presented and link 2 is displaced by an angle $\psi+\varphi$ from both the knee motor and external load (the cam is displaced)

Block A shown in Fig.1 is converted into the follower which can slide up and down via the bushing. Block B is converted into the slope-gear, which is mounted on the slope-carrier that can slide along sliding shafts. The orientation angle of the slope-gear is equivalent to the transmission angle θ and controlled by the stiffness motor through the worm-gear. The worm-gear, the stiffness motor and the slope-gear are mounted on the slope-carrier which can slide horizontally. We use the cam mechanism to convert the rotary motion of link 2 to the linear motion of the follower. We also minimize the impact arising between the surfaces of the cam and the follower by placing there a bearing which dramatically reduces the friction coefficient of contacting surfaces. In addition, in order to ensure the contact there is always a pre-compression force coming from the spring's compression on the cam surface via the follower.

The cam can rotate about the rotational joint O and is connected to link 2 through gear 1 and gear 2 controlled by the knee motor. Due to the mechanical separation of stiffness and knee motor, two independent mechanisms can work in parallel: the position-based control and the stiffness-based control at the joint O. In the absence of external forces, the spring forces the follower into the middle point of the cam. Gear 2 which is rigidly connected to the cam is also held in place by the springs. In order to rotate link 2 the knee motor rotates gear 2 and consequently link 2 which changes

the joint angle ψ about the rotational point O. If an external torque is applied to link 2 during the rotational motion, the cam is passively displaced by an angle φ in either direction. As a result, the total displacement of link 2 is $\varphi + \psi$, as shown in Fig.3c. Since the worm-gear mate is not back-drivable, the stiffness control θ and position control ψ are definitely decoupled. Thus, the MESTRAN has the capability to achieve both position and stiffness control independently. In term of energy efficiency, the worm-gear mate helps the system to avoid having to supply the power when there is no need to change the stiffness. In addition, the linear relationship between the exerted torque and the angular displacement at the joint O can be achieved through a systematic design of the cam profile, which is presented in section II.B.2.

2) Force Analysis

In order to understand the mechanical behaviors, we constructed a model (using Matlab) to perform force analysis and assess the resulting outcome of the MESTRAN prototype. Fig.4 shows the calculation scheme. Parameters are manually selected as shown in Table 1.

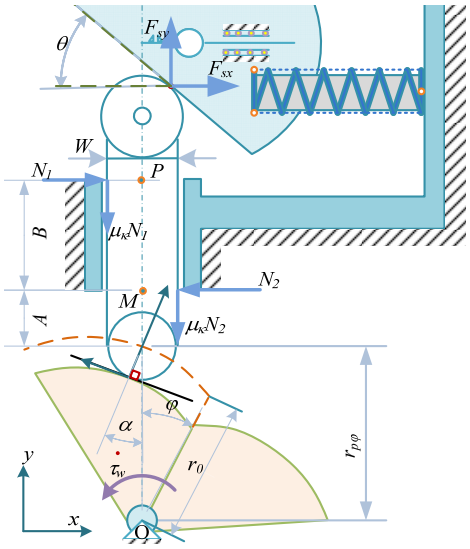

Fig.4 Calculation scheme the configuration where external load is presented. The cam is being deflected by angle φ due to an external load. The follower is being pushed up by force F and in opposite direction, spring pushes the slope-gear against the external load. The system stiffness is set by setting the transmission angle to θ. For the other variables and parameters, see Table 1.

TABLE 1
NOMENCULATURE

Symbols	Variables
δx_{sp}	Deflection of one spring
F_{sy}	Force acting on the follower in y direction
F_{sx}	Force acting on the follower in x direction
N_1	Reaction force from bushing to the follower
N_2	Reaction force from bushing to the follower
$r_{C\phi}$	Cam radius in contacting angle ϕ
Φ	Deflection angle of the cam
F	Normal force on the cam surface
θ	Transmission angle
$r_{p\varphi}$	Pitch radius at angle φ
A	Overhang height of the bushing

Symbols	Parameters	Values
B	Length of the bushing	12mm
W	The follower diameter	8mm
L_0	Spring preload (summed from two springs)	3mm
S_{offset}	Offset of slope-gear	5 mm
K	Spring stiffness	0.64N/mm
μ_k	Kinetic friction coefficient	0.18
μ_r	Rolling friction coefficient	0.01
α	Pressure angle	20
r_{p0}	Initial radius of pitch	18.45mm
ϕ_0	Initial contacting angle	6.5°
r_{conC}	Roller radius	4mm
$r_{C\phi 0}$	Initial contacting radius of the cam profile	15mm
r_{C0}	Initial radius of the cam profile	14mm

The deflection of the spring depends on the preload and pitch radius of the pitch profile.

$$\delta x_{sp} = 0.5\frac{L_0}{k} + \frac{r_{p\varphi} - r_{p0}}{\tan(\theta)} \quad (2)$$

The force components push one end of the follower up as below.

$$F_{sx} = L_0 + 2k\delta x_{sp} \quad (3)$$

$$F_{sy} = F_{sx} / \tan\theta \quad (4)$$

The force and moment at the equilibrium state of the follower is obtained.

$$\sum F_y = -F_{sy} + F\cos\alpha - \mu_k N_1 - \mu_k N_2 + F\mu_r \sin\alpha = 0 \quad (5)$$

$$\sum M_{pointM} = -FA\sin\alpha + N_1 B - N_1\mu_k W + N_2\mu_k W + F\mu_r(r_{rol} + A\cos\alpha) = 0 \quad (6)$$

$$\sum M_{pointP} = -F(A+B)\sin\alpha + N_2 B - N_1\mu_k W + N_2\mu_k W + F\mu_r\left[r_{rol} + (A+B)\cos\alpha\right] = 0 \quad (7)$$

By solving the equation system (5), (6), (7), N_1, N_2 and F are found.

$$N_1 = \frac{-BF_{sy}}{2\mu_k A\sin\alpha(A - W\mu_k) + B(\mu_k\sin\alpha - \cos\alpha)} \quad (8)$$

$$N_2 = N_1\frac{(\mu_k W + A)\sin\alpha}{B} \quad (9)$$

$$F = \frac{N_2 B - N_1\mu_k W + N_2\mu_k W}{(A+B)\sin\alpha - \mu_r\left[r_{rol} + (A+B)\cos\alpha\right]} \quad (10)$$

Using this model and its parameter values shown in Table 1, we can calculate the torque τ_w and the joint stiffness ε at the cam's angular displacement φ and the transmission angle θ.

$$\tau_w(\varphi,\theta) = F(\theta,\varphi)r_{p\varphi}(\varphi)\sin\varphi \quad (11)$$

$$\varepsilon(\varphi,\theta) = \frac{\partial\tau_w(\varphi,\theta)}{\partial\varphi} = \frac{\partial(F(\theta,\varphi)r_{p\varphi}(\varphi)\sin\varphi)}{\partial\varphi} \quad (12)$$

For convenience of control, the curve of the exerted torque τ_w and the angular deflection φ formulated in Eq.11 is linearized. Based on observations illustrated in Fig.5 and the above equations from 2 to 10, we provide a number of

comments: 1-The normal force F is determined by the transmission angle, profile radius and pressure angle. 2–At one desired level of stiffness, the transmission angle is fixed. 3-The pressure angle is constant as shown in the cam design. 4-The profile radius is linear to the normal force and changed according to the angular displacement. 5-When φ is as small as in radian values (0:π/4), φ is approximately linear to sinφ. Therefore, the remaining task for the linearization task now is only to design the cam such that the profile radius is as linear as possible to the angular displacement of link 2.

3) Cam design

As shown in Fig.4, the cam rotates around the rotational joint O and its pitch profile radius $r_{p\varphi}$ is changed according to the angular displacement φ. In order to have the pitch profile radius linear to its angular displacement, we design the pitch profile radius as an exponential function: $r_{p\varphi}=r_{p0}e^{u\varphi}$ in polar coordinates centered at the axis of joint O.

The pressure angle α is calculated at an arbitrary angle of the cam displacement φ as following:

$$\frac{1}{\tan\alpha}=\frac{r_{p\varphi}}{(dr/d\varphi)}=\frac{r_{p0}e^{u\varphi}}{ur_{p0}e^{u\varphi}}=\frac{1}{u} \quad (13)$$

As a result, α is constant at any cam displacement angle. By setting r_{p0} to 18mm and α to 25°, we can calculate the resulting pitch profile function $r_{p\varphi}=18e^{0.4663\varphi}$.

Based on this pitch profile function, the cam profile function $r_{c\varphi}$ is determined as illustrated in Fig.5.

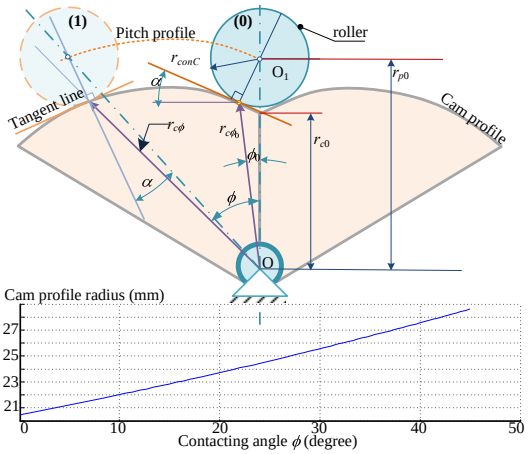

Fig.5 Cam calculation scheme; Upper plot: Cam design scheme. (0): Initial position in unloaded state. Solid circle: roller at rest position. (1): Cam displaced state. Dashed circle: roller when cam displacement at φ. Lower plot: cam profile radius versus the cam displacement. The displacement angle of the cam is designed in the range of ± 40°. See Table 1 for more details.

The initial radius of the cam profile can be obtained as follows.

$$r_{c\phi 0}=\sqrt{(r_{conC}\sin\alpha)^2+(r_{p0}-r_{conC}\cos\alpha)^2} \quad (14)$$

$$\phi_0=\sin^{-1}(r_{conC}\sin\alpha/r_{c\phi_0}) \quad (15)$$

$$r_{c\phi_0}=r_{c0}e^{\phi_0\tan\alpha}\Rightarrow r_{c0}=\frac{r_{c\phi_0}}{e^{\phi_0\tan\alpha}} \quad (16)$$

From Eq.14, 15 and 16, the profile of the cam can be drawn:

$$r_{c\phi}=r_{c0}e^{\phi\tan\alpha} \quad (17)$$

The cam profile presented in Eq.17 is plotted in Fig.5 by using the parameters shown in Table 1. The profile radius and the contacting angle are approximately linear to each other. As mentioned in section III.B.2 the torque-angle relationship can achieve the same level of linearity. By simulating Eq.11, we plot the torque-angle relationship, as shown in Fig.6.

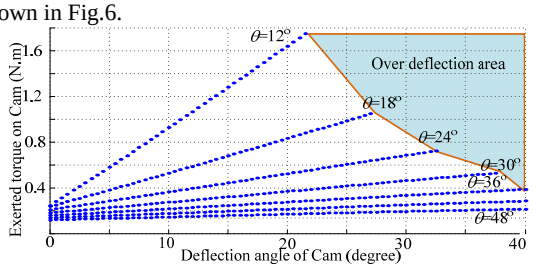

Fig.6 Exerted torque versus angular displacement of the cam at different values of the transmission angle between 17° and 47°. Two springs of 0.64N/mm are used. Over deflection area shows the operating area of the MESTRAN actuator.

Due to the geometrical configuration of the system and the maximum compression of the springs, the operating angle of link 2 is limited to ± 40° and not in the 'over deflection area'. The preload length of the springs increases with the transmission angle. On one hand, in principle when the transmission angle θ decreases to zero, the joint stiffness is infinite in a way to lock the joint rotation. This situation may be necessary in cases where compliance is not desired. When the transmission angle reaches 90° no spring effect is introduced to link 2, i.e zero stiffness.

III. Experiments

A. General Experiment Setup

We have conducted a series of three experiments in order to evaluate and verify the MESTRAN concept. In the first experiment, we examined the fundamental characteristics of torque versus angle of the MESTRAN actuator. In the second, we evaluated the independence of stiffness and position control. Lastly, in the third experiment, we investigated MESTRAN's capability for fast change of stiffness.

The experiment platform consists of a segmented leg which is mounted to a frame by fixing one segment (link 1) to it, as shown in Fig.7. In all experiments, the platform is mounted horizontally to avoid gravitational effects on moving parts. Link 2 can be rotated about the knee joint by the knee motor. The stiffness value can be changed by actuating the stiffness motor. To measure external load, the force sensor is installed on the frame perpendicularly to link 2. The absolute angular displacement of the cam with respect to link 1 is measured by a potentiometer.

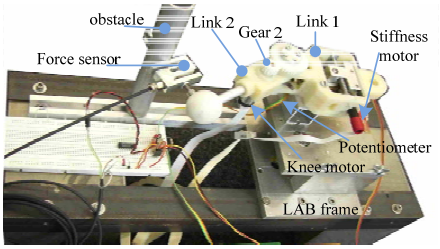

Fig.7 The experimental platform to validate the practical performance of the MESTRAN actuator. Link 2 is set to touch to the force sensor at the point where there is no cam displacement produced and the measured force values are zero. The knee motor actuates link 2 via gear 2 toward the force sensor. The absolute displacement of link2 respected to link 1 is the sum of knee motor encoder and the potentiometer values.

The device specifications are as follows: two springs of 0.64N/mm; Maxon RE-10 brushes motor (stiffness motor), power 1.5W, encoder resolution 16 counts per turn; Maxon–RE max-17 brushes motor (knee motor), power 4.5W, encoder resolution 256 counts per turn; force sensor KD40S made by ME-Meßsysteme GmbH, nominal force range of ±100N, accuracy of 0.1%; controller of 8-bit Atmel-based microcontroller, H-bridge with 3 Amp continuous output current.

B. *Results and Discussion*

1) *Torque versus Angular Displacement*

This experiment is designed to validate the fundamental capability of the MESTRAN actuator. In the initial position, link 2 is set at the point where no cam displacement is produced. This is considered as the zero degree angle point. Then, the knee motor starts displacing link 2 by one degree to press on the force sensor. In each degree, the presented force value is averaged over all measured values at that angle. Fig.8 shows the plot of the mean values and standard deviation values of the torques and the displacement measurements for all 3 trials. These results validate the main concept of MESTRAN actuator which is the ability to change the actuator stiffness by altering the transmission angle.

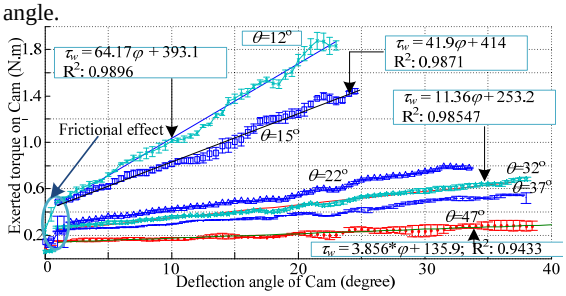

Fig.8 The exerted torque on the cam is plotted respectively to the deflection angle of the cam in six transmission angles, θ=12,15,22,27,37,47 (°). Two linear springs of 0.64N/mm are used. The plotted results are the mean values of exerted torques in each transmission angle and the error bars show deviation of exerted torques. The linear relationship of the experiment data is validated by computing linear regression. The linear functions represent the torque-angle relationship at 47°, 32° and 12°: τ_w=64.17φ+393.1, τ_w=11.36φ+253.2 and τ_w =3.856φ +135.9 with the confidence coefficient 0.98, 0.98 and 0.94, respectively.

At the transmission angle of 47 degrees, the stiffness evaluated by the slope of the torque versus the angle is at the lowest value (3.8Nmm/degree). At the transmission angle of 12 degrees, the stiffness rises up to 64.17 Nmm/degree. Due to frictional effects, the zero stiffness cannot be achieved since if the transmission angle is close to 90 degrees (zero stiffness), then the contact between the follower and the cam cannot be maintained over the full operational range of the link 2. In this design, we set the minimum transmission angle to 12 degrees therefore the maximum achievable stiffness is at 12 degrees. The minimum coefficient of determination R^2 is calculated to be 0.9433, which indicates that the experiment data fits well with the linear function, as shown in Fig.8. In high stiffness values, the operating angle is restricted in a smaller range compared to that in the low stiffness case. This experimental data matches the modeling data very well, as shown in Fig. 6. However under the influence of gravity, the compliance level or transmission angle θ needs to be adjusted to compensate the leg weight. Note that due to the frictional effect, some initial force is needed to start rotating the cam.

2) *Positioning Accuracy Independent from Stiffness*

An important feature of variable compliance actuators is the decoupling between the stiffness and the position control. In the following experiments, we evaluate MESTRAN in its capacity for this requirement. The results are shown in Fig.9.

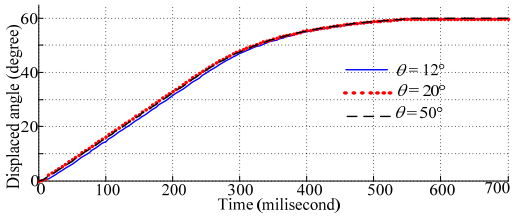

Fig.9 Positioning profile of MESTRAN actuator while it is moving from 0° to 60° in 3 different stiffness values, θ = 12°, 20° and 50°.

We command the knee motor to move link 2 from the zero degree to the 60 degree displacement with three different transmission angles, θ = 12°, 20° and 50°. We use the same control parameters for all trials. The absolute displacement of link 2 plotted in Fig.9 is calculated as the sum of the displacement of the cam and the relative angular displacement of link 2 to the cam. The position profile of link 2 at three stiffness values shows a very small amount of discrepancies.

3) *Speed of Stiffness Change*

Various research works in biomechanics and experimental biology have shown that human leg stiffness is changed during locomotion in one step cycle to accommodate surface stiffness changes [9, 10]. In the context of robot locomotion, the same strategy can be applied in order to reduce impact and gain stability. Therefore, MESTRAN is designed so that it can change its stiffness in one walking step cycle, currently 1Hz. In this experiment, link 2 is actuated until the cam's angular deflection reaches 30°. Please note that link 2 is touching the force sensor and therefore only the cam is moving. The maximum torque threshold is set at 0.5 Nm. If the measured torque is higher than the torque threshold, the stiffness values will be changed in order to keep the incoming torque below the threshold. The experimental processes and results are shown in Fig.10.

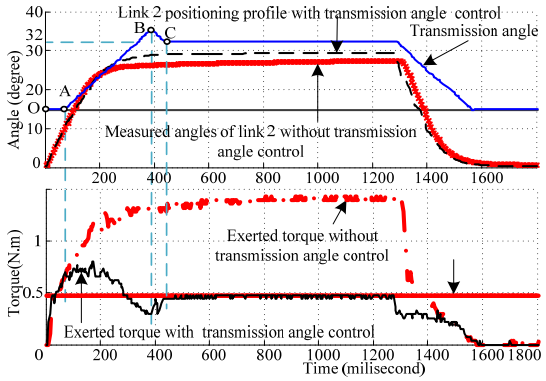

Fig.10 Speed of changing the stiffness of MESTRAN actuator. In the upper plot, the transmission angle and Cam angular displacement with and without adaptive force controller are shown with respect to time. The points O, A, B and C examined system's control steps before it reaches to the desired level. OA: detecting step; AB: roughly reacting step; BC: finely regulating step. In the lower plot, the exerted torque on the cam with and without transmission angle control is visualized.

The initial stiffness is set to the transmission angle of 15°. Then link 2 starts pressing against the force sensor. The experimental process works as follows. During time period O→A, the exerted torque is still lower than the limited torque, therefore there is no reaction of the system yet (O→A). During time period A→B→C, the exerted torque exceeds the threshold and the system regulates the transmission angle until the torque is at the desired torque level. During the time period after C, the system's stiffness stays constant (the transmission angle at 32°) until link 2 returns to the zero degrees.

In comparison, we show the results of this experiment without transmission angle control. The exerted torque without transmission angle control applied to the cam is three times higher than that with the transmission angle control. The time to adjust the stiffness from A to C is about 400 milliseconds, while the stiffness varies from 41.9Nmm/degree to 11.36Nmm/degree as mentioned in Fig.8. These results show that MESTRAN actuator is able to accommodate surface stiffness changes within one step cycle of the 1Hz walking speed.

In summary, three series of experiments have validated the performance of the variable stiffness actuator, MESTRAN in the following criteria: capability to change the stiffness at high rate and large operational range, and independent control of position and stiffness.

IV. Conclusion and Future Work

This paper presents a novel variable stiffness actuator design (MESTRAN), based on the concept of varying the transmission angle to change the force transmission which is a mechanical strategy to achieve varying stiffness. We have conducted modeling analysis, constructed a physical prototype, and carried out various experiments to validate the performance of the actuator. The preliminary results have shown that MESTRAN is capable of varying the joint stiffness with a large operational range and speed, and allows independent control of position and stiffness. We expect that the worm-gear mechanism would address the energy efficiency issue, i.e. the amount of torque required to maintain the same stiffness level. We will examine and verify this hypothesis in the near future. Preliminary experiment results are promising and we plan to integrate the MESTRAN actuator into a quadruped robot. We will carry out further experiments to investigate energy efficiency, self-stability in the context of dynamic locomotion.

Acknowledgement

Thanks to Juan Pablo Carbajal at the AI Laboratory for very useful discussions.

References

[1] P. Sardain, G. Bessonnet, "Force acting on a biped robot. Center of pressure zero moment point," *Systems, Man and Cybernetics, Part A: Systems and Humans, IEEE Transactions on* September 2004.

[2] S. A. Migliore, E. A. Brown and S. P. DeWeerth, "Biologically Inspired Joint Stiffness Control," *Proceedings of the 2005 IEEE, International Conference on Robotics and Automation*, Barcelona, Spain, April 2005.

[3] G. Tonietti, R. Schiavi, and A. Bicchi, "Design and control of a variable stiffness actuator for safe and fast physical human/robot interaction," in *Robotics and Automation, ICRA. 2005; Proceedings of the 2005 IEEE International Conference*, pages 526-531, April 2005.

[4] J. W. Hurst, Chestnutt, A. Rizzi, "The Actuator with Mechanically Adjustable Series Compliance," *Robotics, IEEE Transaction*. Vol.26, Issue 4, pages 597-696, August 2010.

[5] B. Vanderborght, N.G. Tsagarakis, C. Semini, R. Van Ham, D. G. Caldwell, "MACCEPA 2.0: Adjustable compliant actuator with stiffening characteristic for energy efficient hopping," *Robotics and Automation, 2009. ICRA '09. IEEE International Conference on*, pages 544-549, May 2009.

[6] S. Wolf, G. Hirzinger, "A New Variable Stiffness Design: Matching Requirements of the Next Robot Generation," *IEEE International Conference on Robotics and Automation*, Pasadena, USA, May 2008.

[7] L.C. Visser and R. Carloni, R. Ünal, and S. Stramigioli, "Modeling and design of energy efficient variable stiffness actuators*", Proceedings of the IEEE International Conference on Robotics and Automation*, Anchorage, Alaska, USA, May 2010.

[8] A. Jafari, Nikos G. Tsagarakis, Bram Vanderborght and Darwin G. Caldwell, "An Intrinsically Safe Actuator with the Ability to Adjust the Stiffness," *7th IARP Workshop on Technical Challenges for Dependable Robots in Human Environments*, Toulouse, France, June 2010.

[9] A. Arampatzis, G.P. Bruggemann, V. Metzler, "The effect of speed on leg stiffness and joint kinetics in human running," *Journal of Biomechanics*, Vol. 32, pages 1349-1353, Issue 12, December 1999.

[10] D. P. Ferris, C. T. Farley, "Interaction of leg stiffness and surface stiffness during human hopping," *J Appl Physiol.* 82(1):15-22, January 1997.

Appendix C

A variable stiffness mechanism for improving energy efficiency of a planar single-legged hopping robot

Reprinted from:

Hung Q.Vu, Helmut Hauser, and R. Pfeifer, "*A variable stiffness mechanism for improving energy efficiency of a planar single-legged hopping robot*," Advanced Robotics (ICAR), 2013 16th International Conference on 25-29 Nov. 2013, pp.1-7.

A variable stiffness mechanism for improving energy efficiency of a planar single-legged hopping robot

Hung Q. Vu, Helmut Hauser, Derek Leach, and Rolf Pfeifer

Abstract— **Recently, variable stiffness actuators (VSAs) have been considered as actuation approaches to improve energy efficiency of legged locomotion robots. In this paper, we present the design and implementation of a variable stiffness actuator, named L-MESTRAN, which allows for improving energy efficiency of a planar single-legged robot over different stride frequencies. The leg in our setup consists of an actuated hip joint and a passive knee joint equipped with the L-MESTRAN. This mechanism is capable of varying stiffness in a large range, maintaining stiffness with almost no energy, and offers a linear joint stiffness. We empirically demonstrate that the L-MESTRAN actuator can increase energy efficiency for hopping locomotion for various stride frequencies. Furthermore, we also demonstrate the capability of the L-MESTRAN to adjust stiffness to improve energy efficiency during locomotion.**

I. INTRODUCTION

In legged robots, energy efficiency and locomotion versatility are difficult to be achieved at the same time. In fact, energy efficient robots usually exhibit poor versatility [1]. Recently, there have been several robots that can achieve energy efficiency at the same levels of that of humans/animals, but they are constrained to a small range of working conditions [2]–[5]. For example, passivity-based bipedal walkers can produce human-like walking behaviors with a relatively low energetic cost (Cost of Transport (CoT) = 0.2 [6], [7]). However, their mechanical structures are carefully optimized for slightly inclined slopes. In contrast, the ASIMO robot can demonstrate various behaviors, i.e., walking, running, climbing up/down stairs, but the robot's energy efficiency is known to be an order of magnitude worse than humans [8], [9].

A typical way of increasing energy efficiency is utilizing elastic elements as energy storage mechanisms. Such elements can retain kinetic energy as potential energy and release it when necessary [10]. In biological systems, it has been found that animal locomotion can greatly benefit from the energy recoil of tendons [11], [12]. In robotics, compliant joints, which consist of elastic elements, have been widely applied in many robots [13]–[15]. For example, curved-beam hopping robots were designed to exploit their natural dynamics via the elasticity of their beams, achieving energy efficient locomotion [5]. Another example is the elastic bow-leg robot, which can hop up to 50 cm in height and reach 1 m/s in forward speed [16]. However, in these robots, the leg elasticity/stiffness is carefully tuned offline to improve energy efficiency due to the lack of an adjustment mechanism. Therefore, their locomotion behavior is not versatile.

In order to enrich the versatility, among many other locomotion parameters, the stride frequency, i.e., the frequency of leg oscillation, is an important parameter to be considered. As it has been found in biological systems, stride frequency has a significant influence onto locomotion parameters such as: stride length [17], gait patterns [18], [19], stability [20], speed [21], and energy efficiency [22], [23].

From this perspective, recently, the interest to develop VSAs, which are capable of changing stiffness and, therefore, the natural frequency of the structure (e.g., leg), has rapidly increased, resulting in a number of prototypes [24]–[28]. Some VSAs have been used to explore energy efficiency of legged robots. For example, a variable stiffness leg in the RHex robot was used to adjust the natural frequency of the leg for improving energy efficiency and speed [29]. Another example is the in-place hopping leg robot MACCEPA that optimized the knee stiffness to achieve higher hopping height compared to the height obtained when a stiff actuator was used [30]. Hurst et al. have demonstrated on their MABEL robot [31] in in-place hopping experiments that energetically optimal stiffness maximizes the spring restitution. Although all these studies have applied VSAs to increase energy efficiency, they have not considered locomotion versatility, which is a crucial property, especially for autonomous robots. Such robots, which have to interact with unknown and changing environments, should be able to adapt to new environmental conditions with minimum loss of energy efficiency.

Towards this direction, we investigate the applicability of a new VSA design to improve energy efficiency and locomotion versatility. The employed actuator, named L-MESTRAN (Linear MEchanism for varying Stiffness via Transmission ANgle) is an improved version of the original design so-called MESTRAN [32]. Compared to the previous one, the L-MESTRAN offers a linear joint stiffness, instead of an exponential one, and a more compact design. In addition, the symmetrical compliant joint in [32] has been adapted to a uni-directional compliant joint in the L-MESTRAN. We

*This research was funded by three funding sources: (1) the LOCOMORPH project, within European Commission Seventh Framework Programme, Theme ICT-2007.8.5 under grant no 231688, (2) the Swiss National Science Foundation Professorship Grant No. PP00P2123387/1 and the Swiss National Science Foundation under The National Centre of Competence in Research (NCCR) Robotic project, and (3) the European Community Seventh Framework Programme FP7/2007-2013 Challenge 2, Cognitive Systems, Interaction, Robotics Under Grant No.248311-AMARSi.

Hung Quy Vu, Helmut Hauser, and Rolf Pfeifer are with the Artificial Intelligence Laboratory, Department of Informatics, University of Zurich, Switzerland (vqhung,hhauser, pfeifer at ifi.uzh.ch)

Derek Leach is with the Bio-Inspired Robotics Laboratory, Institute of Robotics and Intelligent Systems, Swiss Federal Institute of Technology Zurich, CH-8092 Zurich, Switzerland (derek.leach@mavt.ethz.ch)

978-1-4799-2722-7/13/$31.00 2013 IEEE

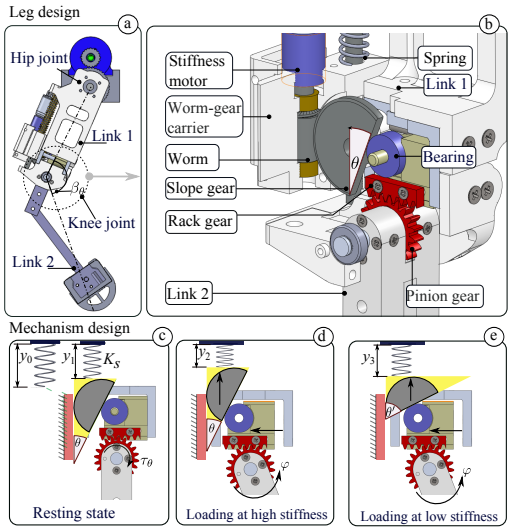

Fig. 1. Variable stiffness leg design. (a) Segmented-leg configuration. (b) Integration of the L-MESTRAN with the knee joint. (c) Mechanism in a unloaded state. (d) Mechanism under load at high stiffness. (e) Mechanism under load at low stiffness. The natural length of the spring is y_0. The length of the spring when the slope angle changes to θ under no load is y_1 . The length of the spring under external load, causing the link deflection φ, is y_2 . The length of the spring under external load at lower stiffness is y_3. The spring constant is K_s.

utilize this mechanism to systematically investigate how to improve energy efficiency in forward hopping locomotion on a segmented leg robot.

This paper is organized as follows: in Section II, the design of the L-MESTRAN mechanism is explained and its characteristics are experimentally validated. Section III presents the hopping experiments on the leg platform and discusses the results. Finally, Section IV presents the conclusions.

II. A MECHANISM TO VARY JOINT STIFFNESS

In this section, we present a newly developed legged platform, which is equipped with the L-MESTRAN at the knee joint. First, we present the general design of the leg and the L-MESTRAN. Second, we derive the static force analysis to investigate the principle of the stiffness variability. We then validate the characteristics of the mechanism.

A. Mechanical design

The hopping leg is equipped with the L-MESTRAN as shown in Fig. 1(a,b). It consists of an actuated hip joint and a passive knee joint that connects link 1 and 2. The hip joint is further connected to a supporting boom as shown in Fig. 6 and described in the next section. The L-MESTRAN mechanism is integrated at the knee joint to actively adjust the knee stiffness. The angle of the slope gear θ in Fig. 1(b) is the parameter that determines the stiffness of the joint, i.e., a lower angle of θ results in a higher knee stiffness (Fig. 1(d)), and vice versa. The stiffness motor is used to control the slope angle θ via the worm-gear. To reduce sliding frictions

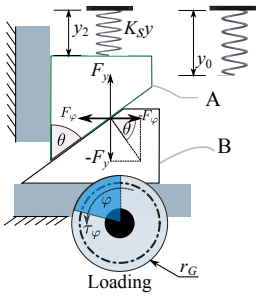

Fig. 2. Schematics for the force analysis. The interaction of the slope gear and the bearing is simplified as the interaction of two blocks, A and B.

between the contacting surfaces, a bearing is mounted on the rack gear block to roll on the slope gear.

In the resting state, i.e., when no external load is applied to link 2, the spring preload $y_0 - y_1$ is increased with the increase of the slope angles resulting in a different preloaded torque τ_θ. Under the loading state, i.e., when a force is exerted on link 2, link 2 rotates counterclockwise by an angle φ to push the rack gear against the slope gear at the angle θ (as in Fig. 1(d)) and compresses the spring with the stiffness K_s by an amount of $y_1 - y_2$. When the slope gear is turned to a larger angle θ' (as in Fig. 1(e)), the amount of spring compression $y_1 - y_3$, under the same displacement φ of link 2, is smaller, i.e., $y_1 - y_3 < y_1 - y_2$, which eventually results in a lower knee stiffness.

We compare the features of the old and the new design based on the MESTRAN [32] concept as follows. First, the stiffness of the knee joint in this design is linear, whereas it was exponential in the previous design. This linearity allows for a decoupling between external load and shaft of the stiffness motor, and, subsequently, a independence of the knee stiffness from the knee deflection. Second, to reduce possible undamped oscillations of the knee in flight phase, we designed the knee joint as a uni-directional compliant joint, instead of a symmetrical compliant joint as the previous one. This modification also improves the sturdiness, and compactness of the leg design. The advantageous characteristics of the original MESTRAN are preserved in the new design, i.e., both designs exhibit a large range of stiffness variability (theoretically, the stiffness can be set from zero to infinity), and both have the capability to maintain the joint stiffness with almost no energy.

B. Mathematical formulation of stiffness variability

To further analyze the performance of the proposed mechanism, this section shows a mathematical formulation of the L-MESTRAN.

As shown in Figure 1(d) and Fig. 2, the external torque rotates the pinion gear by an angle φ and pushes the rack gear with a force F_φ. It results in a force $F_y = K_s(y_0 - y_2)$ that compresses the spring with the spring stiffness K_s by an amount of $y = y_0 - y_2$. The force balance formula along

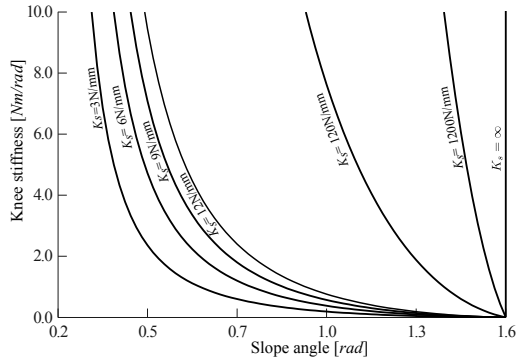

Fig. 3. Theoretical variations of knee stiffness versus the slope angles for various spring constants from 3.5 N/mm to infinity.

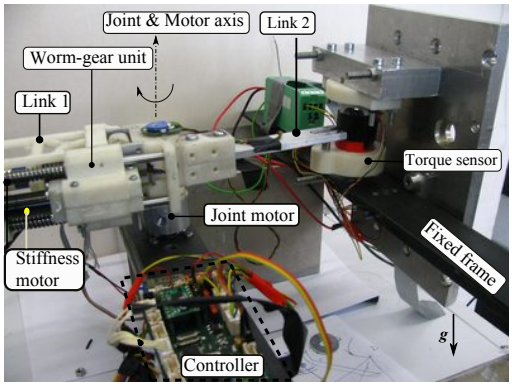

Fig. 4. Experiment setup for measuring torque versus angular deflection. The legged robot, mounted to the joint motor, consists of link 1, worm-gear unit, and link 2. The torque sensor is connected to link 2 in a way that the resulting torque generated by the joint motor can be measured by the torque sensor. The torque sensor is rigidly mounted on the fixed frame.

the axes is

$$F_\varphi = \frac{yK_s}{\tan\theta}. \tag{1}$$

The torque applied on the knee joint can be calculated from the force F_φ acting between the rack gear and the pinion gear and it is

$$\tau_\theta = F_\varphi r_G. \tag{2}$$

When no external torque is applied and the spring is pre-compressed by an amount $y_p = y_0 - y_1$, as shown in Fig. 1, the preloaded torque applied to the joint with respect to the slope angle θ is

$$\tau_\theta = \frac{y_p K_s}{\tan\theta} r_G. \tag{3}$$

The relationship between the link angle φ, slope angle θ, gear radius r_G, compression of the spring y, and translation of the block B (Fig. 2) is

$$x = y\tan\theta = r_G\varphi. \tag{4}$$

From Eq. 1, Eq. 2, Eq. 3 and Eq. 4 we obtain the relationship between the external torque τ_φ and the angular deflection φ

$$\tau_\varphi = \frac{K_s r_G^2}{\tan\theta^2}\varphi + \frac{y_p K_s}{tan\theta} r_G. \tag{5}$$

The rotational joint stiffness at the slope angle of θ is found by differentiating the external torque with respect to the angular deflection as follows:

$$K_\theta = \frac{\partial\tau_\varphi}{\partial\varphi} = \frac{K_s r_G^2}{\tan\theta^2}. \tag{6}$$

As one can see K_θ is defined only by design parameters, but for θ, which can be kept unchanged due to the non back-drivable characteristic of the worm-gear mate. Thus, we can achieve a fixed knee stiffness value with respect to θ. Furthermore, the slope angle θ is the only parameter to change the stiffness online.

C. Effects of spring constants to the knee stiffness

In the presented design, r_G is fixed by the leg design, thus it cannot be easily changed after the leg has been built. However, the spring elements can be replaced manually offline. Therefore, we investigated the influences of the spring constants on the knee joint stiffness to obtain guidelines for spring selection.

The variation of the joint stiffness K_θ versus the slope angle θ at various spring constants K_s according to our theoretical model (Eq. 6) is shown in Fig. 3. For any spring constant (K_s), as the slope angle changes from $\pi/2$ to 0.2 (rad), the joint stiffness increases from zero to infinity, respectively. However, the spring constant can affect the sensitivity of stiffness changes with respect to changes of the slope angle. For example, the spring constant $K_s = 1200\frac{N}{mm}$ results in almost a linear relationship between the slope angle and the stiffness. In contrast, the spring constant $K_s = 6\frac{N}{mm}$ results into large changes of stiffness at lower slope angles and smaller changes at high slope angles.

Given the fact that the efficiency of the worm-gear mate is rather low (about 20-90 (%)), the efficiency of the system could be limited when continuous adjusting stiffness is required. However, such high sensitivity of the knee stiffness changes with the slope angle can accommodate for energy losses and low speed output, since there is only a little actuation effort needed to achieve a large range of stiffness.

D. Identification of the torque-deflection relationship

In this section, we will present the experimental results on the relationship between the joint stiffness and the angular deflection. The results will be compared to the theoretical model in Eq. 6. The experiment setup is shown in Fig. 4. A brief description of the experiment is as follows.

The leg was mounted on the joint motor shaft in the horizontal direction to avoid the effects of gravity. The joint motor was vertically fixed to the frame. The end of link 2 was fixed by the torque sensor, such that the torque on the

TABLE I
EXPERIMENT DEVICES AND SPECIFICATIONS

Items	Specification
Torque sensor	FUTEK MODEL TFF325/ Torque capacity: 12 Nm
Joint motor	Faulhaber 324212CR, 24.7 W/Gear reducer 43:1
Stiffness motor	Maxon RE13, 1.5 W/Gear reducer 131:1
Spring constant	3.5 N/mm
Controllers	Maxon EPOS2 24/2 and Atmega328P

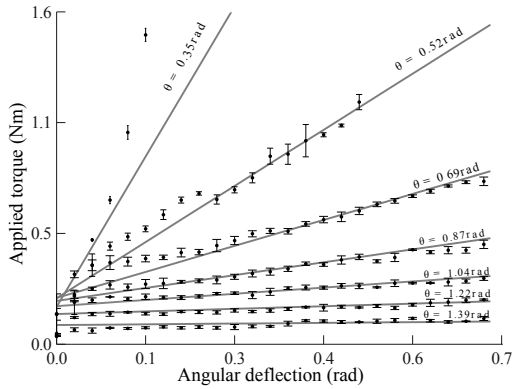

Fig. 5. Theoretical (dashed line) and experimental data (bold dots) of external torques versus angular deflections at the knee joint. The slope angle varies from 1.39 rad to 0.35 rad with an interval of 0.174 rad. The spring constant used in these experiments was 3.5 N/mm. The plotted results are the mean values and the standard deviation of the externally exerted torques.

knee joint was transferred via link 2 to the torque sensor, which was also fixed to the frame. The range of the slope angle was varied from 0.34 -1.36 (rad) with a discretized step of 0.17 rad. At each slope angle step, the joint motor varied the angle of link 1 from 0 - 0.68 (rad) with a step size of 0.017 rad. In order to investigate the reproducibility we conducted the whole process three times. The torque and the angular deflection were measured simultaneously via the Maxon EPOS2 controller. The results are shown in Fig. 5 together with the theoretical predictions, which were obtained from Eq. 6. The experimental specifications are shown in Tab. I.

The results show that regulating the slope angle results in different joint stiffness. Since the slope angle is nonlinear to the knee stiffness, as shown in Fig. 3, when the slope angle was varied in a fixed step, there were more measured joint stiffness at larger angles than that at smaller angles. For the same reason, at higher slope angles, the stiffness changes with respect to the slope angles is smaller than that at lower slope angles.

In summary, the theoretical as well as the experimental results have validated that the L-MESTRAN can be used to vary joint stiffness in a large range, thus, we were able to use it reliably in the hopping experiments as described in the following section.

TABLE II
HOPPING PLATFORM SPECIFICATIONS

Items	Specifications
β_0	134°
Length of link 1	0.115 m
Length of link 2	0.156 m
Weight of link 1	0.33 kg
Weight of link 2	0.08 kg
Weight of hip module	0.6 kg
Total leg weight	1 kg
Spring constant	3.5 N/mm
Hip motor	Faulhaber DC:234212CR 17 W/Gear reducer: 43:1
Stiffness motor	Maxon RE13, 1.5 W/Gear reducer 131:1
Controllers	Atmega328P
Gyros meter	Pololu: LPR550AL
Current sensor	Sparkfun:ACS712
Touch sensor	INTERLINK Electronics: 0.2”

III. HOPPING EXPERIMENTS

The stiffness variability of the L-MESTRAN allows us to systematically investigate on how to improve energy efficiency in hopping locomotion over different stride frequencies by adjusting the knee stiffness. First, we describe the experimental platform. Second, we analyze the hopping behaviors of the leg and present the experimental results. To evaluate the energy efficiency of the hopping leg, we used CoT as a criterion, which is defined as follows:

$$CoT = \frac{P}{M_s \times g \times v}, \tag{7}$$

where P, M_s, g, and v denotes the electrical power consumption, the total mass of the robotic leg, gravitational acceleration, and hopping speed.

A. Experimental setup

A complete leg platform supported by a boom has been constructed as shown in Fig. 6 (see Tab. II for more information). The L-MESTRAN was integrated at the knee joint. The boom with the length of 1.07 m was connected to the boom support and the hip joint. The DC motor was mounted to the hip module that was fixed on the boom. The leg was actuated by the motor via a pair of spur gears with a ratio of 2:1. The total weight consisting of the hip motor, boom, link 2 and link 1 measured at the leg position along the boom was one kg. To detect the flight and stance phase, a touch sensor located underneath the foot was integrated. In addition, the preloaded torque applied from the precompression force of the spring could quickly restore link 2 after being deflected in the stance phase and prevent extra-oscillation of link 2 before the next touch-down commenced. The preloaded torque was also sufficiently large to keep the same stand-still leg posture $(q_1(t=0), q_2(t=0))$(Fig. 6), when the knee stiffness was varied.

Since we were primarily interested in the passive behaviors of the hopping leg in order to study its natural dynamics, we applied a simple position control on the hip motor to

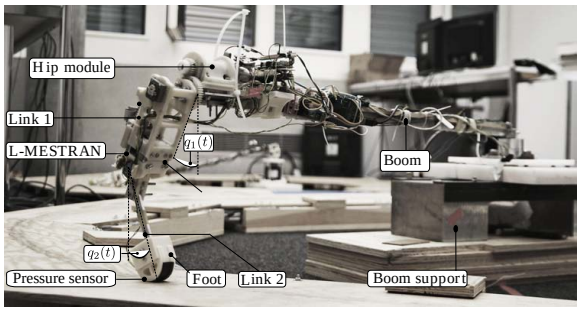

Fig. 6. A mechanical prototype of the single-leg hopping robot with boom support. The variable stiffness mechanism, L-MESTRAN, is equipped at the passive knee joint (see Fig. 1 for more detail).

actuate link 1. The desired trajectory was a simple sinusoidal function defined as

$$q_1(t) = A\sin(2\pi f t) + q_{\text{offset}}, \tag{8}$$

where A: Amplitude of oscillation, f: actuating frequency, t: time, and q_{offset}: offset angle of link 1.

A typical stable hopping behavior (i.e., link angles, joint deflection, hopping speeds, hip motor power) of the leg at 5 Hz is shown in Fig. 7 and Fig. 8. As we can observe, the deflection of the knee joint (q_2) together with the angular trajectories (q_1) shows the asymmetry of the knee joint, while the maximum average speed ($\dot{x}_m$) over 10 hopping cycles was about 0.85 m/s. In general, the leg's behavior is considered reproducible over hopping cycles, thus, we investigate the variations of CoT with stiffness variability at different stride frequencies in the next section.

B. Improving energy efficiency by joint stiffness adjustment

We conducted a series of experiments by using different oscillation frequencies f in the hip joint between 2 and $6Hz$, and varied the knee stiffness K_θ from 0.7 to $4.4Nm/rad$. The values of A and q_{offset} were heuristically found and were set to 0.26 ($15°$) and 0.086 ($5°$), respectively, such that the leg was able to hop forward at all 5 investigated frequencies, i.e., at 2, 3, 4, 5, and 6 (Hz). The robot did not hop under 2 Hz and showed non-reproducible behaviors for frequencies higher than 6 Hz.

For each combination of an actuating frequency and a joint stiffness, we collected data from 3 successful hopping trials. A trial was accepted as being successful, when the robot was able to hop one complete round about the boom support. Since Figure 9 only shows the successful trials, thus, the number of data points are not necessarily the same for each stride frequency.

The experimental results indicate that for all given stride frequencies from 2-6 (Hz), a proper adjustment of the knee stiffness results in a minimum CoT and an almost maximum speed. For example, at 2 Hz, the CoT and the speed are optimal at a knee stiffness of 0.8 Nm/rad. However, at 6 Hz, the stiffnesses for the minimum CoT and the maximum speed are slightly different as 1.7 Nm/rad for a minimum CoT and

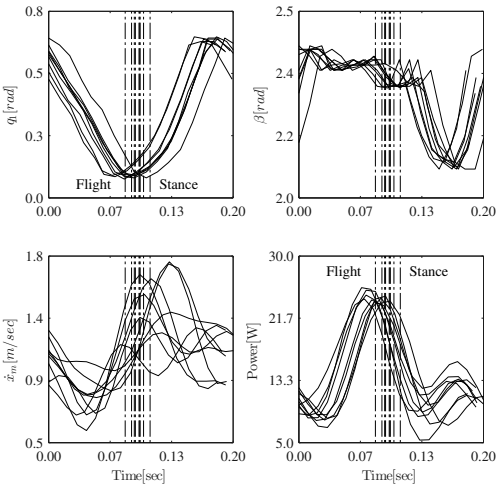

Fig. 8. Time series of link trajectories, forward speed and power consumption during 10 hopping cycles at the stride frequency 5Hz and the knee stiffness 1.8 Nm/rad. The data are plotted in one cycle scale. The dot-dashed vertical line in the middle of all sub-plots indicates the separation of stance and flight phase

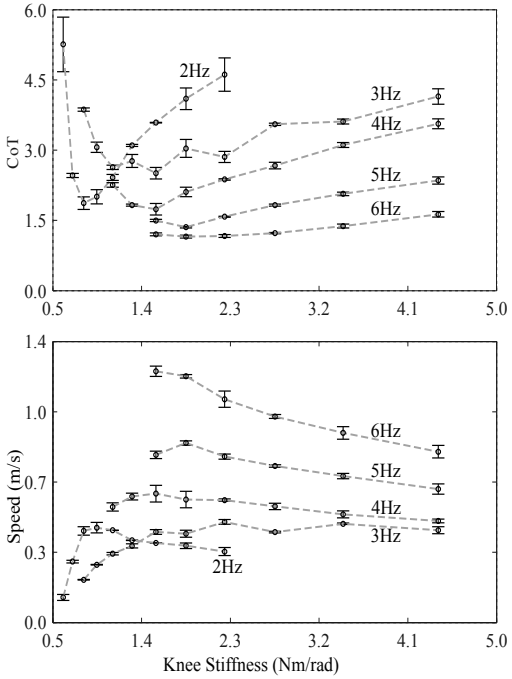

Fig. 9. Averaged CoT and speed versus knee stiffness at different actuating frequencies. The data show by the mean values over 3 successful trials and their standard deviations.

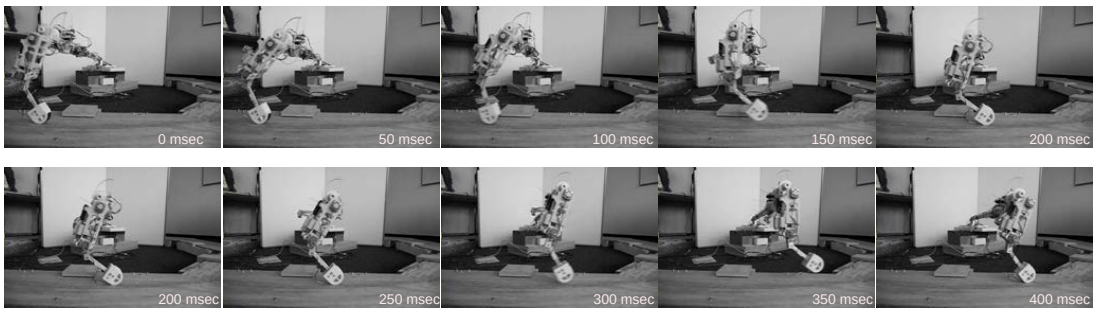

Fig. 7. Time series of two hopping cycles at the hip actuating frequency 5 Hz and the knee stiffness 1.8 Nm/rad.

1.5Nm/rad for a maximum speed. Furthermore, the variations profile of CoT and speed reveal the fact that hopping at lower frequencies, e.g., 2,3,4 (Hz), requires a higher care of adjusting the knee stiffness to achieve low CoT compared to hopping at higher frequencies, e.g., 5,6 (Hz). As shown in Fig. 9, at 6Hz, the changes of the knee stiffness do not cause a large variation of the CoT in contrast to the case when the leg is driven at 2 Hz. In addition, such variation profiles also indicate that the increasing stride frequency with knee stiffness can lead to higher locomotion speed and energy efficiency. From a control point of view, the same setup could be potentially used with adaptive controllers [33], such that the L-MESTRAN actuator would take over the role to automatically change the knee stiffness in accordance to the given stride frequency in an online fashion.

To investigate the capability of the L-MESTRAN actuator for changing the stiffness online and the influences of stiffness changes on the locomotion efficiency, we conducted experiments as described in the next section.

C. On-line adjustment of stiffness for increasing energy efficiency

In the following experiments, we investigated the influences of the knee stiffness adjustment at the stride frequency of 4 Hz. The experiment started by letting the robot hop at a low stiffness. We then increased the stiffness to the optimum value (i.e., 1.5 Nm/rad as shown in Fig.9). Figure 10a shows that when the knee stiffness was adjusted to the optimal value, the speed increased from 0.1 to 0.6 (m/s), while the power consumption was reduced to the half. As a result, the averaged CoT, i.e., computed by the averaged speed and power, dropped from 12 (before stiffness adjustment) to 1 (after stiffness adjustment). The duration for the leg dynamics to transit from the initial stiffness to the optimum was about 6 seconds. In the second experiment, the knee stiffness was set to a high value at the beginning and was decreased to the optimum value (in Fig. 10b). The result was a slightly reduced CoT after 1.6 sec of transition. Although the knee stiffness has been largely changed from 3.5 to 1.5 Nm/rad), the speed only changed in a little bit. However, the power consumption was reduced about 50%.

In both experiments, as expected, the CoT was reduced

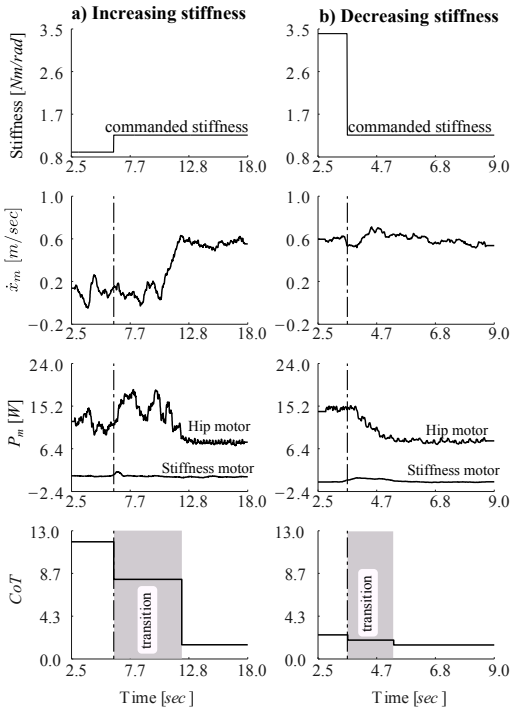

Fig. 10. Hopping behavior under dynamic conditions, i.e., varying the knee stiffness while hopping. (a) Knee stiffness changed from a low value to the optimal value. (b) Knee stiffness was changed from a high value to the optimal value. The gray bars indicate the transition periods of the leg behavior during the stiffness regulation

when the knee stiffness was regulated to the optimal value. However, the results also show that the leg was able to find back into a stable behavior after changing the stiffness. The power measurement of the stiffness motor shows that the L-MESTRAN consumes a remarkably small amount of power to change the stiffness, compared to the amount of power consumed by the hip motor. Furthermore, we would like to point out that to maintain the stiffness, the requiring amount of energy is negligible, since the slope angle is locked mechanically by the non-back drivable characteristic

of the worm-gear mate.

IV. Conclusions and future work

This paper presented the design and evaluation of a variable stiffness actuator, called L-MESTRAN, for energy efficient and versatile locomotion. The results of the static loading experiments have validated simulation results such that (1) the L-MESTRAN is capable of changing the joint stiffness over a large range and (2) it offers a linear joint stiffness. In addition, the dynamic experiments have demonstrated the potential applicability of using the L-MESTRAN to increase energy efficiency in hopping locomotion at various stride frequencies and, therefore, achieve locomotion versatility.

In order to investigate the underlying principle to improve energy efficiency by stiffness adjustment at various stride frequencies, there would be a need for theoretical analysis to reveal the underlying mechanism in future works. In addition, the study of stiffness adjustment found in this paper could also be extended to study hopping locomotion on surfaces with different stiffness, which is a regular condition for legged robots navigating outdoor in environments.

References

[1] A. D. Kuo, "Choosing your steps carefully: Trade-offs between economy and versatility in dynamic walking bipedal robots," *IEEE Robotics & Automation Magazine*, vol. 14, no. 2, pp. 18–29, 2007.

[2] R. Alexander, *Principles of animal locomotion*. Princeton, NJ: Princeton University Press, 2003.

[3] V. Tucker, "Energetic cost of locomotion in animals," *Comparative Biochemistry and Physiology*, vol. 34, no. 4, pp. 841–846, 1970.

[4] T. McGeer, "Passive Dynamic Walking," *International Journal of Humanoid Robotics*, vol. 09, no. 02, pp. 62–82, 1990.

[5] M. Reis and F. Iida, "An energy-efficient hopping robot based on free vibration of a curved beam," *Mechatronics, IEEE/ASME Transactions on*, vol. PP, no. 99, pp. 1–12, 2013.

[6] G. Gabrielli and T. Von Karman, "What price speed?," *Mech. Eng.*, vol. 72, p. 775781, 1950.

[7] S. Collins, A. Ruina, R. Tedrake, and M. Wisse, "Efficient bipedal robots based on passive-dynamic walkers." *Science (New York, N.Y.)*, vol. 307, no. 5712, pp. 1082–5, Feb. 2005.

[8] S. Collins and A. Ruina, "A bipedal walking robot with efficient and human-like gait," in *Robotics and Automation, 2005. ICRA 2005. Proceedings of the 2005 IEEE International Conference on*, 2005, pp. 1983–1988.

[9] Y. Sakagami, R. Watanabe, C. Aoyama, S. Matsunaga, N. Higaki, and K. Fujimura, "The intelligent asimo: system overview and integration," in *IEEE/RSJ International Conference on Intelligent Robots and Systems*, vol. 3, 2002, pp. 2478–2483.

[10] R. M. Alexander, "Three uses for springs in legged locomotion." *I. J. Robotic Res.*, vol. 9, no. 2, pp. 53–61, 1990.

[11] T. Dawson and C. Taylor, "Energetic Cost of Locomotion in Kangaroos." *Nature 246*, pp. 313–314, Nov. 19737.

[12] T. J. Roberts, R. L. Marsh, P. G. Weyand, and C. R. Taylor, "Muscular force in running turkeys: The economy of minimizing work," *Science*, vol. 275, no. 5303, pp. 1113–1115, 1997.

[13] M. Ahmadi and M. Buehler, "The arl monopod ii running robot: control and energetics," in *Robotics and Automation, 1999. Proceedings. 1999 IEEE International Conference on*, vol. 3, 1999, pp. 1689 –1694 vol.3.

[14] U. Scarfogliero, C. Stefanini, and P. Dario, "The use of compliant joints and elastic energy storage in bio-inspired legged robots," *Mechanism and Machine Theory*, vol. 44, no. 3, pp. 580–590, Mar. 2009.

[15] J. Rummel and A. Seyfarth, "Stable Running with Segmented Legs," *The International Journal of Robotics Research*, vol. 27, no. 8, pp. 919–934, 2008.

[16] B. Brown and G. Zeglin, "The bow leg hopping robot," in *Robotics and Automation, 1998. Proceedings. 1998 IEEE International Conference on*, vol. 1, may 1998, pp. 781 –786 vol.1.

[17] F. Danion, E. Varraine, M. Bonnard, and J. Pailhous, "Stride variability in human gait: the effect of stride frequency and stride length," *Gait & Posture*, vol. 18, no. 1, pp. 69–77, 2003.

[18] N. C. Heglund, C. R. Taylor, and T. A. McMahon, "Scaling stride frequency and gait to animal size: mice to horses," *Science*, vol. 186, no. 4169, pp. 1112–1113, 1974.

[19] M. Laurent and J. Pailhous, "A note on modulation of gait in man: effects of constraining stride length and frequency," *Human movement science*, vol. 5, no. 4, pp. 333–343, 1986.

[20] K. G. Holt, S. F. Jeng, R. Ratcliffe, and J. Hamill, "Energetic cost and stability during human walking at the preferred stride frequency," *Journal of Motor Behavior*, vol. 27, no. 2, pp. 164–178, 1995.

[21] N. C. Heglund and C. R. Taylor, "Speed, stride frequency and energy cost per stride: how do they change with body size and gait?" *Journal of Experimental Biology*, vol. 138, no. 1, pp. 301–318, 1988.

[22] A. Minetti and F. Saibene, "Mechanical work rate minimization and freely chosen stride frequency of human walking: a mathematical model," *Journal of experimental biology*, vol. 170, no. 1, pp. 19–34, 1992.

[23] P. Högberg, "How do stride length and stride frequency influence the energy-output during running?" *European Journal of Applied Physiology and Occupational Physiology*, vol. 14, no. 6, pp. 437–441, 1952.

[24] J. W. Hurst and A. Rizzi, "Physically variable compliance in running," in *CLAWAR*, September 2004.

[25] B. Vanderborght, A. Albu-Schaeffer, A. Bicchi, E. Burdet, D. Caldwell, R. Carloni, M. Catalano, O. Eiberger, W. Friedl, G. Ganesh, M. Garabini, M. Grebenstein, G. Grioli, S. Haddadin, H. Hoppner, A. Jafari, M. Laffranchi, D. Lefeber, F. Petit, S. Stramigioli, N. Tsagarakis, M. V. Damme, R. V. Ham, L. Visser, and S. Wolf, "Variable impedance actuators: A review," *Robotics and Autonomous Systems*, pp. –, 2013.

[26] B. Vanderborght, A. Albu-Schaffer, A. Bicchi, E. Burdet, D. Caldwell, R. Carloni, M. Catalano, G. Ganesh, M. Garabini, M. Grebenstein, G. Grioli, S. Haddadin, A. Jafari, M. Laffranchi, D. Lefeber, F. Petit, S. Stramigioli, N. Tsagarakis, M. Van Damme, R. Van Ham, L. C. Visser, and S. Wolf, "Variable impedance actuators: Moving the robots of tomorrow," in *Intelligent Robots and Systems (IROS), 2012 IEEE/RSJ International Conference on*, 2012, pp. 5454–5455.

[27] R. Ham, T. Sugar, B. Vanderborght, K. Hollander, and D. Lefeber, "Compliant actuator designs," *Robotics Automation Magazine, IEEE*, vol. 16, no. 3, pp. 81–94, 2009.

[28] N. L. Tagliamonte, F. Sergi, D. Accoto, G. Carpino, and E. Guglielmelli, "Double actuation architectures for rendering variable impedance in compliant robots: A review," *Mechatronics*, vol. 22, no. 8, pp. 1187–1203, Dec. 2012.

[29] K. C. Galloway, "Variable Stiffness Legs for Robust, Efficient, and Stable Dynamic Running," *Journal of Mechanisms and Robotics*, vol. 5, no. 1, p. 011009, Jan. 2013.

[30] B. Vanderborght, N. G. Tsagarakis, R. Ham, I. Thorson, and D. G. Caldwell, "MACCEPA 2.0: compliant actuator used for energy efficient hopping robot Chobino1D," *Autonomous Robots*, vol. 31, no. 1, pp. 55–65, 2011.

[31] J. W. Hurst, "The electric cable differential leg: a novel design approach for walking and running," *I. J. Humanoid Robotics*, vol. 8, no. 2, pp. 301–321, 2011.

[32] H. Vu, L. Aryananda, F. Sheikh, F. Casanova, and R. Pfeifer, "A novel mechanism for varying stiffness via changing transmission angle," in *Robotics and Automation (ICRA), 2011 IEEE International Conference on*, may 2011, pp. 5076 –5081.

[33] K. J. Åstrom and B. Wittenmark, *Adaptive Control*, 2nd ed., P. Hall, Ed. Addison Wesley Longman, 1995.

Appendix D

Improving energy efficiency of hopping locomotion by using a variable stiffness actuator

Reprinted from: Hung Q. Vu, Yu Xiaoxiang, Fumiya Iida, and Rolf Pfeifer. "Improving energy efficiency of hopping locomotion by using a variable stiffness actuator", submitted to The IEEE/ASME Transactions on Mechatronics, 2014 in Jan. 2014

IEEE/ASME TRANSACTIONS ON MECHATRONICS, VOL. .., NO. .., 2014

Improving energy efficiency of hopping locomotion by using a variable stiffness actuator

Hung Vu, Xiaoxiang Yu, Fumiya Iida, and Rolf Pfeifer

***Abstract*—In recent years, the development of legged locomotion robots that can achieve both efficiency and versatility has been one of the most important challenges in robotics research. In general, fully actuated systems that can achieve many variations of behaviors show comparatively low energy efficiency, while passivity-based systems that exhibit efficient behaviors suffer from enriched behavioral diversity. In order to overcome the tradeoff, there has been an increasing interest in the development of actuation technologies, such as variable stiffness actuators (VSAs) that can autonomously adjust mechanical dynamics. However, although many VSAs have been proposed and developed in the past, researchers are yet to clarify how such actuators can improve both energy efficiency and behavioral diversity. From this perspective, the goal of this paper is to investigate a one-legged hopping robot that is equipped with a class of VSA with the intention of explaining how behavioral diversity can be enhanced with modest impact in the energy efficiency. Through a systematic analysis including both simulation and a real-world robot platform, this paper investigates how the natural dynamics of hopping robots can be varied by the actuator resulting in variations in stride frequencies and locomotion speed while maximizing energy efficiency.**

***Index Terms*—Energy efficiency, leg stiffness, hopping locomotion, variable stiffness mechanism, variable impedance actuators, variable stiffness actuators.**

I. Introduction

THE development of versatile yet energy efficient locomotion robots has been a long-standing challenge in robotics research. On the one hand, fully actuated legged systems such as the humanoid robot ASIMO are capable of large variety of locomotion behaviors including walking, running, and climbing up stairs, whereas the robot's energy efficiency is known to be an order of magnitude worse than humans [1]. On the other hand, an alternative approach has been employed, in which passive dynamics was mainly exploited for efficient locomotion. A series of passivity-based locomotion robots have demonstrated walking behaviors at almost the same level of energy efficiency as those of human locomotion, although these robots are optimized only for this particular motion without any versatility [2].

For energy efficiency, the exploitation of natural mechanical dynamics seems to be an unavoidable option for energy efficiency. Passivity-based walking machines, for example, take advantage of swing leg dynamics to minimize energy consumption in locomotion while maintaining stability [3]. In biology, animals are also known to exploit mechanical dynamics in muscles, tendons and ligaments that store and release energy for efficient locomotion [4], [5]. This finding was further verified in some of the legged robots in which the elastic leg structures were proven to be effective for efficient hopping and running locomotion [6]–[8].

In order to enrich the versatility of passivity-based legged robots, e.g., traveling at various speeds, it is important to consider, among others, the variability of the so-called stride frequency, i.e. the frequency at which a legged system swings its legs. In biological systems, stride frequency was found to be important for two main reasons. First, the stride frequency has been shown to affect the variability of gait patterns such as walk, trot, bound, and gallop in such a way that as the frequency varies, animals usually switch between different gait patterns [9], [10] . Second, energy efficiency is also significantly related to the stride frequency in any of these gait patterns [11], [12]. Moreover, stride frequency is also important for legged locomotion in complex environments. Stride frequency is highly related to the stride length (i.e., distance between footholds) [13], [14], resulting in the speed variations, as well as the ground clearance of swing legs (the maximum height of the toe swing leg), which are crucial performance metrics for locomotion in rough terrains, in particular. However, changing the stride frequency in passivity-based legged robots present a challenging problem because this frequency is essentially determined by the given mechanical design of the robots such as leg length, body mass distributions, and leg stiffness [2], [3]. In principle, no change in these design parameters should result in the loss of energy efficiency.

From this perspective, there has been an increasing interest in the study of variable stiffness actuators (VSAs) which are expected to significantly enhance performances of legged robot locomotion under changes of stride frequency and locomotion speed [15]–[18]. In the past, a variable stiffness mechanism was tested in a hopping robot which demonstrated a larger hopping height if compared to the regular fixed stiffness in the leg [19]. Another variable stiffness mechanism was also investigated in a planar hopping robot for energy efficient locomotion at a fixed stride frequency [20]. A similar approach

This research was funded by three funding sources: (1) the LOCOMORPH project, within European Commission Seventh Framework Programme, Theme ICT-2007.8.5 under grant no 231688, (2) the Swiss National Science Foundation through the National Centre of Competence in Research Robotics, and (3) the European Community Seventh Framework Programme FP7/2007-2013 Challenge 2, Cognitive Systems, Interaction, Robotics under Grant No.248311-AMARSi.

Hung Vu and Rolf Pfeifer are with Artificial Intelligence Laboratory, Department of Informatics, University of Zurich, Switzerland.

Xiaoxiang Yu and Fumyia Iida are with Bio-Inspired Robotics Laboratory, Institute of Robotics and Intelligent Systems, Swiss Federal Institute of Technology Zurich, Switzerland.

Manuscript received ...; revised December

was also applied to a six-legged robot, Rhex, where a variable stiffness mechanism was investigated in terms of the energy efficiency and speed of locomotion [21]. Despite the recent intensive research activities in this research domain, it has not been fully clarified how energy efficiency can be improved over an extended range of stride frequencies such that a legged robot can take advantages of VSAs.

To fill the gap of the important knowledge, the goal of this paper is to provide a theoretical framework about the relationship between leg stiffness variability, energy efficiency and versatility in locomotion. The contributions of this paper is threefold. First, by using a simulation model of one-legged hopping robot, we first obtain a theoretical understanding on the relationship between leg stiffness, stride frequencies and energy efficiency. For this purpose, we employ a minimalistic model of one-legged robot, and prove the degree to which VSAs can contribute to energy efficiency of locomotion over a large range of stride frequency. Second, we propose the design and mechanism of a class of variable stiffness actuator that is able to best characterize the proposed locomotion framework. Third, we run a series of real-world experiments to show the feasibility of the aforementioned statement in practice.

We organize the rest of the paper as follows. In Section 2, we introduce a theoretical model of a one-legged hopping robot and show the analysis of energy efficiency in terms of leg stiffness and stride frequency. In Section 3, we present the design of a physical legged platform equipped with a variable stiffness mechanism L-MESTRAN. Following that we use this platform for the real-world experiments in Section 4 and provide some discussions on the results of the paper in Section 5. Finally, we conclude the paper in Section 6.

II. Analysis of Energy Efficiency in Hopping Locomotion with Different Stride Frequencies

This section introduces a simulation model of a one-legged hopping robot that was investigated in this paper. The theoretical analysis provides an insight into the relationship between energy efficiency and stride frequencies, and serves as a baseline for the more comprehensive experiments with the real-world hardware that is presented later in this paper.

A. A simulation model of a segmented one-legged robot

The following simulation model was developed by considering the simplicity which allowed a systematic analysis, on the one hand, and practicality, on the other hand, such that the model could be verified at the later stage on a real-world platform later. Note that in the real-world platform (Fig. 7), we used a boom arm that was restricted in the pitch direction to realize the planar motion of the legged robot. The hip part of the legged robot was rigidly mounted to the boom arm, thus, its pitching motion can be consider to be small and negligible during locomotion.

The model is assumed to be a one-legged hopping robot in a planar environment, and the leg consists of three masses and two links that are connected through two joints (i.e., hip and knee joints as shown in Fig. 1). In addition, we further assume that the knee joint is equipped with a variable stiffness actuator

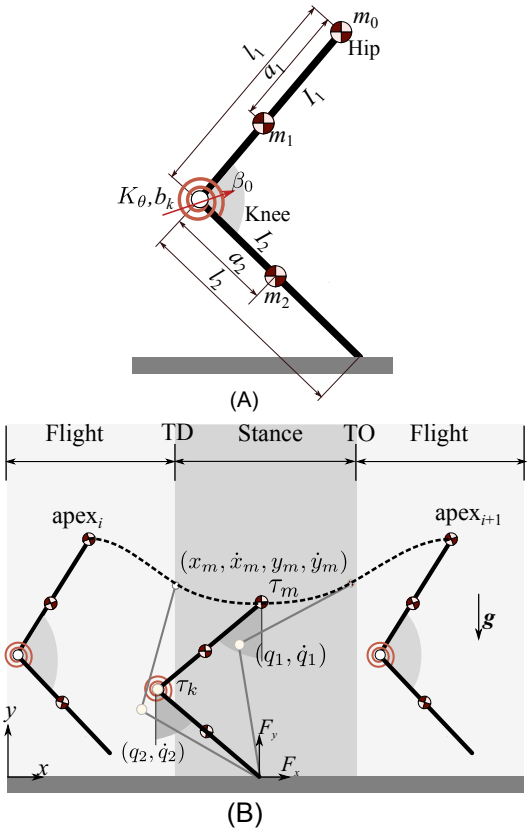

Fig. 1. A model of legged hopping locomotion. (**A**) A two-segmented leg with a knee and hip joints. The knee joint is simulated as a linearly variable stiffness joint. Three point masses m_0, m_1, m_2 are located at the hip joint, the center of mass of the link 1, and 2. (**B**) Hopping behaviors of the two-segmented leg in one cycle. The hopping cycle starts and ends at the apex points. The whole cycle is divided into three distinct phases: Flight, Stance, and Flight.

that dynamically regulates the stiffness of the torsional spring, whereas the hip joint is fully actuated with position control. As a result, the system consists of 12 design parameters (l_1, m_1, I_1, a_1, l_2, m_2, I_2, a_2, m_0, K_θ, b_θ, β_θ) as shown in Fig. 1(a). In particular, l_i and a_i denote the length in the leg geometry and m_i and I_i indicate the mass and inertial. In addition, K_θ, b_θ and β_θ define the characteristics of variable stiffness in the knee joint through stiffness, damping and rest angle, respectively.

Due to the constraint of the hip part to the boom arm in the real-world platform, the pitching degree of freedom of m_0 is not allowed during hopping simulations, as similar to the way human and animal locomotion are typically modeled by the template so-called SLIP (Spring Loaded Inverted Pendulum) [22]. Thus, in the numerical simulation that is described later in this section, we analyze eight state variables of this system:

(i.e., $\vec{u} = [q_1, q_2, x_m, y_m]^T$) and velocity of this vector $\dot{\vec{u}}$. Therefore, the equations of motion of this system can be described as follows:

$$\boldsymbol{M}(\vec{u})\ddot{\vec{u}} + \boldsymbol{B}(\vec{u}, \dot{\vec{u}})\dot{\vec{u}} + \boldsymbol{C}(\vec{u}) = \vec{\boldsymbol{\tau}}, \quad (1)$$

where $\boldsymbol{M}(\vec{u})$ is a 4×4 matrix of the mass and the inertia, $\boldsymbol{B}(\vec{u}, \dot{\vec{u}})$ is a 4×4 Coriolis/Centripetal matrix, $\boldsymbol{C}(\vec{u})$ is a 4×1 gravity-dependent vector, and $\vec{\boldsymbol{\tau}}$ denotes a 4×1 vector of the external generalized forces, which contains the external force components derived from motor torques, ground reaction forces, and spring torque. For the sake of nomenclature, we use the following symbols F_x, F_y, τ_m, and τ_k to represent the horizontal and vertical ground reaction forces, the hip actuated torque, and the knee spring torque, respectively.

Obviously, during the flight phase, the ground reaction force is a zero vector, but during the stance phase, the ground reaction force needs to be computed based on the ground interaction model. In order to simulate the ground reaction forces, a realistic nonlinear spring-damper model based on [23] was applied. The horizontal ground force F_x was modeled as the Coulombs friction in Eq. 2 and the vertical ground force F_y was produced by a nonlinear spring-damper model in Eq. 3.

$$F_x = \begin{cases} F_{slide} = \mu_{sl} F_y \dfrac{\dot{x}_g}{|\dot{x}_g|} & \text{if } F_x > F_{stiction} \\ F_{stiction} = \mu_{st} F_y \dfrac{\dot{x}_g}{|\dot{x}_g|} & \text{otherwise} \end{cases} \quad (2)$$

$$F_y = a\,|y_g|^3\,(1 - b\dot{y_g}), \quad (3)$$

where x_g and y_g are the coordinates of the foot with respect to the ground and $\dot{x}_g$ and $\dot{y}_g$ are the velocities of x_g and y_g. The kinetic and stiction friction coefficients are μ_{sl} and μ_{st}. Two empirical parameters are $a = 0.25 \times 10^9 (N.m^{-3})$ and $b = 1 sec.m^{-1}$.

In order to compute the hip motor torque τ_m, a simple position control policy is utilized in the actuation on the hip joint, so that the leg sinusoidally swings. As such, q_1 follows a sinusoidal signal as $q_1(t) = A\sin(2\pi f t) + q_1(0)$, where $q_1(t)$ denotes the value of q_1 at time t, while A and f denote the amplitude and frequency of the sinusoidal signal, respectively (note that f should match to the stride frequency during steady state hopping locomotion). In order to avoid the undamped oscillations of the leg during the flight phases, there is a constraint on the knee joint deflection such that the joint angle (the angle between two links) cannot be larger than β_θ.

The knee joint of this model is treated as a simple linear rotational spring, thus the torque generated in the joint τ_k should be determined by the joint angle given the stiffness, damping, and rest angle parameters.

In the rest of this section, we start every simulation analysis from an apex of hopping locomotion as shown in Fig. 1(b). Therefore, the initial condition of every simulation experiment can be described by (q_{10}, q_{20}, x_{m0}, y_{m0}, $\dot{q}_{10} = 0$, $\dot{q}_2 = 0$, $\dot{x}_{m0} = 0$, $\dot{y}_{m0} = 0$). The simulation is then switched between two phases, i.e., the stance and the flight phases, where a stance phase begins as soon as the toe touches down the ground (labeled by TD in Fig. 1(b)). The stance phase then is terminated at the point when the vertical component of the ground reaction force $F_y = 0$, and the next flight phase starts (labeled by TO in Fig. 1(b)).

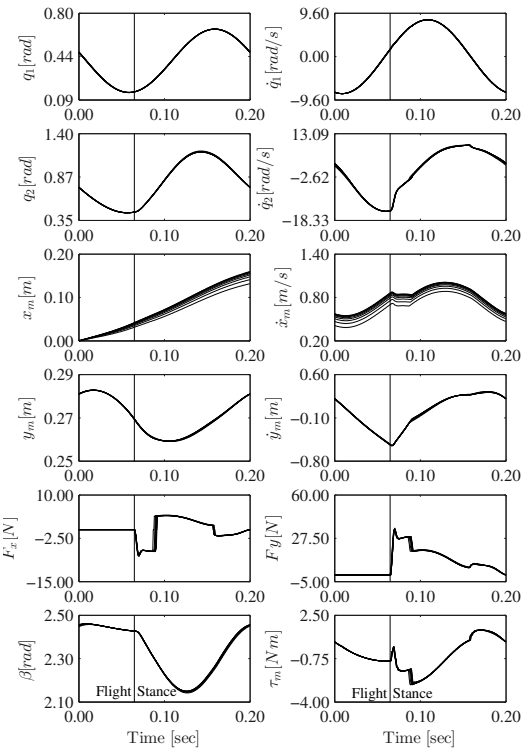

Fig. 2. The trajectories of eight state variables, ground reaction forces, F_x, F_y, knee bending angle β, and required torque τ_m at the hip for 10 cycles of legged hopping, where $f = 5Hz$ and $K_\theta = 4Nm/rad$. The vertical lines located at the middle of each plot indicate the switching moment between flight and stance phases. The forward speeds x_m were plotted as relative distances from the immediate preceding TO position to the current position of the hip point within a hopping cycle.

TABLE I
PARAMETERS OF USED IN ONE-LEG ROBOT LOCOMOTION

Parameters	Value	Parameters	Value
l_1	$0.115m$	l_2	$0.155m$
m_1	$0.32kg$	m_2	$0.080kg$
I_1	$4.1^{-4}kgm^2$	I_2	$8.1^{-6}kgm^2$
a_1	$0.06m$	a_2	$0.1m$
β_θ	$135°$	m_0	$0.6kg$
b_θ	$0.1Ns.m^{-1}$	K_θ	$0.7 - 4.7Nm/rad$

B. Method and stability of simulated locomotion

The proposed model was implemented and used to analyze the behaviors of the hopping leg. For the simulation explained in this section, we employed SimMechanics Toolbox in Matlab

(Mathwork Inc.) with the Runge-Kutta solver and fixed-step size of 0.0002 seconds, and every hopping simulation was conducted over five second periods. The other simulation parameters are listed in Tab. I, and these are mostly compatible with the real-world platform that is described later in this paper.

Using these parameters, the proposed model generally exhibits stable hopping locomotion over a relatively large range of control parameters (e.g., stride frequency and knee joint stiffness). Figure 2 shows a result of typical stable hopping behavior of this simulation model, in which the leg stride frequency $f = 5Hz$ and the knee joint stiffness $K_\theta = 4Nm/rad$ were used. This figure includes the time-series trajectories of the state variables, the torque actuated on the hip joint, and the vertical ground reaction force over 10 hopping cycles, aligned with respect to the TD point in every cycle.

As shown in Fig. 2, the locomotion dynamics is largely smooth regardless of some discrete events such as the transition between flight and stance phases as well as those of sliding and stiction ground interactions (i.e., F_x and F_y in Fig. 2). In the analysis presented in this paper, we consider only the stable locomotion as shown in Fig. 2. The stability can be evaluated through the trajectories of the state variables by analyzing the deviations of the state variables over 10 hopping cycles.

C. Analysis of energy efficiency for different stride frequencies

Throughout this paper, we employed the so-called "Cost of Transport" CoT as the dimensionless measure of energy efficiency in locomotion behaviors. The CoT can be defined as follows:

$$\text{CoT} = \frac{E}{M_{total} g d} = \frac{P}{M_{total} g v}, \tag{4}$$

where M_{total} and g denote the total mass of the leg and gravitational acceleration. d and v are the traveling distance and locomotion speed, and E and P denote the input energy and power. In this paper, we defined the input power in the simulations such that it could be directly compared with the electrical power used in the real-world experiments. In the simulation, the power consumption (P_m) was calculated as a product of the hip torque (τ_m), the current constant (K_A) of the DC motor employed in real-world platform, and the voltage (U) employed to supply the DC motor. The relation is $P_m = \tau_m K_A U$. Similarly, in the real-world experiments, the electrical power consumption was calculated as the product of the current consumption (I) ,i.e., as a product of the generated torque on the employed DC motor and the current constant (K_A), and the used voltage (U) as the relation: $P_m = IU$.

For a systematic analysis, the following experiments investigate energy efficient locomotion behaviors with respect to the different stride frequencies and the knee stiffness. As a baseline of analysis, we also consider the Eigen frequency of the hopping robot model. The Eigen frequency of the model f_e is computed based on the given knee stiffness K_θ and the resonance frequency of the system is linearized by assuming the model is fixed on the ground (see more details in the appendices). As a result, we can analytically derive the Eigen frequency f_e as a function of the knee stiffness K_θ which is depicted in Fig. 3. This figure essentially indicates that the Eigen frequency of the system increases as the system has larger knee stiffness.

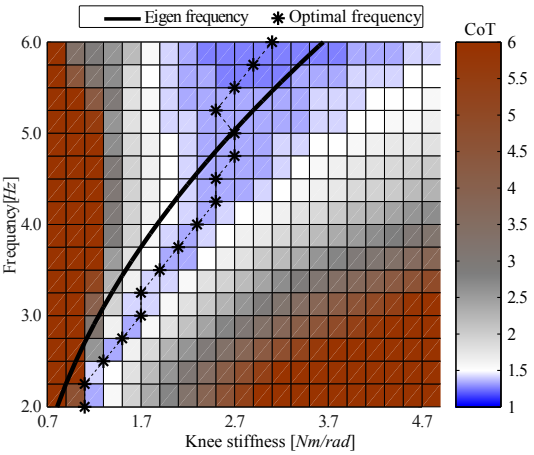

Fig. 3. CoT of hopping locomotion with different knee stiffness K_θ ($0.7 - 4.7Nm/rad$ with every $0.2Nm/rad$) and stride frequency f ($2-6Hz$ with every $0.25Hz$). The bar in the right indicates the relationship between the values of CoT and color. The solid line shows the Eigen frequency f_e with K_θ, while the dashed line connects the points at which the minimum CoT is achieved for each f.

Following that we also analyzed the energy efficiency of hopping locomotion with respect to the different stride frequency and knee stiffness in the same figure. For this analysis, we conducted a number of simulation experiments by varying both knee stiffness and stride frequency and analyzed the lowest cost of transport. Usually, CoT exhibited a concave profile with respect to a stride frequency, thus we were able to identify the optimum CoT, which were depicted by the asterisks in Fig. 3.

In general, because stride frequency is strongly related to locomotion velocity, CoT is usually lower as the stride frequency increases; this was also shown in Fig. 3. More specifically, at the higher stride frequency (depicted at the upper part of the figure), CoT was mostly between 1 and 2 over the range of knee stiffness, whereas it increased up to $CoT = 6$, when the frequency was lower. Nevertheless, it is important to note that the CoT could also be very low when the knee stiffness was set close to the Eigen frequency. For example, even when the stride frequency was set to 3 Hz, CoT could be as low as 1.7 when the knee stiffness was adjusted to 1.7 Nm/rad.

We can learn two important implications from this simulation results. First, variability of knee joint stiffness is very important in order to achieve high energy efficiency in hopping over different stride frequencies. Second, the energy efficiency of hopping locomotion is significantly related to the Eigen frequency of hopping locomotion, thus stiffness adjustment

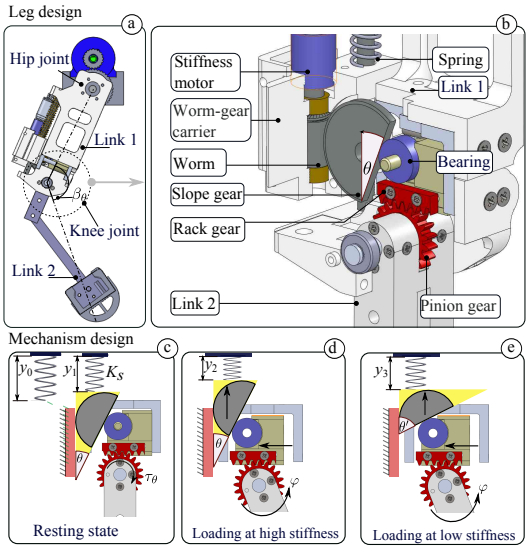

Fig. 4. The mechanical design of a hopping leg with the L-MESTRSAN mechanism. (a) A two-segmented leg. (b) Mechanical structure of the L-MESTRAN mechanism. (c)-(e) show the working principle of the L-MESTRAN mechanism. There are three states: (c) the unloaded state, (d) under load state with a high stiffness, and (e) under load state with a low stiffness.

should be designed and controlled with respect to the Eigen frequency. In the following experiments with the real-word robot platform, we will investigate these predictions from the simulation.

III. Variable Stiffness Mechanism for a One-Legged Hopping Robot

Even though we confirmed the effectiveness of a variable stiffness leg in efficient locomotion over a range of stride frequency, the real-world implementation of variable stiffness mechanisms is not a trivial problem. Prior to testing the target hypothesis of this paper in the real-world experimental platform, this section discusses the basic requirements and characteristics of VSAs, and introduces the system that we employed in this paper.

A. Design of variable stiffness mechanism

The variable stiffness mechanism (VSA) that we investigate in this paper is called L-MESTRAN. As shown in Fig. 4(a and b), the L-MESTRAN was designed to be easily integrated into a one-legged hopping robot while effectively controlling stiffness during locomotion. In the implementation shown in Fig. 4(a), the knee joint stiffness can be actively adjusted using the "stiffness motor" via a worm transmission. The angle of the slope gear θ in Fig. 4(b) is the important parameter that determines the stiffness of the joint, as a lower angle of θ results in a higher knee stiffness(Fig. 4(d)), and vice versa. In the absence of an external load applied to the link 2, due to

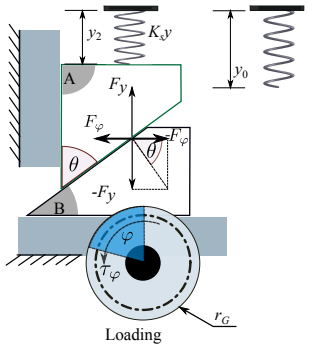

Fig. 5. Schematics for the force analysis. The interaction of the slope gear and the bearing is abstracted as the interaction of two blocks A and B. The natural length of the spring is y_0. With a joint deflection of φ, the linear spring has a compression of $y = y_0 - y_2$.

the geometrical constraints, the spring compression $y_0 - y_1$ (shown in Fig. 4(c)) becomes larger with the increase of the slope angles which results in the different preloaded torque, τ_θ. During operation, when the link 2 is exerted by a load, the joint rotates counter-clockwise by an angle φ to push the rack gear against the slope gear and the spring K_s by an amount of $y_0 - y_2$. In contrast, when the slope gear has a larger angle θ' (as in Fig. 4(e)), the amount of spring compression $y_0 - y_3$ with respect to an angular displacement φ is smaller, which eventually results in a lower knee stiffness.

As briefly mentioned in Section 1, a number of variable stiffness mechanisms have been proposed and analyzed in recent years [21], [24]–[27]. Although all of these mechanisms were designed and controlled to vary stiffness dynamically, we argue that the proposed VSA is more beneficial for the proposed locomotion framework than the other VSAs proposed in the past [28], [29]. First, it has a large range of stiffness variability as theoretically, the stiffness can range from zero to infinity. For example, the stiffness of the joint is zero (i.e.,completely passive) when the slope gear angle θ is $\frac{1}{2}\pi$ (rad), whereas, when θ is zero, it becomes a rigid joint. Second, since the worm-slope gear unit is not back drivable from the slope gear, the mechanism requires no energy to maintain stiffness in contrast to others [30]–[32]. Third, another feature of this actuator lies in the fact that the knee stiffness can be decoupled from the external load; this is not possible with some of others VSAs [16], [25]–[27]. As explained in the next subsection, the joint compliance is linear. In order to understand the principle of stiffness variability, we derive a static force analysis on the mechanism in the following subsection.

B. Mathematical formulation

To further analyze the performance of the proposed mechanism, this subsection shows a mathematical formulation of L-MESTRAN. As shown in Fig. 4(d) and conceptually in Fig. 5. The external torque rotates the pinion gear by an angle φ and pushes the rack gear with a force F_φ. This force applies

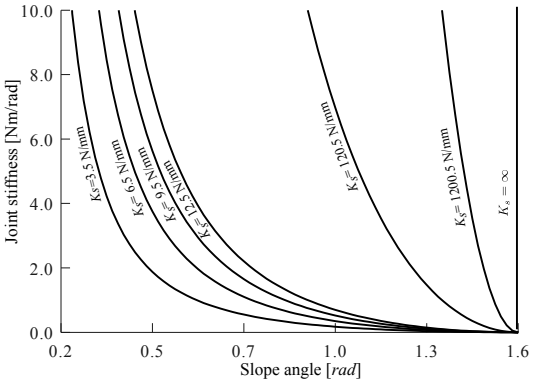

Fig. 6. The theoretical variation of the joint stiffness versus the slope angles at different spring constants from 3.5 N/m to infinite. The spring constant K_s = 3.5 N/mm and the radius $r_G = 12.5mm$ were used in the physical leg.

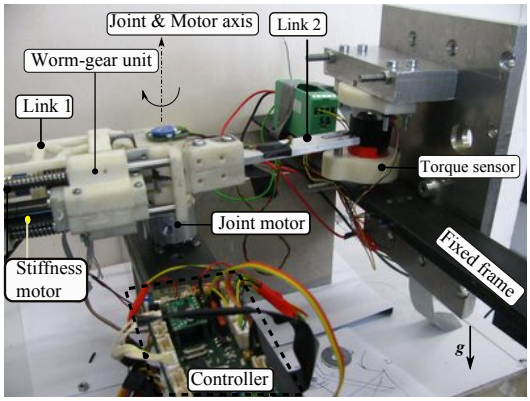

Fig. 7. Experiment setup for measuring torque versus angular deflection. The legged robot, mounted to the joint motor, consists of the link 1, worm-gear unit, and the link 2. The torque sensor is connected to the link 2 in a way that the resulting torque generated by the joint motor can be measured by the torque sensor. The torque sensor is rigidly mounted on the fixed frame.

a force $F_y = K_s(y_0 - y_2)$ on the y axis. As the spring is compressed by an amount of $y = y_0 - y_2$, the force balance formula along axes are

$$F_\varphi = \frac{yK_s}{tan\theta}. \tag{5}$$

The torque applied on the joint can be calculated from the force F_φ acting between the rack gear and the pinion gear is $\tau_\theta = F_\varphi r_G$. In the absence of external torque and the spring precompressed $y_p = y_0 - y_1$, as shown in Fig. 4, the preloaded torque applied on the joint with respect to the slope angle θ is

$$\tau_\theta = \frac{y_p K_s}{tan\theta} r_G. \tag{6}$$

The relationship between the link angles φ, the slope angle θ, gear radius r_G, and the compression of the spring y is

$$x = ytan\theta = r_G\varphi. \tag{7}$$

Therefore, from (Eq. 5), (Eq. 6), and (Eq. 7) we obtain the relationship between the external torque τ_φ and the angular deflection φ is

$$\tau_{(\varphi)} = \frac{K_s r_G^2}{tan\theta^2}\varphi + \frac{y_p K_s}{tan\theta} r_G. \tag{8}$$

The rotational joint stiffness at the slope angle of θ is found by differentiating the external torque with respect to the angular deflection as follows.

$$K_\theta = \frac{\partial \tau_{(\varphi)}}{\partial \varphi} = \frac{K_s r_G^2}{tan\theta^2} \tag{9}$$

The slope angle θ, the pinion gear radius r_G, and the spring constant K_s remains unchanged and are design parameters. Therefore, the knee stiffness is a constant at a given slope angle θ.

The variation of the joint stiffness K_θ versus the stiffness regulator (i.e., slope angle θ) at various spring constants K_s is shown in Fig. 6. As the slope angle changes from $\pi/2$ to 0.2 (rad), for any spring constant(K_s) the joint stiffness could also vary between zero and infinity. But the line with a higher K_s is more close to the right, which implies a certain range of slope angle θ can achieve a larger range of adjustable joint stiffness K_θ.

In order to validate the capability of L-MESTRAN we fabricated a leg with the integration of L-MESTRAN as a variable stiffness-passive knee joint, and identified the torque-deflection relationship. The results of this are presented in the next section.

TABLE II
EXPERIMENT DEVICES AND SPECICICATIONS

Items	Specification
Torque sensor	FUTEK MODEL TFF325/ Torque capacity: $12Nm$
Joint motor	Faulhaber 324212CR, 24.7 W/Gear reducer 43:1
Stiffness motor	Maxon RE13, 1.5 W/Gear reducer 131:1
Spring constant	K_s = 3.5 N/mm
Pinion gear radius	r_G = 12.5 mm
Controllers	Maxon EPOS2 and Atmega328P

C. Feasibility test of the real-world platform

We investigated the characteristics of the joint stiffness in the experiments, where the relationship of the joint torque versus the deflection angle is compared to the theoretical formulation (Eq. 9). The experiment setup is shown in Fig. 7. The leg was mounted on the joint motor shaft in the horizontal direction to avoid the effect of gravity. The joint motor was vertically fixed on the frame. The end of the link 2 was fixed by the torque sensor such that the torque on the link 2 was transferred to the torque sensor. The torque sensor was also fixed on the frame. The experiments were conducted as follows. The range of the slope angle was varied from 0.34 to $1.36rad$ with a discretized step of $0.17rad$. At each slope angle, the joint motor varied the angle of the link 1 from 0 to

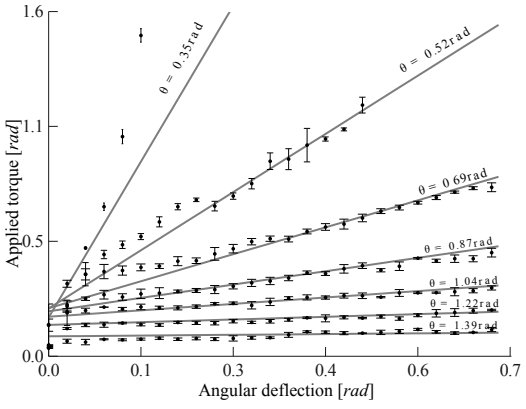

Fig. 8. The relationship between the applied torque τ and joint deflection φ with different slope angle θ when $K_s = 3.5Nm/rad$. The solid lines and dots show the theoretical and actual average results, respectively. The slope angle varies from 1.39 to $0.35rad$ with the interval of $0.174rad$. 3 measurements were conducted to computed the average and standard deviations.

$0.68rad$ with step size of $0.034rad$. In order to investigate the reproducibility we conducted the whole process three times. The torque and the angular deflection were measured simultaneously and the results are shown in Fig. 8 together with the theoretical predictions that were obtained from (Eq. 9).

The results show that regulating the slope angle results in different joint stiffness. When the slope angle increases, the joint stiffness also increases, as theoretically shown in Fig. 6. The preloaded torque τ_θ leads to an offset of applied torque, whereas this offset can be neglected with larger deflection angles. Although some fluctuation exist in experiment, the applied torques linearly rises with deflection angle. The coefficient of the linearity for θ is close to the theoretic stiffness. It shows the L-MESTRAN can, in theory, supply a large range of joint stiffness and exhibit the characteristics of a linear rotational spring.

Thus, we were able to use it reliably during the hopping experiments that are described in the following section.

IV. Experiments of the real-world hopping locomotion

In this section, we explain the locomotion experiments in the real world. Based on the basic insights obtained in Section 3, we investigate the degrees to which the model can explain the relationship between energy efficiency, stride frequency, and knee stiffness.

A. Experimental platform

A one-legged robot platform was constructed as shown in Fig. 9. A boom that rotates around a boom base was connected to the hip joint of the hopping leg. A DC motor with a gear transmission ratio of $2:1$ was mounted on the boom to actuate the leg swing around the hip joint. The leg could hop on a circular wooden floor and a touch sensors that was positioned underneath the foot was used to detect the contact with the ground during hopping processes. The parameters of the platform are listed in Tab. III.

TABLE III
Devices used in the legged hopping platform

Items	Specifications
Hip motor	Faulhaber DC:234212CR,17 W/Gear reducer: 43:1
Controllers	Two Atmega328Ps
Gyros meter	Pololu: LPR550AL
Current sensor	Sparkfun:ACS712
Touch sensor	Interlink Electronics: FSR 400

The values of A and $q_1(0)$ in the hip motor oscillation were heuristically found in the real-world experiment as 0.26 rad (15°) and 0.086 rad (5°), respectively. Since the torque of DC motors was used as control signals in the most practical environment, a simple PID control method was applied to achieve the desired position of q_1.

Based on the one-leg hopping locomotion platform, we conducted a series of hopping experiments. Figure 10 visualizes one-cycled behaviors of one typical stable hopping locomotion with the knee stiffness $K_\theta = 1.8Nm/rad$ and stride frequency $f = 5Hz$. Figure 11 shows the trajectories of the variables in 10 cycles, including the hip joint angle q_1, knee joint angle β, velocity of the hip joint x_m and input power P. The trajectories were plotted in one cycle scale and every cycle started at the beginning of the flight phase. The vertical dashed lines indicate the switch between the flight and stance phases.

As Fig. 11 depicts, the leg was able to achieve 10 cycle continuous hopping locomotion. The trajectories show this locomotion was stable, which is consistent with the results in Section 2.2. During the stance phase, an oscillation β in the sub-figure of Fig. 11, which means that the link 2 vibrated with respect to the link 1 due to the compliant nature of the knee joint. However, this oscillation was largely reduced (smaller than 0.15 rad) due to the preloaded torque in the knee joint. Moreover, the preloaded torque was also helpful to quickly restore the hip and knee joint angles q_1 and q_2 to initial values before the stance phase commenced.

B. Analysis of energy efficiency with stiffness variations

Similar to Section 2.3, we conducted a series of real-world experiments to investigate the energy efficiency of one-leg hopping locomotion with knee stiffness variability. In this experiment, we conducted a series of experiments by using different oscillation frequencies f in the hip joint between 2 and $6Hz$, and varied knee stiffness K_θ from 0.7 to $4.7Nm/rad$. With each set of the parameters, the robot exhibited mostly stable hopping, and we measured the locomotion velocity as well as energy consumption of the robots through the registered data of voltage and current used in the motors. All measured data in this section was the results of the robot hopping in three complete rounds in the experimental arena.

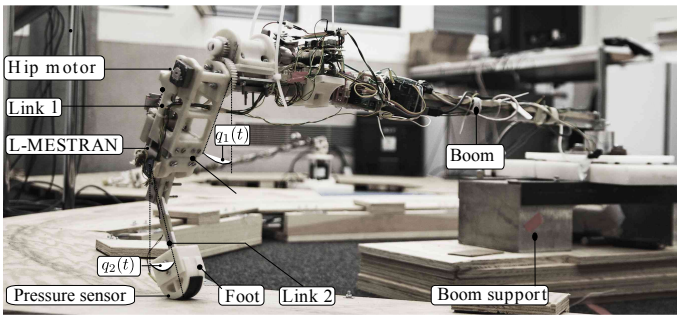

Fig. 9. A legged hopping platform based on the hopping leg equipped with the variable stiffness mechanism L-MESTRAN. The robotic leg is fixed with the boom which is constrained by the boom support. The pitch degree of freedom of the boom is rigidly restricted, thus only the yaw and roll degree of freedoms are released. The hip motor is fixed to the boom and its output torque is transmitted through a gear reducer 1:2 to the link 1. The photo was taken when the leg was at its initial state.

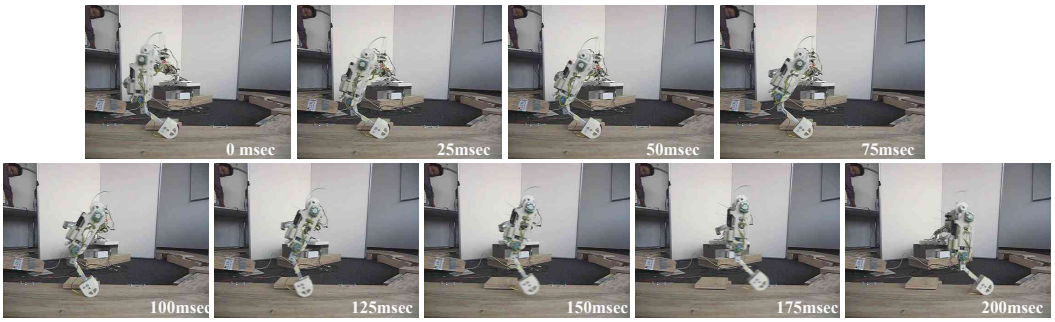

Fig. 10. A typical stable hopping behavior for one hopping cycles when the knee stiffness $K_\theta = 1.8Nm/rad$ and leg stride frequency $f = 5Hz$.

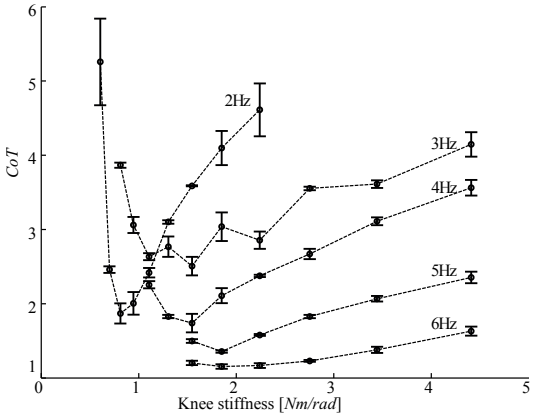

Fig. 12. CoT of legged hopping with the leg stiffness K_θ for different stride frequencies f : 2,3,4,5, and 6 (Hz). The mean values are average of three computed CoTs shown together with standard deviation bars.

In Fig. 12, the average and variations of CoT in real-world experiments were plotted against the knee stiffness over different hip oscillation frequencies. As also found from the simulation experiments (Fig. 3), a minimal CoT with K_θ, namely $K_{\theta opt}$, always existed for each stride frequency f. For example, the minimal CoT of 1.8 or 1 for $f = 2$ or $6Hz$ was achieved when K_θ reached 0.8 or $2Nm/rad$, respectively. In general, as the stride frequency increased, the range of K_θ and $K_{\theta opt}$ shifted towards to the right-hand side, similar to the trend found in the simulation experiments. For example, hopping at 6 Hz was only possible if the knee stiffness was higher than 1.5 Nm/rad, whereas at 2 Hz, the leg could successfully hop only when the knee stiffness was smaller than 2.2 Nm/rad. This trend was similarly observed in the simulation results, as indicated in Fig. 3 and Fig. 13

Through examining the results in Fig. 12, the improvement of the CoT at the different stride frequencies with the stiffness variability can be clarified as follows. At five stride frequencies: 2,3,4,5,6 (Hz), the CoTs were improved 60, 40, 50, 40, and 25 (%), respectively. The minimum amount of 25 % was a significant improvement promoted by a proper setting of the knee stiffness according to the stride frequency. Moreover, the variations of the CoT over different stride frequencies further indicated that hopping at lower frequencies, e.g., 2 and 3 (Hz), requires higher precision of knee stiffness adjustment than hopping at higher frequencies, e.g., 5 and 6 (Hz). In particular, at the stride frequency of 6 Hz, the CoT only increased from

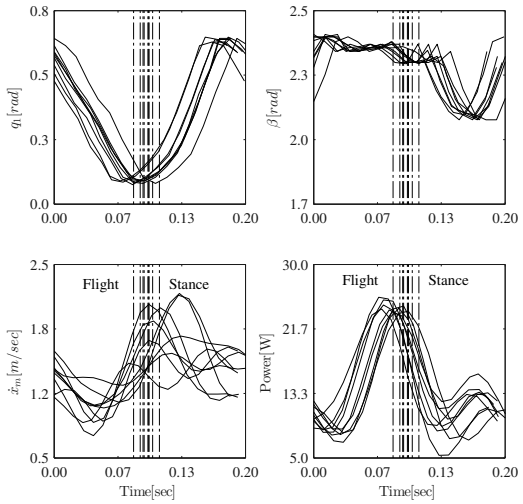

Fig. 11. Trajectories of hopping variables consisting of the angle of the link 1 q_1, the bending angle of the knee joint β, forward speed $\dot{x}_m$, and power consumption P_m in 10 cycles for the hopping behavior shown in Fig. 10, including the hip joint angle q_1, knee joint angle β, velocity of the hip joint x_m and input power P. The trajectories are plotted in one cycle scale from the ith TO to $(i+1)$th TO point and the vertical dashed lines indicate the switch between the flight and stance phases.

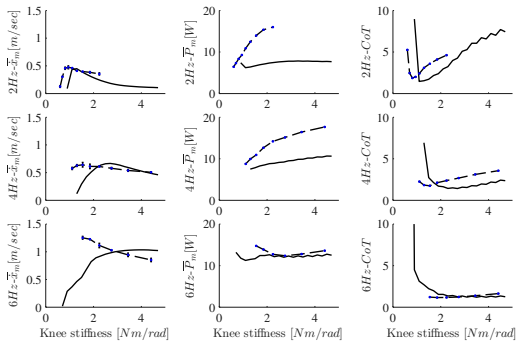

Fig. 13. CoT, average power consumption and average speed of the simulation (continuous lines) and real-world (dashed lines) hopping robot at 2, 4, and 6 (Hz). For each experimental data point, three computed CoT, measured speed, and measured power values were used to calculate the standard deviations.

1.3 to 1.5 (13%) when the knee stiffness varied from 1.5 Nm/rad to 4.7 Nm/rad (313%), whereas, at 2 Hz, a small change as 1Nm/rad of the knee stiffness could result in a rapid increase in CoT of 60%.

From this experimental result, we conclude that the variability of the leg stiffness is necessary for the improvement of the energy efficiency of one-leg robot hopping locomotion over the variations of stride frequencies.

C. Locomotion speed and input power during hopping locomotion

To gain additional insights into the relationship between CoT and the leg stiffness under various stride frequencies, we explore the input power and average locomotion speed that are the numerator and denominator of the calculation of cost of transport (Eq. 4). In this analysis, we use the experimental data from both the simulation and the real-world platforms, and plotted against the knee stiffness as shown in Fig. 13. In general, we observed that the simulation results provided good predictions of the experimental results in terms of the variation trend. Thus, we could use these two results for further investigations.

As shown in Fig. 13, one of the salient characteristics was that both the averaged speed $\bar{\dot{x}}_m$ and the averaged power consumption $\overline{P}_m$ of the locomotion largely varied with respect to the different stride frequency. In particular, maximum locomotion speeds and minimum power consumption changed from about 0.5 m/sec to 1 m/sec and about 6 W to 12 W, respectively, when the stride frequency varied from 2 Hz to 6Hz. In addition, Fig. 13 shows that it was necessary to increase the stride frequency in order to achieved increased speed.

Apart from the stride frequency, the variations of the knee stiffness also significantly influenced the speed, power consumption, and CoT for all three frequencies, i.e., 2,4,6 (Hz). As we can observe from Fig. 13, a proper adjustment of the knee stiffness could result in an increased speed and reduced power consumption, which resulted in a decrease in the CoT. The general trend from Fig. 13 revealed that, it was unavoidable to increase both the knee stiffness and the stride frequency to increase the hopping speed. For example, in the simulation, the maximum speed was achieved at 1 m/sec, when the knee stiffness was set at the maximum level, 4.7 Nm/rad. However, the leg with the maximum stiffness of 4.7 Nm/rad was not able to hop forward if the stride frequency was set at 2 Hz.

Concerning the simulation-reality gap, the difference between the simulation and experimental results was shown in Fig. 13. The simulation and experimental results correlated the most at 2Hz and deviated from each other as the stride frequency increased. This could be explained by the limitation of the model to simulate highly dynamic locomotion. As such, the more dynamically the locomotion performed, the more errors the simulation model accumulated. For more details in this difference, we further discuss the simulation-reality gap in Section 5.3.

V. Discussions

This paper has presented a study of how leg stiffness variability can improve the energy efficiency of legged robot locomotion with various stride frequencies. The theoretical analysis and simulation results provided insights into how the stride frequency relates to the leg stiffness to achieve energy efficient locomotion. We then sought more comprehensive real-world robot explorations to investigate this relationship. We have validated two important findings. First, energy efficiency of hopping locomotion is significantly related to Eigen

frequency of hopping systems. Second, a proper adjustment of knee stiffness at a given stride frequency always results in improved energy efficiency. We derive several points to discuss the overall results as follows.

A. Efficient locomotion with L-MESTRAN leg

VSAs are considered to be new actuation approaches which are capable of changing the intrinsic properties, e.g., Eigen frequency of the structure to which VSAs are mounted. Thus, a legged robot that is equipped with VSAs can potentially adjust its mechanical properties to exploit natural dynamics and, subsequently, improve both energy efficiency and versatility during locomotion. Through conducting a number of experiments on our robot, we have demonstrated that with the use of L-MESTRAN, the legged robot can improve energy efficiency during hopping at various stride frequencies. The minimum CoT of our system was 1.1 at the stride frequency of 6Hz and the knee stiffness setting 1.9 Nm/rad, shown in Fig. 12. This CoT value is indeed not very attractive by number itself, since running humans can achieve energy efficiency of around 0.2 and the other efficient robots without VSAs [3], [6], [33] can also attain the similar level of efficiency.

Comparing the CoT of the L-MESTRAN hopping robot with those of animals and other robots via Tucker diagram [33], [34], it is indicated that hopping locomotion of our robot is as efficient as those of running rabbits. The diagram also shows that the CoT among animals increases with body mass. Light animals, e.g., lizard, usually use more energy to travel over a unit distance than heavy ones, e.g., humans, horse. This trend also applies to artificial mobile machines as heavy machines can travel with lower CoTs than light ones. Based on this comparison, the hopping locomotion of our legged robot is considered to be efficient, and its level of efficiency is comparable to that of biological systems.

Furthermore, we were able to showed that with the use of VSAs, high energy efficiency and diverse behaviors of locomotion can co-exist in the intrinsic property of the leg. This capability of the L-MESTRAN robotic leg is unique among many other so-called "energy efficient robots" in which a very limited behavioral diversity can be exhibited.

B. Future work towards a more efficient hopping locomotion

In this paper, we aimed to explore how knee stiffness adjustment could improve the energy efficiency of hopping locomotion at various stride frequencies, thus, we did not optimize the hopping efficiency over a large parameter set. In implementation of the study, we heuristically chose and fixed other parameters while varying stiffness at various stride frequencies to produce a fair comparison of efficiency among various stride frequencies. This was a very rough constraint we had to impose for the experimental purpose. As a result, the parameter sets that were employed was not optimal to achieve the highest hopping efficiency, and the resulting CoT was greater than 1 as an understandable consequence.

However, the overall level of CoT can be potentially improved when more specific optimization processes can be implemented to explore the optimal parameter sets for a specific range of locomotion behaviors. For example, the optimization can be implemented at one specific stride frequency, that take into account other parameters such as the amplitude and the offset angle of leg oscillation and the knee stiffness. In addition, a simple feedback controller that takes into account the touch sensor of the foot to modify the leg trajectory depending on the contact of the leg with the ground could be necessary to improve energy efficiency of hopping.

C. Simulation-reality gap

In general, the simulation results of the leg model offered fair predictions of the hopping behaviors compared to that of the L-MESTRAN robotic leg. However, there are still some differences between the two results, especially, as the stride frequency increases. As nature of simulation, it seems unavoidable to close the gap between simulation and real-world data, however, it is important to identify sources that potentially cause the discrepancies between the experimental and simulation results in Fig. 13.

First, the ability of the model [23] employed to represent the reaction forces between the foot and the ground can be limited, and this could lead to imprecise predictions of the ground reaction forces in the simulations. The model reproduced the characteristics of the vertical forces as that of one non-linear visco-elastic element, whereas the horizontal force was described by a Coulomb (dry) friction model. The constants used in the model were found by matching results of the model with that of specific experimental results. Hence, the success of the model remains strongly sensitive to specific experimental conditions, therefore, the mismatch between the simulation and experimental results is understandable. Second, since the simulated leg was abstracted from the real robotic leg, there could be differences between behaviors of two PID controllers at the hip actuators of the simulation model and the real robotic leg. As presented in Fig. 2 and Fig. 11, the trajectories of the state variables were repeated in a higher order of precision in the simulation than the repeated trajectories in the experiments.

D. Efficiency of worm-gear mechanism for stiffness modulation

The L-MESTRAN leg was proposed with a worm-gear mechanism to drive the knee stiffness. This mechanism allows for a large torque amplification and speed reduction from the worm to the gear, due to the high gear ratio transmission. Thus, a low torque and high speed motor can be used to realize a large output torque within a compact design. Another important feature concerns the fact that the mechanism is only drivable from the gear if the lead angle of the worm is properly chosen. Our design used a single-thread worm with the lead angle of five degrees. Thus, the external load from the link 2 was decoupled from the stiffness motor's shaft and, subsequently, a constant stiffness setting could be retained without requiring energy.

Nevertheless, the main disadvantage of the worm-gear mechanism concerns the low power transmission efficiency, which is lower than many other gearing mechanisms, i.e.,

TABLE IV
PARAMETERS OF THE WORM-GEAR MECHANISM USED IN L-MESTRAN

Motor	Maxon: RE 13	Φ13 mm
	Efficiency	0.45
	Speed	13000rpm
	Power	1.5W
	Stall torque	3.4mNm
	Continuous torque	1.3mNm
Gearbox	Type	Planetary
	Efficiency	0.75
	Ratio	131
	Stage	3
	Max torque	3.4mNm
Worm-gear	Type	Single thread
	Efficiency	0.45
	Ratio	50
	Coefficient (φ)	0.16
	Helical angle (β)	5°

spur gears (98-99%), helical gears (98-99%), bevel gears (98-99%), crossed helical (70-98%), and worm-gear (20-98%). Especially, increasing the gear ratio causes a decrease in efficiency. Thus, continuous stiffness modulation is actually not recommended for the purpose of energy efficiency when a worm-gear mechanism is employed for setting stiffness.

In the L-MESTRAN design, we did not aim to explore the continuous stiffness modulation, but instead focused on the fixed optimal stiffness for each stride frequency. However, the mechanism was designed to be able to modulate the stiffness continuously during locomotion, as described in the following details.

The specifications of the worm-gear mechanism are shown in Tab. IV. The efficiency of worm-gear mechanism is calculated, based on the relation [35], [36] as follows.

$$\eta_{wormgear} = \frac{tg\beta(1-\varphi tg\beta)}{tg(\beta+\varphi)} = 0.41, \tag{10}$$

where β is the lead angle of the worm and φ is the friction coefficient between steel(worm) and bronze (gear). The total transmission efficiency η_{out} from the motor to the gear, which determines the slope angle (Fig. 11), is calculated as

$$\begin{aligned} \eta_{out} &= \eta_{motor} \times \eta_{gearbox} \times \eta_{wormgear} \\ &= 0.45 \times 0.75 \times 0.45 = 14\% \end{aligned} \tag{11}$$

From the continuous permissible torque of the motor (Tab. IV), it is possible to estimate the continuous torque output τ_o at the slope gear as follows.

$$\begin{aligned} \eta_{out} &= \frac{P_o}{P_m} = \frac{\tau_o\omega_o}{\tau_m\omega_m} \Rightarrow \tau_o = \frac{\eta_{out}\tau_m\omega_m}{\omega_o} \\ &= 0.14 \times 1.3 \times 131 \times 50 = 1.5(Nm) \end{aligned} \tag{12}$$

Similarly, we can obtain the stall torque at the slope gear as 3.1 Nm. In order to regulate the stiffness during locomotion, the torque from the stiffness motor, which is delivered to the slope gear, should be higher then the external torque which is applied at the tip of the foot. In Fig. 2, we can observe that the hip torque trajectory τ_m fluctuates within the same torque range in which the stiffness motor can deliver. Thus, the torque capacity of the stiffness mechanism is sufficient for changing stiffness during locomotion.

The electrical power P_m of the stiffness motor is lost during transmission with the efficiency η =0.14. The speed of the continuous stiffness regulation ω_o can be obtained by considering the motor power P_m and continuous permissible torque τ_o of the stiffness motor.

$$\omega_o = \frac{\eta_{out}P_m}{\tau_o} = \frac{0.14 \times 1.5}{1.5} = 0.14(rad/sec)/8(^\circ/sec) \tag{13}$$

As a result, it takes 3 seconds to regulate from the lowest (0.7Nm/rad) to highest stiffness (4.7 Nm/rad). Although the speed to vary stiffness ($\frac{4.7-0.7}{3} = 1.3Nm/(rad.sec)$ is not very high, the stiffness motor was capable of continuous stiffness modulation during locomotion.

E. Adding VSAs into legged robots: A tradeoff to be solved

While VSAs provide robots with a capability to regulate robot's mechanical dynamics via stiffness variation, integrating VSAs into legged robots usually causes increased weights and added inertia, which degrades robots' performance. As a matter of fact, to the best of the author's knowledge, none of robots with VSAs that control stiffness via back-drivable mechanisms have demonstrated forward dynamic locomotion performances. Although these robots have shown the advantages of using VSAs to improve the hopping efficiency, i.e., hopping height and energy consumption in in-place hopping, their mechanical structure is limited for dynamic locomotion. The ASMACS leg is rather heavy and complex in use [37]. The MACCEPA leg would encounter serious challenges in high stiffness modes, for example, in running locomotion, since its maximally producible stiffness is dependent on the maximum power of motors [31].

Determining the right level of non-back drivability given application requirements is potentially the key to solve the tradeoff [26], [38]–[41]. In this paper, we did not aim at continuous and rapid stiffness modulation during one locomotion cycle, thus, a small and compact worm-gear mechanism with a high gear ratio was used to regulate the stiffness. In exchange, a large range of stiffness can be achieved, no energy is consumed for maintaining a stiffness level, and a light-weighted and robust leg was achieved. Having adopted this design approach, we were able to demonstrate very dynamic locomotion behaviors of the robotic legs with L-MESTRAN at the knee joint. Thus, we were capable of performing systematic studies about the relationship between leg stiffness, stride frequency, and locomotion energy efficiency. Nevertheless, for robotic applications that energy supply is not a critical issue, fully back-drivable mechanisms is beneficial for force and stiffness control [42].

VI. CONCLUSION

The development of a legged robot that is capable of locomotion with high energy efficiency and diverse behaviors remains a significant challenge. For a systematic investigation of this challenge, this paper explored the relationship between energy efficiency, leg stiffness, and stride frequency. Through a series of simulation and real-world experiments of one-legged hopping locomotion, we showed that adjustment of knee joint

stiffness is crucial in order to achieve efficient locomotion with variations of stride frequencies. In particular, we clarified that the energy efficiency of locomotion of the hopping robot can be significantly improved by at least approximately 25% over different stride frequencies with the joint stiffness variability. Furthermore, the model-based analysis suggested that the energy efficiency of hopping locomotion is significantly related to the Eigen frequency of the system, which can be used as an effective indicator of the adjustment of knee stiffness.

There are still a number of questions that need to be investigated in the future. In particular, this paper was limited to an investigation of only a partial set of control and design parameters, and the influences these had requires further clarification. Also it would be very interesting to investigate the design and control of different types of stiffness adjustment mechanisms in the same context. On top of these additional investigations, we will be able to develop a more comprehensive understanding about the efficiency and versatility of various types of legged locomotion such as bipedal or quadrupedal robot locomotion.

APPENDIX

We refer to an equilibrium point of the leg motion when the leg is in steady state (i.e., standstill for our leg robot). We assume the system oscillates harmonically around this point and bears a toque $\vec{\boldsymbol{\tau_e}} = -K(\vec{q} - \vec{q_e})$ from the spring, where $\vec{q_e}$ =$[q_{1e}, q_{2e}]$ is equilibrium configuration of the leg. To obtain the Eigen frequency of the leg, we change the system coordinate to the equilibrium point with a new state vector $\vec{q'} = [q_1 - q_{1e}, q_2 - q_{2e}]$ and remove the first order term. The equation of motion (Eq. 1) is linearized as follows.

$$\boldsymbol{M'}(\vec{q_e})\ddot{\vec{q'}} + (\boldsymbol{K} + \boldsymbol{J}(\vec{q_e}))(\vec{q'}) = \vec{\boldsymbol{\tau_p}}, \tag{14}$$

where $\boldsymbol{M'}$ is 2×2 mass and inertia matrix, $\boldsymbol{J}$ is 2×2 jacobian matrix of gravity-dependent vector, and $\boldsymbol{K}$ is 2×2 stiffness matrix, and $\boldsymbol{\tau_p}$ is 2×1 preloaded torque vector. Then the Eigen frequency of the leg f_e is the Eigen value of $\boldsymbol{M'}^{-1}(\boldsymbol{K} + \boldsymbol{J}(q_e))$.

The mass and inertial matrix $\boldsymbol{M}(q_e)$:

$$\begin{aligned}
\boldsymbol{M}_{e11} &= 2l_1a_1m_1 - l_1^2m_0 - l_1^2m_1 - a_1^2m_1 - I_1 \\
\boldsymbol{M}_{e12} &= l_2a_1m_1cos(q_{10} - q_{20}) - l_1l_2m_1cos(q_{10} - q_{20}) - \\
&\quad l_1l_2mcos(q_{10} - q_{20}) \\
\boldsymbol{M}_{e21} &= l_2a_1m_1cos(q_{10} - q_{20}) - l_1l_2m_1cos(q_{10} - q_{20}) - \\
&\quad l_1l_2m_0cos(q_{10} - q_{20}) \\
\boldsymbol{M}_{e22} &= 2l_2a_2m_2 - l_2^2m_0 - l_2^2m_1 - l_2^2m_2 - a_2^2m_2 - I_2.
\end{aligned}$$

The jacobian matrix $\boldsymbol{J}(q_e)$:

$$\begin{aligned}
\boldsymbol{J}_{e11} &= l_1gm_0 + l_1gm_1 - a_1gm_1 \\
\boldsymbol{J}_{e12} &= 0 \\
\boldsymbol{J}_{e21} &= 0 \\
\boldsymbol{J}_{e22} &= l_2gm_0 + l_2gm_1 + l_2gm_2 - a_2gm_2.
\end{aligned}$$

The stiffness matrix $\boldsymbol{K}$:

$$\begin{aligned}
\boldsymbol{K}_{11} &= -K_\theta \\
\boldsymbol{K}_{12} &= K_\theta \\
\boldsymbol{K}_{21} &= K_\theta \\
\boldsymbol{K}_{22} &= -K_\theta.
\end{aligned}$$

The preloaded torque vector at the slope angle θ : $\vec{\boldsymbol{\tau_p}} = [-\tau_\theta, \tau_\theta]$.

REFERENCES

[1] Y. Sakagami, R. Watanabe, C. Aoyama, S. Matsunaga, N. Higaki, and K. Fujimura, "The intelligent ASIMO: system overview and integration," in *IEEE/RSJ International Conference on Intelligent Robots and Systems*, vol. 3, 2002, pp. 2478–2483.

[2] T. McGeer, "Passive dynamic walking." *I. J. Robotic Res.*, vol. 9, no. 2, pp. 62–82, 1990.

[3] S. Collins, A. Ruina, R. Tedrake, and M. Wisse, "Efficient bipedal robots based on passive-dynamic walkers." *Science (New York, N.Y.)*, vol. 307, no. 5712, pp. 1082–5, Feb. 2005.

[4] R. M. Alexander, "Three uses for springs in legged locomotion." *I. J. Robotic Res.*, vol. 9, no. 2, pp. 53–61, 1990.

[5] R. Blickhan, "The spring-mass model for running and hopping," *Journal of Biomechanics*, vol. 22, no. 11-12, pp. 1217–1227, 1989.

[6] M. Ahmadi and M. Buehler, "The ARL monopod II running robot: control and energetics," in *Robotics and Automation, 1999. Proceedings. 1999 IEEE International Conference on*, vol. 3, 1999, pp. 1689 –1694 vol.3.

[7] M. Reis and F. Iida, "An energy-efficient hopping robot based on free vibration of a curved beam," *IEEE/ASME Transactions on Mechatronics*, 2013.

[8] B. Brown and G. Zeglin, "The bow leg hopping robot," in *Robotics and Automation, 1998. Proceedings. 1998 IEEE International Conference on*, vol. 1, 1998, pp. 781–786 vol.1.

[9] D. F. Hoyt and C. R. Taylor, "Gait and the energetics of locomotion in horses," *Nature*, vol. 292, no. 5820, pp. 239–240, Jul. 1981.

[10] F. Danion, E. Varraine, M. Bonnard, and J. Pailhous, "Stride variability in human gait: the effect of stride frequency and stride length," *Gait & Posture*, vol. 18, no. 1, pp. 69–77, 2003.

[11] N. C. Heglund and C. R. Taylor, "Speed, stride frequency and energy cost per stride: how do they change with body size and gait?" *Journal of Experimental Biology*, vol. 138, no. 1, pp. 301–318, 1988.

[12] A. M. Grabowski and H. M. Herr, "Leg exoskeleton reduces the metabolic cost of human hopping," *Journal of Applied Physiology*, vol. 107, no. 3, pp. 670–678, 2009.

[13] N. C. Heglund, C. R. Taylor, and T. A. McMahon, "Scaling stride frequency and gait to animal size: mice to horses," *Science*, vol. 186, no. 4169, pp. 1112–1113, 1974.

[14] R. Alexander and G. Maloiy, "Stride lengths and stride frequencies of primates," *Journal of Zoology*, vol. 202, no. 4, pp. 577–582, 1984.

[15] Q. Hung Vu, L. Aryananda, F. I. Sheikh, F. Casanova, and R. Pfeifer, "A novel mechanism for varying stiffness via changing transmission angle," in *Proceedings of the RIEEE International Conference on Robotics and Automation*, 2011, pp. 5076–5081.

[16] K. C. Galloway, "Passive variable compliance for dynamic legged robots," Ph.D. dissertation, University of Pennsylvania, 2010.

[17] Y. Huang, B. Vanderborght, R. Van Ham, Q. Wang, M. Van Damme, G. Xie, and D. Lefeber, "Step length and velocity control of a dynamic bipedal walking robot with adaptable compliant joints," *Mechatronics, IEEE/ASME Transactions on*, vol. 18, no. 2, pp. 598–611, 2013.

[18] N. Tsagarakis, M. Laffranchi, B. Vanderborght, and D. Caldwell, "A compact soft actuator unit for small scale human friendly robots," *2009 IEEE International Conference on Robotics and Automation*, pp. 4356–4362, May 2009.

[19] B. Vanderborght, N. G. Tsagarakis, R. Ham, I. Thorson, and D. G. Caldwell, "MACCEPA 2.0: compliant actuator used for energy efficient hopping robot Chobino1D," *Autonomous Robots*, vol. 31, no. 1, pp. 55–65, 2011.

[20] J. W. Hurst, "The electric cable differential leg: a novel design approach for walking and running," *I. J. Humanoid Robotics*, vol. 8, no. 2, pp. 301–321, 2011.

[21] K. C. Galloway, "Variable stiffness legs for robust, efficient, and stable dynamic running," *Journal of Mechanisms and Robotics*, vol. 5, no. 1, p. 011009, Jan. 2013.

[22] R. Full and D. Koditschek, "Templates and anchors: Neuromechanical hypotheses of legged locomotion on land," in *The Journal of Experimental Biology*, vol. 202, 1999, pp. 3325–3332.

[23] K. G. Gerritsen, A. J. van den Bogert, and B. M. Nigg, "Direct dynamics simulation of the impact phase in heel-toe running," *Journal of Biomechanics*, vol. 28, no. 6, pp. 661–668, Jun. 1995.

[24] T. Takuma, S. Hayashi, and K. Hosoda, "3d bipedal robot with tunable leg compliance mechanism for multi-modal locomotion," in *Intelligent Robots and Systems, 2008. IROS 2008. IEEE/RSJ International Conference on*, 2008, pp. 1097–1102.

[25] S. Wolf, O. Eiberger, and G. Hirzinger, "The DLR FSJ: Energy based design of a variable stiffness joint," in *Robotics and Automation (ICRA), 2011 IEEE International Conference on*, may 2011, pp. 5082 –5089.

[26] A. Jafari, N. G. Tsagarakis, I. Sardellitti, and D. G. Caldwell, "A new actuator with adjustable stiffness based on a variable ratio lever mechanism," *Mechatronics, IEEE/ASME Transactions on*, vol. PP, no. 99, pp. 1–9, 2012.

[27] B.-S. Kim, J.-B. Song, and J.-J. Park, "A serial-type dual actuator unit with planetary gear train: Basic design and applications," *Mechatronics, IEEE/ASME Transactions on*, vol. 15, no. 1, pp. 108 –116, feb. 2010.

[28] N. L. Tagliamonte, F. Sergi, D. Accoto, G. Carpino, and E. Guglielmelli, "Double actuation architectures for rendering variable impedance in compliant robots: A review," *Mechatronics*, vol. 22, no. 8, pp. 1187–1203, Dec. 2012.

[29] B. Vanderborght, A. Albu-Schaeffer, A. Bicchi, E. Burdet, D. Caldwell, R. Carloni, M. Catalano, O. Eiberger, W. Friedl, G. Ganesh, M. Garabini, M. Grebenstein, G. Grioli, S. Haddadin, H. Hoppner, A. Jafari, M. Laffranchi, D. Lefeber, F. Petit, S. Stramigioli, N. Tsagarakis, M. V. Damme, R. V. Ham, L. Visser, and S. Wolf, "Variable impedance actuators: A review," *Robotics and Autonomous Systems*, vol. 61, no. 12, pp. 1601 – 1614, 2013.

[30] R. Schiavi, G. Grioli, S. Sen, and a. Bicchi, "VSA-II: a novel prototype of variable stiffness actuator for safe and performing robots interacting with humans," *2008 IEEE International Conference on Robotics and Automation*, pp. 2171–2176, May 2008.

[31] B. Vanderborght, N. G. Tsagarakis, C. Semini, R. Van Ham, and D. G. Caldwell, "MACCEPA 2.0: Adjustable compliant actuator with stiffening characteristic for energy efficient hopping," *Proceedings of the IEEE International Conference on Robotics and Automation (2009)*, pp. 544–549, 2009.

[32] S. Migliore, E. Brown, and S. DeWeerth, "Biologically Inspired Joint Stiffness Control," *Proceedings of the 2005 IEEE International Conference on Robotics and Automation*, no. April, pp. 4508–4513, 2005.

[33] A. D. Kuo, "Choosing your steps carefully: Trade-offs between economy and versatility in dynamic walking bipedal robots," *IEEE Robotics & Automation Magazine*, vol. 14, no. 2, pp. 18–29, 2007.

[34] V. Tucker, "The energetic cost of moving about," *American Scientist*, vol. 63, no. 4, pp. 413–419, 1975.

[35] W. Davis, *Gears for Small Mechanisms*. TEE Publishing, Limited, 1993.

[36] M. Quirini, A. Menciassi, S. Scapellato, C. Stefanini, and P. Dario, "Design and fabrication of a motor legged capsule for the active exploration of the gastrointestinal tract," *Mechatronics, IEEE/ASME Transactions on*, vol. 13, no. 2, pp. 169–179, 2008.

[37] J. W. Hurst, J. E. Chestnutt, and A. A. Rizzi, "An actuator with physically variable stiffness for highly dynamic legged locomotion," in *IEEE International Conference on Robotics and Automation*, vol. 5, 2004, pp. 4662–4667.

[38] B. Lambrecht, A. D. Horchler, and R. Quinn, "A small, insect-inspired robot that runs and jumps," in *Robotics and Automation, 2005. ICRA 2005. Proceedings of the 2005 IEEE International Conference on*, 2005, pp. 1240–1245.

[39] G. C. Haynes, A. Khripin, G. Lynch, J. Amory, A. Saunders, A. A. Rizzi, and D. E. Koditschek, "Rapid pole climbing with a quadrupedal robot," in *Proceedings of the IEEE International Conference on Robotics and Automation*, May 2009, pp. 2767–2772.

[40] D. Robinson, J. Pratt, D. Paluska, and G. Pratt, "Series elastic actuator development for a biomimetic walking robot," *1999 IEEE/ASME International Conference on Advanced Intelligent Mechatronics*, pp. 561–568, 1999.

[41] J. Clark, "Dynamic stability of variable stiffness running," in *2009 IEEE International Conference on Robotics and Automation*, May 2009, pp. 1756–1761.

[42] B. Siciliano and O. Khatib, Eds., *Springer Handbook of Robotics*. Springer, 2008.

Appendix E

Knee stiffness adjustment for energy efficient locomotion of a legged robot on surfaces with different stiffness

Reprinted from: Hung Q. Vu . "*Knee stiffness adjustment for energy efficient locomotion of a legged robot on surfaces with different stiffnes*" Robotics and Biomimetics (ROBIO), 2013 IEEE International Conference on 12-14 Dec. 2013, pp.1825-1831.

Knee stiffness adjustment for energy efficient locomotion of a legged robot on surfaces with different stiffness

Hung Q. Vu and Lorenzo G. Marcantini

***Abstract*— In recent years, there has been an increasing interest in the development of variable stiffness actuators (VSAs) for legged robots. In this paper, we explore how VSAs can be used in legged robots to achieve energy efficient locomotion on compliant surfaces at various stride frequencies. Our legged robot is consisted of an actuated hip joint and a passive knee joint equipped with a VSA, named L-MESTRAN. This VSA is capable of varying stiffness over a large range, maintaining stiffness without consuming energy, and offering a linear joint stiffness. The compliant surface was constructed with stiffness variability. Through simulation and preliminarily experimental results, we show that adjustment of the knee stiffness in the relationship with stride frequency and surface stiffness is beneficial for increasing the energy efficiency of hopping at various stride frequencies.**

I. INTRODUCTION

A number of legged robots have been developed to improve locomotion energy efficiency, however, most of them only performed on stiff surfaces [1], e.g., concrete-like surfaces. In the real world, locomotion does not take place only on stiff surfaces, but compliant, unstructured, and changing environments. Thus, legged robots, which aim for long-time autonomous navigation in outdoor environments, should also be able to adapt to uneven locomotion conditions, e.g., surfaces with different stiffness, while achieving energy efficient locomotion. By contrast, the locomotion capability of biological systems is far superior than that of any existing legged robot, today [2]–[4]. Indeed, animals/humans can efficiently walk or run on compliant surfaces at different locomotion speed.

One of the key features that allows animals/humans to traverse surfaces with different stiffness is the elasticity of their bodys complex muscle-tendon-ligament systems [5]. Such feature provides body and legs compliance to absorb external shocks and efficiently exchange mechanical energy, e.g., kinetic and potential energy, to exploit natural dynamics during locomotion. For example, in single jumping locomotion, it has been found that humans stiffen the legs to land on compliant surfaces and soften them when landing on stiff surfaces [6], [7]. Similarly, the adjustment mechanism of leg stiffness for different surface stiffness has also been found in the in-place hopping experiments [8]. When the ground stiffness reduced from the stiffest value to the least, the leg stiffness of the hopping subjects in the experiments increased more than twice. The total stiffness, i.e., a series combination of the surface and the leg stiffness, remained unchanged regardless of the surface stiffness. In running, Farley et al., found that human runners adjust their leg stiffness to accommodate for changes in the surface stiffness [9]. Such adjustment allows them to maintain their running mechanics over surfaces with different stiffness.

In legged robotic research, the studies of locomotion on compliant surfaces have just been at an early state. Little is known about how to adjust leg stiffness to accommodate for changes of surface stiffness during locomotion. One of the difficulties in such studies could be that in order to cope with changes in the surface stiffness, one would need a VSA [10], [11] to dynamically adjust the stiffness of robotic legs. However, incorporating VSAs into a legged robot usually increases the size, weight, and, inertia, which would, eventually, degrades the agility and efficiency of the legged robot for dynamic locomotion. Furthermore, the interaction of legs and surfaces during locomotion is highly complicated, which involves a number of locomotion parameters: leg stiffness, surface stiffness, leg damming, surface damming, and stride frequency, i.e., the frequency at which the legs swing. Thus, this topic remains challenging in the field of legged robots.

Progressing along this direction, the research presented in this paper preliminarily explored how leg stiffness could be exploited to improve the energy efficiency of robots on compliant surfaces at various stride frequencies. We developed a segmented leg, which incorporated with a VSA, named L-MESTRAN (Linear MESTRAN), at the knee joint to change the stiffness. This VSA is an improved version of the original design, so-called MESTRAN [12]. To vary the stiffness of the surface, we constructed an experimental platform with stiffness variability. This paper is organized as follows. In Section II, a design of the robotic leg is presented and characteristics of the knee joint are shown. Section III presents a legged hopping model and simulation results. Following that, Section IV presents real world hopping experiments to test the simulation results. Finally, Section V and VI will discuss the results and conclude the paper.

*This research was funded by the LOCOMORPH project, within European Commission Seventh Framework Programme, Theme ICT-2007.8.5 under grant no 231688. Additionally, the research has received funding from the European Community Seventh Framework Programme FP7/2007-2013 Challenge 2, Cognitive Systems, Interaction, Robotics Under Grant No. 248311-AMARSi.

Hung Q. Vu is with the Artificial Intelligence Lab, University of Zurich and the Bio-Inspired Robotics Laboratory, Institute of Robotics and Intelligent Systems, Swiss Federal Institute of Technology Zurich, CH-8092 Zurich, Switzerland (vqhung@ifi.uzh.ch)

Lorenzo G. Marcantini is with the Bio-Inspired Robotics Laboratory, Institute of Robotics and Intelligent Systems, Swiss Federal Institute of Technology Zurich, CH-8092 Zurich, Switzerland (lorenzog@student.ethz.ch)

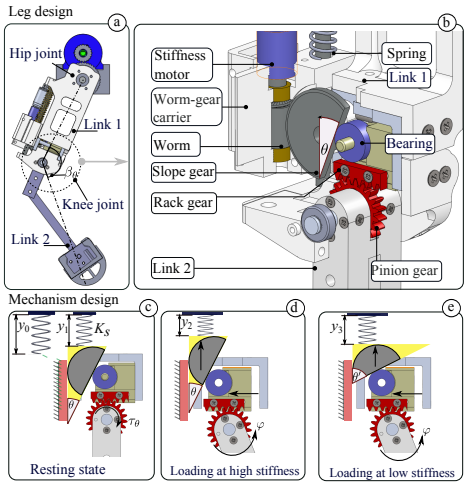

Fig. 1. Variable stiffness leg design. (a) A segmented-leg configuration. (b) Integration of the L-MESTRAN with the knee joint. (c) Mechanism in a unloaded state. (d) Mechanism under load at high stiffness. (e) Mechanism under load at low stiffness. The natural length of the spring is y_0 . The length of the spring when the slope angle changes to θ under no load is y_1 . The length of the spring under external load, causing the link deflection φ, is y_2 . The length of the spring under external load at lower stiffness is y_3. The spring constant is K_s.

II. A MECHANISM TO VARY JOINT STIFFNESS

In this section, we present a newly developed legged platform, which is equipped with L-MESTRAN at the knee joint. First, we present the general design of the leg and L-MESTRAN. Second, we derive the static force analysis to investigate the stiffness variability. We then validate the characteristics of the mechanism in the end of this section.

A. Mechanical design of the robotic leg

The robotic leg is consisted of an actuated hip joint and a passive knee joint, which connects link1 and 2, as shown in Fig. 1(a,b). The hip joint is connected to a boom arm, as shown in Fig. 4, and the knee joint is integrated with L-MESTRAN to actively adjust the knee stiffness. The angle of the slope gear θ in Fig. 1(b) is the parameter that determines the stiffness of the knee joint as a lower angle of θ results in a higher knee stiffness (Fig. 1(d)) and vice versa. The stiffness motor is used to control the slope angle θ via the worm-gear. To reduce sliding frictions between the contacting surfaces, a bearing is mounted to the rack gear to roll on the slope gear.

As shown in Fig. 1, at the resting state, i.e., when no external load is applied to link2, the spring preload $y_0 - y_1$ (Fig. 1c) increases with the slope angles θ, resulting in a preloaded torque τ_θ. At the loading state, i.e., when a force is exerted on link2, link2 rotates in the counterclockwise direction by an angle φ to push the rack gear against the slope gear (Fig. 1(d)). As a result, the spring K_s is compressed by an amount of $y_1 - y_2$. When the slope gear is turned to an

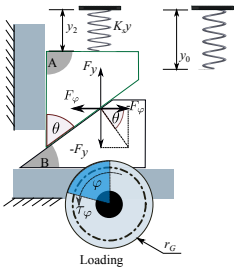

Fig. 2. Schematics for the force analysis. The interaction of the slope gear and the bearing is simplified as the interaction of two blocks, A and B.

angle $\theta'(> \theta)$ (Fig. 1(e)), the amount of spring compression under the same displacement φ is smaller, compared to that when θ is used, which eventually results in a lower knee stiffness.

Similar to the previous MESTRAN [12], the torque formulation of L-MESTRAN under a deflection of φ can be realized as follows:

$$\tau_\varphi = \frac{K_s r_G^2}{tan\theta^2}\varphi + \frac{y_p K_s}{tan\theta} r_G, \tag{1}$$

where the second term in the right-hand size is the preloaded torque applied by the pre-compression of the linear spring with stiffness K_s. The spur gear radius and the compression of the spring are r_G and y_p, respectively. Thus, the rotational joint stiffness at the slope angle of θ is

$$K_\theta = \frac{\partial \tau_\varphi}{\partial \varphi} = \frac{K_s r_G^2}{tan\theta^2}. \tag{2}$$

In (2), K_θ is defined only by design parameters but for θ, which can be kept unchanged due to the non-backdrivable characteristic of the worm-gear mate. We therefore can achieve a linear stiffness at the knee joint, and this linearity can be regulated by controlling θ. Furthermore, this linearity allows for a decoupling between external load and the stiffness motor's shaft, and, subsequently, an independence of the knee stiffness from the knee deflection.

We validated this theoretical characteristic by conducting progressive torque loading experiments using the Futek torque sensor (TFF325) as follows. External torques were applied to the knee joint and the reaction torque was measured by the torque sensor. The applying process was carried out three times at each slope angle θ shown in Fig. 3. Theoretical and experimental results validated that regulating the slope angle results in the different joint stiffness. Further details of this experiments and the features of L-MESTRAN can be found in the author's recently accepted paper [13].

To begin investigating the energy efficiency of the robotic hopping leg on surfaces with different stiffness, we examine the hopping efficiency through a hopping model as presented in the next section.

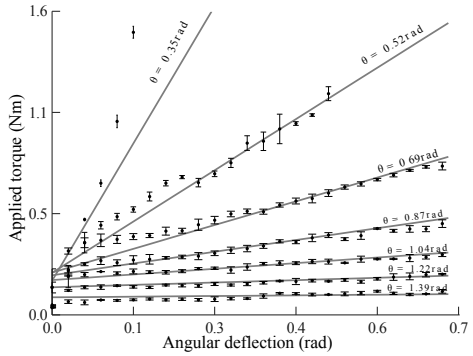

Fig. 3. Theoretical (dashed line) and experimental data (bold dots) of external torques versus angular deflections at the knee joint. The slope angle varies from 1.39 to 0.35 with an interval of 0.174. The plotted results are the mean values of 3 measured torques and the standard deviation of the externally exerted torques.

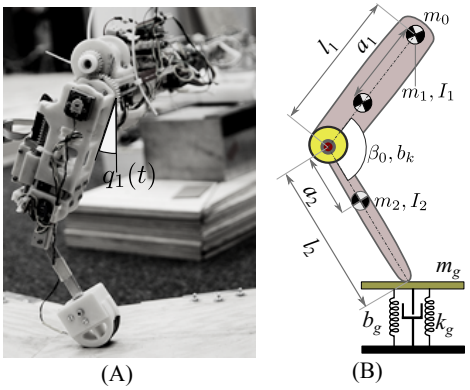

Fig. 4. Mechanical design parameters of the real hopping leg and the leg model on the variable stiffness surface (A and B). The leg model consists of two links with two revolute joints which are referred to as the hip and the knee. The hip joint is considered as damping free whereas the knee joint is modeled with viscous-damping effect b_k. The rest angle formed by two links is β_0. The surface is modeled by a mass m_G supported by a linear spring with viscous damping b_G. The hip part of the leg is mounted on the boom arm which allows the leg hopping around the boom base at the experimental arena.

III. Modeling and Simulation of Hopping on Surfaces with Different Stiffness

A. A hopping model description

All design parameters of this model are presented in Fig. 4A, which closely abstracts the mechanical structure of the real robotic leg, shown in Fig. 4B, and the compliant surface, shown in Fig. 6. Note that since the hip part of the robotic leg was mounted on the boom arm, the hip pitching motion is omitted in the model.

This model consists of a one-legged hopper and a compliant surface in a planar environment. The leg consists of three masses ($m_0, m_1,$ and m_2) and two connecting links

TABLE I
Parameters of used in one-leg robot locomotion

Parameters	Value	Parameters	Value
l_1	0.115 m	l_2	0.155 m
m_1	0.32 kg	m_2	0.080 kg
I_1	4.1^{-4} kgm^2	I_2	8.1^{-6} kgm^2
a_1	0.06 m	a_2	0.1 m
β_θ	135°	m_0	0.6 kg
b_θ	0.1 Ns.m^{-1}	K_θ	0.7-4.7 Nm/rad
b_g	0.05 Ns.m^{-1}	K_g	3000→63000 (N/m)
m_g	0.5 kg		

($l_1$and l_2) at the hip and knee joints. We further assume that the knee joint is equipped with a variable stiffness actuator, which dynamically varies the knee stiffness, whereas the hip joint is fully actuated with position control. The compliant surface is modeled as a mass located on a spring-damper system. As a result, the system consists of 14 design parameters (l_1, m_1, I_1, a_1, l_2, m_2, I_2, a_2, m_0, K_θ, b_θ, β_θ, K_g, b_g, m_g), as shown in Fig. 4. Note that l_i and a_i denote the length in the leg geometry, and m_i and I_i indicate the mass and inertia. In addition, K_θ, b_θ and β_θ define the knee stiffness, the knee damping and the knee rest angle, respectively. The compliant surface is modeled by three parameters which are the stiffness K_g, the damping b_g, and the surface mass m_g. All parameter values are presented in Tab. I.

In order to simulate the surface reaction forces between link 2 and the surface m_g, a realistic nonlinear spring-damper model based on [14] was applied. To actuate the leg, a simple position control policy was utilized at the hip joint to sinusoidally swing the leg. In Fig. 4, q_1, thus, follows a sinusoidal signal as $q_1(t) = A\sin(2\pi ft) + q_1(0)$, where $q_1(t)$ denotes the value of q_1 at time t , and A and f denote the amplitude and frequency of the sinusoidal signal, respectively. The values of A and $q_1(0)$ were heuristically found and fixed at 0.26 rad(15°) and 0.086 rad (5°) during whole experiments. To implement the simulations, we employed SimMechanics Toolbox in Matlab (Mathwork Inc.) with the Runge-Kutta solver and fixed-step size of 0.0002 seconds, and every hopping simulation was conducted over 5 second periods. This model was used to investigate how to improve energy efficiency of the hopping leg via the adjustment of knee stiffness on complaint surfaces.

B. Influences of knee and surface stiffness on locomotion efficiency

In this section, we present the simulation results to investigate the influences of knee stiffness adjustment on the energy efficiency of the hopping leg. To evaluate the energy efficiency of the hopping leg, we used CoT as a dimensionless measure, which is defined as follows.

$$\text{CoT} = \frac{P}{M_s \times g \times v}, \tag{3}$$

where P, M_s, g, and v denotes the power consumption of the hip actuation, the total mass of the robotic leg,

gravitational acceleration, and hopping speed. In order to have a fair comparison of the CoTs of the simulations and real world experiments, the input power of the simulation is calculated as a product of the hip torque at the hip joint, the current constant of the DC motor employed in the real-world experiments, and the voltage used to supplied the DC motor in real-world experiments.

To investigate energy efficient locomotion at various stride frequencies, we simulated the hopping leg at the oscillation frequencies of 3, 4, 5, and 6 (Hz). To cover a large variation range of leg and surface parameters, we systematically varied three important parameters: K_θ, K_g, and f from 1→15 (Nm/rad), 3000→63000 (N/m), and 3-6 (Hz) in a step size of 0.25, 6000, and 1, respectively. The results are expected to provide some primary understandings of locomotion efficiency for real-world investigation, which is carried out later in this paper on the robotic leg. Note that only the combinations of oscillation frequency, knee stiffness and surface stiffness that result in the CoT smaller than 5 are considered to be successful and shown in Fig. 5. The results are presented in Fig. 5.

In overall trend, the range of the knee stiffness, at which the leg can successfully hop, increases with the stride frequency. Within these ranges, a proper adjustment of the knee stiffness always results in a decrease in the CoT and increase in the speed. The maximum speed and minimum CoT are achieved almost at the same knee stiffness. As illustrated in Fig. 5, over all stride frequencies, when the surface stiffness increases, the knee stiffness should be decreased to attain low CoT and high speed, especially, higher stride frequencies: 5 and 6 (Hz). Furthermore, the stiffness variability results in a larger improvement of CoT and speed at higher stiffness surface. Indeed, at the lowest stiffness surface, the CoT and speed are not largely influenced by the stiffness variability.

In summary, the simulation results predict that there is an optimal knee stiffness to achieve low CoT and high speed locomotion for a given stride frequency and surface stiffness. This optimum increases with stride frequency and decrease with surface stiffness. Based on this result, we conducted the real-world experiments to test the simulation results. The next section presents the experimental setup and results.

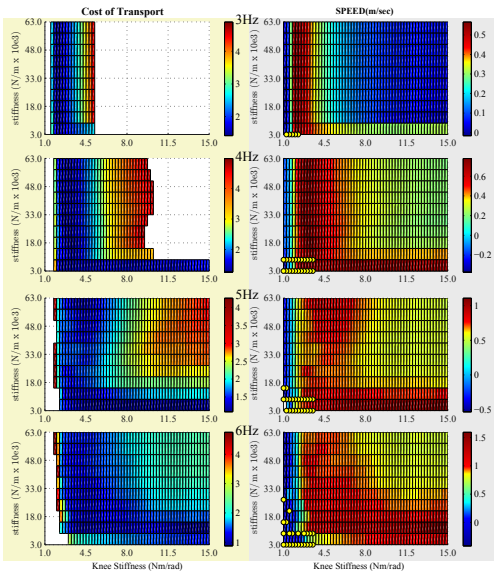

Fig. 5. Exploration of speed and CoT in the variations of knee and track stiffness at the stride frequencies of 3,4,5 and 6 Hz. The yellow dots indicates that the leg hops in a backward direction. The knee stiffness is increased from 1 Nm/rad to 15 Nm/rad with a step size of 0.25 Nm/rad, while the incremental step size of track stiffness is 6000 N/m from 3000 N/m to 63000 N/m.

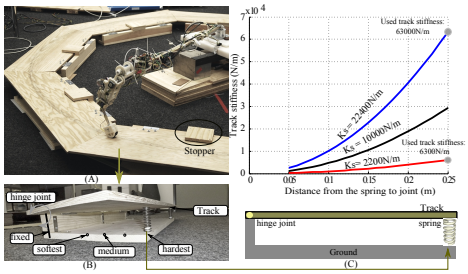

Fig. 6. Variable stiffness track platform with a robotic leg setup. The circular platform is segmented into 8 single tracks. A robotic platform is installed in the center of the track.

IV. Real-world experiments using the L-MESTRAN leg

A. Experimental setup

To investigate locomotion performance, i.e., speed and energy efficiency, of the hopping leg in steady state of locomotion, we constructed a circular track platform that consists of 8 single tracks. Each track could be deflected independently about the hinge joint under load. A boom setup was installed at the center of the track platform to constraint the robotic leg in a circular path. It is possible to independently vary the stiffness of each track in a wide range using a variable stiffness mechanism, as shown in the Fig. 6. The operational principle of such mechanism is based on changing level arm ratio which was investigated in several studies [8], [15], [16]. In our setup, the track compliance, i.e., surface stiffness, were obtained by two linear springs which were positioned underneath the tracks (Fig. 6). The surface stiffness is calculated as follows.

As shown in Fig. 7, when d_{leg} is fixed, a lower value of d_{sp} results in a lower effective stiffness k_{surf} of the track. This design principle allows the surface stiffness to be adjusted across a wide range which is determined by the spring constant and the ratio of d_{leg}/d_{sp}. For simplicity, the angular deflection of the track is assumed to be small and, thus, the robotic leg is assumed to displace only in the vertical direction. This assumption allows us to determine

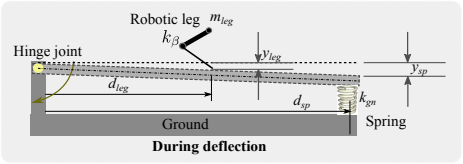

Fig. 7. Track stiffness calculation scheme. $d_{leg}, d_{sp}, k_{sp}, m_{leg}, k_\beta$ are the distance between the hinge joint to the contact point of the robotic leg, the distance between the hinge joint to the spring position, the spring constant, the knee stiffness, and the leg mass.

the displacement of the surface via triangle relationships as

$$y_{leg} = \frac{d_{leg}}{d_{sp}} y_{sp}. \quad (4)$$

Therefore, the effective surface stiffness defined at the leg contact point is

$$k_{surf} = \frac{F_{leg}}{y_{leg}} = k_{sp} \left(\frac{d_{sp}}{d_{leg}} \right)^2. \quad (5)$$

Equation 5 indicates that the surface stiffness can be changed by altering either the spring constant k_{sp} or the ratio d_{sp}/d_{leg}. In our experiments, we used two different springs with the spring constants of 1100 N/m and 11200 N/m. Note that there are two springs for each track, thus the total spring constants are 2200 N/m and 22400 N/m, respectively. Figure 6 shows the stiffness variation of the surface stiffness with respect to the distance from the springs to the hinge joint. For example, when the spring position is changed from 0.05 m to 0.25 m, the track stiffness is varied 6 times with a spring constant of 2200 N/m and 60 times with a spring constant of 22400 N/m, as shown in Fig. 6C.

Due to the track mass (m_g = 0.5 kg), its undamped oscillations can influence the leg motion, especially when the leg approaches the surface right before stance. To eliminate that, we modified the track platform by simply adding a stopper at the zero level of the surface such that the springs could only be compressed as shown in Fig. 6A.

B. Experimental protocols

The goal of these experiments was to find how the knee stiffness adjustment can increase the energy efficiency of the hopping locomotion on compliant surfaces and compare the results to the simulation results.

The surface stiffness was alternatively set at two stiffness levels: stiff ($K_g = 63000$ N/m) and soft ($K_g = 6300$ N/m). The knee stiffness was varied in a large range with respect to the frequency to oscillate the leg as shown in Tab. III. For every pair of hopping parameters, i.e., one frequency and one stiffness, 3 hopping trials were experimented to compute one averaged measure of CoT and speed.To evaluate whether the hopping trials were successful, we used the following criterion. Each hopping trial was considered to be successful if the hopping leg could hop to complete one round on the circular track platform. We implemented this experimental protocol and showed the results in the next section.

TABLE II

PARAMETERS IN THE LEGGED HOPPING PLATFORM

Items	Specifications
L-Mestran spring	3.3 N/mm
Track springs	1100 and 11200 (N/m)
Hip motor	Faulhaber:234212CR,17 W/Gear box: 43:1
Stiffness motor	Maxon RE13, 1.5 W/Gear box: 131:1
Controller	Atmega328P
Gyros meter	Pololu: LPR550AL
Current sensor	Sparkfun:ACS712

TABLE III

STIFFNESS VALUES IN THE EXPERIMENTS. K_θ IS PRESENTED NM/RAD.

Frequencies(Hz)	K_θ	K_θ	K_θ	K_θ	K_θ
3	5	3.2	2.2	1.5	
4	15.2	8.2	5	3.2	2.2
5	15.2	8.2	5	4.2	3.2
6	15.2	8.2	6	4.5	3.5

C. Experimental results

Figure 8 shows the overall experimental results of the robotic leg hopping at four different frequencies of actuation: 3,4,5, and 6 (Hz) on two levels of the track compliance: stiff ($K_g = 63000$ N/m) and soft ($K_g = 6300$ N/m). Two locomotion measures, i.e., forward speed and CoT, were taken into account for analyzing the hopping performances.

1) Locomotion speed: As shown in the upper plots of Fig. 8, the locomotion speed was strongly influenced by changes of the knee stiffness. For example, when the surface stiffness was set at a large value, i.e., 63000 N/m, it is clear that the variation profiles of the speed with respect to the

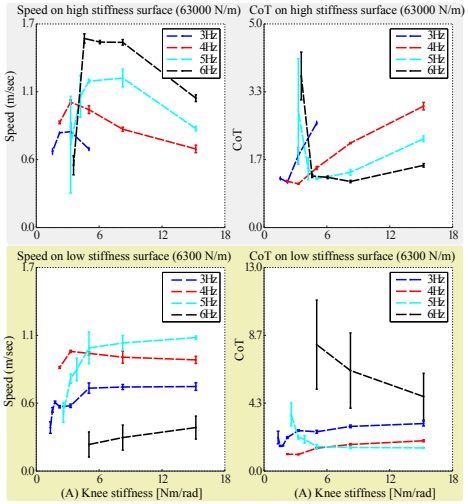

Fig. 8. Knee stiffness versus CoT and speed at various hopping frequencies on surfaces with two different stiffness. The CoT is calculated by the average electrical power and average speed.

knee stiffness show convex shapes. Thus, at a given stride frequency, a highest speed can be achieved when the knee stiffness is properly adjusted .

In the lower plots of Fig. 8, when the surface stiffness reduced to a low level, e.g., 6300 N/m, the influence of the knee stiffness adjustment on the speed decreased. The data trends revealed that after the knee stiffness approached a minimum level, the increase of knee stiffness did not significantly affect the speed. The hopping leg achieved almost the same speed over a large range of the knee stiffness. Furthermore, the speed data also showed that increasing stride frequency requires to increase the knee stiffness in hopping on both levels of surface stiffness. Lastly, from upper and lower figures, it was clear that on the lower stiffness surface, higher knee stiffness was required to achieve the similar level of speed as that achieved on higher stiffness surface.

2) CoT of hopping: As similarly found in the simulation, Figure 8 shows that it is possible to optimize speed and CoT of locomotion over all stride frequencies (3-6 Hz) by a proper adjustment of the knee stiffness since the optimal knee stiffnesses for maximum speed and minimum CoT are almost the same. Moreover, the improvement of CoT by knee stiffness adjustment however reduced when the surface stiffness decreased as shown in the lower plot of Fig. 8. In general, the influence of knee stiffness adjustment on speed was similar to that on CoT.

Note that at the stride frequency of 6 Hz, we recorded very unstable hopping behaviors of the leg on the low stiffness surface, which could be observed by large standard deviations of CoTs and speeds. The reason could be that the stiffness level of the surface in this experiments was too low for hopping at 6 Hz even when the knee stiffness reached its maximum level.

In summary, the experimental results demonstrated that knee stiffness adjustment can accommodate for changes of surface stiffness in order to improve energy efficiency of hopping robots at various stride frequencies. We discuss this result in a comparison with the simulation results in the next section.

V. Discussions

In this paper, we presented a systematic exploration of how knee stiffness adjustment can accommodate for changes of surface stiffness to improve locomotion energy efficiency at various stride frequencies. First, we presented the mechanical design, the theoretical analysis, and the performance evaluation of the adjustable stiffness leg incorporating with L-MESTRAN. We, then, studied hopping locomotion on compliant surfaces by developing a simulation hopping model which closely abstracted the physical properties of the robotic leg and the surface. Following that, based on the simulation results, we conducted a number of experiments to validate the results. The simulation results (Fig. 9) are in agreement with the experimental results (Fig. 8). We derive several discussions as follows.

As shown in Fig. 9 and Fig. 8, the simulation results provided fair predictions to describe the experimental results

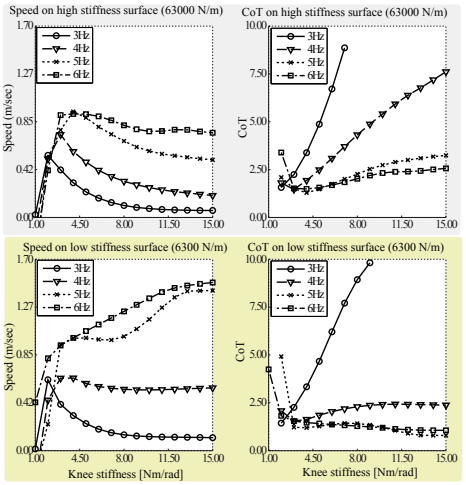

Fig. 9. Knee stiffness versus CoT and speed at various hopping frequencies on two type of substrates: soft and hard. The CoT is calculated by the average electrical power and average speed.

in advance. Both figures shows the convex profiles of the CoT and speed plots with respect to the stiffness adjustment. These profiles validate a simple CoT optimization approach that, for a given stride frequency and surface stiffness, a proper adjustment of knee stiffness can result in the lowest CoT of locomotion. Despite highly complex interaction in leg-surface interaction which involves a number of locomotion parameters: leg stiffness, leg oscillation amplitude, offset angle of leg oscillation, surface stiffness, stride frequency, etc., knee stiffness adjustment is found to be an effective approach to improve energy efficient locomotion at various stride frequencies on different stiffness surfaces.

As inspired by biological systems, we draw some similarities between our results and biological findings.In [17], it has been showed that leg stiffness adjustment accommodates for changes in surface stiffness during human locomotion. The underlying mechanism was revealed later that the adjustment of leg stiffness over changes of surface compliance allows for a decrease in metabolic cost of locomotion [18]. Compared to our results in both the simulation and the experiments, the adjustment of knee stiffness over changes of surface stiffness improves energy efficiency of locomotion. We also found that the optimal knee stiffness, resulting in the highest efficiency of locomotion, increases with the compliance of surface.

VI. Conclusion

Throughout the results from simulation and experiments, we have demonstrated an approach employing the stiffness adjustment mechanism to improve the locomotion energy efficiency of a single-legged hopping robot on compliance surfaces. This approach also allows the robot to advance its locomotion efficiency at multiple stride frequencies, which is beneficial to diversify locomotion behaviors. In the field

of actuator development, we demonstrated the applicability of the VSA, in particular our actuator L-MESTRAN, for improving locomotion efficiency of legged robots under changes of surface stiffness and stride frequency.

VII. ACKNOWLEDGMENTS

Thanks to Fumiya Iida and Amir Jafari at the Bio-Inspired Robotic Lab, ETH Zurich, for technical supports and helpful discussions.

REFERENCES

[1] S. Kajita and B. Espiau, "Legged robots," in *Springer Handbook of Robotics*, B. Siciliano and O. Khatib, Eds. Springer Berlin Heidelberg, 2008, pp. 361–389.

[2] R. Alexander, *Principles of animal locomotion*. Princeton, NJ: Princeton University Press, 2003.

[3] S. Collins and A. Ruina, "A bipedal walking robot with efficient and human-like gait," in *Robotics and Automation, 2005. ICRA 2005. Proceedings of the 2005 IEEE International Conference on*, 2005, pp. 1983–1988.

[4] A. D. Kuo, "Choosing your steps carefully: Trade-offs between economy and versatility in dynamic walking bipedal robots," *IEEE Robotics & Automation Magazine*, vol. 14, no. 2, pp. 18–29, 2007.

[5] A. J. Spence, S. Revzen, J. Seipel, C. Mullens, and R. J. Full, "Insects running on elastic surfaces." *The Journal of experimental biology*, vol. 213, no. 11, pp. 1907–20, Jun. 2010.

[6] R. H. Sanders and B. D. Wilson, "Modification of movement patterns to accomodate to a change in surface compliance in a drop jumping task," *Human movement science*, vol. 11, no. 5, pp. 593–614, 1992.

[7] A. Seyfarth, A. Friedrichs, V. Wank, and R. Blickhan, "Dynamics of the long jump," *Journal of Biomechanics*, vol. 32, no. 12, pp. 1259 – 1267, 1999.

[8] D. P. Ferris and C. T. Farley, "Interaction of leg stiffness and surface stiffness during human hopping," *Journal of applied physiology*, vol. 82, no. 1, pp. 15–22, 1997.

[9] D. P. Ferris, M. Louie, and C. T. Farley, "Running in the real world: adjusting leg stiffness for different surfaces," *Proceedings of the Royal Society of London. Series B: Biological Sciences*, vol. 265, no. 1400, pp. 989–994, 1998.

[10] N. L. Tagliamonte, F. Sergi, D. Accoto, G. Carpino, and E. Guglielmelli, "Double actuation architectures for rendering variable impedance in compliant robots: A review," *Mechatronics*, vol. 22, no. 8, pp. 1187–1203, Dec. 2012.

[11] B. Vanderborght, A. Albu-Schaeffer, A. Bicchi, E. Burdet, D. Caldwell, R. Carloni, M. Catalano, O. Eiberger, W. Friedl, G. Ganesh, M. Garabini, M. Grebenstein, G. Grioli, S. Haddadin, H. Hoppner, A. Jafari, M. Laffranchi, D. Lefeber, F. Petit, S. Stramigioli, N. Tsagarakis, M. V. Damme, R. V. Ham, L. Visser, and S. Wolf, "Variable impedance actuators: A review," *Robotics and Autonomous Systems*, pp. –, 2013.

[12] H. V. Quy, L. Aryananda, F. Sheikh, F. Casanova, and R. Pfeifer, "A novel mechanism for varying stiffness via changing transmission angle," in *Robotics and Automation (ICRA), 2011 IEEE International Conference on*, may 2011, pp. 5076 –5081.

[13] H. Vu, H. Hauser, and R. Pfeifer, "A variable stiffness mechanism for improving energy efficiency of a planar single-legged hopping robot," in *The 16th International Conference on Advanced Robotics, ICAR 2013*, 2013, accepted.

[14] K. G. Gerritsen, A. J. van den Bogert, and B. M. Nigg, "Direct dynamics simulation of the impact phase in heel-toe running," *Journal of Biomechanics*, vol. 28, no. 6, pp. 661–668, Jun. 1995.

[15] A. Jafari, N. G. Tsagarakis, I. Sardellitti, and D. G. Caldwell, "A new actuator with adjustable stiffness based on a variable ratio lever mechanism," *IEEE/ASME Transactions on Mechatronics*, 2012.

[16] J. Choi, S. Hong, W. Lee, S. Kang, and M. Kim, "A robot joint with variable stiffness using leaf springs," *Robotics, IEEE Transactions on*, vol. 27, no. 2, pp. 229–238, 2011.

[17] D. P. Ferris, K. Liang, and C. T. Farley, "Runners adjust leg stiffness for their first step on a new running surface," vol. 32, no. March, pp. 787–794, 1999.

[18] A. E. Kerdok, A. a. Biewener, T. a. McMahon, P. G. Weyand, and H. M. Herr, "Energetics and mechanics of human running on surfaces of different stiffnesses." *Journal of applied physiology (Bethesda, Md. : 1985)*, vol. 92, no. 2, pp. 469–78, Feb. 2002.

Appendix F

Influence of knee and surface stiffness on locomotion stability

The dynamics of hopping locomotion is considered as hybrid dynamics that is characterized by interactions between continuous dynamics, i.e., stance and flight dynamics, and discrete events, i.e., touch-down and take-off. The dynamics of such system exhibits many interesting and complex behaviors such as limit cycles, bifurcation, or chaos. To analyze the stability of the systems, Poincare maps are commonly used. Poincare map is created by sampling the flow of periodic state variables once every cycle (Buchli et al. 2006; Parker and Chua 1987). If the system is stable, the samples will approach the fixed points and the flow will return to the same position once after every cycle. In cases of instability, there are no such fixed points and samples will be diverging. We define the Poincare map as follows.

Considering a dynamical system:

$$\dot{X} = f(X). \tag{F.1}$$

Assuming that X is the state variables of the system defined by the hopping model. Let P be the hyperplane, which is required to intersect with X at X_k^* at the kth intersection. In this case, the Poincare map is the mapping of the state variables from P to itself, obtained by the flow trajectories from one section on P to the next. At the $(k+1)$th intersection of X with P, the Poincare map is defined as follows:

$$X_k = P(X_{k+1}). \tag{F.2}$$

Thus we determine that the system as stable if the state variable flow returns to itself at the next intersections after a period T. This means that the solution X^*, i.e., so-call fixed point, of Eq. F.3 exists.

$$X^* = P(X^*). \tag{F.3}$$

By analyzing the behaviors of state variables at the fixed points, we can determine the stability of the system of Eq. F.1. The stability of the system is also the stability of the fixed point X^*. Applying this theory to our system to analyze hopping stability in the steady state, we identify the limit cycles of all 10 state variables involved in the model. In order to be stable, it is strictly required that all state variables have to return to the fixed points after one hopping cycle. We choose the Poincare section at the TD time, i.e., the point at which the leg touches the surface at the beginning of the stance phase. The evolution of all state variables from a subsequent section TD_n to TD_{n+1} is presented by return maps.

In this section, we analyze the hopping stability in two extreme cases when the surface stiffness is set at the minimum (**low stiffness - 3000 N/m**) and maximum values (**high stiffness - 63000 N/m**). For each stiffness value of surfaces, we show the return maps of three hopping trials at three different values of knee stiffness, i.e., $K_\theta = 1.5Nm/rad$, $K_\theta = 3.5Nm/rad$, and $K_\theta = 5.5Nm/rad$.

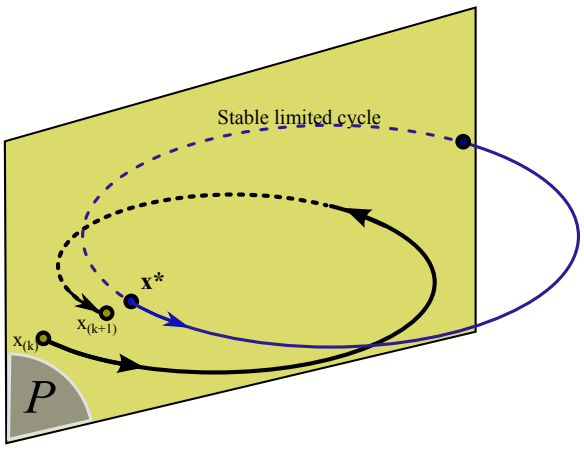

Figure F.1: State variables flows through a Poincare map.

To investigate how hopping stability varies according to stride frequency, we present the return maps of the hopping variables at 2 stride frequencies (3 Hz and 5 Hz). For the stability defined by using the return map, all trajectories of state variables have to converge to the points locate on the diagonal blue-dashed lines on the each return map (see Fig. F.2). These lines contain the points where the samples of the state variables of two adjacent hopping cycles are coincident.

Thus, based on the obtained simulation results, we found that with an appropriate adjustment of the knee stiffness, there always exist a specific stiffness value where the hopping locomotion is self-stabilized, as shown in Fig. F.2, Fig. F.3, Fig. F.4 and Fig. F.5. Notice that since traveling distance is not a periodic variable, the values of x_m in the sub-figure E in Fig. F.2, Fig. F.3, Fig. F.4 and Fig. F.5 are the length of hopping strides. We mention the term "self-stabilized" since the controller of the hopping locomotion is open loop, and is not changed at all trials at one stride frequency. Only the knee stiffness is varied to find the specific value which results in stable hopping. Thus, the behaviors of the robotic leg are shaped from unstable to stable via the stiffness adjustment.

- **Hopping with stride frequency of 3Hz**

  For example, when the simulated leg hops on the low stiffness surface at the stride frequency of 3 Hz, among 3 knee stiffness values, only the lowest knee stiffness $K_\theta = 1.5\,\mathrm{Nm/rad}$ can result in stable hopping as shown by the red circle locations lying on the diagonal lines in Fig. F.2. Likewise, the higher knee stiffness $K_\theta = 3.5\,\mathrm{Nm/rad}$ and $K_\theta = 5.5\,\mathrm{Nm/rad}$ result in unstable hopping. Moreover, we found that the leg only hop at the lowest knee stiffness $K_\theta = 1.5\,\mathrm{Nm/rad}$, whereas, for other knee stiffness, the leg actually sled forward, i.e., no TO was detected. Thus the results show that when the knee stiffness is varied to a specific value, the leg can find its way to achieve stable hopping despite the fact that the surface is highly vibrant. On the higher stiffness surface, i.e., 63000 N/m, we found two values of the knee stiffness resulting in stable hopping, i.e., $K_\theta = 1.5\,\mathrm{Nm/rad}$(red lines), $K_\theta = 3.5\,\mathrm{Nm/rad}$ (blue lines). The highest knee stiffness causes an unstable and slow hopping speed as indicated in Fig. F.3. As the result, no TO is detected when the highest knee stiffness is set. Moreover, the knee stiffness $K_\theta = 3.5\,\mathrm{Nm/rad}$ also results in a quicker convergence of

state variables to the fixed points.

Analyzing the leg hopping dynamics at the stride frequency of 3 Hz, we found that when the surface stiffness is as low as 3000 N/m, increasing the knee stiffness does not help the hopping leg to hop. Instead, reducing knee stiffness could be more conducive to obtain stable hopping. To further investigate the stability behaviors of the hopping leg at a higher stride frequency, we analyze the hoping behaviors at a stride frequency of 5 Hz on both levels of surface compliances, i.e., 3000 N/m and 63000 N/m.

- **Hopping with stride frequency of 5Hz**

  The simulation results at this frequency indicate a clear unstable hopping behavior when the surface stiffness is set at 3000 N/m and the knee stiffness is reduced to the lowest value, i.e., the red circle falls far away the diagonal-blue lines. The leg is almost stumbles in place as shown in Fig. F.4**F** (red lines) and Fig. F.4**L** (red lines). As the knee stiffness is increased as high as $K_\theta = 3.5$ Nm/rad, $K_\theta = 5.5$ Nm/rad, the leg is able to find stable hopping behaviors which are indicated by the blue and cyan lines in Fig. F.4**A-K**. The forward speed is greatly improved as shown in Fig. F.4**L**.

  In the last hopping simulation, the surface stiffness was increased to 63000 N/m. In Fig. F.4**(**F) and Fig. F.5**(**F), we observe that the lowest knee stiffness still results in unstable hopping behavior, whereas higher knee stiffness causes stable hopping. We notice that the increasing stride frequency can enlarge the region of the knee stiffness for stability. Moreover, the trajectories of all state variables quickly converge to the fixed points after starting points, i.e., triangular markers. In addition, we observe that the maximum speed of hopping on the higher stiffness surface is lower than that of hopping on the lower stiffness surface, as.

In this section, we have investigated the stability of the hopping leg model at different stride frequencies (i.e., 3,5 Hz) and the surface stiffness by analyzing the cyclic return of state variables at every TD event. We found that by appropriately regulating the knee stiffness, the hopping leg is always capable of achieving locomotion stability dispite the fact that the surface stiffness varies across a large range. Therefore, in the next section, we can use this model to further investigate the energy efficiency of the hopping leg.

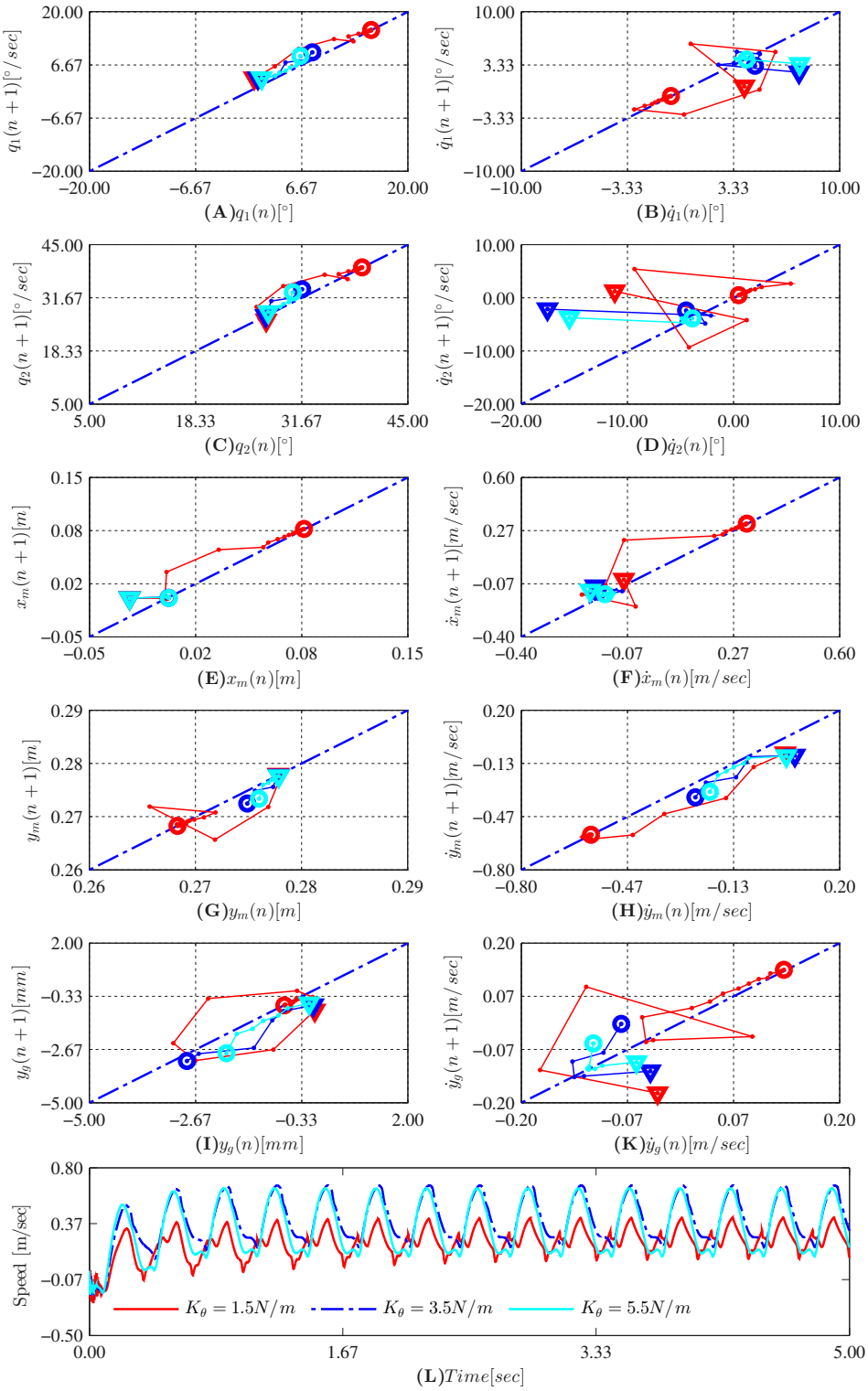

Figure F.2: Return maps of state variables at every TD event with a stride frequency of 3 Hz. The surface stiffness is at the lowest value of 3000 N/m. Three colors (**red, blue, and cyan**) represent three different knee stiffness, $K_\theta = 1.5\,\mathrm{Nm/rad}, K_\theta = 3.5\,\mathrm{Nm/rad}, K_\theta = 5.5\,\mathrm{Nm/rad}$, respectively. The triangular and circular shapes indicate the starting and ending points of state variables. A diagonal blue dotted-dashed line presents all possible points at which the state variables of two subsequent TD events are coincident.

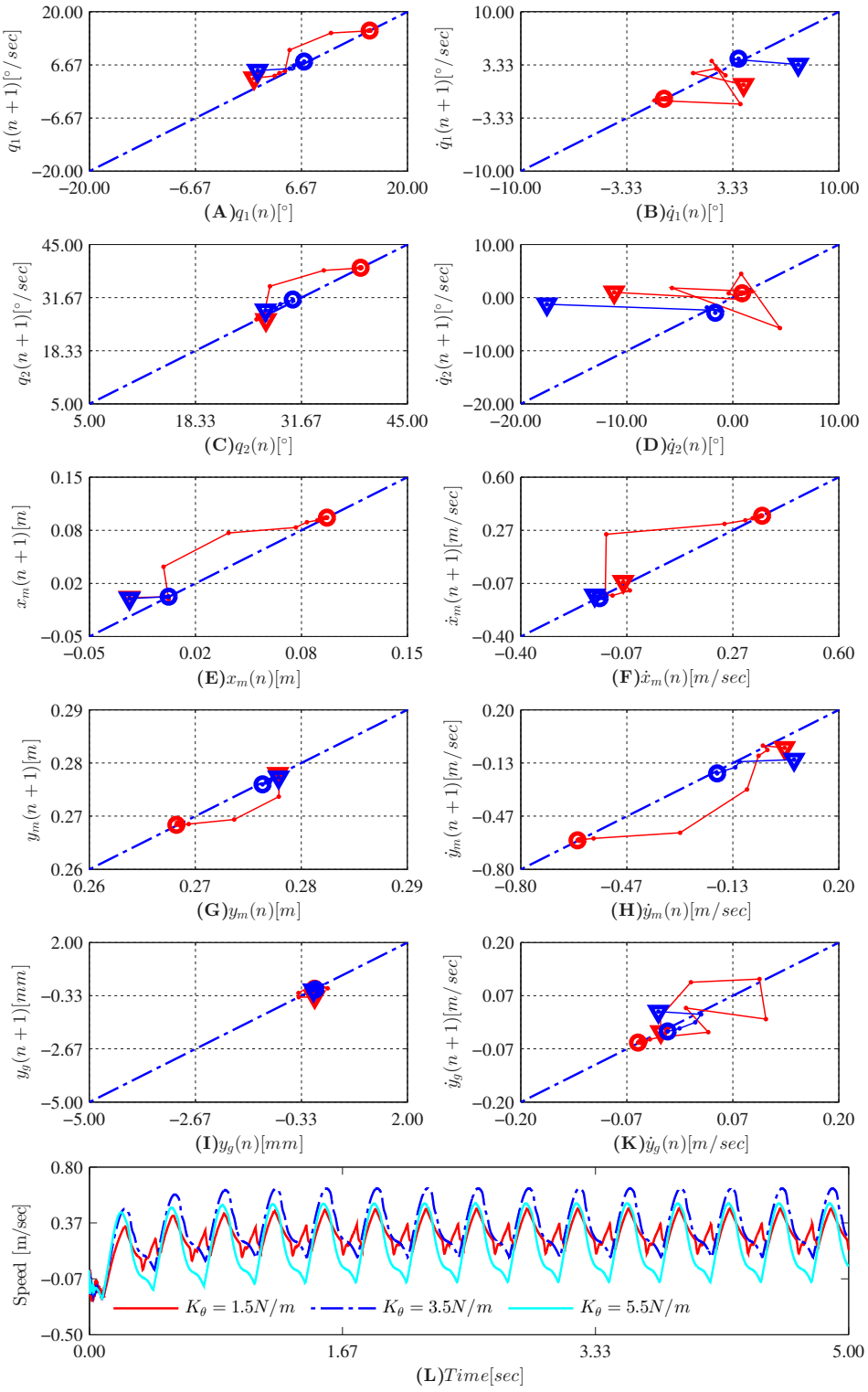

Figure F.3: Return maps of state variables at every TD event with a stride frequency of 3 Hz. The surface stiffness is at the lowest value of 63000 N/m. Three colors (**red, blue, and cyan**) represent three different knee stiffness, $K_\theta = 1.5\,\text{Nm/rad}, K_\theta = 3.5\,\text{Nm/rad}, K_\theta = 5.5\,\text{Nm/rad}$, respectively. The triangular and circular shapes indicate the starting and ending points of state variables. A diagonal blue dotted-dashed line presents all possible points at which the state variables of two subsequent TD events are coincident. The cyan lines are missing since no TO occurred when the stiffness $K_\theta = 5.5\,\text{Nm/rad}$ was set to the knee joint.

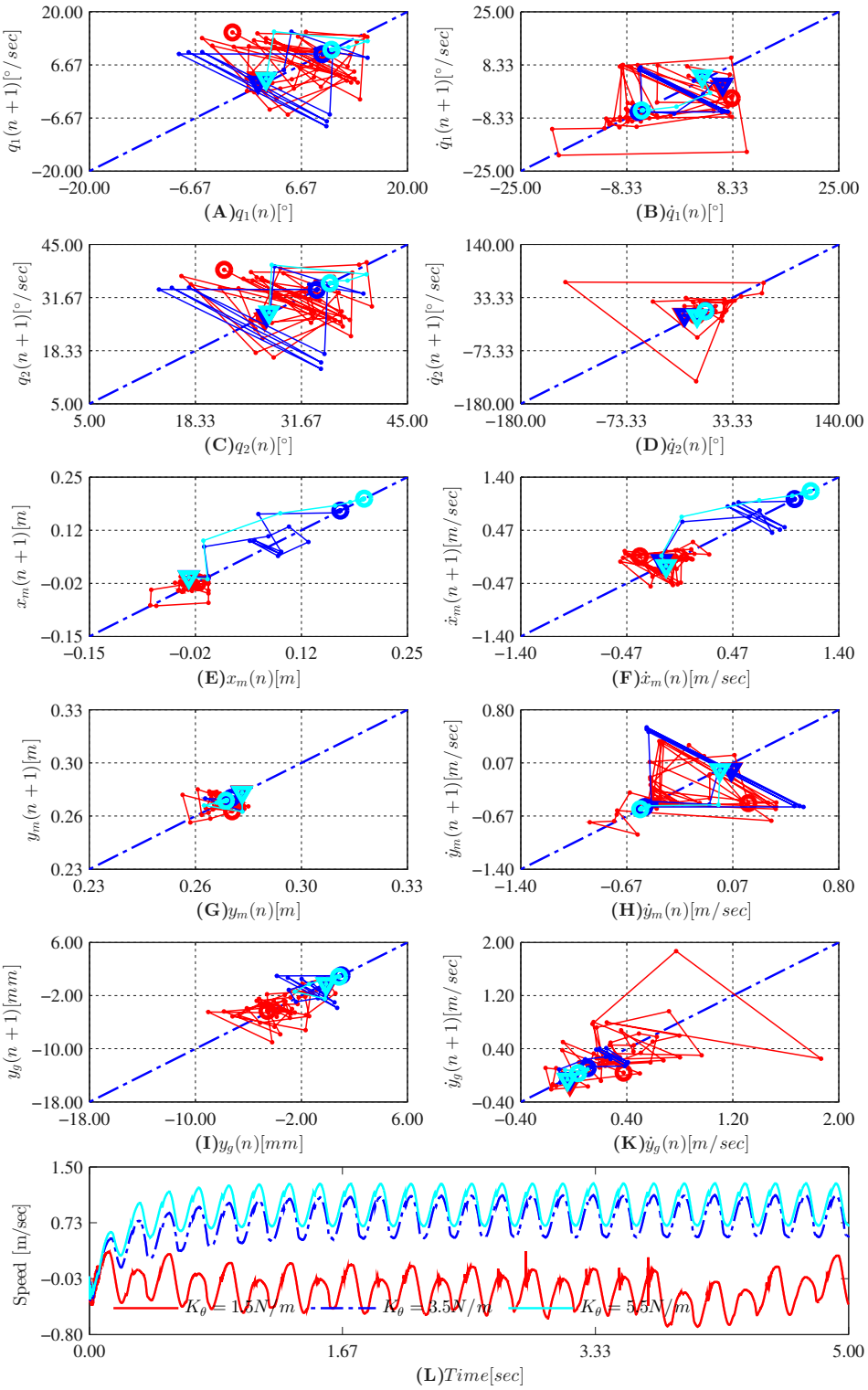

Figure F.4: Return maps of state variables at every TD event with a stride frequency of 5 Hz. The surface stiffness is at the lowest value of 63000 N/m. Three colors (**red, blue, and cyan**) represent three different knee stiffness, $K_\theta = 1.5$ Nm/rad, $K_\theta = 3.5$ Nm/rad, $K_\theta = 5.5$ Nm/rad, respectively. The triangular and circular shapes indicate the starting and ending points of state variables. A diagonal blue dotted-dashed line presents all possible points at which the state variables of two subsequent TD events are coincident. The cyan lines are missing since no TO occurred when the stiffness $K_\theta = 5.5$ Nm/rad was set to the knee joint.

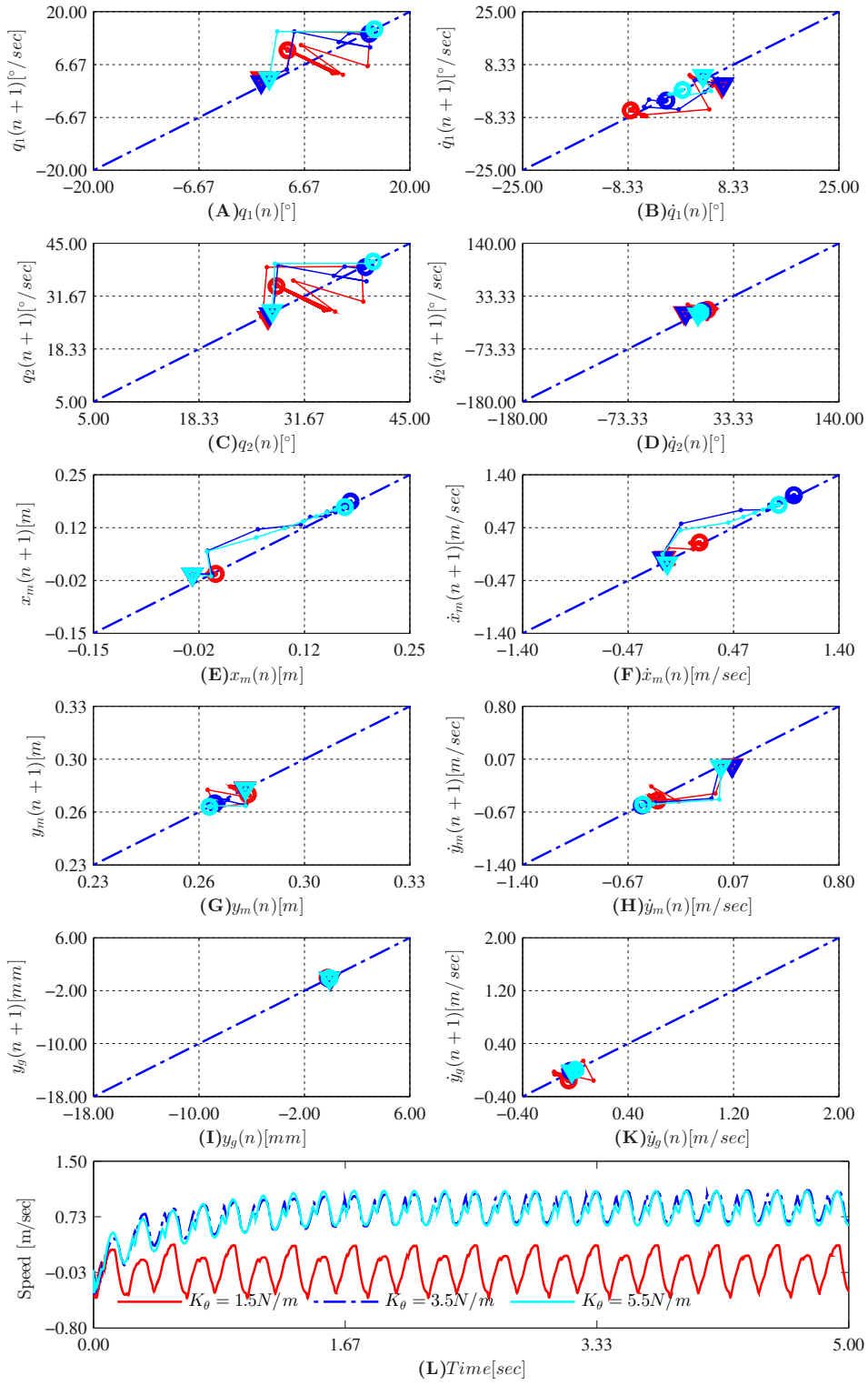

Figure F.5: Return maps of state variables at every TD event with a stride frequency of 5 Hz. The surface stiffness is at the lowest value of 63000 N/m. Three colors (**red, blue, and cyan**) represent three different knee stiffness, $K_\theta = 1.5\,\text{Nm/rad}, K_\theta = 3.5\,\text{Nm/rad}, K_\theta = 5.5\,\text{Nm/rad}$, respectively. The triangular and circular shapes indicate the starting and ending points of state variables. A diagonal blue dotted-dashed line presents all possible points at which the state variables of two subsequent TD events are coincident. The cyan lines are missing since no TO occurred when the stiffness $K_\theta = 5.5\,\text{Nm/rad}$ was set to the knee joint.

Appendix G

Gait Versatility Through Morphological Changes in a New Quadruped Robot

Although this paper is out of the scope of this thesis work, the goal of this paper is well aligned with that of the thesis. The paper investigates the applicability of a new leg actuation approach to achieve energy efficient yet versatile locomotion. I have spent one and a half year to develop this robot, however before starting this thesis work I decided not to include this work in to the thesis. Nevertheless, for a summary of my PhD, I would like to include this paper in Appendix as a brief reference to an alternative approach compared to VSA approach.

Reprinted from: Hung Vu Quy, Gilles Ramstein, Flurin Casanova, Lijin Aryananda, Matej Hoffmann, Farrukh Iqbal Sheikh and Helmut Hauser "Gait Versatility Through Morphological Changes in a New Quadruped Robot," in 2011 International Symposium on Adaptive Motion of Animals and Machines, 2011, pp. 59-60..

Gait Versatility Through Morphological Changes in a New Quadruped Robot

Hung Vu Quy, Gilles Ramstein, Flurin Casanova, Lijin Aryananda, Matej Hoffmann, Farrukh Iqbal Sheikh and Helmut Hauser

Artificial Intelligence Laboratory, University of Zurich, Zurich, Switzerland
Tel: +41 44 635 4592; E-mail: (vqhung, casanova, lijin, hoffmann, fsheikh, hhauser) at @ifi.uzh.ch and gilles187@hotmail.com

Abstract: In dynamic locomotion, robots' morphology and the ability to adapt it online play an important role for energy efficiency and coping with the highly unpredictable perturbations from the environment. In this paper, we present the design and implementation of a quadruped robot, whose morphology is particularly targeted toward energy-efficient dynamic locomotion. We propose a combination of mechanisms, which allows for energy-efficient actuation, ground clearance, and gait versatility through adaptation of morphology (i.e., morphosis). We report on a series of experiments to validate the robot's performance in different locomotion conditions.

Keywords: robot design, legged locomotion, morphological computation, gait versatility, energy efficiency, morphosis

1. INTRODUCTION

Biological systems show amazing locomotion capabilities. The combination of their morphology (musculoskeletal structure, body shape, etc.) and sensory-motor control allows them to traverse many terrains and to switch among gaits to maintain varying levels of speed at optimized energy efficiency. With the goal to match these impressive capabilities, roboticists have put vast efforts to derive inspiration from biology and transfer it into the design of robots' morphology [1]. We have identified the following key factors that need to be addressed in a dynamic legged robot:

- **Power:** In the dynamical running, the robot has to deliver a large amount of energy within a fraction of a second in order to jump off.
- **Compliance:** For energy storage and instant adaptation to external forces, compliant structures have to be integrated into the robot's legs.
- **Ground clearance.** When legs are propagated forward during a swing phase, they need to clear the ground.
- **Gait versatility:** Legged animals are able to locomote in different gaits, mostly, in order to adapt to new terrain or to change speed, at minimized cost of transport [2]. Therefore, it is very important for an agile robot to be able to exhibit different gaits.

To integrate all these, sometimes competing requirements, into a single design is a challenge. For instance, high power-to-weight ratio conflicts with controllability and gait versatility. Specifically used as inspirations in our work are the iSprawl [3] and Scout II [4] robots. The iSprawl robot demonstrates fast and robust dynamic hexapedal locomotion, due to carefully designed compliant properties and the fast and efficient prismatic joint actuations. The Scout II quadruped robot shows several fast and robust running gaits (i.e., trot, bound, and gallop), but only with one rotational degree-of-freedom per leg and linear compliance.

We present a novel solution to address the key factors: the quadruped robot UZH1 (Fig. 1). High power-to-weight ratio was achieved by using only one motor for locomotion per leg. The motors were placed towards the center of mass in order to minimize counter-forces and inertial moments generated. In addition, the motors rotate continuously providing energy-efficient output since they do not "fight" against their own inertia (which is the case as oscillating). The oscillatory movement of the leg is then achieved through a crank-slider mechanism.

The additional design requirements were fulfilled in the following manner: First, compliance was introduced by incorporating springs within the leg structure. Second, ground clearance was already incorporated into the crank-slider mechanism, obtaining an oval foot trajectory. With this adopted mechanism, while we gain a two-dimensional foot trajectory with only one motor per leg, these trajectories are fixed and not controllable. Therefore, third and last, we introduced the missing flexibility that is needed for different gaits through mechanisms that allow the robot to change its leg configuration - which we call *morphosis.* The ground clearance profile (GCP) can be adjusted online (through additional lightweight "morphosis motors") and offline. With the morphosis capabilities our work goes beyond that of K. lida[5].

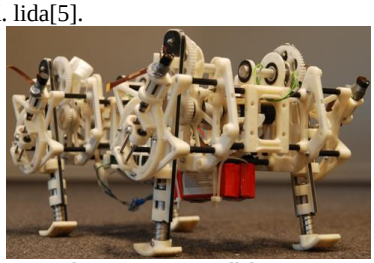

Fig.1 UZH1 Robot Prototype; overall dimension: (LxWxH: 350, 250x200 [mm]); weight: 2.25kg.

The paper is organized as follows, we begin by presenting the design concept and implementation details of the first version of the UZH1 robot. We then describe a series of experiments designed to evaluate the robot's performance.

2. DESIGN AND IMPLEMENTATION

As shown in Fig.2, each leg of the UZH1 robot has two degree of freedoms: a prismatic and a rotary joint.

The first one is a passive compliant joint allowing for energy storage and impact absorption. The second one is controlled by the continuous rotation of a crank disk mounted at the end point of the leg. The leg is constrained by one end point mounted on the crank disk and the slider rotating about the fix point. As a result, the foot produces a GCP as shown in Fig.2 (d).

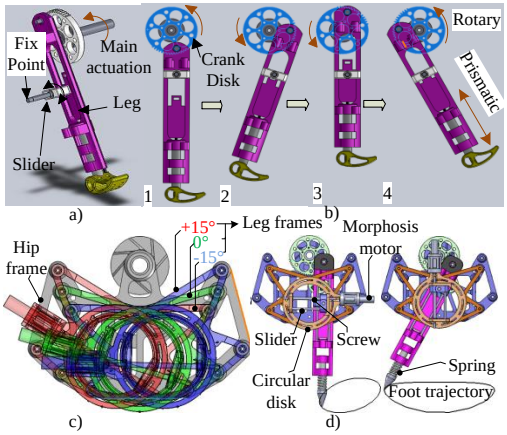

Fig.2 Operational principle of the robot's leg design; (a) main components of the robot leg; (b) from (1)-(4): leg movement in one working cycle; (c-d) online and offline morphosis possibilities influencing the foot trajectory.

In order to provide diverse locomotion capabilities, we introduce two levels of morphosis: online and offline. In the online morphosis, we vary the fix point position in order to provide possibilities to change leg configuration. As shown in Fig.2, the position of the fix point determines the trajectory of the end point of the robot's foot. By moving the fix point along with the screw via the morphosis motor, the foot trajectory, which depends on the offset angle and the oscillating amplitude, can be varied. The influence of the fix point movement on the changing ratio between the offset angle and the oscillating amplitude also depends on the orientation of the screw, shown in Fig. 2 (d).

In the offline morphosis, the circular disk, at which the screw is mounted on, can be rotated in a full circle with resolution of 5° on the leg frame allowing to vary the foot trajectory. Additionally, one can rotate the whole leg frame by 15° to either side. As a result, this creates a larger change of the offset angle, shown in Fig. 2 (c).

3. EXPERIMENT: GAIT VERSATILITY

We investigated the robot's capabilities using a simple CPG architecture [6] without any sensory feedback. The main goal of the presented experiments is to gain insights to the abilities of the compliant, morphological structure of UZH1 in combination with this simple open-loop control.

In a series of experiments, we have jointly explored the space of control (speed, duty factor, phase difference), morphological parameters (slider orientations and fix point positions) and different terrains. These resulted in three different gaits, namely bound, trot, and pace. The highest speeds and the specific resistances are shown in Fig.3.

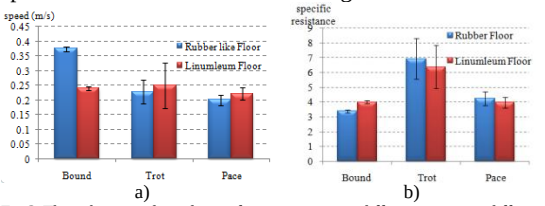

Fig.3 The robot speeds and specific resistances in different gaits on different floor materials.

As a result, the morphological parameters such as the combination of different slider orientations and the fix points at the best speeds were determined through a lot of experiments as shown in the Fig.4.

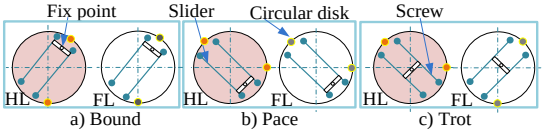

Fig.4 The different slider combinations in different gaits for the best speed; FL: front leg; HL: hind leg.

4. DISCUSSION, CONCLUSION, FUTURE WORK

We presented a novel robot design that aims at dynamic, energy-efficient, yet versatile locomotion. The missing active degrees of freedoms that were sacrificed for the sake of higher power-to-weight ratio were compensated by mechanisms that manipulate the robot's morphology. We have successfully demonstrated the robot's performance in multiple gaits and multiple grounds, with a simple feed-forward controller. We speculate that the robustness that we observed was due to self-stabilization properties of the compliant mechanical structure.

The current level of the energy-efficiency is shown in Fig.3b. We plan to investigate how to improve it with closed-loop control. In addition, we will compare rotary with oscillatory movement regarding energy consumption of the main actuators as future work.

5. REFERENCES

[1] R. Pfeifer, M. Lungarella, and F. Iida, "Self-Organization, Embodiment, and Biologically Inspired Robotics", *Science* 16, 318 (5853), 1088-1093, 2007.

[2] D.F. Hoyt, and C. R. Taylor. "Gait and the energetics of locomotion in horses." *Nature* 292(5820): 239-240, 1981.

[3] S. Kim, J. Clark and M. Cutkosky, "iSprawl: Autonomy, and the Effects of Power Transmission", *Climbing and Walking Robots*, Part VII, pp. 859-867, 2005.

[4] I. Poulakakis, J. A. Smith, and M. Buehler, "Modeling and experiments of untethered quadrupedal running with a bounding gait: The Scout II Robot". *International Journal of Robotics Research*, vol. 24, no. 4, pp. 239-256, April 2005.

[5] K. Iida,Y. Hayami,T. Hira,T. Yasuno,T. Kamano, "Evolutionary Acquisition for Moving Performance of Reduced D.O.F's Quadruped Robot," *SICE-ICASE,2006 International Joint Conference* , pp. 3005-3010, 2006.

[6] S. Pouya, J. Van den Kieboom, A. Sproewitz, and A.J. Ijspeert, Automatic Gait Generation in Modular Robots: to Oscillate or to Rotate? that is the question", *in Proceedings of IROS 2010*.

Appendix H

Matlab model implementation

By combining MATLAB/Simulink and the Symmechanics Toolbox (MathWorks Inc.), we have developed a hopping model on a compliant surface. We imported the complete CAD data consisting of the geometrical and material properties of the leg design from Solidwork (Dassault Systèmes, S. A. (Vélizy, France)) to Simulink. Thus, the numerical model is comparable to the real-world robot. The visualization of the model implementation is shown in Fig. H.1, while the detail schematics is presented in Fig.H.2. We briefly introduce the major parts of the model in the next section.

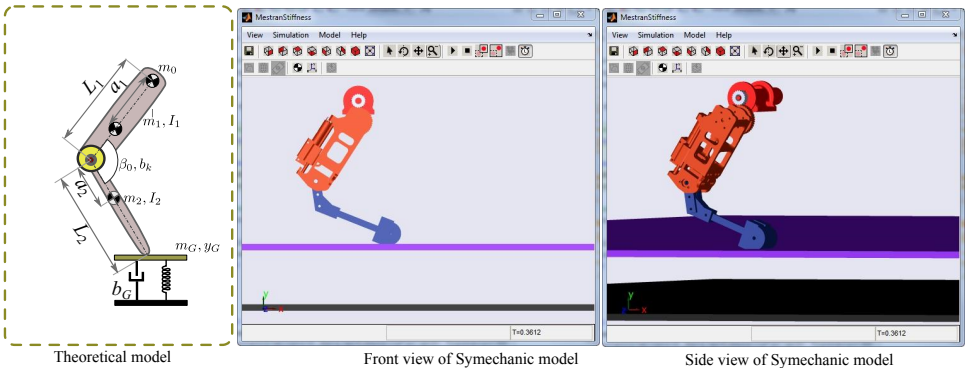

Theoretical model | Front view of Symechanic model | Side view of Symechanic model

Figure H.1: A screen shot the captured model developed in Symechanics and Simulink, Matlab 2012.

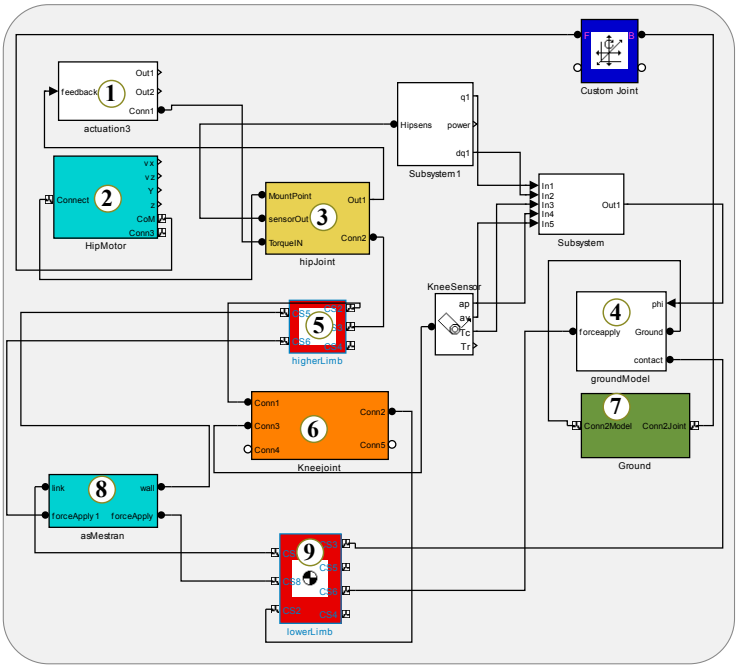

Figure H.2: Complete model of the hopping leg on compliant tracks.

- **(1)** Actuation module: This block implements a PID controller, which produces the required torque to drive the leg to track a desired trajectory, at a sampling frequency of 5 Khz.
- **(2)** Hip module: This block consists of the implementation of the hip motor, the gearbox, and the effective mass of the boom.
- **(3)** Hip joint module: This block implements a revolute joint and an actuator to control link 1, i.e., higherLimb.
- **(4)** Surface module: A collision model (Gerritsen et al. 1995) is implemented in this module which simulates the interaction of the leg with the surface. The detail implementation is shown in Fig. H.3.
- **(5)** The link 1 module: This module only consists of mechanical properties, i.e., mass, inertial, of the link.
- **(6)** Knee joint module: This block consists of a revolute joint which connects link 1 and link 2. This joint is modeled as a variable compliant joint which simulate the characteristics of the L-MESTRAN knee joint as described in the chapter 3.
- **(7)** Surface model: The compliance property of the surface is modeled by a spring mass system consisting of a track and a linear-viscous spring. The detail of this model is shown in Fig. **??**B.

- **(8)** AsMestran: A model of an asymmetrical compliant knee joint is implemented here, since the knee joint in the real robotic leg can be deflected to one-side only.
- **(9)** Link 2: The foot segment of the leg .

Since a discretized PID controller is used to control the leg system, a fixed-step size solver for the Simulink was required. We used a Runge-Kutta solver with a fixed-step size of 0.0002 seconds. This step size is also used as the control frequency (5 KHz) of the PID controller. We simulated every hopping trial for 5 seconds.

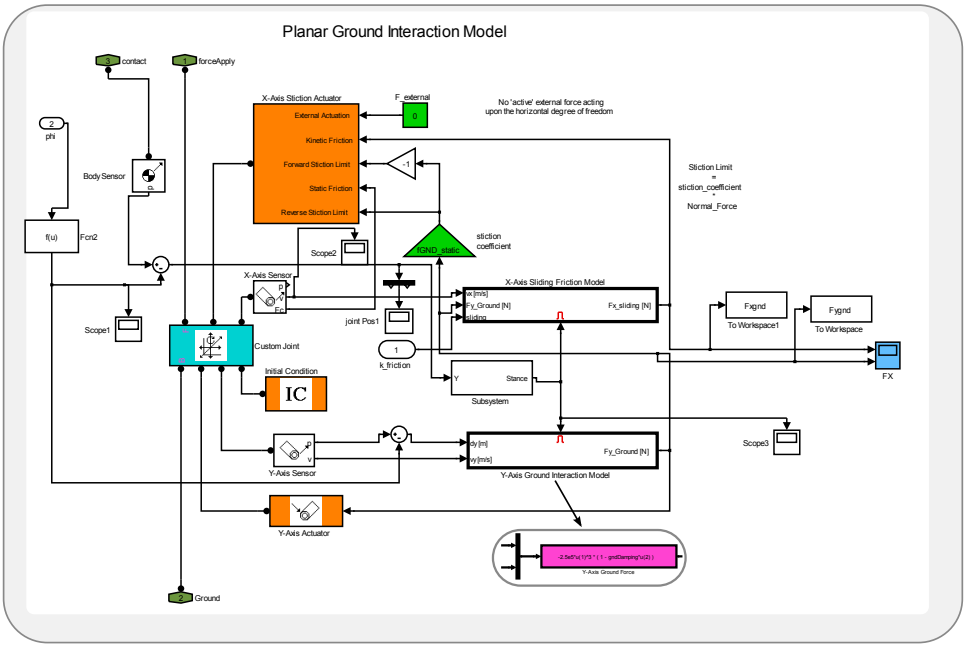

Figure H.3: Implementation of the surface model for the interaction between the leg and the surface.

The detail model implementation of leg and surface interaction is presented in Fig. H.3 .

Using this model, we have implemented a number of simulations to investigate the hopping locomotion of the leg, under changes of various conditions, i.e., knee stiffness, surface stiffness, and stride frequency.

Appendix I

RESUME

Hung Quy Vu

Education

02. 2009 - 11. 2013	**Ph. D., Department of Informatics, University of Zurich**, Switzerland Thesis: "*MESTRAN, a Variable Stiffness Actuator for Energy Efficient Legged Robots*"— Advisor: Prof. Rolf Pfeifer
08. 2006 - 07. 2008	**M.Sc., Department of Mechanical Engineering, Korea University**, Korea Thesis: "*Development of a small field robot with four tracks capable of autonomous stair climbing* "— Advisor: Prof. Jae-Bok Song
09.1999 - 06. 2004	**B.Sc., Department of Mechanical Engineering, Hanoi University of Technology**, Vietnam Thesis: "*Investigation of strength of the GV-503 machining center by using finite element method* "— Advisor: Prof. Toan X. Nguyen

Work Experiences

11. 2013 - Current	**PostDoctoral Research at the Bio-inspired Robotic Laboratory**, Swiss Federal Institute of Technology Zurich, Switzerland (*http://www.birl.ethz.ch/people/Hung_Quy_Vu)* .
02. 2009 - 11. 2013	**Research assistant at Artificial Intelligence Laboratory**, University of Zurich, Switzerland (*http://www.ifi.uzh.ch/ailab).*
08. 2006 - 07. 2008	**Research assistant at Intelligence Robotic Laboratory**, Korea University, Korea (*http://robotics.korea.ac.kr).*
08. 2004 - 08. 2006	**Teacher at CNC Training Center**, Faculty of Mechanical Engineering, Hanoi University of Science and Technology, Vietnam (*http://www.hust.edu.vn)* .

Teaching experiences

Fall 2009 - 2012	**Teaching Assistant**, in 4 semesters at Department of Informatics, University of Zurich, Switzerland Subject: Formal Methods for Computer Science II, Course No. BINF2100, Lecturer: Prof. Rolf Pfeifer

Grants and awards

02. 2009	**Ph. D. candidate** under supervision of Prof. Rolf Pfeifer, Department of Informatics, University of Zurich, Switzerland.
08. 2008	**The ICCAS 2008 Outstanding Paper Award**, selected by ICCAS2008 Award Committee, Korea Institute of Control, Robotics and Systems (ICROS) Secretariat.
06. 2006	**Full 2-year master scholarship** in Germany from the Vietnamese government.
04. 2006	**Integrated Master-Doctoral scholarship** at Intelligence Robotics Laboratory, sponsored by Prof. Jea-Bok Song, Korea University.

Languages

English:	Fluent in speaking, reading, writing (TOEFL 547 in Jan. 2006)
German:	A1 level (Dec. 2010)
Vietnam:	Native language
Korea:	Basic

Computer Experiences

Programming	C, Java (Netbean & Eclipse), **Matlab**, LabView
Office	**Ms. Word, Excel, PowerPoint, Latex**
Graphics	Adobe Illustrator, Adobe Photoshop, **Inkscape**
Mechanical Design	**Solidwork, AutoCAD, Mechanical Desktop**
Mechanic Simulation	**MSC.ADAMS, CosMosDesign Star, Matlab Simulink, Matlab Symmechanics**
CNC technology	**Master CAM**
Computer OS	**Windows**, Ubuntu

**Bold items for professional working proficiency*

Past projects and Experiences

- Member of an European Union funded project Myorobotics from Oct. 2013.
  Reference: *http://Myorobotics.eu*
- Successfully developed a single-leg hopping robot equipped with a new variable stiffness actuator from a concept, design, fabrication, experiment, and data analysis.
  Reference: *http://vqhungvn.blogspot.ch*
- Member of an European Union funded project LOCOMORPH in 4 years from Feb. 2009 to May. 2013. The project was completed successfully on May. 2013.
  Reference: *http://locomorph.eu*
- In-charged person of the Mechanical workshop at the Artificial Intelligence Lab, Department of Informatics, University of Zurich from Feb. 2009 - current. My responsibility is to maintain the quality, and quantity of machine tools under working conditions, to guide new persons to use machines, and guarantee safety in use.
- Successfully developed a new controller to implement a stair-climbing algorithm for the small field robot at the Intelligence Robotics Laboratory, Korea University.
  Reference: *http://vqhungvn.blogspot.ch*
- Successfully complete a master project which was to design, fabricate, and control a new stair climbing robot.
- Participated in the Guard Robot project, at Intelligence Robotics Laboratory, Korea University Sept. 2006 - Jul. 2008.
  Reference: *http://robotics.korea.ac.kr/robotic-systems/guard-robots*
- Experiences in Mechanical Design and Analysis
- G-code/Computer-aided programming (MasterCAM) for CNC machining.
- Machining experienced on various machines (lathe, mill, drill,etc).

Scientific publications

1. Hung Q. Vu, Yu Xiaoxiang, Fumiya Iida, and Rolf Pfeifer. *Improving energy efficiency of hopping locomotion by using a variable stiffness actuator* submitted to The IEEE/ASME Transactions on Mechatronics, 2014 in Jan. 2014
2. Amir Jafari, Hung Q. Vu, Fumiya Iida, *Determinants of Variable Stiffness Mechanisms*, submitted to The International Journal of Robotics Research in Oct. 2013
3. Hung Q. Vu, L. Aryananda, F. I. Sheikh, F. Casanova, and R. Pfeifer, *A novel mechanism for varying stiffness via changing transmission angle*, Robotics and Automation (ICRA), 2011 IEEE International Conference on 9-13 May 2011, pp. 5076-5081.

4. Hung Q.Vu, Helmut Hauser, and R. Pfeifer, *A variable stiffness mechanism for improving energy efficiency of a planar single-legged hopping robot*, Advanced Robotics (ICAR), 2013 16th International Conference on 25-29 Nov. 2013, pp. 1-7.

5. Hung Q. Vu . *Knee stiffness adjustment for energy efficient locomotion of a legged robot on surfaces with different stiffnes* Robotics and Biomimetics (ROBIO), 2013 IEEE International Conference on 12-14 Dec. 2013, pp. 1825-1831.

6. Hung Vu Quy, Gilles Ramstein, Flurin Casanova, Lijin Aryananda, Matej Hoffmann, Farrukh Iqbal Sheikh and Helmut Hauser *Gait Versatility Through Morphological Changes in a New Quadruped Robot*, International Symposium on Adaptive Motion of Animals and Machines, pp. 59-60, 2011.

7. Kim, B.-S., Vu, Q.-H., Song, J.-B., and Yim, C.-H. (2010). Novel design of a small field robot with multi-active crawlers capable of autonomous stair climbing. *Journal of Mechanical Science and Technology*, 24(1):343–350.

8. Vu, H., Kim, B.-S., and Song, J.-B. ((2008)). Autonomous stair climbing algorithm for a small four-tracked robot. *The International Conference on Control, Automation and Systems, ICCAS 2008*, pages 2356–2360.

9. Vu, H., Kim, B.-S., and Song, J.-B. (2008). Multi-tracked robot capable of rough terrain traveling and recoverable from overturn. In *Annual Spring Conference of the KSME*, page 153.

Conference and Other Events

- Presented in International Conference of Robotics and Biomimetics, Schenzhen, China, December, 2013.
- Presented in International Conference of Robot and Automation, ShangHai, China, May, 2011.
- Presented in International Symposium on Adaptive Motion of Animals and Machines, Awaji, Japan, Oct.11-14, 2011.
- Presented my robot and a poster in Swiss National Competence Center of Robotic Research, ETHZ, Zurich, Oct 2012.
- Presented in OCTOPUS and STREP EMBODYi Summer School on Embodied Intelligence Theme, Livorno, Italy, September 20-24, 2010.
- Presented in Multimedia and Cognitive Systems Summer School, University of Zurich, June 8-14, 2009.
- Presented in Spring Annual Meeting of the Korean Society of Mechanical Engineers, Korea, March, 2008.
- Presented my robot, i.e. REMbot, at the ADeKo (Alumninetzwerk Deutschland Korea) exhibition, Korea University, May, 2008.
- Presented my robot at the 17th IFAC(International Federation of Automatic Control) World Congress exhibition, Coex, Seoul, July, 2008.

Personal details

Date of Birth	15th January 1982
Place of Birth	Thainguyen, Vietnam
Nationality	Vietnam
Marital status	Married
Residential status	B permit

Current contact address in 2014

Leonhardstrasse
27, 8092 Zurich,
Switzerland
Phone +41 44 632 43 24
Email vuq@ethz.ch or vqhung@ifi.uzh.ch

References

References are available upon request